Water-wave propagation through Very Large Floating Structures

Benjamin George Carter

Submitted in partial fulfilment of the requirements for the award of
Doctor of Philosophy of Loughborough University

Supervisor: Phil McIver

Acknowledgments

I wish to begin by thanking my supervisor, Professor Phil McIver, for all of the help and guidance that he has provided over the course of my research. I have found him to be very patient, and I feel privileged to have been able to draw from his vast knowledge base.

I would like to thank the staff in the School of Mathematics at Loughborough University for their assistance during my postgraduate, and my undergraduate, studies. I want to express my gratitude to Kieron Moore for the many helpful discussions I have had with him.

Last, but certainly not least, I wish to give a special mention to my parents. Without their encouragement and support, it would have been a lot harder to reach my potential during my education.

Abstract

Proposed designs for Very Large Floating Structures motivate us to understand water-wave propagation through arrays of hundreds, or possibly thousands, of floating structures. The water-wave problems we study are each formulated under the usual conditions of linear wave theory. We study the frequency-domain problem of water-wave propagation through a periodically arranged array of structures, which are solved using a variety of methods.

In the first instance we solve the problem for a periodically arranged infinite array using the method of matched asymptotic expansions for both shallow and deep water; the structures are assumed to be small relative to the wavelength and the array periodicity, and may be fixed or float freely.

We then solve the same infinite array problem using a numerical approach, namely the Rayleigh-Ritz method, for fixed cylinders in water of finite depth and deep water. No limiting assumptions on the size of the structures relative to other length scales need to be made using this method. Whilst we aren't afforded the luxury of explicit approximations to the solutions, we are able to compute diagrams that can be used to aid an investigation into negative refraction.

Finally we solve the water-wave problem for a so-called strip array (that is, an array that extends to infinity in one horizontal direction, but is finite in the other), which allows us to consider the transmission and reflection properties of a water-wave incident on the structures. The problem is solved using the method of multiple scales, under the assumption that the evolution of waves in a horizontal direction occurs on a slower scale than the other time scales that are present, and the method of matched asymptotic expansions using the same assumptions as for the infinite array case.

Contents

Introduction

In recent years there has been a growing interest in the interaction of time-harmonic water waves with very large arrays of fixed or floating structures. This is motivated, for example, by the practical problems of so-called Very Large Floating Structures [1] supported by regular arrangements of floating elements, and arrays of wave power devices [2]. This thesis investigates the water / structure interaction under the theory of linear water waves as described in [3, 4]. The structure of this theory allows us to decompose the wave motion into a scattering problem (where the structures are held fixed) and radiation problem (where each structure is forced to move in the absence of an incident wave): this leads us to consider the two problems separately.

The study of waves through arrays of structures has a long history in the context of water waves, and an extensive review is given in [5], where it is acknowledged that arrays consisting of a small amount of structures can be handled by relatively straightforward extensions of the methods used for single structures. This however, becomes computationally expensive for large arrays and so we look to other methods to describe very large arrays. For arrays of modest size there are well established techniques for the calculation of hydrodynamic interactions: vertical cylinders extending throughout the depth (equivalent to an acoustics problem) is looked at in [6], (their method involves using a plane wave expansion at each cylinder and then linking the expansions together using addition theorems); whilst the work contained in [7] can, in principle, deal with arbitrary array configurations and cater for structures of almost any shape. This work has been further developed in [8], where small arrays are grouped together to form a larger array; in this way the scattering and radiation characteristics of an array for 5120 cylinders was computed.

For larger arrays, properties such as periodicity are exploited; for example, the application of the methods given in [7] to wave scattering by either an infinite or semi-infinite line of periodically arranged structures is described in [9, 10]. Line arrays are also looked at in [11, 12, 13]. Very large arrays consisting of many infinite periodic line arrays stacked together can be treated by an extension of these methods [14, 15, 16]. An alternative is to use asymptotic methods based

on the assumption that individual structures are small compared to other length scales in the problem [17, 18]. In problems of the interaction of water waves with large but finite arrays, quantities of interest include the reflection and transmission properties of the array [15, 17] and the responses of individual elements to wave forcing [18]. Another way of gaining insight into what happens inside large arrays is to consider arrays that extend to infinity in both horizontal directions, as is done in [19].

In much of this literature interest is focussed on the appearance of band gaps, that is frequency ranges for which wave propagation through an infinite medium is not possible. We use band diagrams (plots of the wave frequency against a phase vector associated with the waves under investigation) to graphically show what is happening. In the water-wave problem, and specifically for fixed vertical cylinders that extend throughout the water depth, the band-gap structure has been studied in [20] using approximate and numerical techniques, in [21] using multiple-scattering techniques, and in [19] using asymptotic methods. The study of wave propagation through lattices has a long history in many research fields other than water waves including acoustics and electromagnetism, and an extensive survey of the literature can be found in [22]. The phenomenon of negative refraction – which can be exploited to make superlenses that can refocus a point disturbance on the opposite side of a rectangular slab of material – has been observed both experimentally and theoretically in many contexts including water waves [23] and acoustics [24]. Observation of negative refraction requires an understanding of the band gaps that the material under investigation exhibits [25].

The plan of this thesis is as follows. We introduce the standard linear water wave theory that is used throughout the thesis in Chapter 1. Following the work contained within [26], [3] and [4], we derive the governing equations for a fluid that is inviscid and incompressible and where the fluid motion is assumed to be irrotational, as well as deriving the equation of motion for a constrained body. We present the form that time-harmonic solutions take as well as discussing the decomposition of the velocity potential into a scattering and radiation problem. We also show how to deal with problems where the depth is constant. Three different mathematical problems are considered in chapters 2, 3 and 4. Each problem is formulated by quoting the relevant governing equations and concepts discussed in the first chapter. For the main part the three problems are essentially self-contained and hence can each be read and appreciated on their own, without resort to the other two chapters (and consequently there is significant repetition at the beginning of each chapter to formulate the problem under investigation).

In Chapter 2, solutions for truncated structures arranged in an array that extends to infinity

in both horizontal directions are obtained by the method of matched asymptotic expansions with the principle assumptions that the wavelength is much larger than a characteristic dimension of the structure, and that the separation distance between structures is of the same order of magnitude as the wavelength. This last assumption allows expressions to be obtained for the width of local band gaps, in contrast to homogenisation schemes (for example, [27]) that are valid only for frequencies below those for which band gaps appear in these problems. The assumptions adopted correspond to those made in previous work on two-dimensional problems in acoustics [19, 28] and elasticity [29]. Here, additional simplifying assumptions are made on the depth of the fluid and two cases are considered. First of all, the water is assumed to be shallow so that the depth is much smaller than the wavelength, and secondly the water is assumed to be infinitely deep. In part, these cases are investigated as explicit approximations are relatively easy to obtain. However, it is anticipated that the results for deep water are qualitatively similar to those that would be obtained for water whose depth is of the same order of the wavelength, but is large relative to the dimensions of the structure. By solving the problem asymptotically, the principle aim here is to obtain simple expressions that show explicitly how the frequency of waves with specified wavenumber and propagation direction is affected by the geometry of the structure and the lattice, and by the stiffness of the moorings in the case of a floating structure. For simplicity, we consider only vertically axisymmetric structures constrained to move in the vertical direction. Our asymptotic methods also allow us to describe explicitly the appearance of local band gaps, and hence see how they are affected by various physical parameters.

A numerical approach to the problem is used in Chapter 3. Here we solve the same infinite array problem for truncated cylinders using the Rayleigh-Ritz method by extending the work of [20]. Using this method allows us to get exact solutions for what is essentially the same problem explored in Chapter 2 without having to make an assumption that the structures are small compared to the wavelength, or indeed that the periodicity of the array is of the same order of magnitude as the wavelength. The purpose of this chapter is twofold: to complement *and* extend the asymptotic approach of the previous chapter. The asymptotic work is not helpful enough to investigate negative refraction. (The asymptotic method used in Chapter 2 yields local approximations in wavenumber space, and hence cannot be straightforwardly used to construct complete band diagrams; the results from the Rayleigh-Ritz method can be used to construct full band diagrams allowing us to investigate the conditions required for negative refraction.) We look at finite depth (where of course it is possible to specify parameters corresponding to the shallow water asymptotic solutions) and deep water.

In Chapter 4 we study water-wave propagation through arrays of structures arranged in a two dimensional array stretching to infinity in one horizontal direction but of finite width in the other – we call this a strip array – using the method of multiple scales and matched asymptotic expansions. By having the array wide enough (in the horizontal direction that is of finite length), we expect there to be a clear analogy between the solutions found here and those within Chapter 2; in the same sense, the solutions inside the strip array are perturbations from the plane waves that exist in the absence of any structures. By introducing a slow scale to consider alongside the fast scales, we essentially homogenise a complex geometry – the strip array of structures – to a simpler one; the slow scale describes how the waves change as they propagate through the array of cylinders. By looking at a strip array (where it makes sense to talk of an incident wave), we can look at what happens to waves whose frequencies fall within the band gaps that were found in Chapter 2: as per [30, page 53], adding an edge to an infinite array will allow us to sustain an evanescent mode. Within this chapter we look at both shallow water and the deep water limit (alongside water of finite depth), which is an extension to the work found within [17] and [18] respectively; in both cases we build upon and make more explicit their work by formalising the approach to the method of multiple scales. This is done by considering a full composite solution and using matched asymptotic expansions between inner and outer solutions in one cell, as was done in [31, chapter 4]; in particular, we find that we are able to use the inner solutions from the infinite array solutions, as found in Chapter 2.

Chapter 1

Standard linear wave theory

1.1 Introduction

The formulation of the equations governing the flow of a fluid and its interaction with constrained bodies has been completed following the work of a selection of authors; Crapper [26] as well as Linton and McIver [3] provided the grounding for the fluid equations, whilst Mei [4] demonstrated the derivation of the equations of motion for a constrained body. Courtesy of Linton and McIver, this chapter is concluded by looking at the form that the velocity potential may take under certain conditions: the form of the velocity potential in the case of time-harmonic motion; the decomposition of a water-wave problem into a scattering and radiation problem; and the form of the velocity potential in water of constant depth.

1.2 Fluid equations

We begin by deriving the equation of continuity. Let us assume that the fluid under consideration is incompressible, that is that the density ρ is constant. Consider a closed surface S, fixed in space, with the fluid moving through it. Concentrating our attention on a small segment of the surface, with area $\mathrm{d}S$, we note that in time δt a volume of $\mathrm{d}S(\boldsymbol{u}\cdot\boldsymbol{n})\delta t$ should flow through, where $\boldsymbol{u}$ is the fluid velocity and $\boldsymbol{n}$ is the outward unit normal vector to S. Since the fluid is incompressible the total flow through S must vanish, i.e. the inflow is balanced by the outflow. This means, around the whole surface, we have

$$\int_S \boldsymbol{u}\cdot\boldsymbol{n}\ \mathrm{d}S = 0. \tag{1.2.1}$$

Applying the divergence theorem we find

$$\int_V \nabla \cdot \boldsymbol{u} \, \mathrm{d}V = 0, \tag{1.2.2}$$

where V is the volume of the fluid enclosed by S. For this to be true for any volume this must mean that

$$\nabla \cdot \boldsymbol{u} = 0, \tag{1.2.3}$$

which is the equation of continuity.

Now let us assume that the fluid is irrotational. Mathematically this is expressed as

$$\nabla \times \boldsymbol{u} = 0, \tag{1.2.4}$$

which means that $\boldsymbol{u}$ can be written as the gradient of a velocity potential Φ

$$\boldsymbol{u} = \nabla \Phi. \tag{1.2.5}$$

Subsitution of this result back into the equation of continuity yields Laplace's equation

$$\nabla^2 \Phi = 0. \tag{1.2.6}$$

Because we have assumed that the fluid is irrotational (and will eventually be considering structures present in the fluid) we must make a third assumption on the fluid, that being that the fluid's flow is inviscid. This means that the force on the fluid inside S due to the fluid outside S is purely a pressure, normal to S, denoted $-P\boldsymbol{n}\mathrm{d}S$, where $\boldsymbol{n}$ is the normal vector pointing out of S. The other force acting is due to gravity, which we can write as $\boldsymbol{g}\rho \mathrm{d}V$, acting on an element of volume $\mathrm{d}V$ with $\boldsymbol{g}$ being the acceleration due to gravity times a unit vector pointing vertically downwards. Applying Newton's second law of motion to the fluid inside S in the direction of a general fixed unit vector $\boldsymbol{l}$ we thus have

$$\int_V \boldsymbol{l} \cdot \frac{D\boldsymbol{u}}{Dt} \rho \, \mathrm{d}V = -\int_S P \, \boldsymbol{l} \cdot \boldsymbol{n} \, \mathrm{d}S + \int_V \boldsymbol{l} \cdot \boldsymbol{g} \, \rho \, \mathrm{d}V. \tag{1.2.7}$$

where D/Dt is the material derivative: that is the rate of change moving with the fluid, measured in fixed coordinates. Using the divergence theorem and recalling that $\boldsymbol{l}$ is a constant we see that

this expression is equivalent to

$$\int_V \rho \boldsymbol{l} \cdot \left(\frac{D\boldsymbol{u}}{Dt} + \frac{1}{\rho}\nabla P - \boldsymbol{g} \right) \, \mathrm{d}V = 0, \tag{1.2.8}$$

which we note holds for any volume V and any direction l, so that

$$\frac{D\boldsymbol{u}}{Dt} = -\frac{1}{\rho}\nabla P + \boldsymbol{g} \tag{1.2.9}$$

holds throughout the fluid. This is Euler's equation of motion, and from it we derive Bernoulli's equation. For a general function f the chain rule for partial differentiation gives

$$\frac{Df}{Dt} = \frac{\partial f}{\partial t} + \frac{\partial f}{\partial x}\frac{Dx}{Dt} + \frac{\partial f}{\partial y}\frac{Dy}{Dt} + \frac{\partial f}{\partial z}\frac{Dz}{Dt}, \tag{1.2.10}$$

but, since Dx/Dt, Dy/Dt and Dz/Dt are simply the components of the vector velocity $\boldsymbol{u}$ (z points vertically upwards in our chosen coordinate system), we can rewrite it as

$$\frac{Df}{Dt} = \frac{\partial f}{\partial t} + \boldsymbol{u} \cdot \nabla f \tag{1.2.11}$$

or, when applied to the velocity,

$$\frac{D\boldsymbol{u}}{Dt} = \frac{\partial \boldsymbol{u}}{\partial t} + \boldsymbol{u} \cdot \nabla \boldsymbol{u}. \tag{1.2.12}$$

Recalling that the velocity can be written as the gradient of a velocity potential Φ and using results from vector calculus we thus have

$$\frac{D\boldsymbol{u}}{Dt} = \frac{\partial}{\partial t}(\nabla\Phi) + \frac{1}{2}\nabla \mid \nabla\Phi \mid^2 - \nabla\Phi \times (\nabla \times \nabla\Phi). \tag{1.2.13}$$

But, since Φ was introduced under the assumption that flow is irrotational, the last term disappears and using Euler's equation of motion (1.2.9) yields

$$\frac{\partial}{\partial t}(\nabla\Phi) + \frac{1}{2}\nabla \mid \nabla\Phi \mid^2 + \frac{1}{\rho}\nabla P - \boldsymbol{g} = 0. \tag{1.2.14}$$

But since $\boldsymbol{g} = -g\nabla z$, where g is the magnitude of $\boldsymbol{g}$, this can be written as

$$\nabla \left(\frac{\partial \Phi}{\partial t} + \frac{1}{2} \mid \nabla\Phi \mid^2 + \frac{P}{\rho} + gz \right) = 0. \tag{1.2.15}$$

Finally, integrating gives the Bernoulli equation,

$$\frac{\partial \Phi}{\partial t} + \frac{1}{2} \mid \nabla \Phi \mid^2 + \frac{P}{\rho} + gz = 0 \tag{1.2.16}$$

where we have put the arbitrary function of time that arises because of the integration to zero. (By redefining Φ we get the function of time to cancel).

1.2.1 Boundary conditions on the free surface of the fluid

1.2.1.1 The kinematic condition

A kinematic condition matches the normal component of the velocity of the fluid with that of the particles surrounding it. Let us start by finding the kinematic condition on the free surface. Consider a new closed surface S_M in the fluid, this time moving with the fluid. The same particles always form the surface and fluid originally inside S_M remains there. Let $S(x, y, z, t) = 0$ be the equation of the surface S_M then as x, y, z and t vary for each particle on S_M we have

$$\frac{DS}{Dt} = 0 \tag{1.2.17}$$

for any surface S_M which we may choose. Let S_M be the free surface, which we will define as $z = \eta(x, y, t)$ so that our equation for S_M is

$$S = \eta(x, y, t) - z = 0. \tag{1.2.18}$$

Using (1.2.11) to rewrite (1.2.17) for our newly defined S_M we have

$$\frac{\partial \eta}{\partial t} + \boldsymbol{u} \cdot \nabla \eta - \frac{Dz}{Dt} = 0 \tag{1.2.19}$$

or, in component form,

$$\frac{\partial \eta}{\partial t} + \frac{\partial \Phi}{\partial x}\frac{\partial \eta}{\partial x} + \frac{\partial \Phi}{\partial y}\frac{\partial \eta}{\partial y} = \frac{\partial \Phi}{\partial z} \quad \text{on} \quad z = \eta(x, y, t) \tag{1.2.20}$$

which we call the kinematic free surface condition.

1.2.1.2 The dynamic condition

The so called dynamic condition applies on the free surface and is derived by assuming there is no motion in the air and that pressure there is constant, which we can take to be zero for

simplicity. Hence from Bernoulli's equation we have

$$\frac{\partial \Phi}{\partial t} + \frac{1}{2} \mid \nabla \Phi \mid^2 + g\eta = 0 \quad \text{on} \quad z = \eta(x, y, t). \tag{1.2.21}$$

1.2.2 The kinematic condition on the bed

When the velocity acting normal to the fluid is prescribed, it is more useful to give the kinematic condition in the form that we do here. We note that when there is an impermeable sea (or river) bed with local fluid depth $h(x, y)$, there must be no flow normal to the bed (so that the normal velocity must be zero), hence giving us a bed condition of

$$\frac{\partial \Phi}{\partial n} = 0 \quad \text{on} \quad z = -h(x, y), \tag{1.2.22}$$

where n is a coordinate measured normal to the bed.

1.2.3 The linearised equations

By requiring that the amplitude of the fluid motion is small compared with the wavelength throughout the domain, we can apply the free surface boundary conditions on $z = 0$ and neglect products, giving us

$$\frac{\partial \eta}{\partial t} = \frac{\partial \Phi}{\partial z} \qquad \text{on} \qquad z = 0 \tag{1.2.23}$$

$$\text{and} \quad \frac{\partial \Phi}{\partial t} + g\eta = 0 \qquad \text{on} \qquad z = 0, \tag{1.2.24}$$

as the kinematic and dynamic condition respectively. Differentiating (1.2.24) with respect to t and substituting in (1.2.23) generates

$$\frac{\partial^2 \Phi}{\partial t^2} + g\frac{\partial \Phi}{\partial z} = 0 \quad \text{on} \quad z = 0, \tag{1.2.25}$$

the linearized free surface condition for Φ.

1.3 Equations of motion for a constrained floating body

As in the case of the boundary conditions on the fluid surface there are kinematic and dynamic conditions on the wetted body surface, S_C. Specifically we're interested in so called heave motion, that is motion parallel to the vertical z-axis only, and so after initially considering 6 modes of movement we restrict our attention appropriately.

1.3.1 The kinematic condition

Let the instantaneous position of S_C be described by $z = f(x, y, t)$ so that $S_C = f(x, y, t) - z = 0$. Following the same logic as the kinematic condition for the free surface we have

$$\frac{\partial \Phi}{\partial x}\frac{\partial f}{\partial x} + \frac{\partial \Phi}{\partial y}\frac{\partial f}{\partial y} + \frac{\partial f}{\partial t} = \frac{\partial \Phi}{\partial z} \quad \text{on} \quad z = f(x, y, t), \tag{1.3.1}$$

which is the kinematic condition on S_C which we now need to linearize. Expanding f in powers of the perturbation parameter $\epsilon = kA$ (k is the wavenumber and A typically describes the amplitude of the wave, so that kA is its non-dimensional steepness: by considering kA to be small we are considering a small amplitude motion of an oscillating body) yields

$$z = f^{(0)}(x, y) + \epsilon f^{(1)}(x, y, t) + \epsilon^2 f^{(1)}(x, y, t) + \cdots, \tag{1.3.2}$$

where $f^{(0)}(x, y)$ corresponds to the rest position of S_C, denoted $S_C^{(0)}$. Similarly, we can expand the velocity potential (but we don't require a rest position to be built into this expansion)

$$\Phi = \epsilon \Phi^{(1)} + \epsilon^2 \Phi^{(2)} + \cdots. \tag{1.3.3}$$

Now, to the first order (1.3.1) becomes

$$\Phi_x^{(1)} f_x^{(0)} + \Phi_y^{(1)} f_y^{(0)} + f_t^{(1)} = \Phi_z^{(1)} \quad \text{on} \quad z = f^{(0)}(x, y). \tag{1.3.4}$$

We know $f^{(0)}$ and so we need to find $f^{(1)}$ so that we can write $f_t^{(1)}$. Let the centre of rotation of the rigid body be Q, which has moving coordinate

$$\boldsymbol{X}(t) = \boldsymbol{X}^{(0)} + \epsilon \boldsymbol{X}^{(1)}(t) + \epsilon^2 \boldsymbol{X}^{(2)}(t) + \cdots \quad \text{with} \quad \boldsymbol{X} = (X, Y, Z). \tag{1.3.5}$$

$\boldsymbol{X}^{(0)}$ is the rest position of Q, independent of t. (Note that Q need not coincide with the centre of mass of the body). Denote the coordinate system fixed with the body $\check{\boldsymbol{x}}$ (such that $\check{\boldsymbol{x}} = \boldsymbol{x}$ when the body is at rest). Denote the angular displacement of the body as $\epsilon \boldsymbol{\theta}^{(1)}(t)$ (with components $\epsilon\alpha$, $\epsilon\beta$ and $\epsilon\gamma$ about axes parallel to x, y and z respectively).

The two coordinate systems are related to the first order by

$$\boldsymbol{x} = \check{\boldsymbol{x}} + \epsilon[\boldsymbol{X}^{(1)} + \boldsymbol{\theta}^{(1)} \times (\boldsymbol{x} - \boldsymbol{X}^{(0)})] + O(\epsilon^2). \tag{1.3.6}$$

Rearranging and rewriting in component form we thus have

$$\check{x} = x - \epsilon[X^{(1)} + \beta(z - Z^{(0)}) - \gamma(y - Y^{(0)}], \tag{1.3.7a}$$

$$\check{y} = y - \epsilon[Y^{(1)} + \gamma(x - X^{(0)}) - \alpha(z - Z^{(0)}], \tag{1.3.7b}$$

$$\check{z} = z - \epsilon[Z^{(1)} + \alpha(y - Y^{(0)}) - \beta(x - X^{(0)}]. \tag{1.3.7c}$$

Now, by definition, $\check{\boldsymbol{x}} = \boldsymbol{x}$ when the body is at rest, therefore from $z = f^{(0)}(x, y)$ we must have

$$\check{z} = f^{(0)}(\check{x}, \check{y}). \tag{1.3.8}$$

Putting (1.3.7a - 1.3.7c) into (1.3.8) and using a Taylor series expansion yields

$$\begin{aligned} z = f^{(0)}(x,y) + \epsilon \Big\{ & -f_x^{(0)} \left[X^{(1)} + \beta(z - Z^{(0)}) - \gamma(y - Y^{(0)}) \right] \\ & -f_y^{(0)} \left[Y^{(1)} + \gamma(x - X^{(0)}) - \alpha(z - Z^{(0)}) \right] \\ & + \left[Z^{(1)} + \alpha(y - Y^{(0)}) - \beta(x - X^{(0)}) \right] \Big\}. \end{aligned} \tag{1.3.9}$$

Comparing (1.3.9) with (1.3.2) we see that $f^{(1)}$ can be equated with the curly brackets of (1.3.9) and so differentiating with respect to t yields

$$\begin{aligned} f_t^{(1)} = \Big\{ & -f_x^{(0)} \left[X_t^{(1)} + \beta_t(z - Z^{(0)}) - \gamma_t(y - Y^{(0)}) \right] \\ & -f_y^{(0)} \left[Y_t^{(1)} + \gamma_t(x - X^{(0)}) - \alpha_t(z - Z^{(0)}) \right] \\ & + \left[Z_t^{(1)} + \alpha_t(y - Y^{(0)}) - \beta_t(x - X^{(0)}) \right] \Big\}. \end{aligned} \tag{1.3.10}$$

Putting (1.3.10) into (1.3.4) yields the first-order kinematic condition. This rather cumbersome expression can be written more neatly as

$$\frac{\partial \Phi^{(1)}}{\partial n} = \boldsymbol{X}_t^{(1)} \cdot \boldsymbol{n} + \boldsymbol{\theta}_t^{(1)} \cdot \left[(\boldsymbol{x} - \boldsymbol{X}^{(0)}) \times \boldsymbol{n} \right], \tag{1.3.11}$$

where

$$\boldsymbol{n} = \left[1 + \left(f_x^{(0)} \right)^2 + \left(f_y^{(0)} \right)^2 \right]^{(-1/2)} \left(-f_x^{(0)}, -f_y^{(0)}, 1 \right) \tag{1.3.12}$$

is the unit normal pointing out of the fluid and into the body.

1.3.2 The dynamic condition: conservation of linear momentum

Let M be the mass of the entire floating body (part of which may be above the free surface) and $\boldsymbol{x}^c(t)$ be the position of the centre of mass. Conservation of linear momentum requires that

$$M\boldsymbol{x}^c(t)_{tt} = \iint_{S_C} P\boldsymbol{n}\ \mathrm{d}S - Mg\boldsymbol{e_3} + \underline{\mathbb{F}}, \tag{1.3.13}$$

where P is the magnitude of the pressure on the wetted body surface S_C, the second term is the effect on the body due to gravity and the third term denotes a constraining force from any external support. $\mathbb{F}$ can be expanded as a static and a dynamic part:

$$\underline{\mathbb{F}}(t) = \underline{\mathbb{F}}^{(0)} + \epsilon\underline{\mathbb{F}}^{(1)}(t) + \cdots . \tag{1.3.14}$$

Equation (1.3.6) applies to $\boldsymbol{x}^c(t)$ so that

$$\boldsymbol{x}^c = \check{\boldsymbol{x}}^c + \epsilon\left[\boldsymbol{X}^{(1)} + \boldsymbol{\theta}^{(1)} \times (\boldsymbol{x}^c - \boldsymbol{X}^{(0)})\right] + O(\epsilon^2), \tag{1.3.15}$$

and so the left hand side of (1.3.13) can be written as

$$M\boldsymbol{x}^c(t)_{tt} = \epsilon M\left[\boldsymbol{X}^{(1)}_{tt} + \boldsymbol{\theta}^{(1)}_{tt} \times (\boldsymbol{x}^c - \boldsymbol{X}^{(0)})\right] + O(\epsilon^2). \tag{1.3.16}$$

Now we will deal with the right hand side of (1.3.13). We make use of the linearized Bernoulli equation

$$P = -\rho g f - \epsilon\rho\Phi^{(1)}_t + O(\epsilon^2) \tag{1.3.17}$$

to write the first term as

$$\iint_{S_C}\left(-\rho g f - \epsilon\rho\Phi^{(1)}_t\right)\boldsymbol{n}\ \mathrm{d}S = -\rho g\iint_{S_C} f\boldsymbol{n}\ \mathrm{d}S - \epsilon\iint_{S^{(0)}_C}\rho\Phi^{(1)}_t\boldsymbol{n}\ \mathrm{d}S + O(\epsilon^2) \tag{1.3.18}$$

where $S^{(0)}_C$ is an approximation of S_C. We must now consider the first term – the buoyancy term – of (1.3.18). We have

$$-\rho g\iint_{S_C} f n_3\ \mathrm{d}S = -\rho g\iint_{S_A}\left(f^{(0)} + \epsilon f^{(1)}\right)dxdy \tag{1.3.19}$$

(where n_3 is the component of the normal in the z-direction) as the vertical component, because

on the instantaneous body surface S_C

$$\boldsymbol{n}\ \mathrm{d}S = (-f_x, -f_y, 1)dxdy$$

and the domain of integration S_C may be replaced by the part of the water surface cut out by S_C, that is S_A. Observe that S_A differs from its equilibrium counterpart $S_A^{(0)}$ by $O(\epsilon)$ and since $f^{(0)} = 0$ in the equilibrium free surface (because $z = 0$ on the free surface and the body is at rest / in equilibrium), the surface S_A may be replaced by $S_A^{(0)}$ with an error of order $O(\epsilon^2)$. So (1.3.19) becomes

$$-\rho g \iint\limits_{S_C} f n_3\ \mathrm{d}S = -\rho g \iint\limits_{S_A^{(0)}} f^{(0)} dxdy - \epsilon\rho g \iint\limits_{S_A^{(0)}} f^{(1)} dxdy, \tag{1.3.20}$$

where, of course, $f^{(1)}$ is known (from the derivation of the kinematic condition). Now note that using partial integration we have

$$\iint\limits_{S_A^{(0)}} f_x^{(0)} dxdy = \oint_\Gamma \left[f^{(0)}\right]_{x_-}^{x_+} dy, \tag{1.3.21}$$

where Γ is the edge of $S_A^{(0)}$, that is the water line, and x_+ and x_- refer to points on Γ intersected by a line of constant y. Now, since $f^{(0)} = 0$ on Γ the right hand side of (1.3.21) vanishes; similarly $\iint_{S_A^{(0)}} f_y^{(0)} dxdy = 0$ so that finally we have from (1.3.19)

$$\begin{aligned} -\rho g \iint\limits_{S_C} f n_3\ \mathrm{d}S = &-\rho g \iint\limits_{S_A^{(0)}} f^{(0)} dxdy \\ &-\epsilon\rho g \iint\limits_{S_A^{(0)}} \left[Z^{(1)} + \alpha(y - Y^{(0)}) - \beta(x - X^{(0)})\right] dxdy \end{aligned} \tag{1.3.22}$$

Combining (1.3.16) and (1.3.18) with (1.3.13) yields

$$\begin{aligned} &\epsilon M \left[\boldsymbol{X}_{tt}^{(1)} + \boldsymbol{\theta}_{tt}^{(1)} \times (\boldsymbol{x}^c - \boldsymbol{X}^{(0)})\right] \\ &= \quad -\rho g \iint\limits_{S_C} \left(f^{(0)} + \epsilon f^{(1)}\right) \boldsymbol{n}\ dS \\ &\qquad -\epsilon \iint\limits_{S_C^{(0)}} \rho \Phi_t^{(1)} \boldsymbol{n}\ \mathrm{d}S - Mg\boldsymbol{e_3} + \mathbb{F}^{(0)} + \epsilon \mathbb{F}^{(1)}(t) + O(\epsilon^2). \end{aligned} \tag{1.3.23}$$

At the zeroth order, upon substituting (1.3.22) we have for the third component

$$Mg = \rho g V^{(0)} + \mathbb{F}_3^{(0)}, \tag{1.3.24}$$

which is just Archimedes' Law with $V^{(0)} = \iint_{S_A^{(0)}} f^{(0)} dxdy$ being the submerged volume. At order $O(\epsilon)$ the third component of the linearized momentum equation is

$$\begin{aligned} M\left[Z_{tt}^{(1)} + \alpha_{tt}(y - Y^{(0)}) - \beta_{tt}(x - X^{(0)})\right] \\ = -\rho \iint\limits_{S_C^{(0)}} \Phi_t^{(1)} n_3 \, \mathrm{d}S + \mathbb{F}_3^{(1)}(t) - \rho g \left[I_2^A \alpha - I_1^A \beta + Z^{(1)} A^{(0)}\right] \end{aligned} \tag{1.3.25}$$

where $A^{(0)}$ is the area of $S_A^{(0)}$, $I_1^A = \iint_{S_A^{(0)}} (x - X^{(0)}) dxdy$ and $I_2^A = \iint_{S_A^{(0)}} (y - Y^{(0)}) dxdy$. This third component represents motion in the heave direction.

1.4 Form of solutions

For the main part of this thesis, we will be assuming that the fluid motion is time-harmonic (in chapter 4, where we use the method of multiple scales, we assume that it is the fast-time motion that is time-harmonic), where the frequency is prescribed. For radian frequency ω, we remove time from the problem by writing

$$\Phi(x, y, z, t) = \mathrm{Re}\{\phi(x, y, z)\mathrm{e}^{-\mathrm{i}\omega t}\}, \tag{1.4.1}$$

where ϕ is a complex-valued potential. Substitution of (1.4.1) into (1.2.6) shows that ϕ also satisfies Laplace's equation,

$$\nabla^2 \phi = 0. \tag{1.4.2}$$

In terms of ϕ the linearised free surface condition is found to be

$$\frac{\partial \phi}{\partial z} = K\phi \quad \text{on} \quad z = 0, \tag{1.4.3}$$

where $K = \omega^2/g$, with bed condition

$$\frac{\partial \phi}{\partial n} = 0 \quad \text{on} \quad z = -h(x, y). \tag{1.4.4}$$

Finally we observe that ϕ must also satisfy boundary conditions on any structures that are being considered as part of a problem (which we have just looked at in the previous section) as well as a radiation condition, which states that radiated and scattered waves propagate outwards, away from the structure.

1.4.1 Decomposing the velocity potential

A problem can be decomposed into a scattering problem (where the structure is held fixed) and a radiation problem (where the structure is forced to oscillate in the absence of an incident wave). The solution to a scattering problem maybe decomposed into an incident wave train and the waves caused by diffraction. We now look at how one would attempt to solve a problem by decoupling it.

Consider a typical floating object problem, where the object has been restricted to move in the direction of the z-axis only. The governing equation of motion for the heave direction of the structure is written, from (1.3.25), as

$$M\left[U_3{}^{(1)}\right]_t = -\rho \iint\limits_{S_C^{(0)}} \Phi_t n_3 \, \mathrm{d}S + \mathbb{F}_3(t) - \rho g Z A, \tag{1.4.5}$$

where $U_3^{(1)}$ is the velocity of the structure in the z-direction. We remove time from the problem, as just discussed, by writing

$$U_3 = \mathrm{Re}\{u_3 \mathrm{e}^{-\mathrm{i}\omega t}\}; \quad \Phi = \mathrm{Re}\{\phi \mathrm{e}^{-\mathrm{i}\omega t}\}; \quad Z = \mathrm{Re}\{\zeta \mathrm{e}^{-\mathrm{i}\omega t}\}; \quad \mathbb{F}_3 = \mathrm{Re}\{F \mathrm{e}^{-\mathrm{i}\omega t}\} \tag{1.4.6}$$

and adjusting the governing equations for Φ accordingly so that (1.4.5) becomes

$$(M\omega^2 - \rho g A)u_3 + \omega^2 \rho \iint\limits_{S_C^{(0)}} \phi \; n_3 \, \mathrm{d}S - \mathrm{i}\omega F = 0. \tag{1.4.7}$$

By the linear superposition principle, the solutions of two linear problems can be added together to calculate a total solution to both problems and so we may write

$$\phi = \phi_S + u_3 \phi_R, \tag{1.4.8}$$

where ϕ_S is the part of the solution that is scattered and ϕ_R is the part of the solution that is radiated. Note that u_3 is included here so that we may work with unit velocity in the radiation potential. Recall from the previous section that $\mathbb{F}_3$ originates from constraining forces that may

arise. An idealised force of this nature, in the direction of the Z-axis, will have the form

$$\mathbb{F}_3 = -\kappa Z - \lambda U_3, \tag{1.4.9}$$

where κ is a spring constant, and λ is a damping constant. Because $\zeta = -u_3/\mathrm{i}\omega$ we have

$$F = \frac{\kappa}{\mathrm{i}\omega} u_3 - \lambda u_3. \tag{1.4.10}$$

Putting (1.4.8) and (1.4.10) into (1.4.7) we thus find

$$\begin{aligned}(M\omega^2 - \rho g A)u_3 + \omega^2 \rho \iint\limits_{S_C^{(0)}} \phi_S \; n_3 \; \mathrm{d}S \\ + \; u_3 \omega^2 \rho \iint\limits_{S_C^{(0)}} \phi_R \; n_3 \; \mathrm{d}S - \mathrm{i}\omega F = 0.\end{aligned} \tag{1.4.11}$$

Some of the literature re-writes this expression using the exciting force

$$X_3 = \mathrm{i}\omega\rho \iint\limits_{S_C^{(0)}} \phi_S \; n_3 \; dS, \tag{1.4.12}$$

as well as the added mass and the damping coefficient

$$a_{33} = \rho \mathrm{Re} \iint\limits_{S_C^{(0)}} \phi_R \; n_3 \; dS \tag{1.4.13}$$

$$b_{33} = \rho\omega \mathrm{Im} \iint\limits_{S_C^{(0)}} \phi_R \; n_3 \; dS \tag{1.4.14}$$

respectively, leaving us with

$$\left[\rho g A + \kappa - \omega^2 \left(a_{33} + \frac{\mathrm{i}}{\omega} b_{33} + \frac{\mathrm{i}\lambda}{\omega} + M\right)\right] u_3 = -\mathrm{i}\omega X_3. \tag{1.4.15}$$

Now to find ϕ we note that the field equations (1.4.2-1.4.4) can each be written both in terms of ϕ_S and ϕ_R. To solve for ϕ_S we take the appropriate field equations with the scattering boundary condition

$$\frac{\partial \phi_S}{\partial n} = 0 \quad \text{on the scatterer}'\text{s surface.} \tag{1.4.16}$$

whilst to solve for ϕ_R we take the kinematic condition as derived in the previous section (except

now we are looking at movement of unit velocity in the z direction only) to write

$$\frac{\partial \phi_R}{\partial n} = n_3. \tag{1.4.17}$$

Then we can put our two expressions for ϕ_S and ϕ_R into (1.4.11) and solve for u_3 leaving us with, finally, the solution for ϕ as given in (1.4.8).

1.4.2 Removing the depth dependence

The governing equations for a fluid of constant depth (assuming time-harmonic motion) are as given by (1.4.2-1.4.4), except that the bed condition is applied on $z = -h$, where h is a constant.

We can solve (1.4.2) by separating the variables in Cartesian coordiates. Introducing $\hat{\varphi}$ as a function of x and y and H as a function of z we write

$$\phi(x, y, z) = \hat{\varphi}(x, y)H(z).$$

Substituting this into the governing equations yields

$$-\frac{H''}{H} = \frac{\hat{\varphi}_{xx} + \hat{\varphi}_{yy}}{\hat{\varphi}} \quad \text{in the fluid,} \tag{1.4.18a}$$

$$H' = 0 \quad \text{on} \quad z = -h, \tag{1.4.18b}$$

$$H' = KH \quad \text{on} \quad z = 0, \tag{1.4.18c}$$

where the dependence on x, y and z have been dropped for ease of notation and $'$ denotes the derivative of a function with respect to its argument. In order for (1.4.18a) to be true, both sides must be equal to a constant, which we will label $-k^2$. The ordinary differential equation for H is then

$$H'' - k^2 H = 0, \tag{1.4.19}$$

which, when solved with (1.4.18b), gives

$$H = \cosh kh(\frac{z}{h} + 1) \tag{1.4.20}$$

where the constant has been ignored. Putting $\phi = \hat{\varphi}H$ back into (1.4.2), we see that $\hat{\varphi}$ satisfies

the Helmholtz equation

$$\nabla^2\hat{\varphi} + k^2\hat{\varphi} = 0. \tag{1.4.21}$$

Furthermore, taking $\phi = \hat{\varphi}H$ with (1.4.20) substituted in, and expanding in terms of the parameter kh and equating powers of kh we see that the Helmholtz equation governs flow only at leading orders; beyond that a z dependence is brought back in.

By using (1.4.20) with the free surface condition (1.4.18c) we find the relation

$$K = k \tanh kh, \tag{1.4.22}$$

which is most commonly known as the dispersion relation. This dispersion allows the free surface condition to also be expanded in powers of kh, and hence once can observe that, to leading orders, the free surface condition is taken to be $\dfrac{\partial\hat{\varphi}}{\partial z} = 0$ on $z = 0$.

Chapter 2

Infinite array: method of matched asymptotic expansions

Note: this chapter is based on the publication [32]

2.1 Introduction

The frequency-domain problem of water-wave propagation through a periodically arranged infinite array of structures is solved using the method of matched asymptotic expansions for both shallow and deep water. Solutions are obtained under the principle assumptions that the wavelength is much larger than a characteristic dimension of the structure, and that the separation distance between structures is of the same order of magnitude as the wavelength. This last assumption allows expressions to be obtained for the width of local band gaps, in contrast to homogenisation schemes (for example [27]) that are valid only for frequencies below those for which band gaps appear in these problems. The assumptions adopted correspond to those made in previous work on two-dimensional problems in acoustics [19, 28] and elasticity [29]. Here, additional simplifying assumptions are made on the depth of the fluid and two cases are considered. First of all, the water is assumed to be shallow so that the depth is much smaller than the wavelength, and secondly the water is assumed to be infinitely deep. In part, these cases are investigated as explicit approximations are relatively easy to obtain. However, it is anticipated that the results for deep wave are qualitatively similar to those that would be obtained for water whose depth is of the same order of the wavelength, but is large relative to the dimensions of the structure.

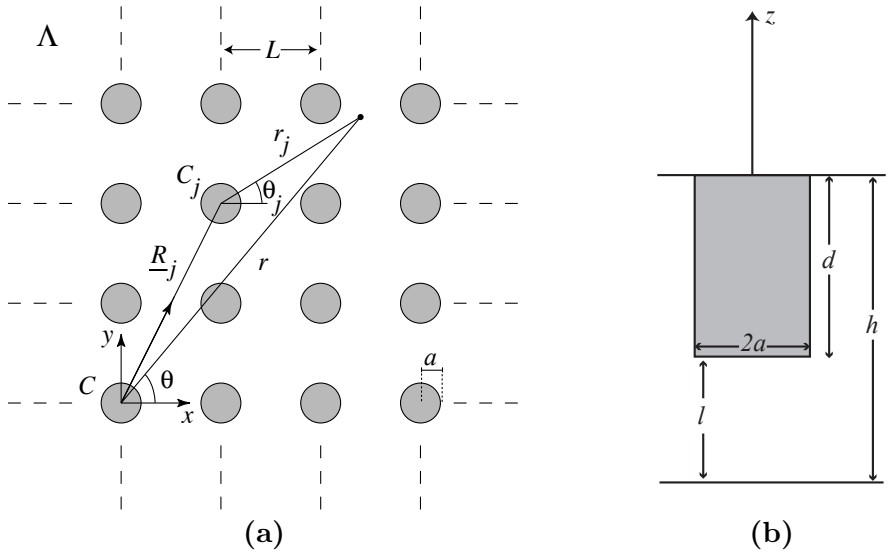

Figure 2.1 (a) Coordinate systems on $z = 0$, and (b) a vertical section of the fluid domain for a surface-piercing circular cylinder.

The problems studied here may be solved using numerical methods, for example by using a boundary-element method based on a periodic Green's function, or by using multiple-scattering techniques. However, the principle aim here is to obtain simple expressions that show explicitly how the frequency of waves with specified wavenumber and propagation direction is affected by the geometry of the structure and the lattice, and by the stiffness of the moorings in the case of a floating structure. For simplicity, we consider only vertically axisymmetric structures constrained to move in the vertical direction. Our asymptotic methods also allow us to describe explicitly the appearance of local band gaps, and hence see how they are affected by various physical parameters. Our method yields local approximations in wave-number space, and hence cannot be straightforwardly used to construct complete band diagrams. The reader is referred to the introduction of this thesis for details of a wider range of references that look at arrays.

The plan of this chapter is as follows. The problem is formulated in § 2.2, and the matching and the non-dimensionalisation of the equations are both discussed. The detailed matching is described for both fixed and floating structures in § 2.3 for shallow water, and in § 2.4 for deep water. The relation between the problems for fixed and floating structures is discussed in § 2.5, and a selection of explicit results for the frequencies of propagating waves are presented and discussed in § 2.6.

2.2 Formulation

Vertically axisymmetric structures C_j with wetted surfaces S_{C_j} are distributed uniformly on an infinite horizontal lattice Λ in water of depth h; the length scale for the lattice periodicity is denoted by L. A horizontal plane is illustrated in figure 2.1a for the particular case of a square lattice. We use Cartesian coordinates (x, y, z), with z directed vertically upwards and origin O in the mean free surface at a chosen lattice point. Global polar coordinates (r, θ) in the horizontal plane are also used. Associated with each cylinder are local horizontal polar coordinates (r_j, θ_j) with origin O_j (so that dropping the j indicates use of the global coordinates) located, relative to O, at the lattice points given by the lattice vectors

$$\boldsymbol{R}_j = n_1\boldsymbol{a}_1 + n_2\boldsymbol{a}_2, \quad n_1, n_2 \in \mathbb{Z},$$

for given linearly independent vectors $\boldsymbol{a}_1$ and $\boldsymbol{a}_2$.

All structures in the lattice are identical, and when held fixed may be either surface-piercing or bottom-mounted. In the case that the structures are allowed to float freely, they are assumed to be surface piercing and moored using identical systems of springs and dampers. Some of the numerical results presented later are for the particular case of a lattice of truncated vertical cylinders in shallow water, and the notations used for this geometry are illustrated in figure 2.1b. If surface-piercing, cylinder j occupies $r_j \leq a$, $-d \leq z \leq 0$, and we define $l = h - d$ to be the gap between the ocean bed and the bottom of the cylinder. For bottom-mounted circular cylinders, the wetted height is still denoted by d and l is the gap between the free surface and the top of the cylinder. More generally, a is used to denote the characteristic size of the structure, which, for a surface-piercing structure, is specifically chosen as the radius of the water-plane area.

The fluid is assumed to be inviscid and incompressible and the fluid motion to be irrotational. The linearised theory of water waves is used throughout so that time-harmonic motions with angular frequency ω may be described by a velocity potential $\mathrm{Re}[\phi(x, y, z)\,\mathrm{e}^{-\mathrm{i}\omega t}]$, where t is time. For all lattice vectors $\boldsymbol{R}_j$, solutions are sought that satisfy the so-called Bloch condition

$$\phi(\boldsymbol{r} + \boldsymbol{R}_j) = \mathrm{e}^{\mathrm{i}\boldsymbol{\beta}^T\boldsymbol{R}_j}\phi(\boldsymbol{r}), \tag{2.2.1}$$

where $\boldsymbol{r} = (x, y)^T$, and $\boldsymbol{\beta} = (q_1, q_2)^T$, $q_1, q_2 \in \mathbb{R}$, is a prescribed vector. The Bloch condition prescribes a phase relationship between the potential values at equivalent points in different cells of the lattice. Given a $\boldsymbol{\beta}$, we seek the frequencies ω that allow non-trivial solutions for ϕ.

In addition to the Bloch condition, the complex-valued potential ϕ satisfies the usual equa-

tions of the linearised theory of water waves [4, Chapter 8]. Thus,

$$\nabla^2\phi = 0 \quad \text{within the fluid domain } \mathcal{D}, \tag{2.2.2}$$

and the linearised condition

$$\frac{\partial\phi}{\partial z} - \frac{\omega^2}{g}\phi = 0 \quad \text{on the free surface } S_F \tag{2.2.3}$$

(g is the acceleration due to gravity) and, for water of constant finite depth,

$$\frac{\partial\phi}{\partial z} = 0 \quad \text{on the bed } S_B, \tag{2.2.4}$$

while for deep water we require that

$$|\nabla\phi| \to 0 \quad \text{as} \quad z \to -\infty. \tag{2.2.5}$$

Here we restrict attention to vertically axisymmetric structures that are either fixed, or constrained to move in the vertical (heave) direction. Hence, on the surface S_C of the particular structure C located at the chosen origin of coordinates

$$\frac{\partial\phi}{\partial n} = u_3 n_3, \tag{2.2.6}$$

where u_3 is the complex amplitude of the structure's vertical velocity, and the coordinate n is measured normal to S_C and directed out of the fluid (n_3 is the component of the unit normal in the z direction). The equation of motion for the structure C (assumed to be surface-piercing) is

$$\left[\omega^2 M + \mathrm{i}\omega\lambda - (\rho g\pi a^2 + \kappa)\right] u_3 = -\rho\omega^2 \iint_{S_C} \phi n_3 \,\mathrm{d}s, \tag{2.2.7}$$

where M is the mass, ρ is the fluid density, κ and λ are respectively the spring and damper constants for the moorings, and s is surface area. The boundary condition and equation of motion for other structures in the lattice are recovered by adjusting the phase of each structure's velocity to ensure that the Bloch condition (2.2.1) is satisfied.

In the absence of structures, the Bloch condition (2.2.1), together with (2.2.2) and (2.2.3) as

well as the appropriate bed condition, are satisfied by plane waves

$$\phi_q(\boldsymbol{r}) = \begin{cases} \mathrm{e}^{\mathrm{i}\boldsymbol{\beta}_q^T \boldsymbol{r}} \cosh k(z+h) & \text{for finite-depth water;} \\ \mathrm{e}^{\mathrm{i}\boldsymbol{\beta}_q^T \boldsymbol{r}} \mathrm{e}^{kz} & \text{for deep water,} \end{cases} \tag{2.2.8}$$

where the wavenumber k is the positive real root of the dispersion relation $\omega^2 = gk \tanh kh$,

$$\boldsymbol{\beta}_q = \boldsymbol{\beta} + \boldsymbol{K}_q, \tag{2.2.9}$$

and each $\boldsymbol{K}_q = 2\pi(m_1\boldsymbol{b}_1 + m_2\boldsymbol{b}_2)$, for $m_1, m_2 \in \mathbb{Z}$ with q representing each ordered pair (m_1, m_2), is a reciprocal lattice vector [30, Appendix B]. The vectors $\{\boldsymbol{b}_1, \boldsymbol{b}_2\}$ satisfy $\boldsymbol{a}_i^T \boldsymbol{b}_j = \delta_{ij}$ for $i, j = 1, 2$, so that $\boldsymbol{K}_q^T \boldsymbol{R}_j = 2\pi p$, $p \in \mathbb{Z}$, for any lattice vector $\boldsymbol{R}_j$. The forms (2.2.8) satisfy Laplace's equation (2.2.2) provided

$$k^2 = \beta_q^2 \quad \text{where} \quad \beta_q = |\boldsymbol{\beta}_q|. \tag{2.2.10}$$

For a given $\boldsymbol{\beta}$ there may be multiple vectors $\boldsymbol{\beta}_q$ that yield the same $|\boldsymbol{\beta}_q|$ and the number of such vectors is denoted by Q. The solutions described later are perturbations of the above quasi-periodic plane waves that exist in the absence of the structures: we will be choosing a frequency and perturbing from the frequencies associated with no structures.

Solutions in the presence of scatterers are obtained by the method of matched asymptotic expansions under the assumption that a characteristic length scale b for the flow around the structure is much smaller than the wavelength $2\pi/k$, so that $\epsilon \equiv kb \ll 1$. In addition, it is assumed that the wavelength is of the same order of magnitude as the cell size L so that $kL = \mathrm{ord}(1)$. (Here, we follow [33] and use ord to denote 'strict order' so that, for example, $kL = \mathrm{ord}(1)$ as $\epsilon \to 0$ does not allow kL to be vanishingly small in the limit.) To facilitate the solution, the fluid domain is split into many inner regions surrounding each structure to distances $r_j \ll k^{-1}$, and an outer region at distances $r_j \gg b$, where b is a length scale for the inner region (the length b will be chosen differently for the shallow and deep water cases). Because of the Bloch condition (2.2.1), it is sufficient to match between the outer region and the inner region containing the global origin O. In particular, the outer expansion of the inner solution is matched with the inner expansion of the outer solution using the formal matching principle that is described in [34]. The inner solution φ up to terms in ϵ^l is denoted $\varphi^{(l)}$, and $\varphi^{(l,m)}$ is its expansion up to ϵ^m after it is written in terms of the outer coordinates kr. Similarly, the outer solution's inner expansion $\hat{\phi}$ up to terms in ϵ^m is denoted $\hat{\phi}^{(m)}$ and $\hat{\phi}^{(m,l)}$

is its expansion up to ϵ^l after it is written in terms of the inner coordinate r/b. Matching is enforced by requiring $\hat{\phi}^{(m,l)} \equiv \varphi^{(l,m)}$ for each m and l when both asymptotic forms are expressed in terms of the same coordinates.

It is convenient to introduce non-dimensional quantities based on the length scale b, chosen differently for shallow and deep water. Thus, for a wave of amplitude $\mathcal{A}$, all lengths are scaled by b and other non-dimensional quantities are defined according to the transformations

$$\phi \to \frac{g\mathcal{A}}{\omega}\phi, \quad u_3 \to \mathcal{A}\omega u_3, \quad M \to \rho b^3 M, \quad \lambda \to \frac{\rho g b^2}{\omega}\lambda, \quad \kappa \to \rho g b^2 \kappa. \tag{2.2.11}$$

In particular, this results in a boundary condition

$$\frac{\partial \phi}{\partial N} = \frac{\omega^2 b}{g} u_3 n_3 \quad \text{on} \quad S_C, \tag{2.2.12}$$

and an equation of motion

$$\left[\frac{\omega^2 b}{g} M + \mathrm{i}\lambda - (W + \kappa)\right] u_3 = -\iint_{S_C} \phi n_3 \, \mathrm{d}S, \tag{2.2.13}$$

where $N = n/b$, $S = s/b^2$ and the non-dimensional water-plane area $W = \pi a^2/b^2$. We have chosen the scalings to study, in particular, the case when the mooring terms are of the same order of magnitude as the hydrostatic spring. It should be noted that the scaled damping λ implicitly depends upon the frequency, but, nevertheless, it is assumed that $\lambda = \mathrm{ord}(1)$ as $\epsilon \to 0$. For both shallow and deep water, three problems are considered: the scattering problem in which the structures are held fixed ($u_3 = 0$), the radiation problem in which the structures are forced to oscillate with velocities consistent with the Bloch condition (the cylinders are not in phase; the motions of different cylinders have a phase difference consistent with the Bloch condition), and the freely-floating problem in which the structures are free to move in the vertical direction.

2.3 Shallow water

In this section the length scale b for the inner regions, introduced in § 2.2, is chosen as the water depth h, and it is assumed that $\epsilon = kh \ll 1$ so that the water is shallow relative to the wavelength. The characteristic size a of each structure is taken to be of the same order of magnitude as the depth, but much smaller than the cell size, so that in addition to the previously stated assumption $kL = \mathrm{ord}(1)$, we have $a/h = \mathrm{ord}(1)$ and $ka \ll 1$ as $\epsilon \to 0$. The vertical length scale for variations in ϕ is h throughout the fluid domain. However, in the inner regions the

horizontal length scale is h, while in the outer region it is k^{-1}. Thus, in terms of the original dimensional coordinates, suitable scaled inner region coordinates are

$$X = x/h, \quad Y = y/h, \quad Z = z/h, \quad R = r_j/h,$$

and the inner potential is $\varphi(X, Y, Z; \epsilon) \equiv \phi(x, y, z)$, while suitable scaled outer region coordinates are

$$x' = kx, \quad y' = ky, \quad Z = z/h, \quad r'_j = kr_j,$$

and the outer potential is $\hat{\phi}(x', y', Z; \epsilon) \equiv \phi(x, y, z)$.

2.3.1 The scattering problem

We now consider the solution to the scattering problem in which each structure is held fixed. In the outer region the motion is wave like and, to the level of approximation considered here, the depth dependence may be separated so that the scattering potential

$$\hat{\phi}_S(x', y', Z) = \hat{\phi}_H(x', y') \cosh \epsilon(Z + 1), \tag{2.3.1}$$

where $\hat{\phi}_H(x', y')$ solves the Helmholtz equation

$$\widehat{\nabla}^2 \hat{\phi}_H + \hat{\phi}_H = 0, \tag{2.3.2}$$

and $\widehat{\nabla}^2$ is the horizontal Laplacian in outer coordinates.

2.3.1.1 Outer solution to leading order

Because of the shallow-water assumption, at leading order in the outer region the solution is independent of Z and is governed by the Bloch condition and the Helmholtz equation (2.3.2), and hence may be constructed using the formalism given for the acoustic problem in [19]. Fundamental solutions of (2.3.2) that also satisfy the Bloch condition are

$$G_n(r', \theta) = \sum_{\boldsymbol{R}_j \in \Lambda} \mathrm{e}^{\mathrm{i}\boldsymbol{\beta}^T \boldsymbol{R}_j} H_n^{(1)}(r'_j) \mathrm{e}^{\mathrm{i}n\theta_j}, \quad n \in \mathbb{Z}, \tag{2.3.3}$$

where $\sum_{\boldsymbol{R}_j \in \Lambda}$ denotes a sum over the entire lattice. The required general solution of equation (2.3.2) has the form

$$\hat{\phi}_H(r', \theta) = \sum_n \mathcal{A}_n G_n(r', \theta), \tag{2.3.4}$$

where $\sum_n$ indicates that the summation is over all integers n. By Graf's addition theorem [35],

$$G_n(r', \theta) = H_n^{(1)}(r')\mathrm{e}^{\mathrm{i}n\theta} + \sum_p (-1)^{n-p} \sigma_{n-p} J_p(r')\mathrm{e}^{\mathrm{i}p\theta}, \tag{2.3.5}$$

where $H_n^{(1)}$ and J_p denote respectively Hankel and Bessel functions, and the lattice sums

$$\sigma_n = \sum_{\boldsymbol{R}_j \in \Lambda}{}' \mathrm{e}^{\mathrm{i}\boldsymbol{\beta}^T \boldsymbol{R}_j} H_n^{(1)}(k\boldsymbol{R}_j)\mathrm{e}^{\mathrm{i}n\alpha_j}, \quad n \in \mathbb{Z} \tag{2.3.6}$$

(the prime indicates that $\boldsymbol{R}_j = \boldsymbol{0}$ is omitted from the sum, and α_j is the angle from the x axis to $\boldsymbol{R}_j$ measured in the anti-clockwise sense). The functions G_n extend the solution for scattering by a single structure by weighting outgoing waves with the factor $\mathrm{e}^{\mathrm{i}\boldsymbol{\beta}^T \boldsymbol{R}_j}$ to account for phase differences within the lattice.

For a chosen β_q (see equation 2.2.9), the lattice sums have the form

$$\sigma_n = \sum_{q=1}^{Q} \frac{\sigma_{n,q}^{(1)}}{(k^2 - \beta_q^2)L^2} + \sigma_n^{(2)} \tag{2.3.7}$$

(consider [36, equation 3.16] for – in the notation found there – kr close to $\beta_m r$), where $\sigma_{n,q}^{(1)}$ and $\sigma_n^{(2)}$ are analytic functions of k within some neighbourhoods of $k = \pm\beta_q$. Solutions in the presence of structures are found by perturbing k away from these values. Note that

$$\sigma_{n,q}^{(1)} = \frac{4\mathrm{i}^{n+1}\mathrm{e}^{\mathrm{i}n\tau_q}}{A/L^2}, \tag{2.3.8}$$

(A is an area of a single cell, which would cancel with L^2 for a square cell, but is kept for generality and consistency with other literature) for angles τ_q defined through

$$\boldsymbol{\beta}_q = \beta_q \boldsymbol{e}_{1q}, \quad \boldsymbol{e}_{pq} = \begin{pmatrix} \cos p\tau_q \\ \sin p\tau_q \end{pmatrix}. \tag{2.3.9}$$

As in [19], we write

$$(k^2 - \beta_q^2)L^2 = \epsilon^2 \Delta_q \tag{2.3.10}$$

where $\Delta_q = \mathrm{ord}(1)$ as $\epsilon \to 0$ (the appearance of ϵ^2 in equation (2.3.10) can be demonstrated as part of the matching, but for simplicity it is included here from the outset). To avoid ϵ appearing in any denominator, we now define

$$g_n(r', \theta) = \epsilon^2 G_n(r', \theta) = g_n^{(1)}(r', \theta) + \epsilon^2 g_n^{(2)}(r', \theta) \tag{2.3.11}$$

where [19, equation 23]

$$g_n^{(1)}(r', \theta) = (-1)^n \sum_{q=1}^{Q} \frac{\sigma_{n,q}^{(1)}}{\Delta_q} \, \mathrm{e}^{\mathrm{i}r' \cos(\theta - \tau_q)}, \tag{2.3.12}$$

which is a combination of plane waves propagating in the directions τ_q, $q = 1, 2, \ldots Q$. The leading-order outer solution is expressed in terms of the phased singular solutions (2.3.11) so that

$$\hat{\phi}_S^{(0)} = \sum_n \mathfrak{a}_n^S \, g_n^{(1)}(r', \theta), \tag{2.3.13}$$

for constants $\mathfrak{a}_n^S$, which has an inner expansion (in terms of inner coordinates)

$$\hat{\phi}_S^{(0,1)} = \sum_n \mathfrak{a}_n^S (-1)^n \sum_{q=1}^{Q} \frac{\sigma_{n,q}^{(1)}}{\Delta_q} \left[1 + \mathrm{i}\epsilon R \boldsymbol{e}_{1q}^T \begin{pmatrix} \cos\theta \\ \sin\theta \end{pmatrix} \right]. \tag{2.3.14}$$

This shows that the primary effect of the outer solution is to 'drive' a flow past each of the cylinders.

2.3.1.2 Inner solution to leading order

The complete inner problem is

$$\nabla^2 \varphi_S = 0 \quad \text{in} \quad \mathcal{D}_i, \tag{2.3.15a}$$

$$\frac{\partial}{\partial Z}\varphi_S = \epsilon(\tanh \epsilon)\, \varphi_S \quad \text{on} \quad S_F, \tag{2.3.15b}$$

$$\frac{\partial}{\partial Z}\varphi_S = 0 \quad \text{on} \quad S_B, \tag{2.3.15c}$$

$$\frac{\partial}{\partial N}\varphi_S = 0 \quad \text{on} \quad S_C, \tag{2.3.15d}$$

where $\mathcal{D}_i$ denotes the fluid domain within the inner region, and N is the inner normal coordinate directed out of the fluid. To facilitate the construction of the inner solution we introduce inner eigenfunctions of the form

$$F_n(R, \theta, Z) = [R^n + \chi_n(R, Z)] \begin{pmatrix} \cos n\theta \\ \sin n\theta \end{pmatrix}, \quad n = 1, 2, 3, \ldots, \tag{2.3.16}$$

which are harmonic throughout the inner region, have zero normal derivative on $S_F \cup S_B \cup S_C$ and, because of the assumption that the structure is vertically axisymmetric, have the property

$$\chi_n(R, Z) \sim \mathfrak{D}_n R^{-n} \quad \text{as } R \to \infty, \tag{2.3.17}$$

where $\mathfrak{D}_n$ is a constant determined by the shape of the structures.

The form of $\hat{\phi}_S^{(0,1)}$ in equation (2.3.14) suggests an inner development of the form

$$\varphi_S^{(1)} = \varphi_0^S + \epsilon \varphi_1^S. \tag{2.3.18}$$

(Formally, we should allow for possible intermediate terms in both the inner and outer solutions; for example, a term should be included here between φ_0^S and $\epsilon\varphi_1^S$. However, such terms would not affect the final results and hence are omitted to simplify the presentation.) The leading-order inner solution is harmonic, satisfies homogeneous boundary conditions and, in order to match with the outer solution, tends to a constant as $R \to \infty$; thus

$$\varphi_0^S = C_0^S, \tag{2.3.19}$$

for some constant C_0^S. The term φ_1^S is also an eigenfunction of the inner problem satisfying a

zero normal derivative on $Z = 0$, and to match with $\hat{\phi}_S^{(0,1)}$ it is required that

$$\varphi_1^S = C_1^S + (\boldsymbol{E}_1^S)^T \left[R + \chi_1(R, Z)\right] \begin{pmatrix} \cos\theta \\ \sin\theta \end{pmatrix}, \tag{2.3.20}$$

for a scalar constant C_1^S and vector constant $\boldsymbol{E}_1^S$ and, hence, the outer expansion of the inner solution required to match with (2.3.14) is

$$\varphi_S^{(1,0)} = C_0^S + \epsilon (\boldsymbol{E}_1^S)^T R \begin{pmatrix} \cos\theta \\ \sin\theta \end{pmatrix}. \tag{2.3.21}$$

2.3.1.3 Leading order matching

When expressed in terms of the outer coordinates, the most singular term at ord(ϵ^2) in the outer expansion of $\varphi_S^{(1)}$ is in $1/r'$, and thus there can be no terms more singular than this at ord(ϵ^2) in the outer solution so that

$$\mathfrak{a}_n^S = 0 \quad \text{for} \quad |n| \geq 2. \tag{2.3.22}$$

Application of the matching principle $\varphi_S^{(1,0)} \equiv \hat{\phi}_S^{(0,1)}$ then gives

$$C_0^S = \sum_{n=-1}^{1} \mathfrak{a}_n^S (-1)^n \sum_{q=1}^{Q} \frac{\sigma_{n,q}^{(1)}}{\Delta_q}, \tag{2.3.23}$$

and

$$(\boldsymbol{E}_1^S)^T = \mathrm{i} \sum_{n=-1}^{1} \mathfrak{a}_n^S (-1)^n \sum_{q=1}^{Q} \frac{\sigma_{n,q}^{(1)}}{\Delta_q} \boldsymbol{e}_{1q}^T. \tag{2.3.24}$$

At this point there are insufficient equations to determine the unknowns, namely C_0^S, $\mathfrak{a}_n^S$ and $\boldsymbol{E}_1^S$, and hence we must continue to a higher order.

2.3.1.4 Outer solution continued

Bearing in mind the Z dependence in the outer form (2.3.1), we continue the outer solution to ϵ^2 as

$$\begin{aligned} \hat{\phi}_S^{(2)} = & \sum_{n=-1}^{1} \mathfrak{a}_n^S \left[\left(1 + \frac{1}{2}\epsilon^2 (Z+1)^2\right) g_n^{(1)}(r', \theta) + \epsilon^2 g_n^{(2)}(r', \theta) \right] \\ & + \epsilon \sum_n \mathfrak{b}_n^S g_n^{(1)}(r', \theta) + \epsilon^2 \sum_n \mathfrak{c}_n^S g_n^{(1)}(r', \theta), \end{aligned} \tag{2.3.25}$$

for new constants $\mathfrak{b}_n^S$ and $\mathfrak{c}_n^S$. With the aid of equations (2.3.8) and (2.3.22), this has an inner expansion (again, ignoring possible intermediate terms)

$$\begin{aligned}\hat{\phi}_S^{(2,2)} = &\sum_{n=-1}^{1} \mathfrak{a}_n^S \left\{ (-1)^n \sum_{q=1}^{Q} \frac{\sigma_{n,q}^{(1)}}{\Delta_q} \left[1 + \mathrm{i}\epsilon R \boldsymbol{e}_{1q}^T \begin{pmatrix} \cos\theta \\ \sin\theta \end{pmatrix} - \frac{1}{4}\epsilon^2 R^2 - \epsilon^2 R^2 \frac{1}{4} \boldsymbol{e}_{2q}^T \begin{pmatrix} \cos 2\theta \\ \sin 2\theta \end{pmatrix} \right] \right\} \\ &+ \epsilon^2 \left\{ \mathfrak{a}_{-1}^S \left[\frac{2\mathrm{i}}{\pi\epsilon R} \mathrm{e}^{-\mathrm{i}\theta} - \sigma_{-1}^{(2)} \right] + \mathfrak{a}_0^S \left[1 + \frac{2\mathrm{i}}{\pi} \left(\log \frac{\epsilon R}{2} + \gamma \right) + \sigma_0^{(2)} \right] \right. \\ &\qquad \left. + \mathfrak{a}_1^S \left[-\frac{2\mathrm{i}}{\pi\epsilon R} \mathrm{e}^{\mathrm{i}\theta} - \sigma_1^{(2)} \right] \right\} \\ &+ \epsilon \sum_n \mathfrak{b}_n^S (-1)^n \sum_{q=1}^{Q} \frac{\sigma_{n,q}^{(1)}}{\Delta_q} \left[1 + \mathrm{i}\epsilon R \boldsymbol{e}_{1q}^T \begin{pmatrix} \cos\theta \\ \sin\theta \end{pmatrix} \right] \\ &+ \epsilon^2 \sum_n \mathfrak{c}_n^S (-1)^n \sum_{q=1}^{Q} \frac{\sigma_{n,q}^{(1)}}{\Delta_q} + \epsilon^2 \sum_{n=-1}^{1} \mathfrak{a}_n^S (-1)^n \sum_{q=1}^{Q} \frac{\sigma_{n,q}^{(1)}}{\Delta_q} \frac{1}{2} (Z+1)^2. \end{aligned} \tag{2.3.26}$$

2.3.1.5 Inner solution continued and final matching

The inner expansion (2.3.26) suggests that the inner region solution should be continued as

$$\varphi_S^{(2)} = C_0^S + \epsilon\varphi_1^S + \epsilon^2 \log\epsilon\, \varphi_{22}^S + \epsilon^2 \varphi_2^S \tag{2.3.27}$$

where φ_1^S is given in equation (2.3.20) and, in order to match with the outer solution, $\varphi_{22}^S = C_{22}^S$, a constant. The inner region problem for φ_2^S is more complex than for lower order inner-region problems because the free surface condition is no longer homogeneous; the complete problem for φ_2^S is

$$\nabla^2 \varphi_2^S = 0 \quad \text{in} \quad \mathcal{D}_i, \tag{2.3.28a}$$

$$\frac{\partial}{\partial Z}\varphi_2^S = C_0^S \quad \text{on} \quad S_F, \tag{2.3.28b}$$

$$\frac{\partial}{\partial Z}\varphi_2^S = 0 \quad \text{on} \quad S_B, \tag{2.3.28c}$$

$$\frac{\partial}{\partial N}\varphi_2^S = 0 \quad \text{on} \quad S_C. \tag{2.3.28d}$$

We construct the solution by writing

$$\varphi_2^S = \varphi_{2A}^S + \varphi_{2B}^S, \tag{2.3.29}$$

where

$$\varphi_{2A}^S = C_0^S \left[Z + \frac{1}{2}\left(Z^2 - \frac{R^2}{2} \right) \right] \tag{2.3.30}$$

is a particular solution of equations (2.3.28a)–(2.3.28c), and the governing equations for φ_{2B}^S are

$$\nabla^2 \varphi_{2B} = 0 \quad \text{in} \quad \mathcal{D}_i, \tag{2.3.31a}$$

$$\frac{\partial}{\partial Z}\varphi_{2B}^S = 0 \quad \text{on} \quad S_F, \tag{2.3.31b}$$

$$\frac{\partial}{\partial Z}\varphi_{2B} = 0 \quad \text{on} \quad S_B, \tag{2.3.31c}$$

$$\frac{\partial}{\partial N}\varphi_{2B}^S = -\frac{\partial}{\partial N}\varphi_{2A}^S \quad \text{on} \quad S_C. \tag{2.3.31d}$$

According to equation (2.3.31d), the problem for φ_{2B}^S involves a non-zero flow across S_C and hence there must be a corresponding non-zero flow to infinity in the inner region. To describe this flow we introduce a particular solution $\Omega(R, \theta, Z)$ of equations (2.3.31a)–(2.3.31d) that satisfies

$$\Omega(R, \theta, Z) = B_{20}^S \log R + o(1) \quad \text{as} \quad R \to \infty. \tag{2.3.32}$$

To determine B_{20}^S we use the result that for a potential φ that is harmonic throughout a region D with a boundary ∂D, then

$$\iint_{\partial D} \frac{\partial \varphi}{\partial N} \, \mathrm{d}S = 0. \tag{2.3.33}$$

Equation (2.3.33) applied to $\varphi = \Omega$ and with $D = \mathcal{D}_i$, the inner region of the fluid domain, yields

$$B_{20}^S = \frac{1}{2\pi} \iint_{S_C} \frac{\partial}{\partial N}\varphi_{2A}^S \, \mathrm{d}S. \tag{2.3.34}$$

The last integral is evaluated by a further application of equation (2.3.33), but with D taken as the interior of the structure, and this gives

$$B_{20}^S = \frac{1}{2\pi} W C_0^S, \tag{2.3.35}$$

where W is the non-dimensional water-plane area; for a surface-piercing structure $W = \pi a^2/h^2$, otherwise $W = 0$. With inner eigenfunctions included as required to match with equation (2.3.26),

$$\varphi_{2B}^S = \Omega(R,\theta,Z) + C_{20}^S + \sum_{\nu=1}^{2} (\boldsymbol{E}_{2\nu}^S)^T \left[R^\nu + \chi_\nu(R,Z)\right] \begin{pmatrix} \cos\nu\theta \\ \sin\nu\theta \end{pmatrix}. \tag{2.3.36}$$

The outer expansion of the inner solution is therefore

$$\begin{aligned} \varphi_S^{(2,2)} = {} & C_0^S + \epsilon \left[C_1^S + (\boldsymbol{E}_1^S)^T \left(R + \mathfrak{D}_1 R^{-1}\right) \begin{pmatrix} \cos\theta \\ \sin\theta \end{pmatrix} \right] + \epsilon^2 \log\epsilon\, C_{22}^S \\ & + \epsilon^2 \left\{ C_0^S \left[Z + \frac{1}{2}\left(Z^2 - \frac{R^2}{2}\right)\right] + B_{20}^S \log R + C_{20}^S + \sum_{\nu=1}^{2} (\boldsymbol{E}_{2\nu}^S)^T R^\nu \begin{pmatrix} \cos\nu\theta \\ \sin\nu\theta \end{pmatrix} \right\} \end{aligned} \tag{2.3.37}$$

and application of the matching principle $\varphi_S^{(2,2)} \equiv \hat{\phi}_S^{(2,2)}$ gives, in particular,

$$B_{20}^S = \mathfrak{a}_0^S \frac{2\mathrm{i}}{\pi} \tag{2.3.38}$$

and

$$\mathfrak{D}_1 (\boldsymbol{E}_1^S)^T = \frac{2\mathrm{i}}{\pi} \left[\mathfrak{a}_{-1}(1,-\mathrm{i}) - \mathfrak{a}_1(1,\mathrm{i})\right]. \tag{2.3.39}$$

It follows from equations (2.3.35) and (2.3.38) that

$$\mathfrak{a}_0^S = -\frac{\mathrm{i}W}{4} C_0^S, \tag{2.3.40}$$

and then, by defining

$$U_q^S = \frac{1}{\Delta_q} \left[\frac{W C_0^S}{\pi} + 2\mathrm{i}\mathfrak{D}_1 (\boldsymbol{E}_1^S)^T \boldsymbol{e}_{1q} \right], \quad q = 1, 2, \ldots, Q, \tag{2.3.41}$$

and using equation (2.3.8), equations (2.3.23) and (2.3.24) may be written as respectively

$$C_0^S = \frac{\pi L^2}{A} \sum_{q=1}^{Q} U_q^S \tag{2.3.42}$$

and

$$(\boldsymbol{E}_1^S)^T = \frac{\pi \mathrm{i} L^2}{A} \sum_{q=1}^{Q} U_q^S \boldsymbol{e}_{1q}^T. \tag{2.3.43}$$

Post multiplying (2.3.43) by $\boldsymbol{e}_{1p}$, $p = 1, 2, \ldots, Q$, and combining the result with (2.3.42) to form U_p^S we get, with the aid of equation (2.3.9),

$$\sum_{q=1}^{Q} \left[\delta_{pq} \Delta_p + \frac{L^2}{A} \left(2\pi \mathfrak{D}_1 \cos(\tau_q - \tau_p) - W \right) \right] U_q^S = 0, \quad p = 1, 2, \ldots Q. \tag{2.3.44}$$

Given a Bloch wave vector $\boldsymbol{\beta}$, equation (2.3.44) is an eigenvalue problem for the allowable values of the wavenumber k, which appears in each Δ_p; see equation (2.3.10).

2.3.2 The radiation problem

In the radiation problem the structure S_C is forced to oscillate with a unit velocity and other structures oscillate with velocities consistent with the Bloch condition. In non-dimensional coordinates, the complete problem for the inner region is

$$\nabla^2 \varphi_R = 0 \quad \text{in} \quad \mathcal{D}_i \tag{2.3.45a}$$

$$\frac{\partial}{\partial Z} \varphi_R = \epsilon (\tanh \epsilon)\, \varphi_R \quad \text{on} \quad S_F, \tag{2.3.45b}$$

$$\frac{\partial}{\partial Z} \varphi_R = 0 \quad \text{on} \quad S_B, \tag{2.3.45c}$$

$$\frac{\partial}{\partial N} \varphi_R = n_3 \quad \text{on} \quad S_C. \tag{2.3.45d}$$

The presence of a non-homogeneous boundary condition on the structure means it is more natural for the inner region solution to guide the form of the solution. The non-homogeneity is at ord(1) and leads to a source-like term in the inner solution at ord(1), which must be matched with a similar term in the outer solution contained within the outer function $g_0^{(2)}(r', \theta)$ introduced in equation (2.3.11). Because of the accompanying term $g_0^{(1)}(r', \theta)/\epsilon^2$, this means that the inner solution actually begins with a term in $1/\epsilon^2$.

2.3.2.1 Outer solution

The outer solution for the radiation problem is constructed in a very similar way to that for the scattering problem. Thus, the outer radiation potential is

$$\hat{\phi}_R(x', y', Z) = \hat{\phi}_H(x', y') \cosh \epsilon (Z + 1). \tag{2.3.46}$$

where $\hat{\phi}_H(x', y')$ satisfies the Bloch condition (2.2.1) and the two-dimensional Helmholtz equation (2.3.2). In terms of the fundamental solutions introduced in equation (2.3.11), and guided

by the structure of the scattering solution (so that some details of the matching are omitted) and the fact that, as noted above, the leading-order inner solution contains terms at ord$(1/\epsilon^2)$, the outer solution up to terms of ord(1) is written

$$\begin{aligned}\hat{\phi}_R^{(0)} &= \sum_n \left\{ \frac{\mathfrak{a}_n^R}{\epsilon^2} \left[\left(1 + \frac{1}{2}\epsilon^2 (Z+1)^2 \right) g_n^{(1)}(r',\theta) + \epsilon^2 g_n^{(2)}(r',\theta) \right] + \frac{\mathfrak{b}_n^R}{\epsilon} g_n^{(1)}(r',\theta) + \mathfrak{c}_n^R g_n^{(1)}(r',\theta) \right\} \\ &= \sum_n \left\{ \left(\frac{\mathfrak{a}_n^R}{\epsilon^2} + \frac{\mathfrak{b}_n^R}{\epsilon} + \mathfrak{c}_n^R + \frac{1}{2}\mathfrak{a}_n^R (Z+1)^2 \right) g_n^{(1)}(r',\theta) + \mathfrak{a}_n^R g_n^{(2)}(r',\theta) \right\}, \end{aligned} \tag{2.3.47}$$

where $\mathfrak{a}_n^R$, $\mathfrak{b}_n^R$ and $\mathfrak{c}_n^R$ are constants which are determined as part of the matching process. A similar argument to that used in the scattering solution gives

$$\mathfrak{a}_n^R = 0 \quad \text{for} \quad |n| \geq 2. \tag{2.3.48}$$

The inner expansion of this outer solution is

$$\begin{aligned}\hat{\phi}_R^{(0,0)} =& \mathfrak{a}_{-1}^R \frac{2\mathrm{i}}{\pi\epsilon R} \mathrm{e}^{-\mathrm{i}\theta} + \mathfrak{a}_0^R \left[1 + \frac{2\mathrm{i}}{\pi} \left(\log \frac{\epsilon R}{2} + \gamma \right) \right] - \mathfrak{a}_1^R \frac{2\mathrm{i}}{\pi\epsilon R} \mathrm{e}^{\mathrm{i}\theta} + \sum_{n=-1}^{1} \mathfrak{a}_n^R \sigma_n^{(2)} \\ &+ \frac{1}{\epsilon^2} \sum_{n=-1}^{1} \mathfrak{a}_n^R (-1)^n \sum_{q=1}^{Q} \frac{\sigma_{n,q}^{(1)}}{\Delta_q} \left[1 + \mathrm{i}\epsilon R \boldsymbol{e}_{1q}^T \begin{pmatrix} \cos\theta \\ \sin\theta \end{pmatrix} - \frac{1}{4}\epsilon^2 R^2 \right. \\ &\left. - \epsilon^2 R^2 \frac{1}{4} \boldsymbol{e}_{2q}^T \begin{pmatrix} \cos 2\theta \\ \sin 2\theta \end{pmatrix} \right] + \frac{1}{\epsilon} \sum_n \mathfrak{b}_n^R (-1)^n \sum_{q=1}^{Q} \frac{\sigma_{n,q}^{(1)}}{\Delta_q} \left[1 + \mathrm{i}\epsilon R \boldsymbol{e}_{1q}^T \begin{pmatrix} \cos\theta \\ \sin\theta \end{pmatrix} \right] \\ &+ \sum_n \mathfrak{c}_n^R (-1)^n \sum_{m=1}^{M} \frac{\sigma_{n,m}^{(1)}}{\Delta_q} + \frac{1}{2}(Z+1)^2 \sum_{n=-1}^{1} \mathfrak{a}_n^R (-1)^n \sum_{q=1}^{Q} \frac{\sigma_{n,q}^{(1)}}{\Delta_q}. \end{aligned} \tag{2.3.49}$$

2.3.2.2 Inner solution

The inner expansion (2.3.49) of the outer solution requires an inner solution in the form

$$\varphi_R^{(0)} = \frac{1}{\epsilon^2}\varphi_{02}^R + \frac{1}{\epsilon}\varphi_{01}^R + \log\epsilon\, \varphi_{00}^R + \varphi_0^R, \tag{2.3.50}$$

where φ_{02}^R and φ_{00}^R are both constants which we denote by C_{02}^R and C_{00}^R respectively and φ_{01}^R has the same form as φ_1^S as given in (2.3.20). The problem for φ_0^R depends on φ_{02}^R and is

$$\nabla^2\varphi_0^R = 0 \quad \text{in} \quad \mathcal{D}_i, \tag{2.3.51a}$$

$$\frac{\partial}{\partial Z}\varphi_0^R = C_{02}^R \quad \text{on} \quad S_F, \tag{2.3.51b}$$

$$\frac{\partial}{\partial Z}\varphi_0^R = 0 \quad \text{on} \quad S_B, \tag{2.3.51c}$$

$$\frac{\partial}{\partial N}\varphi_0^R = n_3 \quad \text{on} \quad S_C. \tag{2.3.51d}$$

We construct a solution by writing

$$\varphi_0^R = \varphi_{0A}^R + \varphi_{0B}^R, \tag{2.3.52}$$

where

$$\varphi_{0A}^R = C_{02}^R\left[Z + \frac{1}{2}\left(Z^2 - \frac{R^2}{2}\right)\right] \tag{2.3.53}$$

is a particular solution of equations (2.3.51a)–(2.3.51c). Similar arguments to those used for the construction of φ_{2B}^S in equation (2.3.36) give

$$\varphi_{0B}^R = \Omega(R,\theta,Z) + C_0^R + \sum_{\nu=1}^{2}(\boldsymbol{E}_{0\nu}^R)^T\left[R^\nu + \chi_\nu(R,Z)\right]\begin{pmatrix}\cos\nu\theta\\ \sin\nu\theta\end{pmatrix}, \tag{2.3.54}$$

where now

$$\Omega(R,\theta,Z) = B_0^R\log R + o(1) \quad \text{as} \quad R\to\infty \tag{2.3.55}$$

and

$$B_0^R = \frac{1}{2\pi}W\left(C_{02}^R - 1\right). \tag{2.3.56}$$

The outer expansion of $\varphi_R^{(0)}$ is

$$\begin{aligned}\varphi_R^{(0,0)} = {}& \frac{1}{\epsilon^2}\left\{C_{02}^R\right\} + \frac{1}{\epsilon}\left\{C_{01}^R + (\boldsymbol{E}_{11}^R)^T\left[R + \mathfrak{D}_1 R^{-1}\right]\begin{pmatrix}\cos\theta\\ \sin\theta\end{pmatrix}\right\} + \log\epsilon\, B_{00}^R \\ & + C_{02}^R\left[Z + \frac{1}{2}\left(Z^2 - \frac{R^2}{2}\right)\right] + B_0^R\log R + C_0^R + \sum_{\nu=1}^{2}(\boldsymbol{E}_{0\nu}^R)^T R^\nu\begin{pmatrix}\cos\nu\theta\\ \sin\nu\theta\end{pmatrix}.\end{aligned} \tag{2.3.57}$$

2.3.2.3 Matching

Application of the matching principle $\varphi_R^{(0,0)} = \hat{\phi}_R^{(0,0)}$ gives, in particular,

$$C_{02}^R = \sum_{n=-1}^{1} \mathfrak{a}_n^R (-1)^n \sum_{q=1}^{Q} \frac{\sigma_{n,q}^{(1)}}{\Delta_q}, \tag{2.3.58}$$

$$\mathfrak{D}_1 (\boldsymbol{E}_{11}^R)^T = \frac{2\mathrm{i}}{\pi} \left[\mathfrak{a}_{-1}^R(1,-\mathrm{i}) - \mathfrak{a}_1^R(1,\mathrm{i}) \right], \tag{2.3.59}$$

$$(\boldsymbol{E}_{11}^R)^T = \mathrm{i} \sum_{n=-1}^{1} \mathfrak{a}_n^R (-1)^n \sum_{q=1}^{Q} \frac{\sigma_{n,q}^{(1)}}{\Delta_q} \boldsymbol{e}_{1q}^T, \tag{2.3.60}$$

$$B_0^R = \mathfrak{a}_0^R \frac{2\mathrm{i}}{\pi}. \tag{2.3.61}$$

By defining

$$U_q^R = \frac{1}{\Delta_q} \left[2B_0^R + 2\mathrm{i}\mathfrak{D}_1 (\boldsymbol{E}_{11}^R)^T \boldsymbol{e}_{1q} \right], \quad q = 1, 2, \ldots, Q, \tag{2.3.62}$$

equations (2.3.58) and (2.3.60) may be written as

$$C_{02}^R = \frac{\pi L^2}{A} \sum_{q=1}^{Q} U_q^R \tag{2.3.63}$$

$$(\boldsymbol{E}_{11}^R)^T = \frac{\pi \mathrm{i} L^2}{A} \sum_{q=1}^{Q} U_q^R \boldsymbol{e}_{1q}^T. \tag{2.3.64}$$

Post multiplying (2.3.64) by $\boldsymbol{e}_{1p}$ for $p = 1, 2, \ldots Q$, and combining the result with (2.3.63) to form U_p^R we get, with the aid of (2.3.56),

$$\sum_{q=1}^{Q} \left[\delta_{pq} \Delta_p + \frac{L^2}{A} \left(2\pi \mathfrak{D}_1 \cos(\tau_q - \tau_p) - W \right) \right] U_q^R = -\frac{W}{\pi}, \quad p = 1, 2, \ldots, Q, \tag{2.3.65}$$

which determines the U_q^R when $\boldsymbol{\beta}$ and k are given.

2.3.3 Freely-floating structures

Under the shallow-water approximation

$$\frac{\omega^2 b}{g} \equiv \frac{\omega^2 h}{g} = \epsilon^2 \left[1 + O(\epsilon^2) \right] \quad \text{as} \quad \epsilon = kh \to 0 \tag{2.3.66}$$

and, to a first approximation, the frequency is proportional to the wavenumber. For a freely-floating structure the first approximation to the body boundary condition (2.2.12) is

$$\frac{\partial \varphi}{\partial N} = \epsilon^2 u_3 n_3 \quad \text{on} \quad S_C, \tag{2.3.67}$$

where for this problem we drop the superscript R. This modifies equation (2.3.56) to

$$B_0 = \frac{1}{2\pi} W \left(C_{02} - \epsilon^2 u_3 \right), \tag{2.3.68}$$

and hence the system (2.3.65) becomes

$$\sum_{q=1}^{Q} \left[\delta_{pq} \Delta_p + \frac{L^2}{A} \left(2\pi \mathfrak{D}_1 \cos(\tau_q - \tau_p) - W \right) \right] U_q = -\frac{W \epsilon^2 u_3}{\pi}, \quad p = 1, 2, \ldots, Q. \tag{2.3.69}$$

The leading order inner region solution is

$$\varphi^{(0)} = \frac{C_{02}}{\epsilon^2}, \tag{2.3.70}$$

which, by an application of equation (2.3.33) over the interior of S_C, gives a leading-order approximation to the integral term in the equation of motion (2.2.13)

$$\iint\limits_{S_C} \frac{C_{02}}{\epsilon^2} n_3 \, \mathrm{d}S = \frac{C_{02}}{\epsilon^2} \iint\limits_{S_C} \frac{\partial Z}{\partial N} \, \mathrm{d}S = \frac{C_{02}}{\epsilon^2} W. \tag{2.3.71}$$

Thus, dropping the inertia term, which is of ord(ϵ^2) relative to the hydrostatic and mooring terms, from equation (2.2.13) the solution for u_3 is

$$u_3 = \frac{\pi L^2 W}{\epsilon^2 A (W + \kappa - \mathrm{i}\lambda)} \sum_{q=1}^{Q} U_q \tag{2.3.72}$$

and therefore equation (2.3.69) becomes

$$\sum_{q=1}^{Q} \left[\delta_{pq} \Delta_p + \frac{L^2}{A} \left(2\pi \mathfrak{D}_1 \cos(\tau_q - \tau_p) - \frac{W(\kappa - \mathrm{i}\lambda)}{W + \kappa - \mathrm{i}\lambda} \right) \right] U_q = 0, \quad p = 1, 2, \ldots, Q. \tag{2.3.73}$$

As in the scattering problem, this is an eigenvalue problem to determine the allowable values of k. Notice that allowing the spring to be infinitely stiff is equivalent to holding the structures still, and in the limit as $\kappa \to \infty$ the scattering solution is recovered from equation (2.3.73).

2.4 Deep water

In this section the water is assumed to be infinitely deep so that the wavenumber $k = \omega^2/g$. We assume that the structures are surface piercing and that each structure has a characteristic size a and a water-plane area πa^2. The length scale b introduced in § 2.2 is taken to be a, and it is assumed to be much smaller than the wavelength $2\pi/k$ so that $\epsilon = ka \ll 1$. As before, the wavelength is assumed to be of the same magnitude as the cell size L, so that $kL = \mathrm{ord}(1)$ as $\epsilon \to 0$, and hence $a/L \ll 1$. In the inner region the motion takes place on the length scale a, but in the outer region the motion takes place on the length scale k^{-1}. Hence suitable inner coordinates are

$$X = x/a,\ Y = z/a,\ Z = z/a,\ R = r_j/a,$$

and the inner region potential $\varphi(X, Y, Z, \epsilon) \equiv \phi(x, y, z)$, while suitable outer coordinates are

$$x' = kx,\ y' = ky,\ z' = kz,\ r'_j = kr_j,$$

and the outer potential $\hat{\phi}(x', y', z', \epsilon) \equiv \phi(x, y, z)$. Spherical coordinates with origin at O are used; these are denoted by $(\tilde{R}, \psi, \theta) = (\tilde{R}, \cos^{-1}(Z/\tilde{R}), \theta)$ for the inner region, and $(\tilde{r}, \psi, \theta) = (\tilde{r}, \cos^{-1}(z'/\tilde{r}), \theta)$ for the outer region.

2.4.1 The scattering problem

2.4.1.1 Outer solution to leading order

We first consider the scattering problem in which the structures are held fixed. The outer solution is constructed with the aid of so-called multipole solutions of the Laplace equation that satisfy the free-surface condition, and that are singular at an origin in the free surface. From [3, equation B.75], after scaling and taking the limit as the submergence tends to zero, suitable multipoles are

$$\hat{\phi}_{mn}(r', z') = \frac{1}{2}\left[\frac{P_m^n(\cos\psi)}{(\tilde{r})^{m+1}} + \frac{(-1)^m}{(m-n)!}\oint_0^\infty \frac{\mu+1}{\mu-1}\mu^m \mathrm{e}^{\mu z'} J_n(\mu r')\,\mathrm{d}\mu\right], \quad z' < 0, \quad m \geq n \geq 0, \tag{2.4.1}$$

where P_m^n denotes the associated Legendre function of the first kind, J_n denotes a Bessel function of the first kind and $\oint$ denotes an integration path passing beneath the pole. (The factor of one half is introduced to compensate for the fact that in the limit of zero submergence two

singularities meet on the free surface.) For later use we note that [3, equation B.74],

$$\hat{\phi}_{00}(r',z') = \frac{1}{\tilde{r}} + \pi \mathrm{i} \sum_{p=0}^{\infty} \frac{\tilde{r}^p}{p!} P_p(\cos\psi) - \sum_{p=0}^{\infty} (-1)^p \frac{\partial}{\partial \nu} \left\{ \frac{\tilde{r}^\nu}{\nu!} P_v(\cos\psi) \right\}_{\nu=p}. \tag{2.4.2}$$

From [3, equation B.63],

$$\frac{P_m^n(\cos\psi)}{(\tilde{r})^{m+1}} = \frac{(-1)^n}{(m-n)!} \int_0^\infty \mu^m \mathrm{e}^{\mu z'} J_n(\mu r') \,\mathrm{d}\mu, \quad z' < 0, \quad m \geq n \geq 0, \tag{2.4.3}$$

so that the right-hand side of equation (2.4.1) may be rewritten as a single integral term. Moving the path of integration on to the positive imaginary axis, and using properties of Hankel functions (in particular [35, equation 9.6.4]), we obtain

$$\hat{\phi}_{mn} = K_{mn}(r',z') + \frac{(-1)^m}{(m-n)!} \pi \mathrm{i}\, \mathrm{e}^{z'} H_n^{(1)}(r') \tag{2.4.4}$$

where we have picked up a residue from the pole (given by the second term) and

$$K_{mn}(r',z') = \begin{cases} \dfrac{2(-1)^{m/2}}{\pi(m-n)!} \displaystyle\int_0^\infty \frac{\nu^{m+1}}{\nu^2+1} \left(\nu \cos\nu z' + \sin \nu z'\right) K_n(\nu r') \,\mathrm{d}\nu & (m-n) \text{ even;} \\ \dfrac{2(-1)^{(m+n+1)/2}}{\pi(m-n)!} \displaystyle\int_0^\infty \frac{\nu^{m}}{\nu^2+1} \left(\nu \cos\nu z' + \sin \nu z'\right) K_n(\nu r') \,\mathrm{d}\nu & (m-n) \text{ odd.} \end{cases} \tag{2.4.5}$$

Here $H_n^{(1)}$ denotes the Hankel function of the first kind, and K_n denotes the modified Bessel function of the second kind.

For the outer region problem, the Bloch condition is satisfied by combining solutions $\hat{\phi}_{mn}$ that are singular at the lattice points using an appropriate phase function. To this end we define the functions

$$G_{mn}(r',\theta,z') = \sum_{\boldsymbol{R}_j \in \Lambda} \mathrm{e}^{\mathrm{i}\boldsymbol{\beta}^T \boldsymbol{R}_j} \hat{\phi}_{m|n|}(r_j', z') \mathrm{e}^{\mathrm{i}n\theta_j}, \tag{2.4.6}$$

which are analogous to those in equation (2.3.3). After splitting off the term corresponding to

$\boldsymbol{R}_j = 0$ and using the decomposition (2.4.4), together with Graf's addition theorem, we get

$$\begin{aligned} G_{mn}(r',\theta,z') = \hat{\phi}_{m|n|}(r',z')\mathrm{e}^{\mathrm{i}n\theta} + {\sum_{\boldsymbol{R}_j\in\Lambda}}' \mathrm{e}^{\mathrm{i}\boldsymbol{\beta}^T\boldsymbol{R}_j} K_{m|n|}(r'_j,z')\mathrm{e}^{\mathrm{i}n\theta_j} \\ + \frac{(-1)^m}{(m-|n|)!}\pi\mathrm{i}\mathrm{e}^{z'}\xi_n \sum_p (-1)^{n-p}\sigma_{n-p}J_p(r')\mathrm{e}^{\mathrm{i}p\theta}. \end{aligned} \tag{2.4.7}$$

for

$$\xi_n = \begin{cases} 1 & n \geq 0; \\ (-1)^n & n \leq 0. \end{cases}$$

Note that the ξ_n originates from the fact that

$$H^{(1)}_{|n|}(r') = \begin{cases} H^{(1)}_n(r') & n \geq 0 \\ (-1)^n H^{(1)}_n(r') & n \leq 0. \end{cases}$$

There are two lattice sums in (2.4.7); the first of the two sums has no singularities as a function of k (see appendix A.1), while the second, involving σ_{n-p}, is very similar to that appearing in the shallow-water solution.

As before we will use the ansatz

$$(k^2 - \beta_q^2)L^2 = \epsilon^2\Delta_q \tag{2.4.8}$$

with $\Delta_q = \mathrm{ord}(1)$ as $\epsilon \to 0$, and this is appropriate for most of the deep-water results presented here. However, as discussed later in section 2.6.2, it does not cover all possible cases. With the aid of equation (2.4.8), we may write

$$\begin{aligned} G_{mn}(r',\theta,z') = \hat{\phi}_{m|n|}(r',z')\mathrm{e}^{\mathrm{i}n\theta} + {\sum_{\boldsymbol{R}_j\in\Lambda}}' \mathrm{e}^{\mathrm{i}\boldsymbol{\beta}^T\boldsymbol{R}_j} K_{m|n|}(r'_j,z')\mathrm{e}^{\mathrm{i}n\theta_j} \\ + \frac{(-1)^m}{(m-|n|)!}\pi\mathrm{i}\,\mathrm{e}^{z'}\xi_n \sum_p (-1)^{n-p}\left[\sum_{q=1}^{Q}\frac{\sigma^{(1)}_{n-p,q}}{\epsilon^2\Delta_q} + \sigma^{(2)}_{n-p}\right] J_p(r')\mathrm{e}^{\mathrm{i}p\theta}, \end{aligned} \tag{2.4.9}$$

and it is again convenient to define

$$g_{mn}(r',\theta,z') = \epsilon^2 G_{mn}(r',\theta,z') = g^{(1)}_{mn}(r',\theta,z') + \epsilon^2 g^{(2)}_{mn}(r',\theta,z'), \tag{2.4.10}$$

where $g^{(1)}_{mn}$ contains the terms in $\sigma^{(1)}_{n,q}$, and $g^{(2)}_{mn}$ all other terms. Note that, from equation [35, equation 9.1.41],

$$g^{(1)}_{mn}(r',\theta,z') = \frac{(-1)^m}{(m-|n|)!}\pi \mathrm{i}\, \mathrm{e}^{z'}\xi_n(-1)^n \sum_{q=1}^{Q} \frac{\sigma^{(1)}_{n,q}}{\Delta_q}\, \mathrm{e}^{\mathrm{i}r'\cos(\theta-\tau_q)}, \tag{2.4.11}$$

which is a combination of deep-water plane waves.

The leading order outer region solution is written as

$$\hat{\phi}^{(0)}_S = \sum_{m,n} \mathfrak{a}^S_{mn} g^{(1)}_{mn}(r',\theta,z'), \tag{2.4.12}$$

where $\sum_{m,n} \equiv \sum_{n=-\infty}^{\infty}\sum_{m=|n|}^{\infty}$, and this has an inner expansion

$$\hat{\phi}^{(0,1)}_S = \sum_{m,n} \mathfrak{a}^S_{mn} \frac{(-1)^{m+n}}{(m-|n|)!}\xi_n \pi \mathrm{i} \sum_{q=1}^{Q} \frac{\sigma^{(1)}_{n,q}}{\Delta_q}\left[1 + \epsilon\tilde{R}\cos\psi + \mathrm{i}\epsilon\tilde{R}\sin\psi\, \boldsymbol{e}^T_{1q}\begin{pmatrix}\cos\theta\\ \sin\theta\end{pmatrix}\right]. \tag{2.4.13}$$

2.4.1.2 Inner solution

The complete inner problem is

$$\nabla^2\varphi_S = 0 \quad \text{in} \quad \mathcal{D}_i, \tag{2.4.14a}$$

$$\frac{\partial}{\partial Z}\varphi_S = \epsilon\varphi_S \quad \text{on} \quad S_F, \tag{2.4.14b}$$

$$|\nabla\varphi| \to 0 \quad \text{as} \quad Z \to -\infty, \tag{2.4.14c}$$

$$\frac{\partial}{\partial N}\varphi_S = 0 \quad \text{on} \quad S_C. \tag{2.4.14d}$$

The form of $\hat{\phi}^{(0,1)}_S$ in equation (2.4.13) suggests an inner solution

$$\varphi^{(1)}_S = \varphi^S_0 + \epsilon\varphi^S_1 \tag{2.4.15}$$

(as before, possible intermediate terms are omitted to simplify the presentation). Substitution of (2.4.15) into the inner problem shows that φ^S_0 and φ^S_1 are each harmonic functions satisfying the following:

$$\frac{\partial}{\partial Z}\varphi^S_0 = 0 \quad \text{on} \quad S_F, \qquad \frac{\partial}{\partial N}\varphi^S_0 = 0 \quad \text{on} \quad S_C, \tag{2.4.16}$$

$$\frac{\partial}{\partial Z}\varphi^S_1 = \varphi^S_0 \quad \text{on} \quad S_F, \qquad \frac{\partial}{\partial N}\varphi^S_1 = 0 \quad \text{on} \quad S_C. \tag{2.4.17}$$

To match with the outer region, it is necessary to take

$$\varphi_0^S = C_0^S, \tag{2.4.18}$$

and

$$\varphi_1^S = C_1^S + C_0^S(Z + \chi_0) + (\boldsymbol{E}_1^S)^T \left[\tilde{R} \sin\psi \begin{pmatrix} \cos\theta \\ \sin\theta \end{pmatrix} + \boldsymbol{\chi}_1 \right] \tag{2.4.19}$$

where C_0^S, C_1^S and $\boldsymbol{E}_1^S$ are constants, $C_0^S Z$ is a particular solution introduced to satisfy the non-homogeneous free-surface condition for φ_1^S, and χ_0 and $\boldsymbol{\chi}_1$ are harmonic functions that satisfy

$$\frac{\partial}{\partial Z}\chi_0 = 0 \quad \text{on} \quad S_F, \qquad \frac{\partial}{\partial N}\chi_0 = -\frac{\partial Z}{\partial N} = -n_3 \quad \text{on} \quad S_C, \tag{2.4.20}$$

$$\frac{\partial}{\partial Z}\boldsymbol{\chi}_1 = 0 \quad \text{on} \quad S_F, \qquad \frac{\partial}{\partial N}\boldsymbol{\chi}_1 = -\frac{\partial}{\partial N}\left[\tilde{R} \sin\psi \begin{pmatrix} \cos\theta \\ \sin\theta \end{pmatrix} \right] \quad \text{on} \quad S_C. \tag{2.4.21}$$

Furthermore, using [37, § 2.9], as $\tilde{R} \to \infty$

$$\chi_0 \sim \frac{B_0^S}{\tilde{R}} \quad \text{and} \quad \boldsymbol{\chi}_1 \sim \underline{\underline{\mathrm{M}}} \frac{\sin\psi}{\tilde{R}^2} \begin{pmatrix} \cos\theta \\ \sin\theta \end{pmatrix}, \tag{2.4.22}$$

for some constant B_0^S and matrix $\underline{\underline{\mathrm{M}}}$ that are determined by the shape of the structures.

To calculate the constant B_0^S we consider the flow due to the potential χ_0 and equate the flux out of the body surface S_C, to the flux out of the half sphere S_∞ at the outer 'boundary' of the inner region. The flux out of S_C is found by applying equation (2.3.33) to the interior of the structure to get

$$-\iint_{S_B} \frac{\partial}{\partial N}\chi_0 \,\mathrm{d}S = -\iint_{S_B} (-n_3) \,\mathrm{d}S = \iint_W (-n_3) \,\mathrm{d}S = \pi, \tag{2.4.23}$$

where the non-dimensional water-plane area $W = \pi$ (in this calculation, it is important to note that N is directed into S_C so that, for consistency, n_3 is negative on W). The flux out of the outer boundary of the inner region is

$$\iint_{S_\infty} \frac{\partial}{\partial N}\chi_0 \,\mathrm{d}S = \lim_{\tilde{R}\to\infty} \int_{\pi/2}^{\pi} \int_0^{2\pi} \frac{\partial}{\partial \tilde{R}} \left[\frac{B_0^S}{\tilde{R}} \right] \tilde{R}^2 \sin\psi \,\mathrm{d}\theta \,\mathrm{d}\psi = -2\pi B_0^S \tag{2.4.24}$$

and hence

$$B_0^S = -\frac{1}{2}. \tag{2.4.25}$$

When expressed in terms of the outer coordinates, the most singular term at ord(ϵ^2) in the outer expansion of $\varphi_S^{(1)}$ is in $1/\tilde{r}$. Thus, there can be no terms more singular than this at ord(ϵ^2) in the outer solution and, taking in to account the singular terms in $\hat{\phi}_{mn}$ as shown in equation (2.4.1), this gives

$$\mathfrak{a}_{mn}^S = 0 \quad \text{for} \quad m \neq 0. \tag{2.4.26}$$

The outer expansion of the inner solution

$$\varphi_S^{(1,0)} = C_0^S + \epsilon \left\{ C_0^S Z + (\boldsymbol{E}_1^S)^T \tilde{R} \sin\psi \begin{pmatrix} \cos\theta \\ \sin\theta \end{pmatrix} \right\} \tag{2.4.27}$$

which when matched with $\hat{\phi}_S^{(0,1)}$, given in equation (2.4.13), yields

$$C_0^S = \mathfrak{a}_{00}^S \pi \mathrm{i} \sum_{q=1}^{Q} \frac{\sigma_{0,q}^{(1)}}{\Delta_q} = -\mathfrak{a}_{00}^S \frac{4\pi L^2}{A} \sum_{q=1}^{Q} \frac{1}{\Delta_q}. \tag{2.4.28}$$

2.4.1.3 Outer solution continued and final matching

The outer region solution is continued as

$$\hat{\phi}_S^{(2)} = \mathfrak{a}_{00}^S \left\{ g_{00}^{(1)}(r',\theta,z') + \epsilon^2 g_{00}^{(2)}(r',\theta,z') \right\} + \epsilon \sum_{m,n} \mathfrak{b}_{mn}^S g_{mn}^{(1)}(r',\theta,z') + \epsilon^2 \sum_{m,n} \mathfrak{c}_{mn}^S g_{mn}^{(1)}(r',\theta,z') \tag{2.4.29}$$

and then, from equation (2.4.2), this has an inner expansion

$$\begin{aligned} \hat{\phi}_S^{(2,1)} = \mathfrak{a}_{00}^S \Bigg\{ & \pi \mathrm{i} \sum_{q=1}^{Q} \frac{\sigma_{0,q}^{(1)}}{\Delta_q} \left[1 + \epsilon \tilde{R} \cos\psi + \mathrm{i}\epsilon \tilde{R} \sin\psi \, \boldsymbol{e}_{1q}^T \begin{pmatrix} \cos\theta \\ \sin\theta \end{pmatrix} \right] + \frac{\epsilon}{\tilde{R}} \Bigg\} \\ & + \epsilon \sum_{m,n} \mathfrak{b}_{mn} \frac{(-1)^{m+n}}{(m-n)!} \pi \mathrm{i} \sum_{q=1}^{Q} \frac{\sigma_{n,q}^{(1)}}{\Delta_q} \end{aligned} \tag{2.4.30}$$

Because of the properties of χ_0 and $\boldsymbol{\chi}_1$ as $\tilde{R} \to \infty$, we have an inner solution outer expansion

$$\varphi_S^{(1,2)} = C_0^S + \epsilon \left\{ C_1^S + C_0^S \left(Z - \frac{1}{2\tilde{R}} \right) + (\boldsymbol{E}_1^S)^T \tilde{R} \sin\psi \begin{pmatrix} \cos\theta \\ \sin\theta \end{pmatrix} \right\} \tag{2.4.31}$$

and the matching principle $\varphi_S^{(2,1)} \equiv \hat{\phi}_S^{(1,2)}$ yields, in particular,

$$\mathfrak{a}_{00}^S = -\frac{1}{2} C_0^S, \tag{2.4.32}$$

equations (2.4.28) and (2.4.32) give

$$\sum_{q=1}^{Q} \frac{1}{\Delta_q} = \frac{A}{2\pi L^2}; \tag{2.4.33}$$

this is similar in form to [28, equation (35)], where acoustic wave propagation through a lattice of Dirichlet scatterers is considered. To unify the deep- and shallow-water cases we define

$$U_q^S = -\mathfrak{a}_{00}^S \frac{4\pi L^2}{A} \frac{1}{\Delta_q} \quad q = 1, 2, \ldots Q, \tag{2.4.34}$$

(the precise form of this substitution is chosen for consistency with the radiation problem that follows) to obtain

$$\sum_{q=1}^{Q} \left[\delta_{pq} \Delta_q - \frac{2\pi L^2}{A} \right] U_q^S = 0, \quad p = 1, 2, \ldots Q, \tag{2.4.35}$$

as the eigenvalue relation to determine the allowable values of k.

2.4.2 The radiation problem

With a unit vertical velocity applied to S_C, the complete inner problem is

$$\nabla^2 \varphi_R = 0 \quad \text{in} \quad \mathcal{D}_i, \tag{2.4.36a}$$

$$\frac{\partial}{\partial Z} \varphi_R = \epsilon \varphi_R \quad \text{on} \quad S_F, \tag{2.4.36b}$$

$$\frac{\partial}{\partial N} \varphi_R = n_3 \quad \text{on} \quad S_C, \tag{2.4.36c}$$

$$|\nabla \varphi_R| \to 0 \quad \text{as} \quad Z \to -\infty. \tag{2.4.36d}$$

As in § 2.3.2, the non-homogeneity in the body boundary condition gives a source-like term in the inner solution at ord(1) that here behaves like $1/\tilde{R} = \epsilon/\tilde{r}$, as $\tilde{R} \to \infty$. This must be matched with a similar term in the outer solution contained within an outer function $\epsilon g_{00}^{(2)}(r', \theta, z')$ and, because of the accompanying term $g_{00}^{(1)}(r', \theta)/\epsilon$, this means that the inner solution begins with a term in $1/\epsilon$ (see also a similar solution for open water in [38, § 7.1]). Thus the inner and outer

solutions are written respectively as

$$\varphi_R^{(0)} = \frac{1}{\epsilon}\varphi_{01}^R + \varphi_0^R, \tag{2.4.37}$$

and

$$\hat{\phi}_R^{(1)} = \frac{1}{\epsilon}\mathfrak{a}_{00}^R\left(g_{00}^{(1)} + \epsilon^2 g_{00}^{(2)}\right) + \sum_{m,n}\mathfrak{b}_{mn}^R g_{mn}^{(1)} + \epsilon\sum_{m,n}\mathfrak{c}_{mn}^R g_{mn}^{(1)}, \tag{2.4.38}$$

where once again we have been guided by the solution to the scattering problem, and possible intermediate terms are omitted as they would not contribute to the results obtained. The above outer solution has an inner expansion

$$\begin{aligned}\hat{\phi}_R^{(1,0)} = \frac{1}{\epsilon}\mathfrak{a}_{00}^R\left[\pi\mathrm{i}\sum_{q=1}^{Q}\frac{\sigma_{0,q}^{(1)}}{\Delta_q}\left(1 + \mathrm{i}\epsilon\tilde{R}\sin\psi\,\boldsymbol{e}_{1q}^T\begin{pmatrix}\cos\theta\\ \sin\theta\end{pmatrix} + \epsilon Z\right) + \frac{\epsilon}{\tilde{R}}\right] \\ + \sum_{m,n}\mathfrak{b}_{mn}^R\frac{(-1)^{m+n}}{(m-n)!}\pi\mathrm{i}\sum_{q=1}^{Q}\frac{\sigma_{n,q}^{(1)}}{\Delta_q}.\end{aligned} \tag{2.4.39}$$

The inner harmonic function φ_{01}^R satisfies homogeneous boundary conditions, must match with a constant, and hence is itself a constant that is here denoted by C_{01}^R. The problem for φ_0^R is then

$$\nabla^2\varphi_0^R = 0 \quad \text{in} \quad \mathcal{D}_i, \tag{2.4.40a}$$

$$\frac{\partial}{\partial Z}\varphi_0^R = C_{01}^R \quad \text{on} \quad S_F, \tag{2.4.40b}$$

$$\frac{\partial}{\partial N}\varphi_0^R = n_3 \quad \text{on} \quad S_C, \tag{2.4.40c}$$

$$|\nabla\varphi_0^R| \to 0 \quad \text{as} \quad Z \to -\infty. \tag{2.4.40d}$$

To match with the outer solution the appropriate form for this inner solution is

$$\varphi_0^R = C_0^R + C_{01}^R(Z + \chi_0) - \chi_0 + \boldsymbol{E}_1^R\left[\tilde{R}\sin\psi\begin{pmatrix}\cos\theta\\ \sin\theta\end{pmatrix} + \boldsymbol{\chi}_1\right], \tag{2.4.41}$$

where χ_0 and $\boldsymbol{\chi}_1$ are the functions introduced in equations (2.4.20) and (2.4.21), respectively. The term in Z on the right-hand side of equation (2.4.41) satisfies the non-homogeneous condition on S_F, while the second term in χ_0 satisfies the non-homogeneous condition on S_C. This

inner solution has an outer expansion

$$\varphi_R^{(0,1)} = \frac{1}{\epsilon}C_{01}^R + C_0^R + C_{01}^R Z - (C_{01}^R - 1)\frac{1}{2\tilde{R}} + (\boldsymbol{E}_1^R)^T \tilde{R}\sin\psi \begin{pmatrix}\cos\theta\\ \sin\theta\end{pmatrix}. \tag{2.4.42}$$

The matching principle $\varphi_R^{(0,1)} \equiv \hat{\phi}_R^{(1,0)}$ gives, in particular,

$$C_{01}^R = \mathfrak{a}_{00}^R \pi \mathrm{i} \sum_{q=1}^{Q} \frac{\sigma_{0,q}^{(1)}}{\Delta_q} = -\mathfrak{a}_{00}^R \frac{4\pi L^2}{A} \sum_{q=1}^{Q} \frac{1}{\Delta_q}, \tag{2.4.43}$$

and

$$\mathfrak{a}_{00}^R = -\frac{1}{2}(C_{01}^R - 1), \tag{2.4.44}$$

so that with

$$U_q^R = -\mathfrak{a}_{00}^R \frac{4\pi L^2}{A}\frac{1}{\Delta_q}, \quad q = 1, 2, \ldots Q, \tag{2.4.45}$$

equations (2.4.43) and (2.4.44) give

$$\sum_{q=1}^{Q}\left[\delta_{pq}\Delta_q - \frac{2\pi L^2}{A}\right] U_q^R = -\frac{2\pi L^2}{A}, \quad p = 1, 2, \ldots Q \tag{2.4.46}$$

as the equation to determine the U_q^R.

2.4.3 Freely-floating structures

For deep water $\omega^2 b/g \equiv \omega^2 a/g = \epsilon$, so that the wavenumber is proportional to the frequency squared, and for a freely-floating structure the body boundary condition (2.2.12) is

$$\frac{\partial\varphi}{\partial N} = \epsilon u_3 n_3 \quad \text{on} \quad S_C, \tag{2.4.47}$$

where for this problem we again drop the superscript R. This modifies equation (2.4.44) to

$$\mathfrak{a}_{00} = -\frac{1}{2}(C_{01} - \epsilon u_3) \tag{2.4.48}$$

and so that the system (2.4.46) becomes

$$\sum_{q=1}^{Q}\left[\delta_{pq}\Delta_q - \frac{2\pi L^2}{A}\right]U_q = -\frac{2\pi L^2}{A}\epsilon u_3, \quad p = 1, 2, \ldots Q. \tag{2.4.49}$$

The leading order inner solution is

$$\varphi_{01} = \frac{C_{01}}{\epsilon}, \tag{2.4.50}$$

and hence, to leading order, the solution of the equation of motion (2.2.13) is

$$u_3 = \frac{W}{\epsilon(W + \kappa - \mathrm{i}\lambda)}\sum_{q=1}^{Q} U_q, \tag{2.4.51}$$

where now the non-dimensional water-plane area is $W = \pi$. Thus, from equation (2.4.49), the eigenvalue problem for freely-floating structures in deep water is

$$\sum_{q=1}^{Q}\left[\delta_{pq}\Delta_p - \frac{2\pi L^2}{A}\frac{\kappa - \mathrm{i}\lambda}{\pi + \kappa - \mathrm{i}\lambda}\right]U_q = 0, \quad p = 1, 2, \ldots Q. \tag{2.4.52}$$

Again, taking the spring to be infinitely stiff recovers the scattering solution.

2.5 Structure of the problems

In each of the shallow- and deep-water cases the solutions obtained have the following structures. For the scattering problems, there are homogeneous systems

$$\underline{\underline{\mathrm{A}}}(k;\boldsymbol{\beta})\boldsymbol{U}^S = \mathbf{0} \tag{2.5.1}$$

and, given a Bloch vector $\boldsymbol{\beta}$, non-trivial solutions for $\boldsymbol{U}^S$ are possible for wavenumbers k satisfying

$$\det \underline{\underline{\mathrm{A}}}(k;\boldsymbol{\beta}) = 0; \tag{2.5.2}$$

the set of such wavenumbers is denoted by Ω_β. For the radiation problems the systems have the form

$$\underline{\underline{\mathrm{A}}}(k;\boldsymbol{\beta})\boldsymbol{U}^R = s_1\boldsymbol{j} \tag{2.5.3}$$

for some constant s_1, where $\underline{\underline{\mathrm{A}}}(k;\boldsymbol{\beta})$ is the matrix that appears in the scattering equation (2.5.1), and $\boldsymbol{j}$ is the vector of ones with length Q. For fixed $\boldsymbol{\beta}$, non-trivial solutions for the vector $\boldsymbol{U}^R$ are certainly possible for wavenumbers k satisfying

$$\det\underline{\underline{\mathrm{A}}}(k;\boldsymbol{\beta}) \neq 0, \tag{2.5.4}$$

that is for $k \notin \Omega_\beta$. For a $k \in \Omega_{\boldsymbol{\beta}}$, solutions for $\boldsymbol{U}^R$ are possible provided the orthogonality condition

$$(\boldsymbol{U}^S)^T\boldsymbol{j} = \sum_{q=1}^{Q} U_q^S = 0 \tag{2.5.5}$$

is satisfied [39, p. 224], where $\boldsymbol{U}^S$ is any solution of equation (2.5.1) for the chosen k. Thus, when it exists, the solution to the radiation problem for $k \in \Omega_\beta$ is not unique as any combination of the available scattering solutions may be added to it. Detailed examination of the inner solutions shows that the condition (2.5.5) is equivalent to there being zero vertical force on each structure in the scattering problem. This is not purely a property of the present solution obtained using asymptotic methods. If the exact radiation potential ϕ^R is assumed to exist for a $k \in \Omega_{\boldsymbol{\beta}}$, then an application of Green's theorem to ϕ^R and the exact scattering potential ϕ^S over a single cell of the lattice yields

$$\iint_{S_C} \phi^S n_3 \,\mathrm{d}S = 0, \tag{2.5.6}$$

which again states that the vertical force on the structure due to the scattering potential is zero, and provides a necessary condition for the existence of the radiation potential when $k \in \Omega_{\boldsymbol{\beta}}$.

In the case of freely-floating structures, there is a homogeneous system of the form

$$\left(\underline{\underline{\mathrm{A}}}(k;\boldsymbol{\beta}) + s_2\underline{\underline{\mathrm{J}}}\right)\boldsymbol{U} = \boldsymbol{0} \tag{2.5.7}$$

for some constant s_2, where again $\underline{\underline{\mathrm{A}}}(k;\boldsymbol{\beta})$ is the matrix that appears in the scattering equation (2.5.1), and $\underline{\underline{\mathrm{J}}}$ is the $Q \times Q$ matrix of ones. For given $\boldsymbol{\beta}$, non-trivial solutions for $\boldsymbol{U}$ are possible only for wavenumbers k satisfying

$$\det\left(\underline{\underline{\mathrm{A}}}(k;\boldsymbol{\beta}) + s_2\underline{\underline{\mathrm{J}}}\right) = 0, \tag{2.5.8}$$

and the set of such wavenumbers is denoted $\hat{\Omega}_{\boldsymbol{\beta}}$. In general, if $k \in \hat{\Omega}_{\boldsymbol{\beta}}$ then $k \notin \Omega_{\boldsymbol{\beta}}$, so that, apart

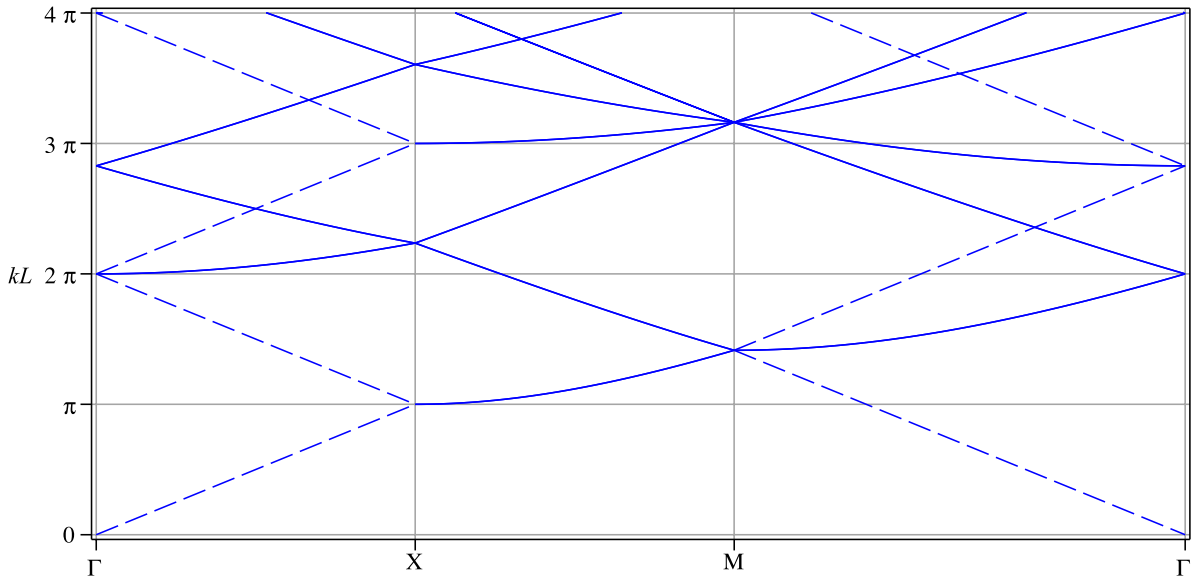

Figure 2.2 Position of poles in wavenumber (or, equivalently, frequency) space for a square lattice with cell side L for $Q = 1$ (– – –) and $Q = 2$ (———): the abscissae is the modulus of $\boldsymbol{\beta} = (q_1, q_2)$ along the edges of the first irreducible Brillouin zone so that ΓX corresponds to $q_1 L \in [0, \pi]$ and $q_2 L = 0$, XM corresponds to $q_2 L \in [0, \pi]$ and $q_1 L = 0$, and $M\Gamma$ corresponds to $q_1 L = q_2 L \in [0, \pi]$.

from possible special cases, allowing the cylinders to float freely changes the wavenumbers of the waves that may propagate through the lattice. The special cases arise when equation (2.5.5) is satisfied so that also $\underline{\underline{\mathrm{J}}}\boldsymbol{U}^S = \mathbf{0}$; the solution to the scattering problem then solves the freely-floating problem as well, but with no motion of the structures as there is no vertical force acting upon them. A similar situation arises in [40], where wave trapping by a structure in open water is investigated (a trapped wave is a free oscillation of an infinite fluid that has finite energy).

2.6 Results

We present here results for both shallow water and deep water and, throughout, the non-dimensional wavenumber kL is used as a frequency parameter.

The poles of the lattice sums represent the plane-wave solutions given in (2.2.10) that exist in the absence of structures. For a square array of cell side L and a wave vector $\boldsymbol{\beta} = (q_1, q_2)$, these plane waves have wavenumbers

$$kL = \sqrt{(q_1 L + 2\pi m_1)^2 + (q_2 L + 2\pi m_2)^2}, \quad m_1, m_2 \in \mathbb{Z}, \tag{2.6.1}$$

and these solutions are shown in figure 2.2 along the edges of the irreducible part of the first

Brillouin zone [30, p. 36]; thus, the abscissa is the modulus of $\boldsymbol{\beta}L$ and ΓX corresponds to $q_1 L \in [0, \pi]$ and $q_2 L = 0$, XM corresponds to $q_2 L \in [0, \pi]$ and $q_1 L = \pi$, and $M\Gamma$ corresponds to $q_1 L = q_2 L \in [0, \pi]$. It is possible to get formulas for any part of the Brillouin zone. However, for consistency with standard practice, we focus our attention on the edges of the Brillouin zone under the assumption that the extreme values of the frequency occur there for each band (we hence acknowledge that maxima and minima can occur away from the Brillouin edge). All numerical results presented here are for a square array of cell side L. For any given wave vector $\boldsymbol{\beta}L$, the solutions with a structure present are perturbations of the values of kL given by equation (2.6.1). Recall that we assume $kL = \mathrm{ord}(1)$ and so it is acceptable to consider perturbation of the modes illustrated in figure 2.2. It should be noted that when either $q_1 L$ or $q_2 L$ is a (non-zero) integer multiple of π there are no single-mode solutions. For example, with $s, t \in \mathbb{Z}$ and $q_1 = s\pi$, taking $m_1 = t$ or $m_1 = -t - s$ both yield the same kL unless $s = t = 0$. A similar argument applies to fixed $q_2 L = s\pi$.

2.6.1 Perturbation of a single plane wave

2.6.1.1 Shallow water

First of all, solutions that are perturbations of a single plane wave are discussed; such plane waves correspond to the dashed lines in figure 2.2. From equation (2.3.44), the shallow-water solution for a fixed structure yields

$$kL = \beta_1 L \left\{ 1 + \frac{h^2}{A} \left(2\pi \mathfrak{D}_1 - W \right) \right\}^{-1/2}. \tag{2.6.2}$$

Note that $h^2/A = \epsilon^2/k^2 A = \mathrm{ord}(\epsilon^2)$ as $\epsilon \to 0$ as, by assumption, $k^2 A = \mathrm{ord}(1)$. The non-dimensional water-plane area $W = \pi a^2/h^2$ for a surface-piercing structure, but $W = 0$ otherwise. For the case of a truncated vertical cylinder of radius a and height $d \leq h$, the dipole coefficient $\mathfrak{D}_1 \in [0, a^2/h^2]$. When the cylinder extends throughout the depth, $\mathfrak{D}_1 = a^2/h^2$ and equation (2.6.2) reduces to [19, equation 60], that is

$$(kL)^2 = (\beta_1 L)^2 \left\{ 1 + \frac{\pi a^2}{A} \right\}^{-1}.$$

For a truncated circular cylinder, the variation of the dipole coefficient $\mathfrak{D}_1$ with the submerged cylinder length d/h is shown in figure 2.3 (the method of computation for $\mathfrak{D}_1$ is described in Appendix A.2; because of the identical leading-order inner boundary conditions on the free surface and bed, $\mathfrak{D}_1$ is the same for bottom-mounted and surface-piercing cylinders of the same

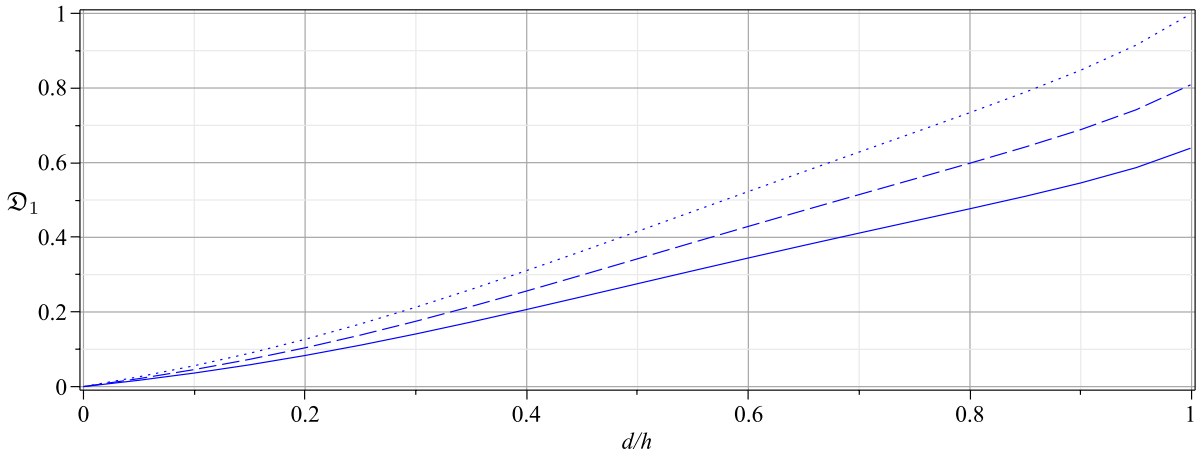

Figure 2.3 Variation of the dipole coefficient $\mathfrak{D}_1$ with the depth of submergence d/h for $a/h = 0.8$ (——) , $a/h = 0.9$ (– – –), $a/h = 1$ (· · · · · ·).

radius and height). It is notable that for a surface-piercing structure the sign of the term in round brackets in equation (2.6.2) changes sign when $\mathfrak{D}_1 = W/2\pi = a^2/2h^2$, so that the presence of a long cylinder decreases the frequency of a wave with given Bloch wavenumber β_1, while a short cylinder increases the frequency. For a submerged structure, for which $W = 0$, the frequency is always decreased by the presence of the structures.

For a freely-floating structure in shallow water, let us first consider no damping in the moorings so that $\lambda = 0$. In this case, equation (2.3.73) gives the single mode solution

$$kL = \beta_1 L \left\{ 1 + \frac{h^2}{A} \left(2\pi\mathfrak{D}_1 - W + \frac{W^2}{W+\kappa} \right) \right\}^{-1/2} \tag{2.6.3}$$

so that for a freely-floating structure ($W \neq 0$) with zero damping and mooring stiffness $\kappa > 0$, the frequencies of propagating waves are reduced when compared with those for a fixed structure as given in equation (2.6.2). For $\lambda \neq 0$, the single mode solution is

$$\beta_1 L = kL \left\{ 1 + \frac{h^2}{A} \left(2\pi\mathfrak{D}_1 - W + \frac{W^2}{W+\kappa-\mathrm{i}\lambda} \right) \right\}^{1/2} \tag{2.6.4}$$

and expansion in $h^2/A = \mathrm{ord}(\epsilon)$ yields

$$\beta_1 L = kL \left\{ 1 + \frac{h^2}{2A} \left(2\pi\mathfrak{D}_1 - W + \frac{W^2(W+\kappa+\mathrm{i}\lambda)}{|W+\kappa-\mathrm{i}\lambda|^2} \right) + O(\epsilon^2) \right\}, \tag{2.6.5}$$

which shows explicitly that, for a fixed frequency, damping in the moorings gives a wavenumber with a positive imaginary part correctly corresponding to decay of the wave amplitude with distance. The decay rate depends on a number of parameters, including the water-plane area

and the spring stiffness.

2.6.1.2 Deep water

For fixed surface-piercing structures in deep water with $Q = 1$ we have that

$$kL = \beta_1 L \left\{ 1 - \frac{2\pi a^2}{A} \right\}^{-1/2}. \tag{2.6.6}$$

so that, in contrast to shallow water, the wave frequency is always increased by the presence of the structure. The equivalent result for freely-floating structures in deep water without damping is

$$kL = \beta_1 L \left\{ 1 - \frac{2\pi a^2 \kappa}{A(\pi + \kappa)} \right\}^{-1/2}, \tag{2.6.7}$$

showing again that allowing the structures to float decreases the frequencies of propagating modes when compared with those for a fixed structure. In the absence of moorings ($\kappa = 0$), within the constraints of this long-wave approximation the structure 'rides the waves' and there is no change in frequency.

2.6.2 Perturbation of two plane waves

2.6.2.1 Shallow water

The emergence of localised band gaps when structures are introduced can be demonstrated explicitly by the present theory for $Q = 2$ when, in the absence of damping, the shallow water solution for a freely-floating structure in equation (2.3.73) yields

$$\det \begin{pmatrix} \Delta_1 + \dfrac{L^2}{A}\left[2\pi\mathfrak{D}_1 - W_\kappa\right] & \dfrac{L^2}{A}\left[2\pi\mathfrak{D}_1 \cos(\tau_1 - \tau_2) - W_\kappa\right] \\ \dfrac{L^2}{A}\left[2\pi\mathfrak{D}_1 \cos(\tau_1 - \tau_2) - W_\kappa\right] & \Delta_2 + \dfrac{L^2}{A}\left[2\pi\mathfrak{D}_1 - W_\kappa\right] \end{pmatrix} = 0, \tag{2.6.8}$$

where $W_\kappa = W\kappa/(W + \kappa)$. By the definitions of Δ_1 and Δ_2, this is a quadratic polynomial in the frequency parameter k^2. To illustrate the main ideas we consider first the neighbourhood of the point $(q_1 L, q_2 L, kL) = (\pi, 0, \pi)$ for which

$$\boldsymbol{\beta}_1 L = (q_1 L, 0)^T \quad \text{and} \quad \boldsymbol{\beta}_2 L = (q_1 L - 2\pi, 0)^T, \tag{2.6.9}$$

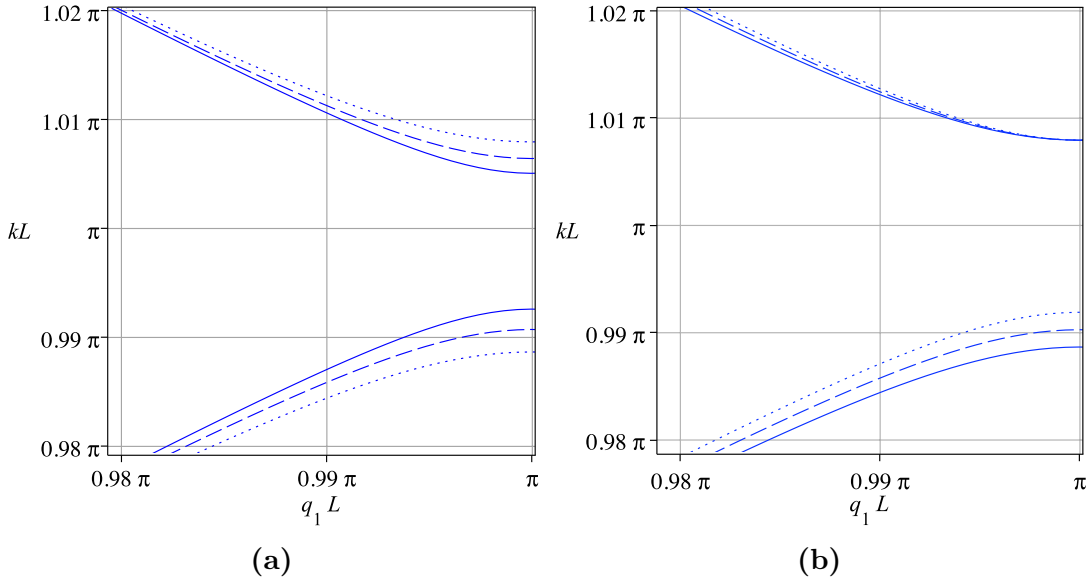

Figure 2.4 Perturbation of two plane waves for fixed surface-piercing cylinders in shallow water for $L/h = 20$: (a) kL *vs.* q_1L for $d/h = 0.8$ with $a/h = 0.8$ (——) , $a/h = 0.9$ (– – –), $a/h = 1$ (· · · · · ·); (b) kL *vs.* q_1L for $a/h = 1$ with $d/h = 0.8$ (——), $d/h = 0.7$ (– – –), $d/h = 0.6$ (· · · · · ·).

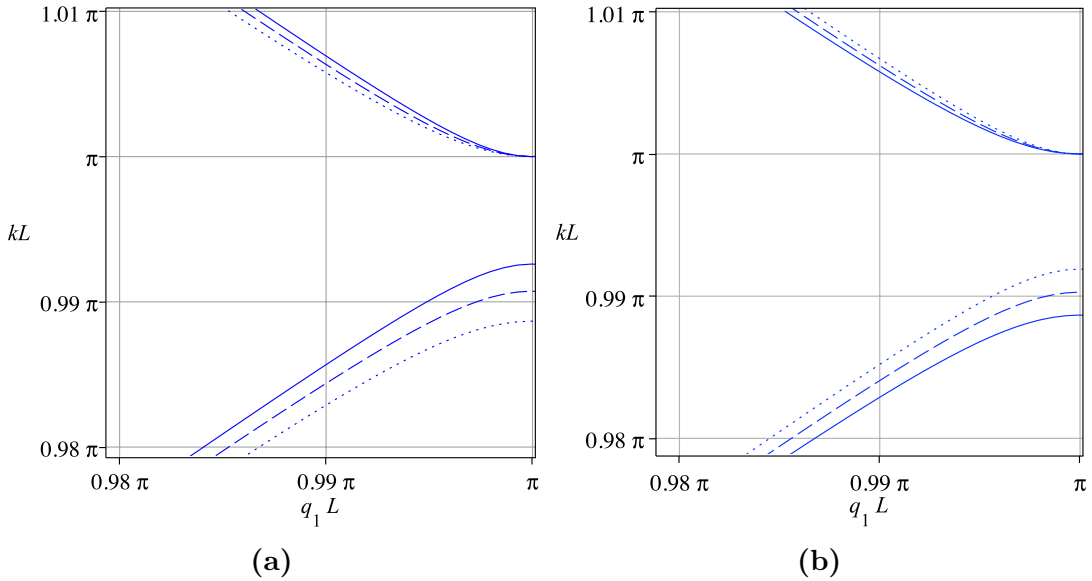

Figure 2.5 Perturbation of two plane waves for bottom-mounted cylinders in shallow water for $L/h = 20$: (a) kL *vs.* q_1L for fixed $d/h = 0.8$ with $a/h = 0.8$ (——) , $a/h = 0.9$ (– – –), $a/h = 1$ (· · · · · ·) and (b) kL *vs.* q_1L for $a/h = 1$ with $d/h = 0.8$ (——), $d/h = 0.7$ (– – –), $d/h = 0.6$ (· · · · · ·).

so that the propagation directions are $\tau_1 = 0$ and $\tau_2 = \pi$. (Note: there is nothing special about choosing this region, we are free to choose any region, as long as we are mindful that choosing a frequency too high could violate our small parameter assumptions.) In the limit as $q_1 L \to \pi$ equation (2.6.8) gives the two positive roots

$$kL = \frac{\pi}{\sqrt{1 + 4\pi h^2 \mathfrak{D}_1 / A}}, \ \frac{\pi}{\sqrt{1 - 2h^2 W_\kappa / A}}. \tag{2.6.10}$$

(For a fixed circular cylinder extending throughout the depth, so that $W_\kappa = W = \pi a^2/h^2$ and $\mathfrak{D}_1 = a^2/h^2$, these roots reduce to those in [19, equation (69)] when the latter is amended to reflect the circular, rather than elliptical, cylinder used here.) The difference between the roots in equation (2.6.10) shows the appearance of a local band gap as the structures' size a/h, and hence $\mathfrak{D}_1$ and W_κ, increase from zero; this is illustrated for the square array of cell side L in figure 2.4a for fixed surface-piercing cylinders, and in figure 2.5a for fixed bottom-mounted cylinders. Interestingly, since the only parameter that contains information about the length of the cylinders is $\mathfrak{D}_1$, these results show that only the lower edge of the band gap is affected by the depth of submergence. On the other hand, only the upper edge of the band gap is affected by whether the structure is surface piercing or bottom mounted, and by allowing it to float freely. When a surface-piercing structure is allowed to float freely, the frequency at the upper edge of the band gap is reduced (because $W_\kappa < W$ for $\kappa > 0$), which is consistent with the single mode solutions discussed in the previous subsection, while the lower gap edge is unaffected; this is shown graphically in figure 2.6.

We now consider circumstances under which the orthogonality condition (2.5.5) may be satisfied for the shallow-water solutions. Let us consider the case when $\Delta_q \equiv \Delta$ for $Q = 2$ (corresponding to identical vectors $\boldsymbol{\beta}_q$) so that, from (2.5.1), we have the eigenvalue equation

$$\underline{\underline{\mathrm{M}}} \boldsymbol{U}^S = \Delta \boldsymbol{U}^S \tag{2.6.11}$$

for a symmetric matrix $\underline{\underline{\mathrm{M}}}$ that has entries

$$\begin{aligned} m_{11} = m_{22} &= -\frac{L^2}{A}\left[2\pi\mathfrak{D}_1 - W\right] \\ m_{12} = m_{21} &= -\frac{L^2}{A}\left[2\pi\mathfrak{D}_1 \cos(\tau_1 - \tau_2) - W\right] \end{aligned} \tag{2.6.12}$$

One of the eigenvalues of the matrix $\underline{\underline{\mathrm{M}}}$ is $\Delta = m_{11} + m_{12}$ and the corresponding eigenvector is $(1, -1)^T$, so that in this case the orthogonality condition is satisfied and the scattering and

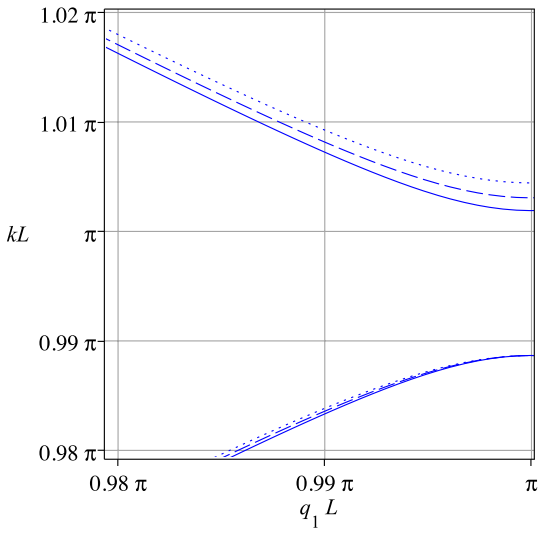

Figure 2.6 Perturbation of two plane waves for freely-floating surface-piercing cylinders in shallow water for $L/h = 20$, $d/h = 0.8$ and $a/h = 1$: kL *vs.* q_1L for $\kappa = 1$ (——), $\kappa = 2$ (– – –), $\kappa = 4$ (· · · · · ·).

radiation solutions both exist. The second eigenvalue is $\Delta = m_{11} - m_{12}$ with corresponding eigenvector $(1, 1)^T$ so that, in this case, the orthogonality condition is not satisfied and the radiation solution does not exist. To illustrate this consider the specific point in wavenumber space for which $(q_1L, q_2L) = (\pi, 0)$ and kL lies in a neighbourhood of π. Here, from the first eigenvalue we obtain $kL = \pi/\sqrt{1 - 2h^2W/A}$ (considering only positive roots) for which both the scattering and radiation solutions both exist, whilst for the second eigenvalue $kL = \pi/\sqrt{1 + 4\pi h^2\mathfrak{D}_1/A}$ and only the scattering solution exists. These values of kL are just the band gap boundaries given in (2.6.10), when amended for the scattering problem.

2.6.2.2 Deep water

For deep water, equation (2.4.52) with $Q = 2$ once more gives a quadratic polynomial in k^2. Again considering the neighbourhood of the point $(q_1L, q_2L, kL) = (\pi, 0, \pi)$ and taking the limit as $q_1L \to \pi$, we find the positive roots are

$$kL = \pi, \quad \frac{\pi}{\sqrt{1 - 4\pi a^2\kappa/(\pi + \kappa)A}}, \tag{2.6.13}$$

showing that only the upper edge of the band gap is affected as the water-plane radius increases from zero, and by allowing the structure to move. These explicit analytical results are illustrated graphically for a fixed structure in figure 2.7a, and for a freely-floating structure in figure 2.7b.

We now consider the implications of the orthogonality condition (2.5.5) for the existence of deep-water radiation solutions. Again we take $\Delta_q \equiv \Delta$ for $q = 1, \ldots, Q$ so that equation (2.5.1)

yields

$$\underline{\underline{\mathrm{J}}}\boldsymbol{U}^S = \Delta'\boldsymbol{U}^S \tag{2.6.14}$$

for $\Delta' = (A/2\pi L^2)\Delta$. The $Q \times Q$ matrix of ones $\underline{\underline{\mathrm{J}}}$ has $(Q-1)$ eigenvalues equal to zero, and one eigenvalue equal to Q. A zero eigenvalue is potentially problematic as, when adopting the ansatz in equation (2.4.8), we make the assumption that each $\Delta_q = \mathrm{ord}(1)$ as $\epsilon \to 0$. In fact, for these zero eigenvalues obtained from equation (2.4.8), a modified ansatz $(k^2 - \beta_q^2)L^2 = \epsilon^3\Delta_q$ leads to non-zero eigenvalues; in other words the changes to the values of kL made by introducing the structures are of $\mathrm{ord}(\epsilon^3)$ rather than of $\mathrm{ord}(\epsilon^2)$; further details are available in the appendix (see § A.3).

We now continue with the examination of the orthogonality condition (2.5.5). For a zero eigenvalue, from any row of the eigenvalue problem (2.6.14) $\boldsymbol{j}^T\boldsymbol{U}^S = 0$ so that the orthogonality condition is always satisfied for solutions associated with the eigenvalues equal to zero. To understand the case $\Delta' = Q$, we consider first the eigenvector equation we have from $\Delta' = 0$, namely

$$\boldsymbol{j}^T\boldsymbol{U}^S = u_1^S + u_2^S + \ldots u_Q^S = 0. \tag{2.6.15}$$

This is the equation of a $(Q-1)$-dimensional hyperplane in Q-dimensional space, with a normal $\boldsymbol{j}$. For a symmetric matrix, such as $\underline{\underline{\mathrm{J}}}$, the eigenvectors corresponding to distinct eigenvalues are orthogonal. Thus, $\boldsymbol{j}$ is parallel to the eigenvectors associated with the simple eigenvalue $\Delta' = Q$, so that $\boldsymbol{j}^T\boldsymbol{U}^S \neq 0$, and the orthogonality condition is not satisfied.

The conclusion from the above is that the scattering and radiation solutions may coexist when $\Delta' = 0$, but the radiation solution does not exist when $\Delta' = Q$. To illustrate this we again consider $(q_1L, q_2L) = (\pi, 0)$ and $kL \approx \pi$, so that $\Delta_1 = \Delta_2 = (k^2L^2 - \pi^2)/(k^2a^2) \equiv \Delta$. For $\Delta = 0$, $kL = \pi$ (considering only positive roots) and the scattering and radiation solutions may coexist, whilst for the second eigenvalue $\Delta = (2\pi L^2/A)Q = 4\pi L^2/A$ we obtain $kL = \pi/(1 - 4\pi a^2/A)$ and the radiation solution does not exist. As in the shallow-water case above, these values of kL are just the band gap boundaries given in (2.6.13), when amended for the scattering problem.

2.6.2.3 Evanescent modes

As discussed in [30, p. 52], evanescent modes that decay as they propagate correspond to a complex wave vector $\boldsymbol{\beta}$ and exist for frequencies within a band gap, even in the absence of

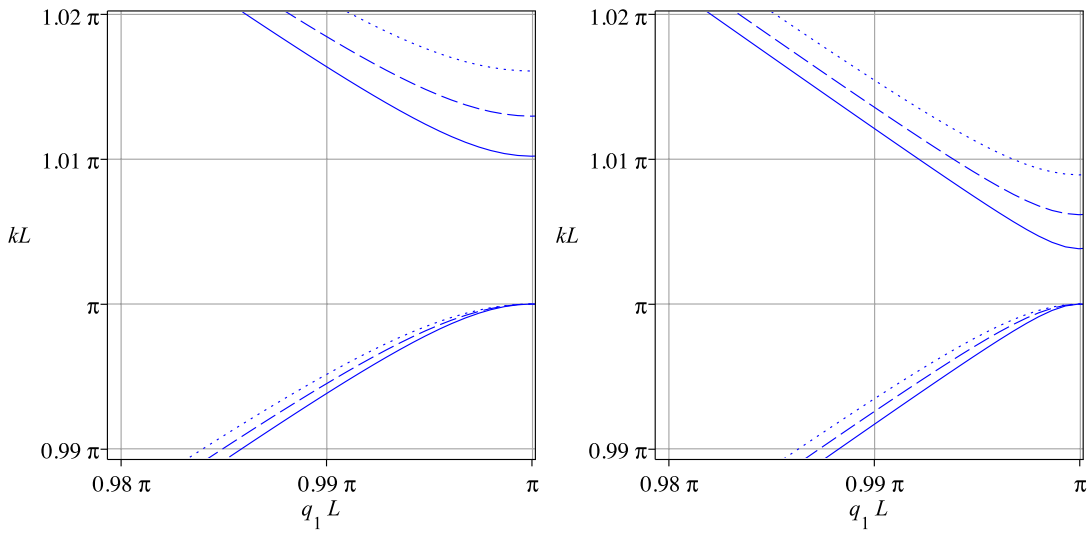

Figure 2.7 Perturbation of two plane waves for surface-piercing structures in deep water: kL *vs.* q_1L for (a) a fixed structure of radius $a/L = 0.04$ (——) , $a/L = 0.045$ (– – –) , $a/L = 0.05$ (· · · · · ·); (b) freely-floating structures for $a/L = 0.05$ with $\kappa = 1$ (——), $\kappa = 2$ (– – –), $\kappa = 4$ (· · · · · ·).

damping on the motion of the structure. To illustrate this we once again consider a neighbourhood of $(q_1L, q_2L, kL) = (\pi, 0, \pi)$ and put $(q_1L, q_2L) = (\pi + \mathrm{i}v, 0)$. Within the band gap, the quantity v is the damping rate with distance of the evanescent mode. For the shallow-water case, equation (2.6.8) then gives a quadratic in v^2, namely

$$v^4 + b_v v^2 + c_v = 0, \tag{2.6.16}$$

where

$$b_v = (\alpha_D + \alpha_W)(kL)^2 + 2\pi^2, \quad c_v = \alpha_D\alpha_W(kL)^4 - \pi^2(\alpha_D + \alpha_W)(kL)^2 + \pi^4, \tag{2.6.17}$$

$$\alpha_D = 1 + \frac{4\pi h^2}{A}\mathfrak{D}_1, \quad \text{and} \quad \alpha_W = 1 - \frac{2h^2}{A}W_\kappa. \tag{2.6.18}$$

The band gap corresponds to real v which requires $c_v \leq 0$; the edges of the gap are at $c_v = 0$ and solving this equation for kL reproduces the values in equation (2.6.10). As frequency varies across the gap, v^2 increases from zero at the lower edge, to a maximum at the mid point, and then reduces to reach zero again at the upper edge of the gap.

2.6.2.4 Structure of the two-mode solutions

As can be seen in figure 2.2, the number of solutions is conserved as wavenumber space is traversed. For example, we see that the two mode solution at $(q_1L, q_2L, kL) = (\pi, 0, \pi)$ branches in to two single mode solutions as q_1L decreases towards zero (with $q_2L = 0$, i.e. in the region ΓX of figure 2.2) but one double mode solution as q_2L increases towards π (with $q_1L = \pi$). For this same region in wavenumber space, when cylinders are present we can use the present approximations to demonstrate how the solutions are preserved as the wavenumber space is traversed; without loss of generality, we focus our attention on the scattering solutions. For the lowest single mode in ΓX, $(m_1, m_2) = (0, 0)$, and for the next (upper) single mode $(m_1, m_2) = (-1, 0)$. In the shallow-water case this gives

$$\begin{aligned} \frac{(q_1L)^2}{(kL)^2_{lower}} &= \left\{1 + \frac{h^2}{A}\left(2\pi\mathfrak{D}_1 - W\right)\right\}, \\ \frac{(q_1L - 2\pi)^2}{(kL)^2_{upper}} &= \left\{1 + \frac{h^2}{A}\left(2\pi\mathfrak{D}_1 - W\right)\right\}. \end{aligned} \tag{2.6.19}$$

On the other hand, in a neighbourhood of the double pole solution at $(q_1L, q_2L, kL) = (\pi, 0, \pi)$, i.e. when $\boldsymbol{\beta}_1 L = (q_1L, 0)^T$ and $\boldsymbol{\beta}_2 L = (q_1L - 2\pi, 0)^T$, there are two positive roots (denoted k_1 and k_2) which, when expanded in terms of $h^2/A = \mathrm{ord}(\epsilon^2)$, yield

$$\begin{aligned} \frac{(q_1L)^2}{(k_1L)^2} &= 1 + (2\pi\mathfrak{D}_1 - W)\frac{h^2}{A} - \frac{(2\pi - q_1L)^2(2\pi\mathfrak{D}_1 + W)^2}{4\pi(\pi - q_1L)}\frac{h^4}{A^2} + \ldots \\ \frac{(q_1L - 2\pi)^2}{(k_2L)^2} &= 1 + (2\pi\mathfrak{D}_1 - W)\frac{h^2}{A} + \frac{(q_1L)^2(2\pi\mathfrak{D}_1 + W)^2}{4\pi(\pi - q_1L)}\frac{h^4}{A^2} + \ldots. \end{aligned} \tag{2.6.20}$$

Clearly, these are equivalent to the single pole solutions in equation (2.6.19) up to $\mathrm{ord}(h^2/A)$, but at $\mathrm{ord}(h^4/A^2)$ the expansions fail as $q_1L \to \pi$ (or equivalently become a better approximation to the single mode solutions as q_1L moves away from π towards zero). Formally, the two-pole solution is valid only within a neighbourhood of $(q_1L, q_2L) = (\pi, 0)$ such that $(k^2 - \beta_q^2)L^2 = O(\epsilon^2)$, where $\Delta_q = \mathrm{ord}(1)$; see equation (2.3.10). However, equation (2.6.20) shows that the two-pole solution works well *throughout* ΓX (which is surprising because we perturbed at a single point). The same phenomena is observed with the two-pole deep-water solution. For

example, the expansions in a^2/A of the equivalent two-pole deep water solutions are

$$\begin{aligned}\frac{(q_1L)^2}{k_1^2} &= 1 - 2\pi\frac{a^2}{A} + \frac{\pi(q_1L)^2}{(\pi - q_1L)}\frac{a^4}{A^2} + \dots \\ \frac{(q_1L - 2\pi)^2}{k_2^2} &= 1 - 2\pi\frac{a^2}{A} - \frac{\pi(-q_1L + 2\pi)^2}{(\pi - q_1L)}\frac{a^4}{A^2} + \dots\end{aligned} \tag{2.6.21}$$

which, on truncation, recover the equivalent one-mode solutions that follow from equation (2.6.6).

We can also see explicitly how the cylinders' radius affects a two pole solution over an extended region of wavenumber space. Consider the lowest bold line (i.e. where $Q = 2$) within ΓX in figure 2.2. For this two pole solution $(m_1, m_2) = (0, 1)$ and $(m_1, m_2) = (0, -1)$ to give the wave vectors

$$\boldsymbol{\beta}_1 L = (q_1L, 2\pi)^T \quad \text{and} \quad \boldsymbol{\beta}_2 L = (q_1L, -2\pi)^T. \tag{2.6.22}$$

Equation (2.3.44) yields a quartic polynomial (in k) and, in the case of circular cylinders extending throughout the depth, the two positive roots are

$$kL = \frac{(q_1L)^2 + 4\pi^2}{\sqrt{(q_1L)^2 + 4\pi^2(1 + 4\pi a^2/A)}} \equiv (kL)_{\text{lower}} \tag{2.6.23}$$

and

$$kL = \frac{(q_1L)^2 + 4\pi^2}{\sqrt{(1 + 2\pi a^2/A)(q_1L)^2 + 4\pi^2(1 - 2\pi a^2/A)}} \equiv (kL)_{\text{upper}}. \tag{2.6.24}$$

The gap between these curves depend on the radius of the cylinder and is

$$(kL)_{\text{upper}} - (kL)_{\text{lower}} = \frac{\pi[12\pi^2 - (q_1L)^2]}{\sqrt{(q_1L)^2 + 4\pi^2}}\frac{a^2}{A} + O\left(\frac{a^4}{A^2}\right) \quad \text{as} \quad a/L \to 0. \tag{2.6.25}$$

This shows explicitly that the introduction of the cylinder splits the two-mode solution in to two separated modes that do not cross.

Chapter 3

Infinite array: the Rayleigh-Ritz method

3.1 Introduction

This chapter is concerned with solving numerically the problem of water-wave propagation through both surface-piercing and bottom-mounted truncated cylinders arranged on an infinite array in water of finite depth, and surface-piercing truncated cylinders arranged on an infinite array in deep water. The motivation for doing so is twofold: to complement the asymptotic approach of chapter 2 and to extend the work found there. We now note that, to investigate all angle negative refraction (AANR), we need complete band diagrams, which were not straightforward to produce using the asymptotic work. Furthermore, we will see later that we require a complete band gap (among other conditions which are difficult to explain here) around the whole Brillouin zone – rather than just a localised one – for negative refraction to occur; such a band gap requires large radii, typically large enough to possibly violate the assumptions we made in obtaining asymptotic solutions. Negative refraction hence serves as a motivation for presenting complete band diagrams for cylinders that extend throughout the depth, as well as truncated cylinders.

The numerical method we will be employing is the Rayleigh-Ritz method. The method allows us to solve an eigenvalue problem by replacing a continuous system with a system of a finite number of degrees of freedom for which the eigenvalues can be found numerically. The theory here follows the approach given in Duff & Naylor [41] and Linton & McIver [3], albeit that we generalise the theory to allow easy incorporation of a Bloch condition. We are able to show that minimising a function subject to a particular constraint is equivalent to solving water-wave

problems: (i) we can show equivalence between minimising a function subject to a particular constraint and the calculation of eigenvalues of the negative Laplacian corresponds to solving a constant depth water-wave problem; (ii) by changing the constraint, we then show that the resulting minimising problem is equivalent to the calculation of eigenvalues where they appear instead in one of the boundary conditions, corresponding to solving the water-wave problem for truncated cylinders. This provides us with a method for allowing us to consider the case of truncated circular cylinders.

The plan of this chapter is as follows. The problem is formulated in §3.2 and the theory of variational methods is introduced in §3.3, whilst the general eigenvalue problems are established in §3.4 (the work for cylinders extending throughout the depth is an account of the work found in [20]) before being solved numerically. Finally, a selection of explicit results, as well as a discussion about the convergence of the method and comparison with the asymptotic work found in chapter 2, is given in §3.5. As part of the results we look at negative refraction and explain its link to a material's complete band gap (we expand the results of [20] by linking a discussion on negative refraction to the complete band diagrams for cylinders that extend throughout the depth). As far as we can see, this link has not been explained explicitly in the current literature. This link motivates the drawing of complete band diagrams to search for complete band gaps in the case of truncated cylinders. The reader that is reading this thesis from beginning to end is reminded that it was the author's intention that the chapters were, for the most part, self-contained and there is hence a lot of repetition between the problem formulation found here and that used in Chapter 2.

3.2 Problem formulation

Vertically axisymmetric structures C_j with wetted surfaces S_{C_j} are distributed uniformly on an infinite horizontal lattice Λ in water of depth h; the length scale for the lattice periodicity is denoted by L. A horizontal plane is illustrated in figure 3.1a for the particular case of a square lattice. We use Cartesian coordinates (x, y, z), with z directed vertically upwards and origin O in the mean free surface at a chosen lattice point. Global polar coordinates (r, θ) in the horizontal plane are also used. Associated with each cylinder are local horizontal polar coordinates (r_j, θ_j) with origin O_j (so that dropping the j indicates use of the global coordinates) located, relative to O, at the lattice points given by the lattice vectors

$$\boldsymbol{R}_j = n_1\boldsymbol{a}_1 + n_2\boldsymbol{a}_2, \quad n_1, n_2 \in \mathbb{Z},$$

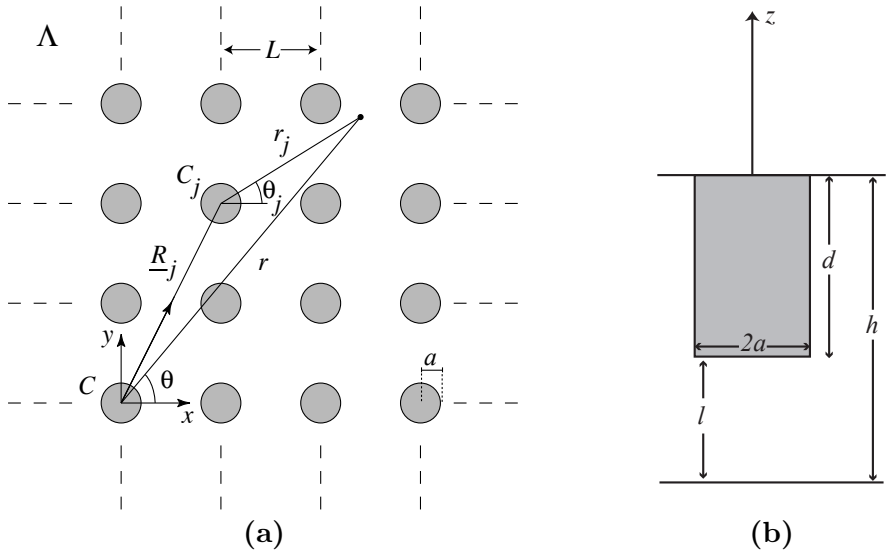

Figure 3.1 (a) Coordinate systems on $z = 0$, and (b) a vertical section of the fluid domain for a surface-piercing circular cylinder.

for given linearly independent vectors $\boldsymbol{a}_1$ and $\boldsymbol{a}_2$.

All structures in the lattice are identical, and when held fixed may be either surface piercing or bottom mounted. Some of the numerical results presented later are for the particular case of a lattice of truncated vertical cylinders in shallow water, and the notations used for this geometry are illustrated in figure 3.1b. If surface piercing, cylinder j occupies $r_j \leq a$, $-d \leq z \leq 0$, and we define $l = h - d$ to be the gap between the ocean bed and the bottom of the cylinder. For bottom-mounted circular cylinders, the wetted height is still denoted by d and l is the gap between the free surface and the top of the cylinder. More generally, a is used to denote the characteristic size of the structure which, for a surface-piercing structure, is specifically chosen as the radius of the water-plane area.

The fluid is assumed to be inviscid and incompressible and the fluid motion to be irrotational. The linearised theory of water waves is used throughout so that time-harmonic motions with angular frequency ω may be described by a velocity potential $\mathrm{Re}[\phi(x, y, z)\,\mathrm{e}^{-\mathrm{i}\omega t}]$, where t is time. For all lattice vectors $\boldsymbol{R}_j$, solutions are sought that satisfy the so-called Bloch condition

$$\phi(\boldsymbol{r} + \boldsymbol{R}_j) = \mathrm{e}^{\mathrm{i}\boldsymbol{\beta}^T \boldsymbol{R}_j}\phi(\boldsymbol{r}), \tag{3.2.1}$$

where $\boldsymbol{r} = (x, y)^T$, and $\boldsymbol{\beta} = (q_1, q_2)^T$, $q_1, q_2 \in \mathbb{R}$, is a prescribed vector. The Bloch condition prescribes a phase relationship between the potential values at equivalent points in different cells of the lattice. Given a $\boldsymbol{\beta}$, we seek the frequencies ω that allow non-trivial solutions for ϕ.

For consistency with [20], W and L is the dimensional width and length of a single cell of a rectangular lattice: for a square lattice take $W/L = 1$. For this geometry, the Bloch condition implies the four independent conditions

$$\left.\begin{aligned} &\phi(1/2, y, z) = \mathrm{e}^{\mathrm{i}q_1 L}\phi(-1/2, y, z), \\ &\frac{\partial}{\partial x}\phi(1/2, y, z) = \mathrm{e}^{\mathrm{i}q_1 L}\frac{\partial}{\partial x}\phi(-1/2, y, z), \end{aligned}\right\} \quad |y| \leq \frac{W}{2L},$$

$$\left.\begin{aligned} &\phi(x, W/2L, z) = \mathrm{e}^{\mathrm{i}q_2 L}\phi(x, -W/2L, z), \\ &\frac{\partial}{\partial y}\phi(x, W/2L, z) = \mathrm{e}^{\mathrm{i}q_2 L}\frac{\partial}{\partial y}\phi(x, -W/2L, z), \end{aligned}\right\} \quad |x| \leq \frac{W}{2L}, \tag{3.2.2}$$

which are valid in a chosen fundamental cell of the array. Once ϕ is established in the fundamental cell, 3.2.1 provides the extension to the other cells. Hence it is sufficient to consider just one cell of the array by solving (in the fundamental cell) the field equation with the free surface condition and boundary conditions to enforce no flow through the cylinders' walls and the bed.

In addition to the Bloch condition, the complex-valued potential ϕ satisfies the usual equations of the linearised theory of water waves [4, Chapter 8]. Thus

$$\nabla^2\phi = 0 \quad \text{within the fluid domain } \mathcal{D}, \tag{3.2.3}$$

and the linearised condition

$$\frac{\partial\phi}{\partial z} - \frac{\omega^2}{g}\phi = 0 \quad \text{on the free surface } S_F \tag{3.2.4}$$

(g is the acceleration due to gravity) and, for water of constant finite depth

$$\frac{\partial\phi}{\partial z} = 0 \quad \text{on the bed } S_B, \tag{3.2.5}$$

while for deep water we require that

$$|\nabla\phi| \to 0 \quad \text{as} \quad z \to -\infty. \tag{3.2.6}$$

Here we restrict attention to vertically axisymmetric structures that are fixed. Hence, on the

surface S_C of the particular structure C located at the chosen origin of coordinates

$$\frac{\partial \phi}{\partial n} = 0, \tag{3.2.7}$$

where the coordinate n is measured normal to S_C and directed out of the fluid.

In the absence of structures, the Bloch condition (3.2.1), together with (3.2.4) and the appropriate bed condition, are satisfied by plane waves

$$\phi_q(\boldsymbol{r}) = \begin{cases} \mathrm{e}^{\mathrm{i}\boldsymbol{\beta}_q^T \boldsymbol{r}} \cosh k(z+h) & \text{for finite-depth water,} \\ \mathrm{e}^{\mathrm{i}\boldsymbol{\beta}_q^T \boldsymbol{r}} \mathrm{e}^{kz} & \text{for deep water,} \end{cases} \tag{3.2.8}$$

where the wavenumber k is the positive real root of the dispersion relation $\omega^2 = gk \tanh kh$,

$$\boldsymbol{\beta}_{mn} = \boldsymbol{\beta} + \boldsymbol{K}_{mn}, \tag{3.2.9}$$

and each $\boldsymbol{K}_{mn} = 2\pi(m\boldsymbol{b}_1 + n\boldsymbol{b}_2)$, for $m, n \in \mathbb{Z}$, is a reciprocal lattice vector [30, Appendix B]. (Note that, unlike in the other chapters of this thesis, we do not use q to represent each ordered pair of integers (m, n) for the reason being that some of the expressions contained later in this chapter are actually easier to interpret by showing explicitly the two components that make up each $\boldsymbol{\beta}_{mn}$.) The vectors $\{\boldsymbol{b}_1, \boldsymbol{b}_2\}$ satisfy $\boldsymbol{a}_i^T \boldsymbol{b}_j = \delta_{ij}$ for $i, j = 1, 2$, so that $\boldsymbol{K}_{mn}^T \boldsymbol{R}_j = 2\pi p$, $p \in \mathbb{Z}$, for any lattice vector $\boldsymbol{R}_j$. The forms (3.2.8) satisfy Laplace's equation (3.2.3) provided

$$k^2 = \beta_{mn}^2 \quad \text{where} \quad \beta_{mn} = |\boldsymbol{\beta}_{mn}|. \tag{3.2.10}$$

For a given $\boldsymbol{\beta}$ there may be multiple vectors $\boldsymbol{\beta}_{mn}$ that yield the same $|\boldsymbol{\beta}_{mn}|$ and the number of such vectors is denoted by Q.

We use the non-dimensional coordinates

$$x' = x/L, \quad y' = y/L, \quad z' = z/L, \quad r_j' = r_j/L.$$

and, for a wave of amplitude $\mathcal{A}$, a non-dimensional velocity potential is defined according to the transformation

$$\phi \to \frac{g\mathcal{A}}{\omega}\phi. \tag{3.2.11}$$

3.3 Theory of variational methods for eigenvalue problems

The full variational method is discussed to demonstrate the recovery of a water-wave problem for constant depth. We then briefly describe the variational method for the water-wave problem for truncated cylinders, before looking at the Rayleigh-Ritz method which can be used to obtain approximations for the resulting eigenvalue problems. The theory given here is generalised to complex-valued potentials to allow easy incorporation of the Bloch condition. We include within this theory section a description of a comparison principle which is used to calculate appropriate bounds for our solutions.

3.3.1 Eigenvalues for the negative Laplacian and the recovery of the constant depth water-wave problem

Consider the problem of minimising a functional

$$\mathcal{E}(v) = \iint_{\mathcal{D}} |\nabla v|^2 \ dV \equiv \iint_{\mathcal{D}} \nabla v \cdot \nabla v^* \ dV \tag{3.3.1}$$

for a trial function v (the superscript asterisk denotes the complex conjugate), required to have piecewise continuous first derivatives and be continuous in the two-dimensional domain $\mathcal{D}$, with boundary $S + S_V$ (S_V is taken to be the cell walls, S is everything else making up the boundary of $\mathcal{D}$), subject to the constraint

$$\mathcal{H}(v) = \iint_{\mathcal{D}} |v|^2 \ dV \equiv \iint_{\mathcal{D}} vv^* \ dV = 1 \tag{3.3.2}$$

(which is included to omit the trivial solution). For later use we define

$$\mathcal{E}(v, w) = \iint_{\mathcal{D}} \nabla v \cdot \nabla w^* \ dV \quad \text{and} \tag{3.3.3}$$

$$\mathcal{H}(v, w) = \iint_{\mathcal{D}} vw^* \ dV. \tag{3.3.4}$$

The theory of Lagrange multipliers indicates we should look for the minimum of

$$\mathcal{E}(v) - \lambda\mathcal{H}(v) = \iint_{\mathcal{D}} |\nabla v|^2 - \lambda v^2 \ dV \tag{3.3.5}$$

for Lagrange multiplier λ. Suppose the minimum of this function is at $v = v_0$, and let us perturb a small distance from this point by writing $v = v_0 + \epsilon v_1$ for $\epsilon \ll 1$ where v_0 and v_1 must both

also satisfy the Bloch condition (as it is not a *natural* condition – more on this meaning of a natural condition shortly). Since v_0 is a minimum, the inequality

$$\mathcal{E}(v) - \lambda\mathcal{H}(v) \geq \mathcal{E}(v_0) - \lambda\mathcal{H}(v_0) \tag{3.3.6}$$

must hold. Note that

$$\mathcal{E}(v) = \mathcal{E}(v_0 + \epsilon v_1) = \mathcal{E}(v_0) + \epsilon\left[\mathcal{E}(v_0, v_1) + \mathcal{E}(v_1, v_0)\right] + \epsilon^2\mathcal{E}(v_1) \tag{3.3.7}$$

and

$$\mathcal{H}(v) = \mathcal{H}(v_0 + \epsilon v_1) = \mathcal{H}(v_0) + \epsilon\left[\mathcal{H}(v_0, v_1) + \mathcal{H}(v_1, v_0)\right] + \epsilon^2\mathcal{H}(v_1). \tag{3.3.8}$$

Substituting these into the inequality above yields the relationship

$$\begin{aligned}\epsilon\left\{\mathcal{E}(v_0, v_1) + \mathcal{E}^*(v_0, v_1) - \lambda\left[\mathcal{H}(v_0, v_1) + \mathcal{H}^*(v_0, v_1)\right]\right\} + \epsilon^2\left[\mathcal{E}(v_1) - \lambda\mathcal{H}(v_1)\right] \\ = \frac{\epsilon}{2}\mathrm{Re}\left[\mathcal{E}(v_0, v_1) - \lambda\mathcal{H}(v_0, v_1)\right] + \epsilon^2\left[\mathcal{E}(v_1) - \lambda\mathcal{H}(v_1)\right] \geq 0.\end{aligned} \tag{3.3.9}$$

Lemma 1 *For every v_0 and v_1 we have that*

$$\mathrm{Re}\left[\mathcal{E}(v_0, v_1) - \lambda\mathcal{H}(v_0, v_1)\right] = 0. \tag{3.3.10}$$

Proof We perform a proof by contradiction. By assuming that

$$\mathrm{Re}\left[\mathcal{E}(v_0, v_1) - \lambda\mathcal{H}(v_0, v_1)\right]$$

is greater than and less than zero respectively, we arrive at a contradiction in each case:

- For $\mathrm{Re}\left[\mathcal{E}(v_0, v_1) - \lambda\mathcal{H}(v_0, v_1)\right] > 0$, let us choose $\epsilon < 0$ such that the magnitude of the second term in (3.3.9) is smaller than the magnitude of the first; in order for (3.3.9) to be true one must have $\mathrm{Re}\left[\mathcal{E}(v_0, v_1) - \lambda\mathcal{H}(v_0, v_1)\right] < 0$, which is a contradiction;
- For $\mathrm{Re}\left[\mathcal{E}(v_0, v_1) - \lambda\mathcal{H}(v_0, v_1)\right] < 0$, let us choose $\epsilon > 0$ such that the magnitude of the second term in (3.3.9) is smaller than the magnitude of the first; in order for (3.3.9) to be true one must have $\mathrm{Re}\left[\mathcal{E}(v_0, v_1) - \lambda\mathcal{H}(v_0, v_1)\right] > 0$, which is a contradiction;

and the truth of the lemma is established.

Lemma 1 is equivalent to writing

$$\mathrm{Re}\left[\iint_{\mathcal{D}} \nabla v_0 \cdot \nabla v_1^* - \lambda v_0 v_1^* \; dV\right] = 0, \tag{3.3.11}$$

From Green's first identity, we know that

$$\iint_{\mathcal{D}} \nabla v_1^* \cdot \nabla v_0 \; dV = -\iint_{\mathcal{D}} v_1^* \nabla^2 v_0 \; dV + \int_{S+S_V} v_1^* \nabla v_0 \cdot \boldsymbol{n} \; dS \tag{3.3.12}$$

for a normal $\boldsymbol{n}$ pointing out of $\mathcal{D}$ which, when substituted into (3.3.11), yields

$$\mathrm{Re}\left[-\iint_{\mathcal{D}} \left(\nabla^2 v_0 + \lambda v_0\right) v_1^* \; dV + \int_{S+S_V} v_1^* \nabla v_0 \cdot \boldsymbol{n} \; dS\right] = 0 \tag{3.3.13}$$

where it is noted that

$$\begin{aligned}\int_{S_V} v_1^* \nabla v_0 \cdot \boldsymbol{n} \; dS = &\int_{-W/2L}^{W/2L} (-1) \frac{\partial}{\partial x} v_0\left(-\frac{1}{2}, y\right) \; v_1^*\left(-\frac{1}{2}, y\right) + \frac{\partial}{\partial x} v_0\left(\frac{1}{2}, y\right) \; v_1^*\left(\frac{1}{2}, y\right) \; dy \\ &+ \int_{-1/2}^{1/2} (-1) \frac{\partial}{\partial y} v_0\left(x, -\frac{W}{2L}\right) \; v_1^*\left(x, -\frac{W}{2L}\right) + \frac{\partial}{\partial y} v_0\left(x, \frac{W}{2L}\right) \; v_1^*\left(x, \frac{W}{2L}\right) \; dx.\end{aligned} \tag{3.3.14}$$

By using equation (3.2.2) we see that the integrals on opposite cell walls cancel so that the complete integral over S_V vanishes by the Bloch condition (making it a necessary condition). At the minimum point, that is when $v = v_0$, we must have that all coefficients of v_1 are zero, i.e.

$$\nabla^2 v_0 + \lambda v_0 = 0 \quad \text{in} \quad \mathcal{D}, \tag{3.3.15}$$

$$\frac{\partial v_0}{\partial n} = 0 \quad \text{on} \quad S. \tag{3.3.16}$$

This is to say that a minimum v_0 of $\mathcal{E}(v)$ subject to the constraint $\mathcal{H}(v)$ is equivalent to finding an eigenfunction $\phi = v_0$, with an associated eigenvalue $k^2 = \lambda$, of the negative Laplacian in a domain $\mathcal{D}$ with a zero Neumann condition on the boundary S. Note that this boundary condition is known as a *natural* one, so called because it is satisfied through the choice of $\mathcal{E}(v)$ and $\mathcal{H}(v)$.

3.3.2 Eigenvalues appearing in one of the boundary conditions and the recovery of the water-wave problem for truncated cylinders

The variational method is given in outline to demonstrate the recovery of the water-wave problem for truncated cylinders. Consider the problem of minimising the function

$$\mathcal{E}(v) = \iiint_{\mathcal{D}} |\nabla v|^2 \ dV \equiv \iiint_{\mathcal{D}} \nabla v \cdot \nabla v^* \ dV \tag{3.3.17}$$

for a trial function v, required to have piecewise first derivatives in a volume $\mathcal{D}$, with boundary $S_V + S_F + S$ (where S_V, S_F and S represents the cell walls, free surface and everything else that bounds $\mathcal{D}$ respectively), subject to the constraint

$$\mathcal{H}(v) = \iint_{S_F} |v|^2 \ dV \equiv \iint_{S_F} vv^* \ dV = 1. \tag{3.3.18}$$

so that

$$\mathcal{E}(v, w) = \iiint_{\mathcal{D}} \nabla v \cdot \nabla w^* \ dV \quad \text{and} \tag{3.3.19}$$

$$\mathcal{H}(v, w) = \iint_{S_F} vw^* \ dV. \tag{3.3.20}$$

We look for a minimum using the method of Lagrange multipliers, for Lagrange multiplier λ. Like we did previously, by considering a perturbation away from the minimum (so that $v = v_0 + \epsilon v_1$), applying Lemma 1 to the resultant inequality and then using Green's first identity yields the result

$$-\iiint_{\mathcal{D}} v_1 \nabla^2 v_0 \ dV + \iint_{S_N} v_1 \nabla v_0 \cdot \boldsymbol{n} \ dS + \iint_{S_F} v_1 \nabla v_0 \cdot \boldsymbol{n} \ dS - \lambda \iint_{S_F} v_1 v_0 \ dS = 0 \tag{3.3.21}$$

(where the integrals across the cell walls S_V vanish by the Bloch condition, which again is an essential condition rather than a natural one) which is equivalent to

$$-\iiint_{\mathcal{D}} v_1 \nabla^2 v_0 \ dV + \iint_{S} v_1 \frac{\partial v_0}{\partial n} \ dS + \iint_{S_F} \left(\frac{\partial v_0}{\partial n} - \lambda v_0 \right) v_1 \ dS = 0. \tag{3.3.22}$$

At a minimum point, we must have that any coefficients of v_1 are equal to zero; that is that

$$\nabla^2 v_0 = 0 \quad \text{in} \quad \mathcal{D}, \tag{3.3.23}$$

$$\frac{\partial v_0}{\partial n} - \lambda v_0 = 0 \quad \text{on} \quad S_F, \tag{3.3.24}$$

$$\frac{\partial v_0}{\partial n} = 0 \quad \text{on} \quad S. \tag{3.3.25}$$

For an infinite array problem, the trial function v_0 will need to be defined so that the Bloch condition is satisfied on the walls of the cell.

3.3.3 The Rayleigh-Ritz method

The Rayleigh quotient is defined as

$$\mathcal{R}(v) = \frac{\mathcal{E}(v)}{\mathcal{H}(v)}; \tag{3.3.26}$$

the problem of minimising $\mathcal{E}(v)$ subject to the constraint $\mathcal{H}(v)$ using the method of Lagrange multipliers is equivalent to minimising the Rayleigh quotient. The maximum-minimum principle is applied to find the eigenvalues $\lambda_1 \leq \lambda_2, \ldots,$ of the infinite-dimensional system defined through the Rayleigh quotient:

The maximum-minimum principle: *Let $\mu_1, \mu_2, \ldots, \mu_n, \ldots$ denote the successive minimum values of the Rayleigh quotient $\mathcal{R}$, subject for $n > 1$ to the $n-1$ orthogonal constraints*

$$\mathcal{H}(v_1, u) = 0, \quad \mathcal{H}(v_2, u) = 0, \quad \ldots, \quad \mathcal{H}(v_{n-1}, u) = 0 \tag{3.3.27}$$

defined by a given sequence of functions $v_1, v_2, \ldots, v_{n-1}, \ldots$. Then

$$\mu_1 = \lambda_1, \quad \mu_2 \leq \lambda_2, \quad \ldots, \quad \mu_u \leq \lambda_n, \quad \ldots \tag{3.3.28}$$

with equality in these relations up to λ_n only if $v_1 = u_1, v_2 = u_2, \ldots, v_{n-1} = u_{n-1}$, where the u_k are the eigenfunctions and the λ_k the corresponding eigenvalues.

This principle says that, when we apply the Rayleigh-Ritz numerical method, we are given upper bounds for the eigenvalues. As per [3, §8.2.3] strengthening the conditions in a minimum problem (by imposing conditions additional to the natural boundary condition for example) does not diminish the minimum. Conversely weakening the conditions does not increase the

minimum. The Rayleigh-Ritz method numerically approximates the eigenvalues by replacing the continuous system by a system of a finite number of degrees of freedom for which the eigenvalues can be found by solving a polynomial equation; that is, it provides us with a way of creating the trial function v.

We begin by writing v as

$$v = \sum_{k=1}^{n} a_k f_k, \tag{3.3.29}$$

for undetermined coefficients a_k and basis functions f_k, defined over the domain of the system, that are chosen by inspection or otherwise (we will use plane waves that exist in the absence of structures as a guide) to be as good approximations to the eigenfunctions as we can find. By analogy with the full variational problem, we shall try to find the minimum of the Rayleigh quotient $\mathcal{R}$ (which is now a function of the n variables a_k). This minimum value will be taken as the approximate eigenvalue; the minimising process will also yield approximate eigenfunctions. As already mentioned, minimising the Rayleigh quotient is equivalent to the Lagrangian multiplier problem of finding the minimum of $\mathcal{E}(v) - \Lambda\mathcal{H}(v)$.

From our chosen form of u we have that

$$\mathcal{E}(v) - \Lambda\mathcal{H}(v) = \sum_{k,l=1}^{n} a_k a_l \left[\mathcal{E}(f_k, f_l) - \Lambda\mathcal{H}(f_k, f_l)\right]. \tag{3.3.30}$$

By defining two $n \times n$ matrices $\underline{\underline{\mathrm{E}}}$ (with elements $e_{kl} = \mathcal{E}(f_k, f_l) = e_{lk}$) and $\underline{\underline{\mathrm{H}}}$ (with elements $h_{kl} = \mathcal{H}(f_k, f_l) = h_{lk}$) we must hence minimise

$$\mathcal{E}(v) - \Lambda\mathcal{H}(v) = \sum_{k,l=1}^{n} \left(e_{kl} - \Lambda h_{kl}\right) a_k a_l. \tag{3.3.31}$$

Differentiating with respect to a_k and equating the result to zero yields

$$\sum_{k,l=1}^{n} \left(e_{kl} - \Lambda h_{kl}\right) a_l = 0 \quad \text{for} \quad k = 1, \ldots, n \tag{3.3.32}$$

Denoting by $\boldsymbol{a}$ the column vector with components $a_1, \ldots, a_n$ allows us to rewrite the last expression in matrix form

$$\underline{\underline{\mathrm{E}}}\boldsymbol{a} = \Lambda\underline{\underline{\mathrm{H}}}\boldsymbol{a} \tag{3.3.33}$$

which is a generalised eigenvalue problem.

For sets of functions $f_1, \ldots, f_n$ that are orthogonal to each other with respect to the constraint $\mathcal{H}$, the matrix $\underline{\underline{\mathrm{H}}}$ will be the unit matrix so that $\underline{\underline{\mathrm{E}}}\boldsymbol{a} = \Lambda\boldsymbol{a}$ and then the vectors satisfying (3.3.33) will be the eigenvectors and the values of Λ the eigenvalues of the matrix $\underline{\underline{\mathrm{E}}}$. When $\underline{\underline{\mathrm{H}}}$ is not unit we premultiply both sides of (3.3.33) by the inverse of $\underline{\underline{\mathrm{H}}}$, that is $\underline{\underline{\mathrm{H}}}^{-1}$, so that $\underline{\underline{\mathrm{H}}}^{-1}\underline{\underline{\mathrm{E}}}\boldsymbol{a} = \Lambda\boldsymbol{a}$; we then call the vectors $\boldsymbol{a}$ eigenvectors of $\underline{\underline{\mathrm{E}}}$ with respect to $\underline{\underline{\mathrm{H}}}$ (and similarly for eigenvalues). In either case for $\underline{\underline{\mathrm{H}}}$, the eigenvalue problem may now be solved using standard numerical techniques. If the approximate eigenvalues are arranged in increasing order so that

$$\Lambda_1 \leq \Lambda_2 \leq \cdots \leq \Lambda_n \tag{3.3.34}$$

then they are upper bounds for the eigenvalue of the original infinite-dimensional system problem, i.e.

$$\lambda_1 \leq \Lambda_1, \quad \lambda_2 \leq \Lambda_2, \quad \ldots, \quad \Lambda_u \leq \lambda_n. \tag{3.3.35}$$

3.3.3.1 Comparison Principle

A comparison principle, described in [42, § 3.7], can be used to obtain simple bounds for the problem. We adapt the proof for the principle contained within [42] to allow for the fact that our potentials are complex. The comparison principle states if, after an appropriate transition of the liquid domains in question then, under the assumption that the principle holds, each (calculation of the upper bound for the) eigenvalue corresponding to the original domain will be bounded by an eigenvalue corresponding to the new domain. Furthermore, we note that the eigenvalues increase with the mass of fluid (and hence provide an upper bound for the upper bound of the eigenvalues corresponding to the original domain); conversely the eigenvalues decrease (providing a lower bound for the upper bound of the eigenvalues) as the liquid is decreased.

Before proving the comparison principle, we begin by introducing the first comparison theorem as given in [42, § 1.6], which states that if λ'_n (and respectively λ_n) denotes the nth eigenvalue of two eigenvalue problems $\mathcal{P}'$ (and respectively $\mathcal{P}$) with admissible spaces (which for us, amounts to the eigenvalues problems being such that the free surfaces have been chosen to coincide) and with Rayleigh quotients $\mathcal{R}$ and $\mathcal{R}'$ satisfying

$$\mathcal{R}(v) \geq \mathcal{R}'(v), \tag{3.3.36}$$

then we have

$$\lambda_n \geq \lambda'_n. \tag{3.3.37}$$

We now prove the comparison principle for the geometry of a cell of our array. We adapt ever so slightly the proof given in [42, § 3.7] because our velocity potentials are complex, which modifies the details found there. We wish to show that for a domain of fluid $\mathcal{D}'$ contained within another domain $\mathcal{D}$ (where the free surface remains the same for both domains), the eigenvalues associated with the water-wave problem defined in $\mathcal{D}'$ are less than or equal to the eigenvalues associated with the water-wave problem defined in $\mathcal{D}$. We recall that the surface of the volume of fluid $\mathcal{D}$ is $S_F + S_V + S$. The reduced domain $\mathcal{D}'$ has defining surface $S_F + S'_V + S'$ (so that the free surfaces for each domain are the same) and is defined such that $\mathcal{D} \subset \mathcal{D}'$. The mathematical water-wave problems – the need to solve the fluid equation, the free surface condition, the bed condition and the no flow condition through the cylinders and walls (which we later see is deduced from the Bloch condition) – in each domain are denoted by $\mathcal{P}$ and $\mathcal{P}'$. The respective Rayleigh quotients are

$$\mathcal{R}(f) = \frac{\iiint\limits_{\mathcal{D}} |\nabla v_f|^2 \ dV}{\iint\limits_{S_F} |f|^2 \ dS} \quad \text{and} \quad \mathcal{R}'(f) = \frac{\iiint\limits_{\mathcal{D}'} |\nabla v'_f|^2 \ dV}{\iint\limits_{S_F} |f|^2 \ dS} \tag{3.3.38}$$

Here f is defined on S_F while v_f (or v'_f) is the corresponding harmonic lifting; that is, for a given f, v_f (or v'_f) solves the Laplace equation in $\mathcal{D}$ (or $\mathcal{D}'$) subject to the boundary condition $v_f = f$ (or $v'_f = f$) on S_F, together with the appropriate conditions on the structure, bed and cell walls (f, v_f and v'_f are each complex). In this form for a Rayleigh quotient, the trial functions are defined over the free surface rather than the fluid domain. This is useful for the proof of the comparison principle but not for the computations of the eigenvalues.

Let us show that $\mathcal{R}(v_f) \geq \mathcal{R}'(v'_f)$. Since the denominators of $\mathcal{R}$ and $\mathcal{R}'$ are identical the comparison is equivalent to showing that

$$I = \iiint\limits_{\mathcal{D}} |\nabla v_f|^2 \ dV - \iiint\limits_{\mathcal{D}'} |\nabla v'_f|^2 \ dV \geq 0. \tag{3.3.39}$$

We can write I as

$$I = \iiint_{\mathcal{D}\setminus\mathcal{D}'} |\nabla v_f|^2 \ dV + \iiint_{\mathcal{D}'} \left(|\nabla v_f|^2 - \left|\nabla v_f'\right|^2 \right) \ dV \tag{3.3.40}$$

By using the identity

$$|a|^2 - |b|^2 = |a-b|^2 + 2\mathrm{Re}\{b(a^* - b^*)\} \tag{3.3.41}$$

where $|a|^2 \equiv a \cdot a^*$, with $a = \nabla v_f$ and $b = \nabla v_f'$, we obtain

$$I = \iiint_{\mathcal{D}\setminus\mathcal{D}'} |\nabla v_f|^2 \ dV + \iiint_{\mathcal{D}'} \left|\nabla v_f - \nabla v_f'\right|^2 \ dV + 2 \iiint_{\mathcal{D}'} \nabla v_f' \cdot \left(\nabla v_f - \nabla v_f'\right) \ dV, \tag{3.3.42}$$

the first two terms of which are positive. We will now show that the last term is equal to zero, which will complete the proof.

Define $(\delta v)^*$ to be the difference between two velocity potentials which are equal on the free surface (so that $\delta v = 0$ on S_F). Multiplying the field equation (for problem $\mathcal{P}'$) by $(\delta v)^*$ and integrating through the volume yields

$$\iiint_{\mathcal{D}'} (\nabla^2 v_f')(\delta v)^* \ dV = 0. \tag{3.3.43}$$

The Laplacian is the divergence of the gradient so that we have

$$\iiint_{\mathcal{D}'} \nabla \cdot (\nabla v_f')(\delta v)^* \ dV = 0, \tag{3.3.44}$$

and after applying a vector calculus identity and the divergence theorem we are left with

$$\iint_{S'} (\delta v)^* \nabla v_f' \cdot \boldsymbol{n} \ dS + \iiint_{\mathcal{D}'} \nabla v_f' \cdot \nabla (\delta v)^* \ dV = 0. \tag{3.3.45}$$

The integrand of the first term is equivalent to $(\delta v)^*(\partial v_f'/\partial n)$ and it is hence easy to see that the first term must be equal to zero (by definition $(\delta v)^* = 0$ on S_F and the boundary conditions make the integrals disappear everywhere else). We are hence left with

$$\iiint_{\mathcal{D}'} \nabla v_f' \cdot \nabla (\delta v)^* \ dV = 0. \tag{3.3.46}$$

Choosing $(\delta v)^* = v_f - v_f'$ (satisfying the definition of $(\delta v)^*$ being the difference of two velocity

potentials which are equal on the free surface) shows that the last term of (3.3.42) is equal to zero, thus concluding that $I \geq 0$. According to the first comparison theorem, if λ'_n (and respectively λ_n) denotes the nth eigenvalue of the problem $\mathcal{P}'$ (and respectively $\mathcal{P}$), then we have

$$\lambda_n \geq \lambda'_n. \tag{3.3.47}$$

3.4 Obtaining the generalised eigenvalue problems

This subsection is split into two parts; we treat the problem of cylinders that extend throughout the whole depth separate from truncated cylinders; this is because the depth dependence may be removed from the former and thus the eigenvalue problem is different.

3.4.1 Cylinders extending throughout the depth

We give here an account of the problem solved in McIver [20]. For cylinders extending throughout the depth, there is no gap between their base and the ocean bed so that $l = 0$. For water of constant depth h, the water-wave problem (3.2.3)-(3.2.7) reduces to the Helmholtz equation with a condition on a particular body,

$$\nabla^2\phi + k^2\phi = 0 \quad \text{in} \quad \mathcal{D} \tag{3.4.1}$$

$$\frac{\partial\phi}{\partial n} = 0 \quad \text{on} \quad S_C, \tag{3.4.2}$$

where k is the real positive root of the dispersion relation $K = k\tanh kh$ for frequency parameter $K = \omega^2/g$, as well as the Bloch condition (3.2.2).

Consider the trial function

$$v = \sum_{m,n=-P}^{P} A_{mn} \mathrm{e}^{\mathrm{i}(\boldsymbol{\beta}L + \boldsymbol{K}_{mn}L)\cdot\boldsymbol{r'}}, \tag{3.4.3}$$

which is chosen to satisfy the Bloch condition (the body condition is a natural condition and need not be incorporated) for constants A_{mn}. The Rayleigh quotient, as given in (3.3.26) for (3.3.1) and (3.3.2) in original coordinates, leads to the generalised eigenvalue problem

$$\sum_{m,n=-P}^{P} \left(e_{klmn} - \Lambda L^2 h_{klmn}\right) a_{mn} = 0 \quad \text{for} \quad k,l = -P,\ldots,P \tag{3.4.4}$$

for non-dimensional eigenvalues ΛL^2. By the theory laid out in §3.3.1, v is equivalent to the velocity potential ϕ for the water-wave problem for cylinders extending throughout the depth; the square root of the eigenvalues ΛL^2 are equivalent to the non-dimensional wavenumber kL so that $k = \sqrt{\Lambda}$. We note that

$$h_{klmn} = \iint_{\mathcal{D}} \mathrm{e}^{\mathrm{i}(\boldsymbol{\beta} L + \boldsymbol{K}_{kl} L)\cdot \boldsymbol{r'}} \mathrm{e}^{-\mathrm{i}(\boldsymbol{\beta} L + \boldsymbol{K}_{mn} L)\cdot \boldsymbol{r'}} \, ds' \tag{3.4.5}$$

$$e_{klmn} = C_1 h_{klmn}, \tag{3.4.6}$$

where

$$C_1 = (q_1 L + 2\pi k)(q_1 L + 2\pi m) + \left(q_2 L + 2\pi l \frac{L}{W}\right)\left(q_2 L + 2\pi n \frac{L}{W}\right), \tag{3.4.7}$$

are the elements of matrices $\underline{\underline{\mathrm{H}}}$ and $\underline{\underline{\mathrm{E}}}$ respectively (when calculating the quantities $\mathcal{E}(v, v^*)$ and $\mathcal{H}(v, v^*)$ the complex conjugate of v comes from the definition of the inner product; see [3, equation (8.61,8.62)]). We have that

$$\begin{aligned} h_{klmn} &= \iint_{S_V} \mathrm{e}^{\mathrm{i}(\boldsymbol{K}_{kl} L - \boldsymbol{K}_{mn} L)\cdot \boldsymbol{r'}} \, ds' - \iint_{S_C} \mathrm{e}^{\mathrm{i}(\boldsymbol{K}_{kl} L - \boldsymbol{K}_{mn} L)\cdot \boldsymbol{r'}} \, ds' \\ &= \int_0^{W/L} \int_0^1 \mathrm{e}^{\mathrm{i}(\boldsymbol{K}_{kl} L - \boldsymbol{K}_{mn} L)\cdot (x', y')^T} \, dx' dy' - \int_0^{a/L} \int_0^{2\pi} \mathrm{e}^{\mathrm{i}(\boldsymbol{K}_{kl} L - \boldsymbol{K}_{mn} L)\cdot \boldsymbol{r'}} \, r' d\theta dr' \\ &\equiv I_1 - I_2. \end{aligned} \tag{3.4.8}$$

The calculation for I_2 when $k \neq m$ and $l \neq n$ is non-trivial, and we give its calculation here as an aside. When $k \neq m$ and $l \neq n$ we have

$$\begin{aligned} I_2 &= \int_0^{a/L} \int_0^{2\pi} \mathrm{e}^{\mathrm{i}(\boldsymbol{K}_{kl} L - \boldsymbol{K}_{mn} L)\cdot \boldsymbol{r'}} \, r' d\theta dr' \\ &= \int_0^{a/L} \int_0^{2\pi} \mathrm{e}^{\mathrm{i} r |\boldsymbol{K}_{klmn} L| \cos(\theta - \tau_{klmn})} \, r' d\theta dr' \end{aligned}$$

where τ_{klmn} is the angle $(\boldsymbol{K}_{kl} L - \boldsymbol{K}_{mn} L)$ makes with x-axis and

$$|\boldsymbol{K}_{klmn} L| = 2\pi \sqrt{(k-m)^2 + (l-n)^2 \frac{L^2}{W^2}}.$$

From [35, equation 9.1.41], the integral over θ only exists for J_0, and so

$$I_2 = \int_0^{a/L} 2\pi J_0(|\boldsymbol{K}_{klmn} L| r') \, r' dr'.$$

for the Bessel function of the first kind and order zero J_0. Following a change of variables $\rho = |\boldsymbol{K}_{klmn}L|r'$

$$I_2 = \int_0^{|\boldsymbol{K}_{klmn}L|a/L} \frac{2\pi}{|\boldsymbol{K}_{klmn}L|^2} J_0(\rho)\ \rho d\rho,$$

and then using [35, equation 9.1.30] we thus have

$$I_2 = \frac{2\pi}{|\boldsymbol{K}_{klmn}L|}\frac{a}{L}J_1\left(|\boldsymbol{K}_{klmn}L|\frac{a}{L}\right).$$

for the Bessel function of the first kind and order one J_1 (upon changing back to our original coordinates).

The integrals are thus given as

$$I_1 = \begin{cases} 0 & ;k \neq m \text{ and } l \neq n \\ \dfrac{W}{L} & ;k = m \text{ and } l = n \end{cases} \tag{3.4.9}$$

and

$$I_2 = \begin{cases} -\dfrac{2\pi}{|\boldsymbol{K}_{klmn}L|}\dfrac{a}{L}J_1\left(|\boldsymbol{K}_{klmn}L|\dfrac{a}{L}\right) & ;k \neq m \text{ and } l \neq n \\ -\dfrac{\pi a^2}{L^2} & ;k = m \text{ and } l = n. \end{cases} \tag{3.4.10}$$

We conclude this subsection by reminding the reader of the notation,

$$e_{klmn} = C_1(I_1 - I_2), \tag{3.4.11}$$

$$h_{klmn} = I_1 - I_2, \tag{3.4.12}$$

which is pointed out for ease of comparison with the next sections.

3.4.2 Truncated circular cylinders

We now build a depth dependent function into the trial solutions in order to obtain the eigenvalue problems for truncated cylinders. The depth dependence, and indeed the boundaries of the integrals across the cylinders, are kept general for succinct presentation. Once the exact nature of the matrices are established, we specify the depth dependence (which is different for deep water and water of finite depth) and the boundaries of the integral across the cylinders (different for

surface-piercing and bottom-mounted structures).

Consider the trial function

$$v = \sum_{m,n=-P}^{P} A_{mn} D_{mn}(z') \phi_{mn}(\boldsymbol{r'}) \tag{3.4.13}$$

$$= \sum_{m,n=-P}^{P} A_{mn} D_{mn}(z') \mathrm{e}^{\mathrm{i}(\boldsymbol{\beta} L + \boldsymbol{K}_{mn} L)\cdot \boldsymbol{r'}}, \tag{3.4.14}$$

for as yet unspecified vertical functions $D_{mn}(z')$, which is chosen to satisfy the Bloch condition (the body condition is a natural condition and need not be incorporated) for constants A_{mn}. We recall that

$$\beta_{mn} L = |\boldsymbol{\beta} + \boldsymbol{K}_{mn}| = \sqrt{(q_1 L + 2\pi m)^2 + (q_2 L + 2\pi n L/W)^2}.$$

The Rayleigh quotient, as given in (3.3.26) for (3.3.1) and (3.3.2) in original coordinates, leads to the generalised eigenvalue problem

$$\sum_{m,n=-P}^{P} \left(e_{klmn} - \Lambda L h_{klmn}\right) A_{mn} = 0 \quad \text{for} \quad k,l = -P, \ldots, P \tag{3.4.15}$$

for non-dimensional eigenvalues ΛL. By the theory laid out in §3.3.2, v is hence equivalent to the velocity potential ϕ for the water-wave problem for truncated cylinders; comparing the natural condition which arises from the variational method with the free surface condition generates the relationship between ΛL and kL:

$$\Lambda L \equiv kL \tanh kh. \tag{3.4.16}$$

We note that

$$h_{klmn} = \iint_{S_F} D_{kl}(0) \phi_{kl}(\boldsymbol{r'}) D^*_{mn}(0) \phi^*_{mn}(\boldsymbol{r'}) \, ds' \tag{3.4.17}$$

$$e_{klmn} = \iiint_{V} \left[C_1 D_{kl}(z') D^*_{mn}(z') + \frac{d}{dz'} D_{kl}(z') \frac{d}{dz'} D^*_{mn}(z') \right] \phi_{kl}(\boldsymbol{r'}) \phi^*_{mn}(\boldsymbol{r'}) \, dv', \tag{3.4.18}$$

where V is the volume of the cell, S_F is the free surface and

$$C_1 = (q_1 L + 2\pi k)(q_1 L + 2\pi m) + \left(q_2 L + 2\pi l \frac{L}{W}\right)\left(q_2 L + 2\pi n \frac{L}{W}\right), \tag{3.4.19}$$

are the elements of matrices $\underline{\underline{\mathrm{H}}}$ and $\underline{\underline{\mathrm{E}}}$ respectively. Using the definitions of I_1 and I_2 introduced in §3.4.1, we hence have

$$h_{klmn} = D_{kl}(0)D_{mn}(0)[I_1 - I_2] \tag{3.4.20}$$

and

$$\begin{aligned} e_{klmn} = I_1 \int_{-h/L}^{0} \left[C_1 D_{kl}(z')D_{mn}(z') + \frac{d}{dz'}D_{kl}(z')\frac{d}{dz'}D_{mn}(z') \right] dz' \\ - I_2 \int_{S_L}^{S_U} \left[C_1 D_{kl}(z')D_{mn}(z') + \frac{d}{dz'}D_{kl}(z')\frac{d}{dz'}D_{mn}(z') \right] dz'. \end{aligned} \tag{3.4.21}$$

For water of finite depth, we choose

$$D_{mn}(z') = \frac{\cosh[\beta_{mn}L(z' + h/L)]}{\cosh(\beta_{mn}h)} \tag{3.4.22}$$

and in the calculation of e_{klmn} we integrate through the structure's lower and upper integral bounds $S_L = -h/L$ and $S_U = -(h/L - d/L)$ for bottom-mounted cylinders or $S_L = -d/L$ and $S_U = 0$ for surface-piercing cylinders. For deep water, we choose

$$D_{mn}(z') = \mathrm{e}^{\beta_{mn}Lz'} \tag{3.4.23}$$

and in the calculation of e_{klmn} from equation (3.4.21) we calculate the first integral in the limit $h/L \to \infty$, whilst the second integral is calculated between the structure's lower and upper integral bounds $S_L = -d/L$ and $S_U = 0$.

3.5 Results

The work contained within this results section is essentially split into three parts; (i) a discussion about the convergence of the current Rayleigh-Ritz solutions, including a demonstration of how the numerical solutions found here compare with the approximate asymptotic solutions obtained in chapter 2; (ii) calculation of localised band gaps, presented alongside a quantitative and qualitative comparison of the band gaps obtained numerically with those found asymptotically; (iii) an investigation into the phenomenon of all angle negative refraction (AANR) and hence a presentation of complete band diagrams: the investigation into AANR requires that we produce complete band gap diagrams, something which we were unable to do using the asymptotic methods of the previous chapter.

For the benefit of quick identification of the results being presented in the figures and tables of this section, we introduce the notation FDBM (finite-depth water, bottom-mounted cylinders), FDSP (finite-depth water, surface-piercing cylinders) and DW (surface-piercing cylinders in deep water).

3.5.1 Convergence

We discuss the convergence of the Rayleigh-Ritz solutions for each of the three cases under consideration: (i) bottom-mounted and (ii) surface-piercing truncated cylinders in water of finite depth and (iii) truncated cylinders in deep water. The approach of discussing the convergence of the three cases is to begin by presenting tables of values for each case to show how the solutions converge as the truncation parameter N is increased, then we apply the comparison principle and finally demonstrate the agreement of the numerical solutions here with the previous asymptotic results and in particular show how the asymptotic results start to disagree as the wavenumber (non-dimensionalised by the cylinders' radii) ka grows beyond the restrictions of the assumptions made in obtaining the asymptotic solutions.

3.5.1.1 Finite depth: bottom-mounted truncated cylinders

Table 3.1 shows the upper bounds calculated for the first two eigenvalues at the point $\boldsymbol{\beta}L = (9\pi/10, 0)^T$ in the case of short (that is, $d/h = 0.2$) bottom-mounted truncated cylinders. At least 14 significant figures, which is more than is being displayed in the table, is obtained with $N = 2$ for radii of $a/L = 0.05$ (same order of magnitude as the radii used in the asymptotic work) or a wider radii of $a/L = 0.2$ (radii that probably violates the assumptions of the asymptotic work). Clearly this is a very good level of convergence, but the same cannot be said for taller cylinders. Table 3.2 shows the upper bounds calculated for the first two eigenvalues at the point $\boldsymbol{\beta}L = (9\pi/10, 0)^T$ for when $d/h = 0.9$. Here $N = 2$ is sufficient for at least four significant figures, but even with $N = 12$ we have still not reached the level of convergence obtained with $N = 2$ for the short cylinders. Furthermore, the radii seems to have little effect on the speed of convergence implying that it is the cylinders' length that is the important variable in these calculations. Physically, this is because longer cylinders disturb the free surface (where most of the fluid motion happens) more than the shorter cylinders.

For bottom-mounted truncated cylinders in water of finite depth, a lower bound is created by considering an empty cell with depth equal to the gap for the original solution that we are attempting to bound (i.e. removing fluid from the original domain). An upper bound is provided

N	a/L	ΛL	
2	0.050	2.80749361764	3.44877240724
4	0.050	2.80749361764	3.44877240724
2	0.200	2.80427596862	3.44726474230
4	0.200	2.80427596862	3.44726474230

Table 3.1 FDBM short: Eigenvalues ΛL for wave propagation through a square array of short ($d/h = 0.2$) bottom-mounted cylinders in water of finite depth ($h/L = 1$).

N	a/L	ΛL	
2	0.050	2.79509653256	3.43520231075
4	0.050	2.79509215260	3.43518889113
6	0.050	2.79509196780	3.43518825987
8	0.050	2.79509196188	3.43518823659
10	0.050	2.79509196177	3.43518823600
12	0.050	2.79509196177	3.43518823599
2	0.200	2.59521236105	3.21637048083
4	0.200	2.59520294254	3.21606336956
6	0.200	2.59520258367	3.21606010131
8	0.200	2.59520256547	3.21606004666
10	0.200	2.59520256479	3.21606004553
12	0.200	2.59520256477	3.21606004547

Table 3.2 FDBM long: Eigenvalues ΛL for wave propagation through a square array of long ($d/h = 0.9$) bottom-mounted cylinders in water of finite depth ($h/L = 1$).

by considering an empty cell with the depth equal to the original depth (i.e. adding fluid to the original domain). As an example, lower and upper bounds at the point $\boldsymbol{\beta} L = (9\pi/10, 0)^T$ are contained within table 3.3 for a typical solution (i.e. a solution which we are trying to bound). The upper bound from the comparison principle is close to the upper bounds for the eigenvalues obtained as the cylinders get thinner (this is to be expected, given that the upper bound here is calculated by considering radii equal to zero, which is mathematically equivalent to infinitely thin cylinders). The calculated lower bound is, however, nowhere near the eigenvalues calculated for radii of $a/L = 0.5$, which is the largest radii that the geometry of the problem allows for. (Radii of $a/L = 0.5$ is chosen for illustrative purposes only: one should note that cylinders of this radii would be taking up an entire cell of the lattice – in the case of cylinders extending throughout the depth – or essentially describing a platform – in the case of truncated cylinders – and would hence no longer be describing the water-wave problem we set out to solve). However,

Description	h/L	d/L	a/L	ΛL	
Lower bound	0.1	N/A	0	0.778794465	1.148849427
Typical solution (thin cylinders)	1	0.9	0.05	2.795096533	3.435202311
Typical solution (wide cyldiners)	1	0.9	0.5	1.536830783	2.070015413
Upper bound	1	N/A	0	2.807707918	3.448873128

Table 3.3 FDBM: Lower and upper bounds for eigenvalues ΛL calculated using the comparison principle, along with typical solutions, for bottom-mounted cylinders in water of finite depth.

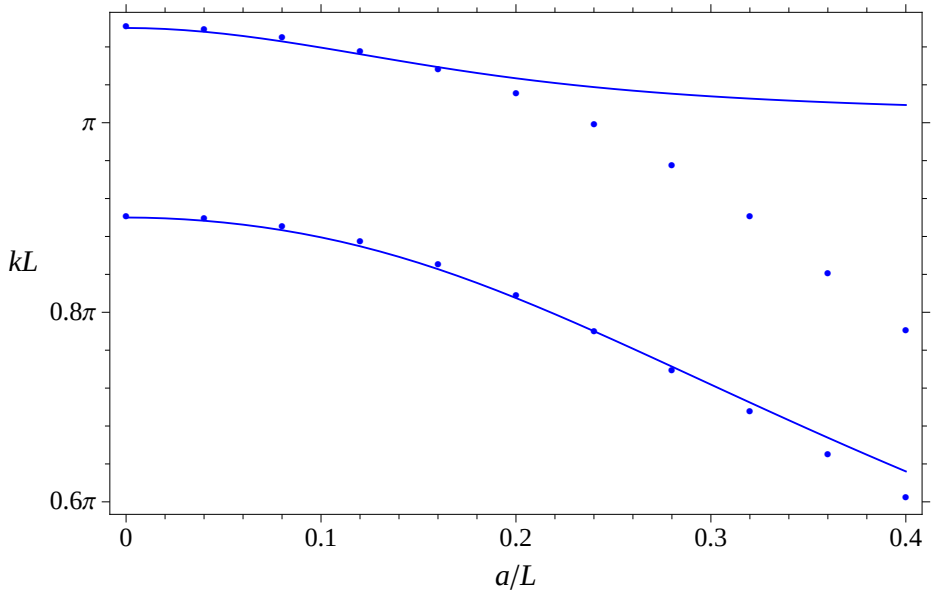

Figure 3.2 FDBM: Comparison of the asymptotic approximations (——) with the numerical solutions (· · ·) for bottom-mounted cylinders in water of finite depth ($h/L = 0.05$ and $d/h = 0.8$).

fortunately table 3.2 demonstrates that the convergence of the upper bounds for the eigenvalues (as calculated using the Rayleigh-Ritz method) for wide bottom-mounted truncated circular cylinders in water of finite depth is good enough that an application of the comparison principle is not necessary to make further comment about the reliability of the results obtained.

Figures 3.2 shows a comparison of the current numerical solutions with the approximations obtained using the method of matched asymptotic expansions (MAE) for bottom-mounted cylinders in water of finite depth at the point $\boldsymbol{\beta} L = (9\pi/10, 0)^T$. The asymptotic work assumed water of shallow depth so, for this reason, the depth we use in our numerical calculations is $h/L = 0.05$. Recall that the MAE solutions were obtained under the assumption that – among others – $a/L \ll 1$ and $kL = \text{ord}(1)$. Increasing a/L (so that, for fixed kL, ka increases) too much will violate the MAE assumptions meaning we would expect the asymptotic solutions to cease to agree with the numerical results (which, of course, have been calculated without making

N	a/L	d/L	ΛL	
2	0.05	0.2	2.81370237	3.456117993
4	0.05	0.2	2.813212619	3.455529271
6	0.05	0.2	2.812801759	3.455019076
8	0.05	0.2	2.812468392	3.454602032
10	0.05	0.2	2.812197723	3.454263596
12	0.05	0.2	2.811972411	3.453983094
2	0.2	0.2	2.742732854	3.690081574
4	0.2	0.2	2.718540105	3.662469469
6	0.2	0.2	2.711379388	3.647983754
8	0.2	0.2	2.709513799	3.640841262
10	0.2	0.2	2.70857744	3.637897079
12	0.2	0.2	2.706882165	3.636710581
2	0.05	0.9	2.806586895	3.449365785
4	0.05	0.9	2.806091424	3.448769629
6	0.05	0.9	2.805676678	3.448257252
8	0.05	0.9	2.805339939	3.447838366
10	0.05	0.9	2.805066402	3.44749836
12	0.05	0.9	2.80483863	3.447216561
2	0.2	0.9	2.604512281	3.598144953
4	0.2	0.9	2.569022738	3.580969025
6	0.2	0.9	2.550532702	3.572496405
8	0.2	0.9	2.538945395	3.567478035
10	0.2	0.9	2.530895416	3.564197628
12	0.2	0.9	2.524806959	3.561958362

Table 3.4 FDSP: Eigenvalues ΛL for wave propagation through a square array of short and long surface-piercing cylinders in water of finite depth ($h/L = 1$).

assumptions on the size of a/L). Sure enough figure 3.2 demonstrates a reasonable agreement in the MAE solutions for ka up to approximately 0.65 (corresponding to, say, $a/L \approx 0.28$ and $kL \approx 0.74\pi$ for the lower branch or $a/L \approx 0.2$ and $kL \approx 1.04\pi$ for the upper branch).

3.5.1.2 Finite depth: surface-piercing truncated cylinders

Table 3.4 shows a particularly poor convergence of the upper bounds for the eigenvalues calculated using the Rayleigh-Ritz method for surface-piercing truncated cylinders in water of finite depth. (At least, the convergence is poor when compared to the quick convergence for bottom-mounted cylinders). We gain no more than a couple of significant figures of agreement as the truncation level is increased up to $N = 12$, seemingly regardless of whether we are considering thin, wide, short or tall cylinders. That said, convergence to two significant figures for ΛL

Description	d/L	a/L	ΛL	
Lower bound	1	0.05	2.806490197	3.449329909
Typical solution	0.9	0.05	2.806586895	3.449365785
Upper bound	0	0.05	2.828057249	3.475207933

Table 3.5 FDSP: Lower and upper bounds for eigenvalues ΛL calculated using the comparison principle, along with a typical solution, for surface-piercing cylinders ($a/L = 0.05$) in water of finite depth ($h/L = 1$)

provides us with solutions for kL – upon using equation (3.4.16) – that are reasonable enough for the scale of the plots contained within this results section. Figure 3.3 shows a comparison of the current numerical solutions with the approximations found using MAE at the point $\boldsymbol{\beta} L = (9\pi/10, 0)^T$. A reasonable agreement between the numerical solutions and the MAE solutions is demonstrated for ka up to approximately 0.4 (corresponding to, say, $a/L \approx 0.14$ and $kL \approx 0.88\pi$ for the lower branch or $a/L \approx 0.12$ and $kL \approx 1.1\pi$ for the upper branch).

Lower and upper bounds calculated using the comparison principle are given in table 3.5 for surface-piercing cylinders in water of finite depth. Bearing in mind that the free surface cannot be changed when applying the comparison principle, we are unable to amend the radii of the cylinders to obtain the bounds. The bounds, however, can be obtained by adding fluid to or removing fluid from the domain which in turn is done by changing the length of the cylinders. We calculate the lower bound by extending the cylinder's length throughout the depth (i.e. remove fluid from the domain) and calculate the upper bound by setting the length of the cylinder to zero (i.e. adding fluid to the domain).

In comparing the results obtained for bottom-mounted and surface-piercing cylinders, we note that for bottom-mounted cylinders the MAE expansions seem to be closer to the numerical results for a higher value of ka. One would expect that a bottom-mounted cylinder would affect a plane wave less than one which pierces the free surface, because most of the fluid motion happens on the free surface. With a much simpler free surface for bottom-mounted structures, there is less approximating taking place in the solutions arising from MAE (see equation 2.3.44 and note that the term in W disappears for bottom-mounted cylinders). We should therefore not be surprised by the apparent greater agreement of the MAE solutions for bottom-mounted cylinders. Furthermore, for the bottom-mounted cylinders, the calculations are much easier because I_2, given in equation (3.4.10), reduces to zero on the free surface when the cylinders aren't piercing the free surface and hence the calculation of h_{klmn} is simplified.

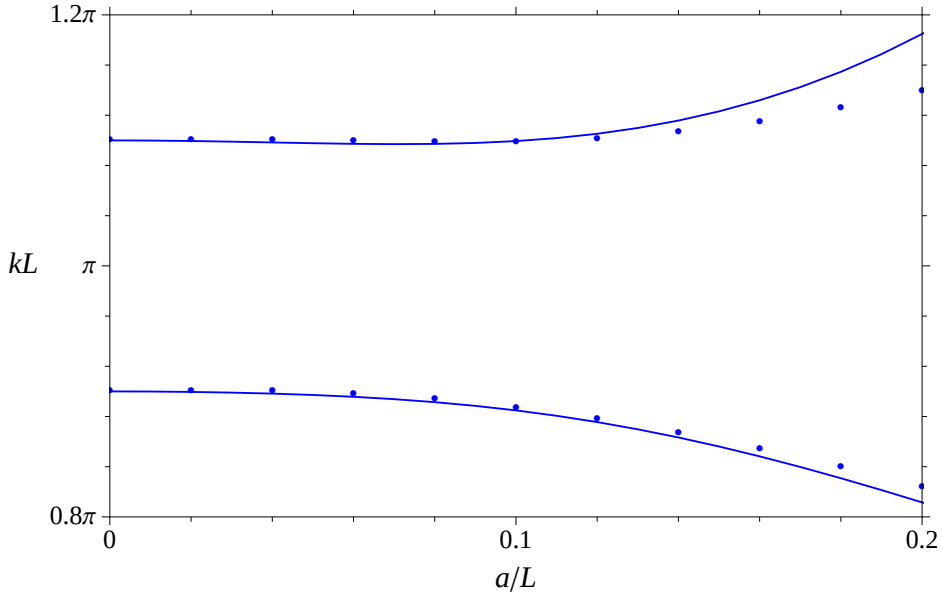

Figure 3.3 FDSP: Comparison of the asymptotic approximations (——) with the numerical solutions (· · ·) for surface-piercing cylinders in water of finite depth ($h/L = 0.05$ and $d/h = 0.9$).

3.5.1.3 Deep water

Again, due to the nature of the more complicated free surface for surface-piercing structures, the upper bounds for the eigenvalues calculated using the Rayleigh-Ritz method do not converge as quickly as the bottom-mounted cylinders in water of finite depth, as is demonstrated in table 3.6. Table 3.7 shows the lower and upper bounds calculated using the comparison principle (fluid is removed from the domain by extending the length of the cylinder to infinity in its limit and fluid is added to the domain by reducing the length of the cylinder to a disc on the free surface, providing a lower and upper bound respectively). Figure 3.4 shows the comparison between the MAE and numeric results at the point $\boldsymbol{\beta}L = (9\pi/10, 0)^T$. Reasonable agreement is demonstrated for ka up to approximately 0.2 (corresponding to, say, $a/L \approx 0.08$ and $kL \approx 0.9\pi$ for the lower branch or $a/L \approx 0.06$ and $kL \approx 1.1\pi$ for the upper branch).

3.5.2 Comparison with asymptotic local band gaps

Figures 3.5 and 3.6 show how a localised band gap depends on the radii and length of cylinders for bottom-mounted and surface-piercing cylinders respectively. The parameters – and area of focus, i.e. around the point $(kL, q_1L, q_2L) = (\pi, \pi, 0)$ – have all been chosen so that a direct comparison with the band gaps presented in chapter 2 is possible. Qualitatively, on comparing the solutions here with their counterparts obtained using MAE (see figures 2.4 and 2.5) we see the same behaviour: a band gap is introduced (and widens) as a/h increases from 0; only the

N	a/L	d/L	$\Lambda L = kL$	
2	0.05	0.05	2.843014242	3.475137071
4	0.05	0.05	2.84263031	3.474626339
6	0.05	0.05	2.842303572	3.474207223
8	0.05	0.05	2.842029431	3.473850664
10	0.05	0.05	2.841803102	3.473552434
12	0.05	0.05	2.84161362	3.473300432
2	0.2	0.05	2.961565049	3.81530871
4	0.2	0.05	2.9575804	3.80619052
6	0.2	0.05	2.954150137	3.801401641
8	0.2	0.05	2.952387549	3.798945297
10	0.2	0.05	2.95100335	3.796872605
12	0.2	0.05	2.950083918	3.795553418
2	0.05	0.9	2.826370353	3.4562405
4	0.05	0.9	2.825875223	3.455644688
6	0.05	0.9	2.825460609	3.455132562
8	0.05	0.9	2.825123982	3.4547139
10	0.05	0.9	2.824850588	3.454374111
12	0.05	0.9	2.824622995	3.454092527
2	0.2	0.9	2.62729939	3.602667943
4	0.2	0.9	2.592173054	3.585784808
6	0.2	0.9	2.574024597	3.577495782
8	0.2	0.9	2.562728227	3.572605094
10	0.2	0.9	2.554928836	3.569420496
12	0.2	0.9	2.548928379	3.567080263

Table 3.6 DW: Eigenvalues $\Lambda L = kL$ at $\boldsymbol{\beta} L = (9\pi/10, 0)^T$ for wave propagation through a square array of long bottom-mounted truncated circular cylinders (height $d/h = 0.2, 0.9$, radii a/L) in water of finite depth.

lower edge is affected by the length of the cylinder d/L; only the upper edge is affected by whether the cylinders are surface piercing or bottom mounted. One can, however, notice small discrepancies (that we will shortly explain) between the local band gap calculated numerically and the local band gap approximated using MAE: the numerical results do not seem to agree with the asymptotic solutions in these somewhat zoomed-in ranges (when, say, compared to the range used in figure 3.3) of kL. For example, the lower branch of figure 3.6a for $a/h = 1$ approximately passes through $(q_1 L, kL) = (\pi, 0.993\pi)$; the solutions obtained using MAE suggest the equivalent result is approximately $(q_1 L, kL) = (\pi, 0.988\pi)$. As stated, this discrepancy can however be explained: around this point, $\epsilon = kh \approx \pi/20 \approx 0.16$, whilst the difference between the asymptotic and numerical solutions is approximately $0.005\pi \in (\epsilon^2, \epsilon^3)$, which is approximately

Description	d/L	$\Lambda L = kL$	
Lower bound	∞	2.826232648	3.45618596
Typical solution	1	2.826310872	3.456213305
Typical solution	0.9	2.826370353	3.4562405
Typical solution	0.05	2.843014242	3.475137071
Upper bound	0	2.847896173	3.482154942

Table 3.7 DW: Lower and upper bounds for eigenvalues $\Lambda L = kL$ calculated using the comparison principle, along with typical solutions, for truncated cylinders ($a/L = 0.05$) in deep water.

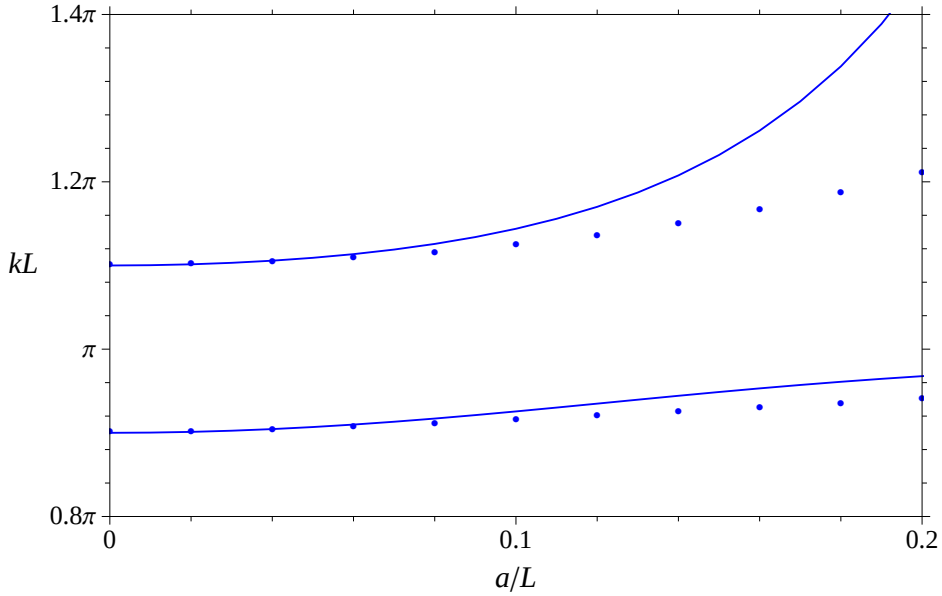

Figure 3.4 DW: Comparison of the asymptotic approximations (——) with the numerical solutions (· · ·) for truncated cylinders ($d/L = 0.05$) in deep water.

the size of higher order terms that were not included within the approximate solutions.

Further, it is evident from the results presented in figure 3.7 that the agreement between the numerical and asymptotic results start to improve as we move further away from the point $(kL, q_1L, q_2L) = (\pi, \pi, 0)$. The asymptotic solutions are perturbations from the no-cylinder case represented by the poles of the lattice sums; larger perturbations are occurring at the point $(kL, q_1L, q_2L) = (\pi, \pi, 0)$ (i.e. more is happening, a band gap is being introduced).

Figure 3.8 shows how a localised band gap depends on the radii and length of cylinders in the case of surface piercing cylinders in deep water. Again the parameters – and area of focus, i.e. around the point $(kL, q_1L, q_2L) = (\pi, \pi, 0)$ – have all been chosen so that a direct comparison with the band gaps presented in chapter 2 is possible. We should note that a/L represents the characteristic size of the structures for the asymptotic solutions; we were not specifically

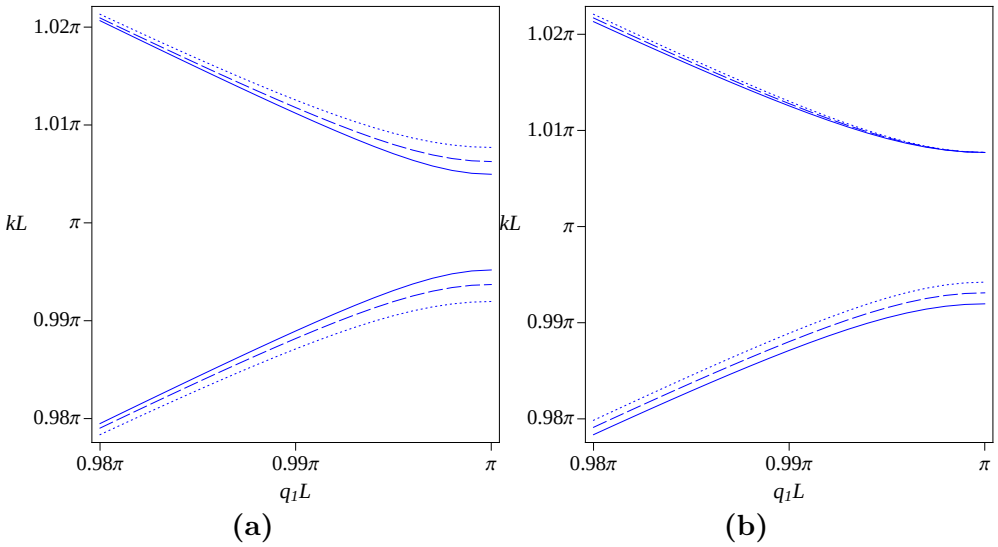

Figure 3.5 FDSP: Two plane waves for surface-piercing cylinders in water of finite depth for $h/L = 0.05$: (a) kL *vs.* q_1L for fixed $d/h = 0.8$ with $a/h = 0.8$ (——) , $a/h = 0.9$ (– – –), $a/h = 1$ (· · · · ·) and (b) kL *vs.* q_1L for $a/h = 1$ with $d/h = 0.8$ (——), $d/h = 0.7$ (– – –), $d/h = 0.6$ (· · · · ·).

looking at cylinders there and the current numerical results allow us to see the effect the depth of submergence of the cylinder has on the solutions (see figure 3.8b). For a reasonable comparison between the asymptotic and numerical solutions, the results shown here have for the most part been generated using d/L to be approximately $2a/L$ (only approximately, because naturally we wish to only vary *one* parameter to study its affect on the band gap).

Whilst the upper edge of the band gap behaves in the same way (that is, the frequency increases as a/L increases) for the numerical and asymptotic (see figure 2.7a) solutions, the numerical solutions here demonstrate that there is a point on the lower branch of the band gap where the curves of varying radii cross. As d/L is decreased through $d/L = 0.05$ (figure 3.9a), the crossing point where the frequencies coincide for varying radii moves closer towards $q_1L = \pi$, so that for $d/L = 0$ (representing infinitesimal discs on the free surface and shown in figure 3.9b) we have that there is no crossing point. Having no crossing point is the behaviour that was demonstrated by the asymptotic solutions in figure 2.7a. In obtaining the asymptotic solutions of chapter 2, we assumed that the depth of submergence was small compared to the deep water and could therefore be neglected. It therefore makes sense that the discs on the free surface here correspond to the structures investigated in the asymptotic work.

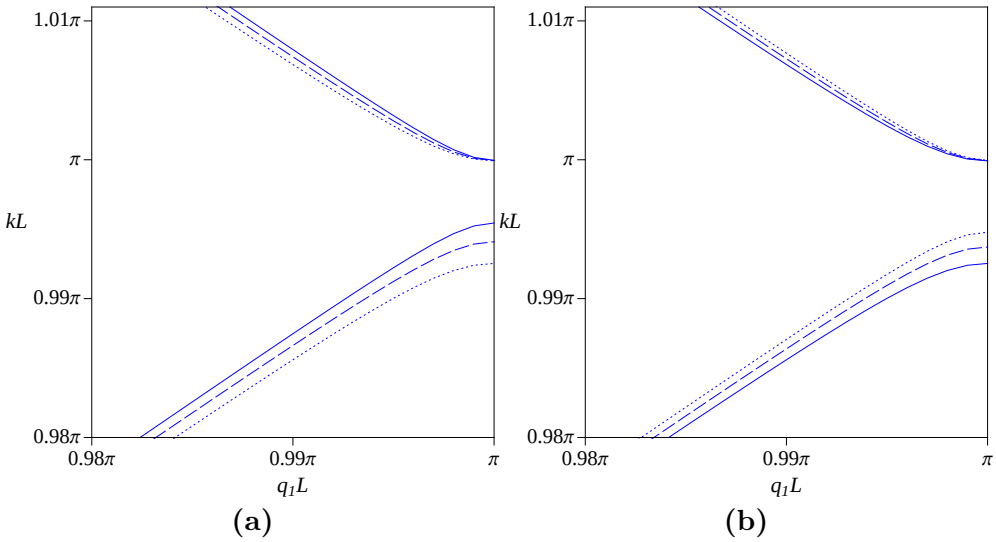

Figure 3.6 FDBM: Two plane waves for bottom-mounted cylinders in water of finite depth for $h/L = 0.05$: (a) kL *vs.* q_1L for fixed $d/h = 0.8$ with $a/h = 0.8$ (——) , $a/h = 0.9$ (– – –), $a/h = 1$ (· · · · ·) and (b) kL *vs.* q_1L for $a/h = 1$ with $d/h = 0.8$ (——), $d/h = 0.7$ (– – –), $d/h = 0.6$ (· · · · ·).

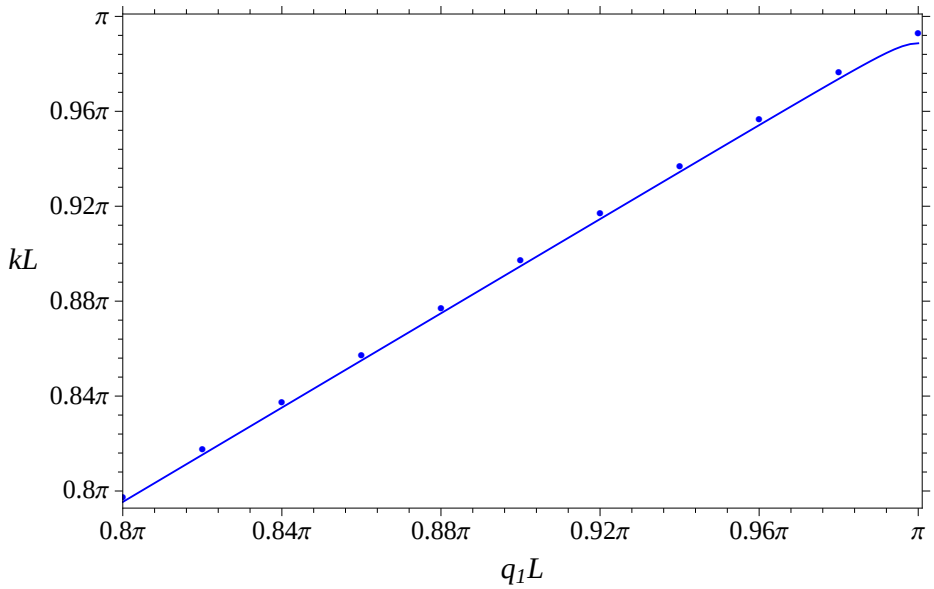

Figure 3.7 FDBM: Comparison (as q_1L varies) of the asymptotic approximations (——) with the numerical solutions (· · ·) for bottom-mounted cylinders in water of finite depth ($h/L = 0.05$, $a/h = 1$ and $d/h = 0.8$) using truncation parameter $N = 6$.

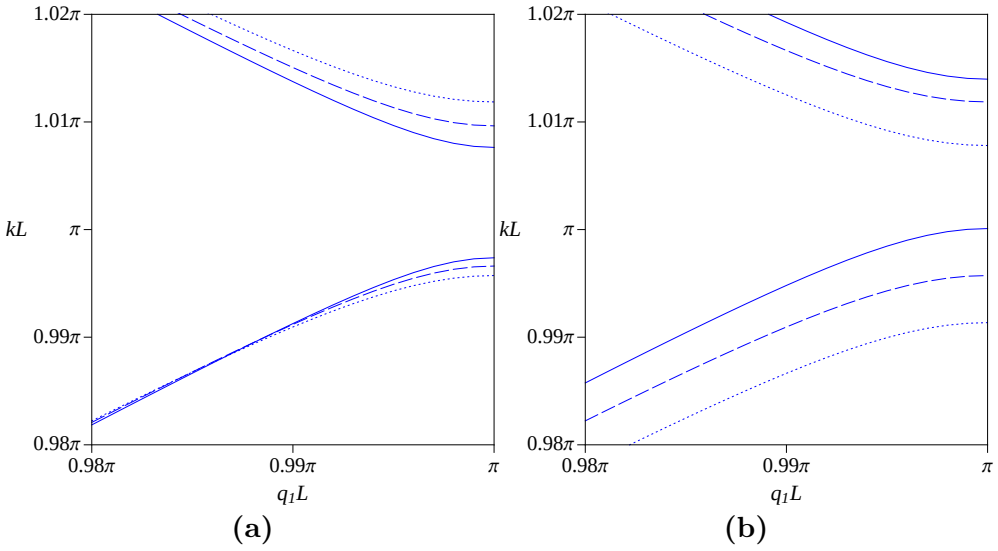

Figure 3.8 DW: Two plane waves for surface-piercing cylinders in deep water: (a) kL *vs.* q_1L for fixed $d/L = 0.1$ with $a/L = 0.04$ (——) , $a/L = 0.045$ (– – –), $a/L = 0.05$ (· · · · · ·) and (b) kL *vs.* q_1L for $a/L = 0.05$ with $d/L = 0.01$ (——), $d/L = 0.05$ (– – –), $d/L = 0.6$ (· · · · · ·).

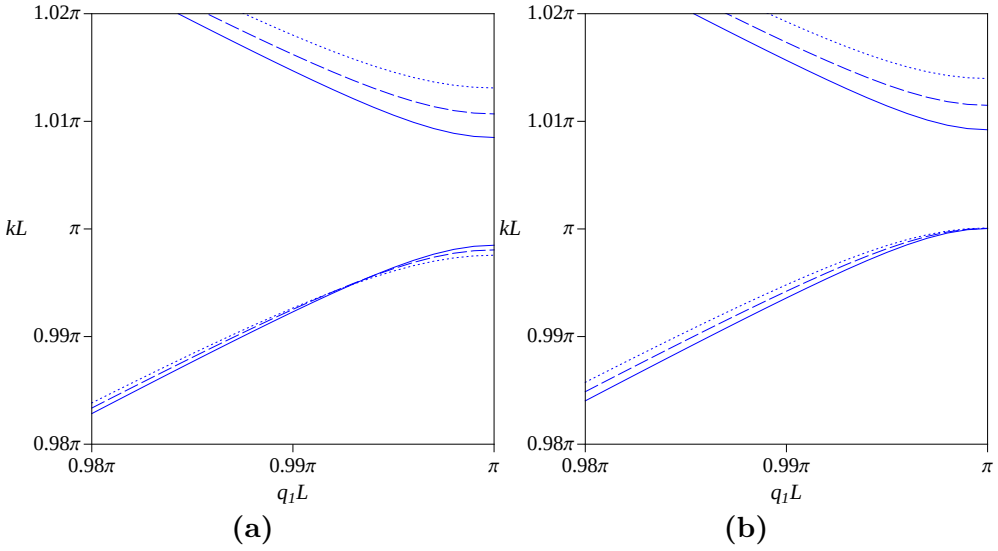

Figure 3.9 Two plane waves for (a) surface-piercing cylinders in deep water showing kL *vs.* q_1L for fixed $d/L = 0.05$ with $a/L = 0.04$ (——) , $a/L = 0.045$ (– – –), $a/L = 0.05$ (· · · · · ·) and (b) horizontal discs lying on the free surface showing kL *vs.* q_1L for fixed $d/L = 0$ with $a/L = 0.04$ (——) , $a/L = 0.045$ (– – –), $a/L = 0.05$ (· · · · · ·).

3.5.3 Negative refraction and complete band diagrams

It has been noted elsewhere in this thesis that an advantage of the numerical approach used in this chapter over the asymptotic work of chapter 2 is the ability to construct what we call complete band diagrams (that is, a diagram that shows the frequency around the *whole* edge of the reduced Brillouin zone; the asymptotic work – whilst giving us the ability to write explicit approximations – only realistically afforded us the ability to create localised band diagrams). To observe the phenomenon of negative refraction – which has been observed in different contexts such as water-waves [23] and acoustics [24] – a complete band diagram is useful to understand the band gaps that the material under investigation exhibits [25].

Waves undergo refraction when they pass through the boundary separating one medium from another. Usually the refracted wave lies on the opposite side of the surface normal to that which the incident wave lies on; we refer to such refraction as *positive* refraction. However *negative* refraction has been observed both theoretically [43, 44] and experimentally [45, 46]. Negative refraction occurs when the incident and the refracted wave both lie on the same side of the surface normal. All angle negative refraction (AANR) is when all incident angles are negatively refracted. As part of the presentation of our numerical results, we will be considering the geometry of the strip array required to observe AANR. Alongside the complete band diagrams, we use the corresponding so called constant frequency contours (CFCs) (a contour plot showing the frequencies for all wave vectors inside the Brillouin zone, i.e. not just its boundary) to produce schematic diagrams which indicate how an incident wave is refracted.

The approach of this subsection is to begin by describing qualitatively (i.e. for a general, unspecified geometry of structures) how the complete band diagrams and corresponding CFCs are used to construct schematic diagrams to determine how an incident wave is refracted: the two schematic diagrams we give as examples show both positive and negative refraction respectively. Once this process has been explained, we will be in a position to start focusing on particular structural geometries and we begin by looking at cylinders that extend throughout the depth: we give a detailed analysis of the geometric conditions required for AANR. We see that (among other conditions) one necessary condition for negative refraction is that a complete band gap is required (i.e. that is to say that there must exist a range of frequencies that never occur around the whole edge of the Brillouin zone). This in turn motivates us to search for complete band gaps in the case of truncated cylinders in water of finite depth: we present complete band diagrams showing whether or not a complete band gap exists.

3.5.3.1 Band diagrams, constant frequency contour plots and schematic diagrams

The point of this sub-subsection is not to quantify any results just yet: it is simply to explain the process of using a band diagram and its corresponding CFCs to produce the schematic diagrams that, in turn, allow for an easy representation of what happens to a given wave incident on an array of structures. We don't specify the geometry of the structures (i.e. for the purposes of this discussion, it is not important whether the cylinders extend throughout the depth or are truncated), all we say is that the band gap diagram and subsequent CFCs correspond to an array of structures which exhibits AANR (for some frequencies).

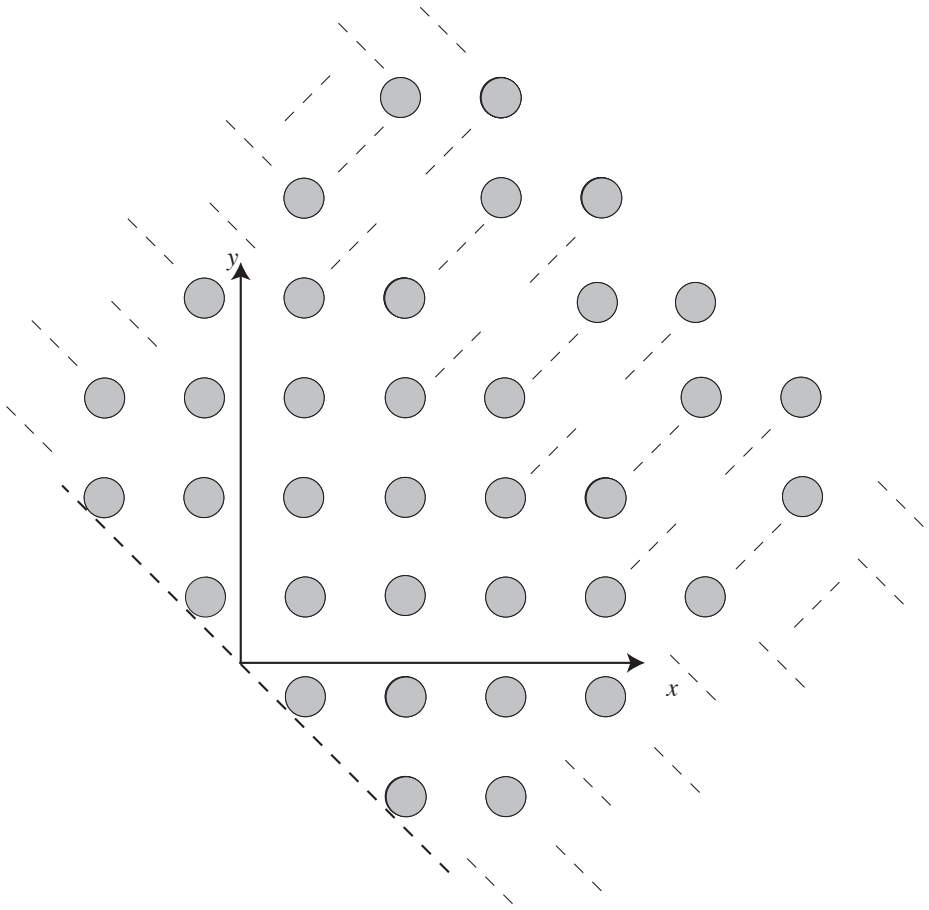

Figure 3.10 Orientation of the strip array; an incident wave acting on the left edge of the array in the direction of $(x, y) = (1, 0)$ – i.e. the same direction as phase vectors lying on the ΓX boundary in the first Brillouin zone – is non-normal to the array.

For consistency with other authors, we choose to have the open water / strip array surface interface (i.e. left edge of the array, as viewed from above) lying at an angle of $\pi/4$ radians (in an anti-clockwise direction) from the y-axis so that the surface interface between the open water and the edge of the strip array lies perpendicular to $M\Gamma$, as in figure 3.10. Orientating the strip array in this way means that by choosing an incident wave which propagates in the direction

of the ΓX Brillouin boundary (as we will do for ease of presentation), it will be incident on the array's left edge at a non-normal angle. For a given incident wave direction, we seek to understand the conditions required for AANR.

To understand negative refraction, one needs to be able to make use of CFCs. The idea is to choose a frequency that corresponds to an incident wave in open water and a refracted wave inside the array. We will demonstrate how refraction moves from positive to negative as the frequency changes. We begin by choosing a fixed wavenumber $kL = kL_1$; this value of kL_1 corresponds to the two phase vectors $\boldsymbol{\beta} L_1^I$ (in open water) and $\boldsymbol{\beta} L_1^S$ (inside the strip array). Figure 3.11a shows the CFC diagram for open water, whilst 3.11b shows the CFC diagram inside the array. For each chosen value of kL, we draw schematically the directions of the refracted wave and, more specifically, whether it has been positively or negatively refracted.

Let us give a step-by-step account of the method described in [30, Ch. 10] and [23], which describes how to draw the CFC for kL_1 as given in figure 3.11c:

1 For our chosen frequency kL_1, superimpose the (black) contour for the incident medium (open water) and the (red) contours for the transmitted medium (inside the array) onto the same axes;

2 Mark on the incident wave $\boldsymbol{\beta} L_1^I$;

3 Draw a line (green, dashed) that goes through $\boldsymbol{\beta} L_1^I$ and is perpendicular to the surface interface (between open water and the strip array);

4 The place(s) where this (green, dashed) line intersects the (red) contours for inside the strip array determines the refracted wave(s) $\boldsymbol{\beta} L_1^S$; the refracted waves act perpendicular to the (red) contour and in the direction of increasing frequency. Note that although the red contours may be intersected in more than one place, it may not correspond to distinct refracted waves; it might, for example, violate boundary conditions for example that the only incoming wave is the incident wave or it might be an equivalent wave that has already been accounted for in a different Brillioun zone.

Thus figure 3.11c corresponds to positive refraction. For a wavenumber fixed at position kL_2, with corresponding phase vectors $\boldsymbol{\beta} L_2^I$ and $\boldsymbol{\beta} L_2^S$, we employ the same methods to create another diagram as shown in figure 3.11d, which corresponds to negative refraction.

The value of kL where the 'jump' from positive refraction to negative refraction occurs is important to us, because it gives a range of frequencies for which negative refraction may occur.

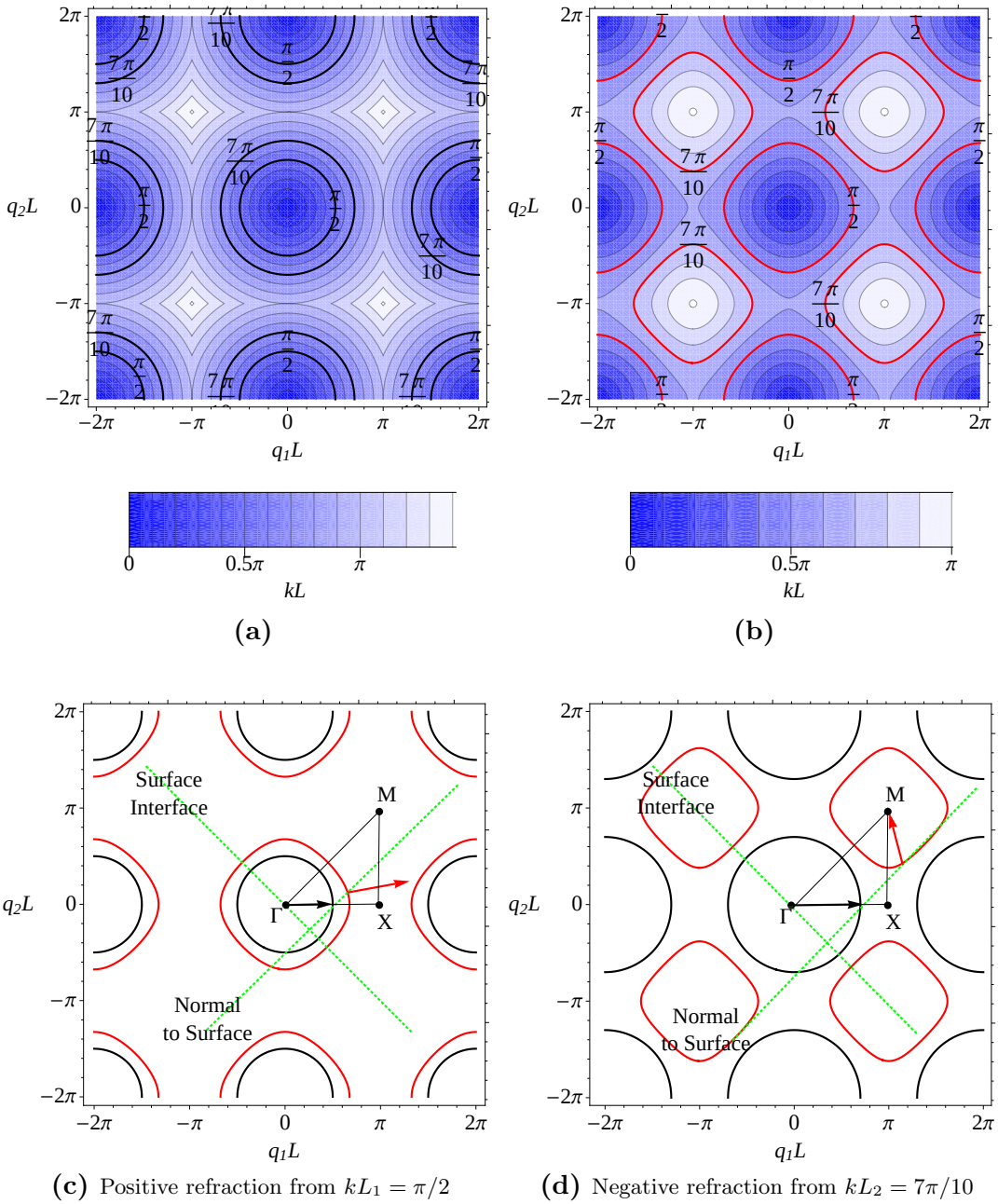

Figure 3.11 Constant frequency contours for (a) open water and (b) inside an array, with selected contours highlighted. The constant frequency contours for open water and inside an array are superimposed onto the same set of axes for (c) $kL_1 = \pi/2$ and (d) $kL_2 = 7\pi/10$ in (c) and (d)

The minimum of this range is the value of kL for which $\boldsymbol{\beta}L = (\pi, 0)^T$ (which coincides with the lower branch of the local band gap) and has a maximum of the value of kL for which $\boldsymbol{\beta}L = (\pi, \pi)$ (which coincides with the lowest branch of the global band gap for the geometry under consideration). Below this frequency, CFCs are centred on the Γ point and above it CFCs are centred at the M point; this has been demonstrated in [23] and [25], for example.

3.5.3.2 Cylinders extending throughout the depth

It is thus evident that an investigation of negative refraction becomes an investigation of how the contours behave. This sub-subsection looks at the behaviour of the contours for the specific case of cylinders extending throughout the depth and how the radii of the cylinders affect the contours.

As we have seen, when we introduce cylinders, we are able to choose frequencies such that the contour corresponding to the refracted wave (inside the array) is centred on M. However, it is evident that simply introducing cylinders (by increasing a/L from zero) so that there exists contours centred on M is not enough to show that a wave has been negatively refracted: the line that goes through $\boldsymbol{\beta}L_1^I$ and is perpendicular to the surface interface (the green dashed line in the schematic diagrams) must at least meet a refracted wave contour. If it doesn't meet (as in figure 3.12) then that means that we are in a localised band gap (for fixed $q_2L = 0$) and the incident wave does not propagate through the array.

Figure 3.12 demonstrates that for smaller cylinders, where $a/L = 0.15$, there is no such negative refraction for our chosen incident wave. We need to choose a high enough frequency (close to $kL = \pi$, corresponding to an incident wave $\boldsymbol{\beta}L^I = (q_1L, 0)$ for q_1L also close to π) to ensure that the refracted wavenumber lies inside XM on the band diagram shown in figure 3.12a. As is shown in figure 3.12b we have chosen a frequency large enough such that the associated contour is centred on M. However, the schematic diagrams shown in figure 3.12c demonstrates that the contours do not indicate negative refraction: this is because, for our incident wave in the direction of $(1, 0)^T$, the line going through the incident wave and acting perpendicular to the surface interface does not go through the corresponding contour for the incident wave. However, when $a/L = 0.35$, it is becomes apparent that we can select demonstrate negative refraction as shown in figure 3.13: figure 3.13a shows the band diagram, figure 3.13b shows the refracted contours with a chosen frequency highlighted, which is then used to create the schematic diagram shown in figure 3.13c.

Other than giving us contours large enough, there are other – perhaps more subtle – changes

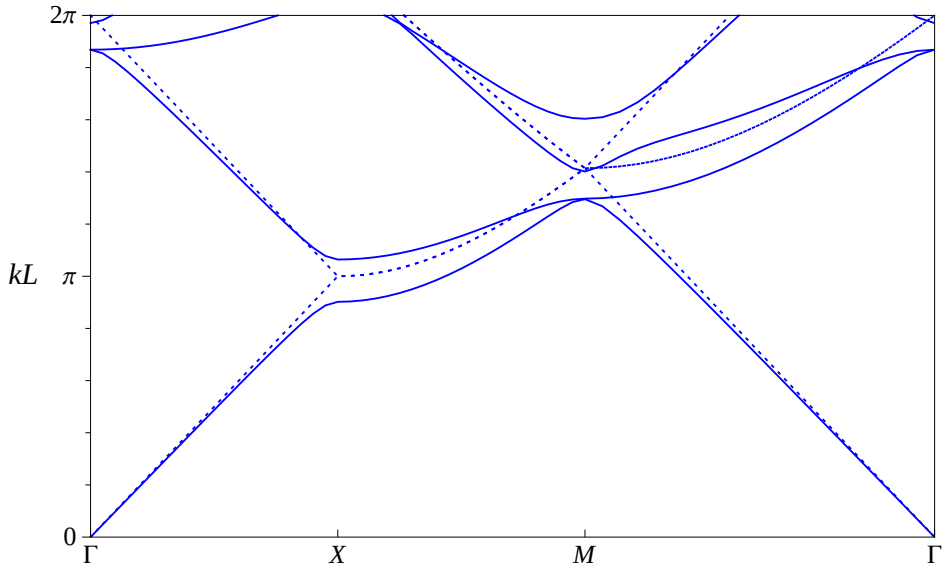

(a) Band diagram for cylinders of width $a/L = 0.15$ (——) and $a/L = 0$ (· · · · · ·) (i.e. open water).

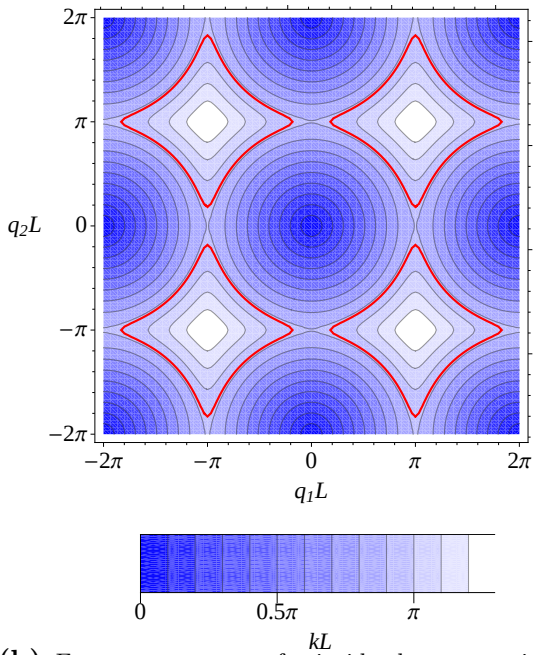

(b) Frequency contours for inside the array, with $kL = 0.92\pi$ highlighted.

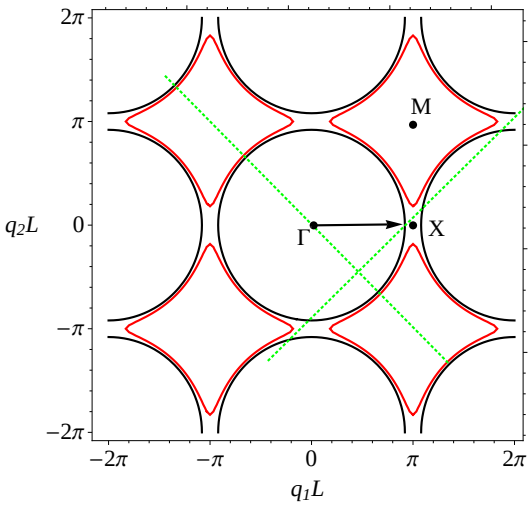

(c) Schematic diagram showing frequency contours at $kL = 0.92\pi$ for outside (black) and inside (red) the array.

Figure 3.12 Frequency diagrams for cylinders of radii $a/L = 0.15$, which extend throughout the depth.

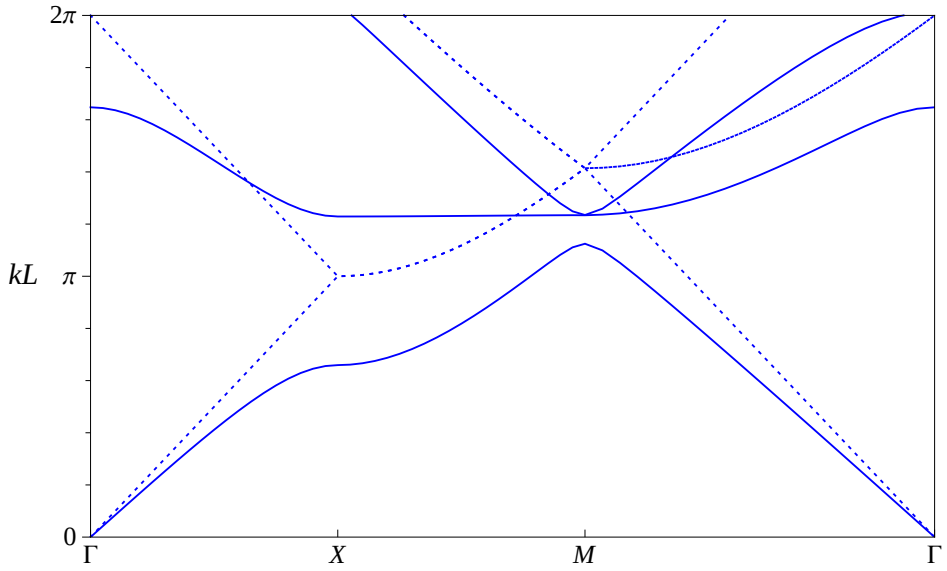

(a) Band diagram for cylinders of width $a/L = 0.35$ (——) and $a/L = 0$ (· · · · · ·) (i.e. open water).

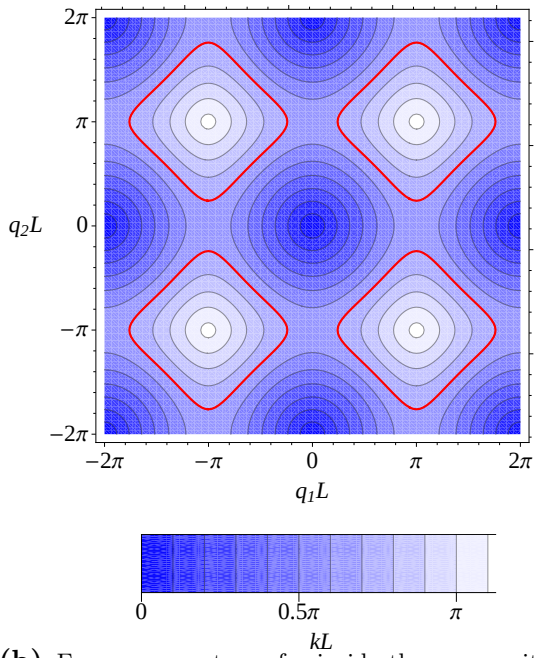

(b) Frequency contours for inside the array, with $kL = 0.7\pi$ highlighted.

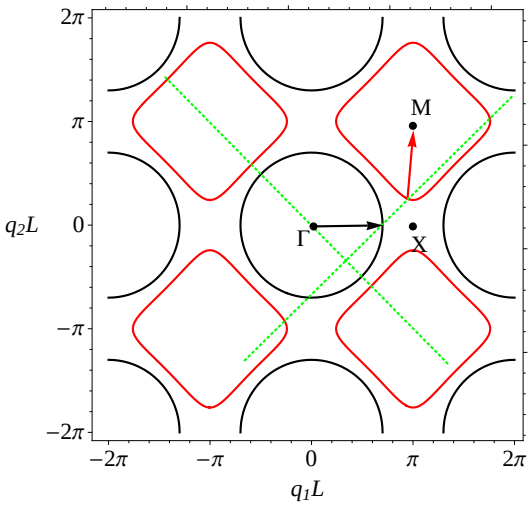

(c) Schematic diagram showing frequency contours at $kL = 0.7\pi$ for outside (black) and inside (red) the array.

Figure 3.13 Frequency diagrams for cylinders of radii $a/L = 0.35$, which extend throughout the depth.

in the geometry that using wider cylinders affords us. Comparing the refracted contours between figures 3.12b and 3.13b, one sees that they go from being concave (for narrow cylinders) to convex (for wider cylinders). Furthermore, comparing the band gap diagrams in figures 3.12a and 3.13a, we see that there is not a complete band gap for the narrow cylinders, but there is for the wider cylinders. By complete band gap we mean there are a range of frequencies that never occur around the whole edge of the Brillouin zone. Thus we have conjectured that there are three conditions for AANR, namely (i) a complete band gap exists; (ii) the contours associated with the refracted wave are convex, which ensures the refracted wave is pointing in the correct direction; (iii) the contours associated with the refracted wave need to be large enough. It just so happens that as the cylinders become sufficiently large, these three conditions are more easily satisfied.

We must point out that we've said nothing about looking at incident waves acting in a different direction for our chosen frequency and whether or not they give rise to negative refraction: the point of this exercise has been to understand how the occurrence of AANR is related to a given incident wave, and to hence motivate us to look at complete band gaps. The current literature does not appear to have made this relationship between the complete band gap and negative refraction as explicit as this.

3.5.3.3 Truncated cylinders

The relationship between negative refraction and complete band gaps is what motivates us to search for complete band gaps for truncated cylinders. Figure 3.14 shows a complete band gap for the case of surface-piercing structures in water of finite depth: figure 3.14a shows the band gap being introduced for approximately $a/h = 0.3$ when the length of the cylinders is fixed to $d/h = 0.8$, whilst figure 3.14b shows that changing the length of the cylinders whilst keeping the radii fixed at $a/h = 0.35$ does not have such a big effect to whether or not the band gap is present. Figure 3.15 suggests that there are no complete band gaps for the case of bottom-mounted cylinders. In both figures presented there, we have chosen the length of cylinders to be long to make their presence largest: in figure 3.15a increasing the cylinders' radii up to the maximum mathematically allowed ($a/L = 0.5$) doesn't introduce a complete band gap, whilst figure 3.15b demonstrates that there is still no complete band gap for bottom-mounted cylinders with the largest possible radii in shallow water (so that $a/h = 10$).

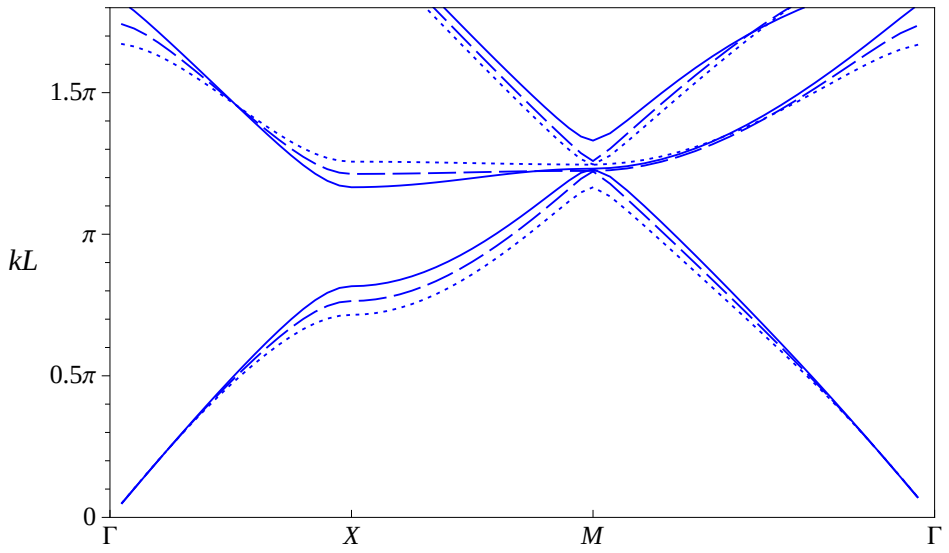

(a) kL *vs.* βL for fixed $d/h = 0.8$ and $h/L = 1$ with $a/h = 0.25$ (——) , $a/h = 0.3$ (– – –), $a/h = 0.35$ (· · · · · ·).

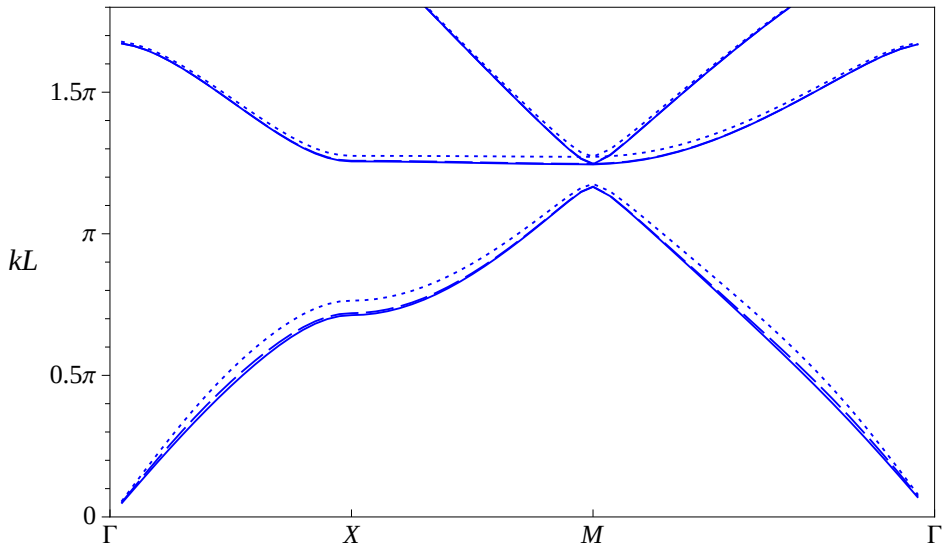

(b) kL *vs.* βL for fixed $a/h = 0.35$ and $h/L = 1$ with $d/h = 0.9$ (——), $d/h = 0.7$ (– – –), $d/h = 0.4$ (· · · · · ·).

Figure 3.14 Complete band diagrams for surface-piercing cylinders in water of finite depth.

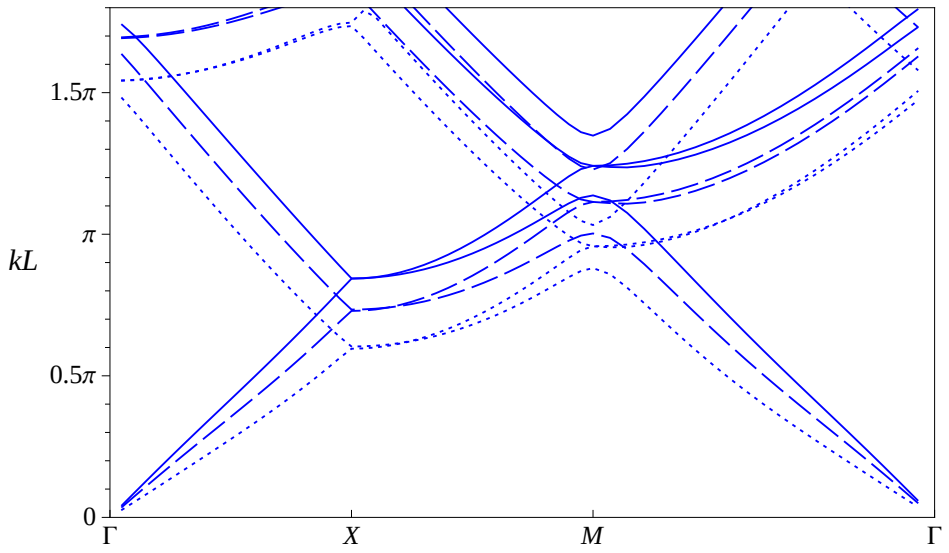

(a) *kL vs.* βL for fixed $d/h = 0.9$ and $h/L = 1$ with $a/h = 0.3$ (——) , $a/h = 0.4$ (– – –), $a/h = 0.5$ (· · · · · ·).

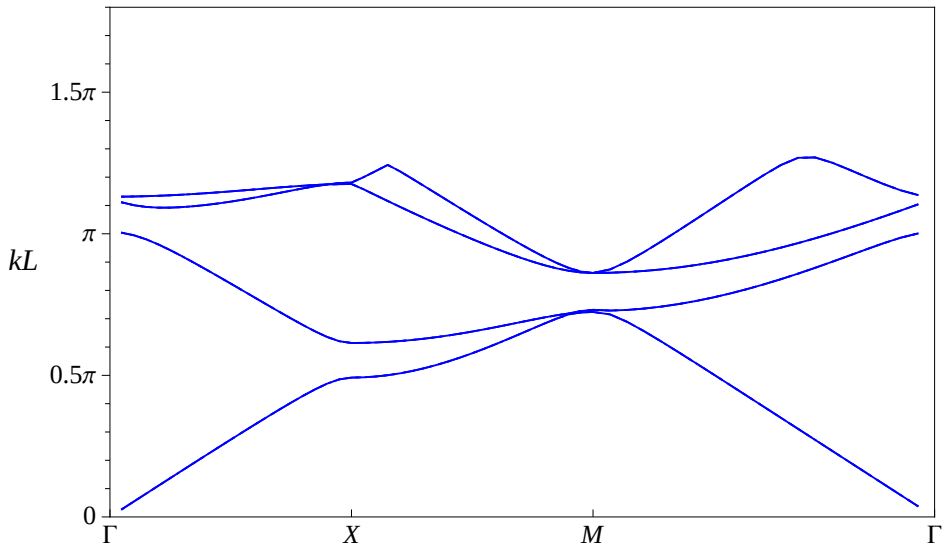

(b) *kL vs.* βL for the first four eigenvalues for fixed $a/L = 0.5$, $h/L = 0.05$ and $d/h = 0.9$ (——).

Figure 3.15 Complete band diagrams for bottom-mounted cylinders in water of finite depth.

Chapter 4

Strip array: methods of matched asymptotic expansions & multiple scales

4.1 Introduction

We consider here water-wave propagation through structures arranged in a two-dimensional array stretching to infinity in one horizontal direction but of finite width in the other – we call this a strip array – using the method of multiple scales and matched asymptotic expansions. By having the array wide enough (in the horizontal direction that is of finite length), we expect there to be a clear analogy between the solutions found here with the infinite array problem; in the same sense, the solutions inside the strip array are perturbations from the plane waves that exist in the absence of any structures. By introducing a slow scale to consider with the fast scales we essentially homogenise a complex geometry - the strip array of structures - to a simpler one; the slow scale describes how the waves change as they propagate through the array of cylinders (we would expect, for example, the waves to only gradually loose their amplitude as it moved through the array). In the infinite array work, we were able to find localised band gaps and hence determine the frequencies of waves which were *allowed* to exist in an array of structures. Now that we are looking at a strip array (where it makes sense to talk of an incident wave) we can consider what happens when we give an incident wave a frequency that falls within these band gaps: as per [30, page 53], adding an edge to an infinite array will allow us to sustain an evanescent mode. Our results will be presented alongside the results from our infinite array solutions, so we can see the relationship between the solutions.

We look first at the case of shallow water by extending the methods found in [17], although we consider truncated cylinders rather than cylinders extending throughout the depth of the water allowing us also to look at the radiation problem as well as freely floating cylinders. Before considering the deep water limit an account is also given here of the finite depth case, which was solved in [18] (where the scattering and radiation problems for small structures on the free surface was considered), although we adjust their scalings so that we can consider what happens in the deep water limit. In both cases we build upon and make more explicit the work completed in [17] and [18] to formalise their approach to the method of multiple scales by considering a full composite solution and using matched asymptotic expansions between inner and outer solutions in one cell, as was done in [31, chapter 4]; in particular, we find that we are able to use the inner solutions from the infinite array solutions, as found in chapter 2. The reader that is reading this thesis from beginning to end is reminded that it was the author's intention that the chapters were, for the most part, self-contained and there is hence a lot of repetition between the problem formulation found here and that used in chapters 2 and 3.

4.2 Formulation

Vertically axisymmetric structures C_j with wetted surfaces S_{C_j} are distributed uniformly on a horizontal lattice Λ that is infinite in one horizontal direction but of finite width s in the other direction (illustrated in figure 4.1a for the particular case of a square lattice) in water of depth h; the length scale for the lattice periodicity is denoted by L. All structures in the lattice are identical and are moored using identical systems of springs and dampers. We use Cartesian coordinates (x, y, z), with z directed vertically upwards and origin O in the mean free surface at a chosen lattice point. Global polar coordinates (r, θ) in the horizontal plane are also used. Associated with each cylinder are local horizontal polar coordinates (r_j, θ_j) with origin O_j (so that dropping the j subscript indicates the use of global coordinates) located, relative to O, at the lattice points given by the lattice vectors

$$\boldsymbol{R}_j = n_1\boldsymbol{a}_1 + n_2\boldsymbol{a}_2, \quad n_1, n_2 \in \mathbb{Z},$$

for given linearly independent vectors $\boldsymbol{a}_1$ and $\boldsymbol{a}_2$.

The fluid is assumed to be inviscid and incompressible and the fluid motion to be irrotational. The linearised theory of water waves is used throughout so that time-harmonic motions with angular frequency ω may be described by a velocity potential $\mathrm{Re}[\phi(x, y, z)\,\mathrm{e}^{-\mathrm{i}\omega t}]$, where t is time.

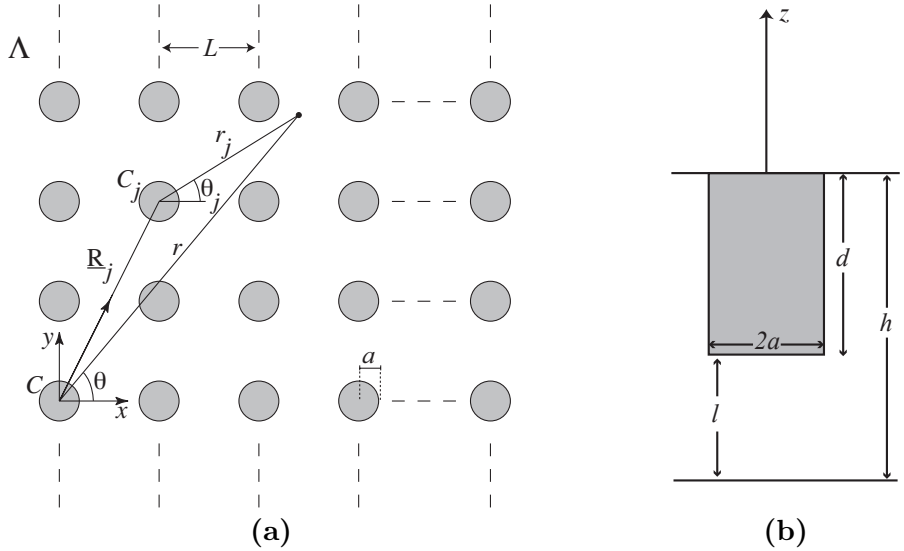

Figure 4.1 (a) Coordinate systems on $z = 0$, and (b) a vertical section of the fluid domain for a surface-piercing circular cylinder.

For all lattice vectors $\boldsymbol{R}_j$, solutions are sought that satisfy the so-called Bloch condition

$$\phi(\boldsymbol{r} + \boldsymbol{R}_j) = \mathrm{e}^{\mathrm{i}\boldsymbol{\beta}^T \boldsymbol{R}_j} \phi(\boldsymbol{r}), \tag{4.2.1}$$

where $\boldsymbol{r} = (x, y)^T$, and $\boldsymbol{\beta} = (q_1, q_2)^T$, $q_1, q_2 \in \mathbb{R}$, is a prescribed vector. The Bloch condition prescribes a phase relationship between the potential values at equivalent points in different cells of the lattice. Given a $\boldsymbol{\beta}$, we seek the frequencies ω that allow non-trivial solutions for ϕ.

In addition to the Bloch condition, the complex-valued potential Φ satisfies the usual equations of the linearised theory of water waves [4, Chapter 8]. Thus

$$\nabla^2 \Phi = 0 \quad \text{within the fluid } \mathcal{D}, \tag{4.2.2}$$

and the linearised condition

$$\frac{\partial^2 \Phi}{\partial t^2} + g \frac{\partial \Phi}{\partial z} = 0 \quad \text{on the free surface } S_F \tag{4.2.3}$$

(g is the acceleration due to gravity). For water of constant finite depth

$$\frac{\partial \Phi}{\partial z} = 0 \quad \text{on the bed } S_B, \tag{4.2.4}$$

while for deep water we require that

$$|\nabla\Phi| \to 0 \quad \text{as} \quad z \to -\infty. \tag{4.2.5}$$

Here we restrict attention to vertically axisymmetric structures that are either fixed, or constrained to move in the vertical (heave) direction. Hence, on the surface S_C of the particular structure C located at the chosen origin of coordinates

$$\frac{\partial\phi}{\partial n} = u_3 n_3, \tag{4.2.6}$$

(the relationship between Φ and ϕ will be explained explicitly – and differently – for the shallow and finite depth / deep-water problems within the relevant sections of this chapter: for now we just need note that ϕ is the time-independent part of Φ) where u_3 is the complex amplitude of the structure's vertical velocity, and the coordinate n is measured normal to S_C and directed out of the fluid (n_3 is the component of the unit normal in the z direction). The equation of motion for the structure C (assumed to be surface piercing) is

$$\left[\omega^2 M + \mathrm{i}\omega\lambda - (\rho g\pi a^2 + \kappa)\right] u_3 = -\rho\omega^2 \iint_{S_C} \phi n_3 \,\mathrm{d}s, \tag{4.2.7}$$

where M is the mass, ρ is the fluid density, κ and λ are respectively the spring and damper constants for the moorings, and s is surface area. The boundary condition and equation of motion for other structures in the lattice are recovered by adjusting the phase of each structure's velocity to ensure that the Bloch condition (4.2.1) is satisfied.

In the absence of structures, the Bloch condition (4.2.1), together with (4.2.3) and the appropriate bed condition, are satisfied by plane waves

$$\phi_q(\boldsymbol{r}) = \begin{cases} \mathrm{e}^{\mathrm{i}\boldsymbol{\beta}_q^T \boldsymbol{r}} \cosh k(z+h) & \text{for finite-depth water,} \\ \mathrm{e}^{\mathrm{i}\boldsymbol{\beta}_q^T \boldsymbol{r}} \mathrm{e}^{kz} & \text{for deep water,} \end{cases} \tag{4.2.8}$$

where the wavenumber k is the positive real root of the dispersion relation $\omega^2 = gk\tanh kh$,

$$\boldsymbol{\beta}_q = \boldsymbol{\beta} + \boldsymbol{K}_q, \tag{4.2.9}$$

and each $\boldsymbol{K}_q = 2\pi(m_1\boldsymbol{b}_1 + m_2\boldsymbol{b}_2)$, for $m_1, m_2 \in \mathbb{Z}$ with q representing each ordered pair (m_1, m_2), is a reciprocal lattice vector [30, Appendix B]. The vectors $\{\boldsymbol{b}_1, \boldsymbol{b}_2\}$ satisfy $\boldsymbol{a}_i^T\boldsymbol{b}_j = \delta_{ij}$ for

$i, j = 1, 2$, so that $\boldsymbol{K}_q^T \boldsymbol{R}_j = 2\pi p$, $p \in \mathbb{Z}$, for any lattice vector $\boldsymbol{R}_j$. The forms (4.2.8) satisfy Laplace's equation (4.2.2) provided

$$k^2 = \beta_q^2 \quad \text{where} \quad \beta_q = |\boldsymbol{\beta}_q|. \tag{4.2.10}$$

For a given $\boldsymbol{\beta}$ there may be multiple vectors $\boldsymbol{\beta}_q$ that yield the same $|\boldsymbol{\beta}_q|$ (which we denote as β, and take to mean the unperturbed wavenumber) and the number of such vectors is denoted by Q. The solutions described later are perturbations of the above quasi-periodic plane waves that exist in the absence of the structures.

Solutions in the presence of structures are obtained by using the method of multiple scales and matched asymptotic expansions under the assumption that a characteristic length scale b for the flow around the structure is much smaller than the wavelength $2\pi/k$, so that $\epsilon \equiv kb \ll 1$. In addition, it is assumed that the wavelength is of the same order of magnitude as the cell size L so that $kL = \text{ord}(1)$. (Here, we follow [33] and use ord to denote 'strict order' so that, for example, $kL = \text{ord}(1)$ as $\epsilon \to 0$ does not allow kL to be vanishingly small in the limit.) To facilitate the solution, the fluid domain is split into many inner regions surrounding each structure to distances $r_j \ll k^{-1}$, and an outer region at distances $r_j \gg b$, where b is a length scale for the inner region (the length b will be chosen differently for the shallow and deep water cases). Because of the Bloch condition (4.2.1), it is sufficient to match between the outer region and the inner region containing the global origin O. In particular, the outer expansion of the inner solution is matched with the inner expansion of the outer solution using the formal matching principle that is described in [34]. The inner solution φ up to terms in ϵ^l is denoted $\varphi^{(l)}$, and $\varphi^{(l,m)}$ is its expansion up to ϵ^m after it is written in terms of the outer coordinates kr. Similarly, the outer solution's inner expansion $\hat{\phi}$ up to terms in ϵ^m is denoted $\hat{\phi}^{(m)}$ and $\hat{\phi}^{(m,l)}$ is its expansion up to ϵ^l after it is written in terms of the inner coordinate r/b. Matching is enforced by requiring $\hat{\phi}^{(m,l)} \equiv \varphi^{(l,m)}$ for each m and l when both asymptotic forms are expressed in terms of the same coordinates.

It is convenient to introduce non-dimensional quantities based on the length scale b, chosen differently for shallow and deep water. Thus, for a wave of amplitude $\mathcal{A}$, all lengths are scaled by b and other non-dimensional quantities are defined according to the transformations

$$\phi \to \frac{g\mathcal{A}}{\omega}\phi, \quad u_3 \to \mathcal{A}\omega u_3, \quad M \to \rho b^3 M, \quad \lambda \to \frac{\rho g b^2}{\omega}\lambda, \quad \kappa \to \rho g b^2 \kappa. \tag{4.2.11}$$

In particular, this results in a boundary condition

$$\frac{\partial \phi}{\partial N} = \frac{\omega^2 b}{g} u_3 n_3 \quad \text{on} \quad S_C, \tag{4.2.12}$$

and an equation of motion

$$\left[\frac{\omega^2 b}{g} M + \mathrm{i}\lambda - (W + \kappa) \right] u_3 = - \iint_{S_C} \phi n_3 \, \mathrm{d}S, \tag{4.2.13}$$

where $N = n/b$, $S = s/b^2$ and the non-dimensional water-plane area $W = \pi a^2/b^2$. We have chosen the scalings to study, in particular, the case when the mooring terms are of the same order of magnitude as the hydrostatic spring. It should be noted that the scaled damping λ implicitly depends upon the frequency but, nevertheless, it is assumed that $\lambda = \mathrm{ord}(1)$ as $\epsilon \to 0$. For both shallow and deep water, three problems are considered: the scattering problem in which the structures are held fixed ($u_3 = 0$), the radiation problem in which the structures are forced to oscillate with velocities consistent with the Bloch condition, and the free-floating problem in which the structures are free to move in the vertical direction.

4.3 Shallow water

We look for solutions as $k \to \beta$ and the length scale b introduced in § 4.2 is chosen to be $b = h$, and it is assumed that $\epsilon = kh \ll 1$. Each cylinder's radius a is taken to be much smaller than the wavelength, so that also $ka \ll 1$, and a/h, d/h and kL are all assumed to be $\mathrm{ord}(1)$ as $\epsilon \to 0$, a notation borrowed from (and defined in) [33]. The vertical length scale for variations in ϕ is h throughout the fluid domain. However, in the inner regions the horizontal length scale is h, while in the outer region it is β^{-1}. Thus, in terms of the original dimensional coordinates, suitable scaled inner region coordinates are

$$X = x/h, \quad Y = y/h, \quad Z = z/h, \quad R = r_j/h,$$

and the inner potential is $\varphi(X, Y, Z; \epsilon) \equiv \phi(x, y, z)$, while suitable scaled outer region coordinates are

$$x' = \beta x, \quad y' = \beta y, \quad Z = z/h, \quad r'_j = \beta r_j,$$

and the outer potential is $\hat{\phi}(x', y', Z; \epsilon) \equiv \phi(x, y, z)$. For the purposes of generating numerical results, we use a specific geometry for the structures: cylinder j occupies $r_j \leq a$, $-d \leq z \leq 0$,

and we define $l = h - d$ to be the gap between the ocean bed and the bottom of the cylinder. For the scattering problem, as well as looking at truncated surface-piercing cylinders, we also look at bottom-mounted circular cylinders; in this case cylinder j occupies $r_j \leq a$, $-1 \leq z \leq -d$, so that d is the gap between the free surface and the top of the cylinder and we define d to be the gap. For $\beta h \ll 1$, we expect our solutions to satisfy the dispersion relation $\omega^2 = g\beta \tanh \beta h \simeq g\beta^2 h$ and so it is appropriate to choose

$$t' = \beta\sqrt{gh}\, t$$

as our non-dimensional fast-time quantity. It is known (for example, see [3]) that the scattered wave – and hence a radiated wave, since it is just a variation of a scattered wave – from a single cylinder is ord(ϵ^2), so that the combined effect is ord(1) when the number of cylinders present is ord($1/\epsilon^2$). This suggests that we also need to define slow scale coordinates

$$\hat{X} = \epsilon^2 x', \quad \hat{Y} = \epsilon^2 y', \quad T = \epsilon^2 t',$$

to describe the evolution of waves as they propagate through the array. We assume that the fast motion of the waves is time harmonic by writing

$$\Phi = \mathrm{Re}\left[\hat{\phi}(x', y', Z; \hat{X}, \hat{Y}, T)\mathrm{e}^{-\mathrm{i}t'}\right] \tag{4.3.1}$$

so that fast-time is separated out of the problem (the slow variation in space takes place as we move horizontally across the array: there is no slow vertical motion, thus (4.3.1) is independent of the slow vertical coordinate). Hence we note that our differential operators become

$$\frac{\partial}{\partial x'} \to \frac{\partial}{\partial x'} + \epsilon^2 \frac{\partial}{\partial \hat{X}} \quad ; \quad \frac{\partial^2}{\partial x'^{\,2}} \to \frac{\partial^2}{\partial x'^{\,2}} + 2\epsilon^2 \frac{\partial}{\partial x'}\frac{\partial}{\partial \hat{X}} + \mathrm{O}(\epsilon^4), \tag{4.3.2}$$

where the relationship between y' and $\hat{Y}$ follows similarly so that we also have

$$\overline{\nabla}^2 \to \overline{\nabla}^2 + 2\epsilon^2 \overline{\nabla} \cdot \widehat{\nabla}, \tag{4.3.3}$$

where $\overline{\nabla}^2$ and $\widehat{\nabla}^2$ are the horizontal Laplacians in outer region fast coordinates and slow coordinates respectively. Furthermore we have

$$\frac{\partial}{\partial t'} \to \epsilon^2 \frac{\partial}{\partial T} \quad \text{so that} \quad \frac{\partial^2}{\partial t'^{\,2}} \to \epsilon^4 \frac{\partial^2}{\partial T^2}. \tag{4.3.4}$$

4.3.1 The scattering problem

4.3.1.1 Outer problem

The outer region problem is stated as

$$\epsilon^2\overline{\nabla}^2\Phi + \frac{\partial^2\Phi}{\partial Z^2} = 0 \quad \text{in the fluid,} \tag{4.3.5a}$$

$$\epsilon^2\frac{\partial^2\Phi}{\partial t'^2} + \frac{\partial\Phi}{\partial Z} = 0 \quad \text{for} \quad Z = 0 \quad \text{and} \quad |r| > a, \tag{4.3.5b}$$

$$\frac{\partial\Phi}{\partial Z} = 0 \quad \text{on} \quad Z = -1. \tag{4.3.5c}$$

Using the form for Φ given in (4.3.1) generates the multiple scales problem of

$$\epsilon^2\left(\overline{\nabla}^2 + 2\epsilon^2\overline{\nabla}\cdot\widehat{\nabla}\right)\hat{\phi}^S + \frac{\partial^2\hat{\phi}^S}{\partial Z^2} = 0 \quad \text{in the fluid,} \tag{4.3.6a}$$

$$\epsilon^2\left(-\hat{\phi}^S - 2\mathrm{i}\epsilon^2\frac{\partial\hat{\phi}^S}{\partial T} + \epsilon^4\frac{\partial^2\hat{\phi}^S}{\partial T^2}\right) + \frac{\partial\hat{\phi}^S}{\partial Z} = 0 \quad \text{for} \quad Z = 0 \quad \text{and} \quad |r| > a, \tag{4.3.6b}$$

$$\frac{\partial\hat{\phi}^S}{\partial Z} = 0 \quad \text{on} \quad Z = -1. \tag{4.3.6c}$$

Motivated by the infinite array solution, where our outer solutions were constructed from fundamental solutions of the form $g_n = g_n^{(1)} + \epsilon^2 g_n^{(2)}$, consider the ansatz

$$\hat{\phi}^S = \hat{\phi}_0^S + \epsilon^2\hat{\phi}_2^S + \epsilon^4\hat{\phi}_4^S.$$

Going forward, we drop the superscript S from our velocity potentials. Substituting this ansatz into the system (4.3.6) yields

$$\frac{\partial^2}{\partial Z^2}\hat{\phi}_0 = 0 \quad \text{in the fluid,} \tag{4.3.7a}$$

$$\frac{\partial}{\partial Z}\hat{\phi}_0 = 0 \quad \text{for} \quad Z = 0 \quad \text{and} \quad |r| > a, \tag{4.3.7b}$$

$$\frac{\partial}{\partial Z}\hat{\phi}_0 = 0 \quad \text{on} \quad Z = -1, \tag{4.3.7c}$$

$$\frac{\partial^2}{\partial Z^2}\hat{\phi}_2 = -\overline{\nabla}^2\hat{\phi}_0 \quad \text{in the fluid,} \tag{4.3.8a}$$

$$\frac{\partial}{\partial Z}\hat{\phi}_2 = \hat{\phi}_0 \quad \text{for} \quad Z = 0 \quad \text{and} \quad |r| > a, \tag{4.3.8b}$$

$$\frac{\partial}{\partial Z}\hat{\phi}_2 = 0 \quad \text{on} \quad Z = -1, \tag{4.3.8c}$$

$$\frac{\partial^2}{\partial Z^2}\hat{\phi}_4 = -\overline{\nabla}^2\hat{\phi}_2 - 2\overline{\nabla}\cdot\widehat{\nabla}\hat{\phi}_0 \quad \text{in the fluid,} \tag{4.3.9a}$$

$$\frac{\partial}{\partial Z}\hat{\phi}_4 = \hat{\phi}_2 + 2\mathrm{i}\frac{\partial}{\partial T}\hat{\phi}_2 \quad \text{for} \quad Z = 0 \quad \text{and} \quad |r| > a, \tag{4.3.9b}$$

$$\frac{\partial}{\partial Z}\hat{\phi}_4 = 0 \quad \text{on} \quad Z = -1. \tag{4.3.9c}$$

From (4.3.7) we can show that $\hat{\phi}_0$ does not depend on Z and by using this fact in conjunction with the system of equations (4.3.8) we show that $\hat{\phi}_0$ satisfies

$$\overline{\nabla}^2\hat{\phi}_0 + \hat{\phi}_0 = 0 \tag{4.3.10}$$

everywhere (i.e. the scaled Helmholtz equation encompasses information about the free surface and bed as well as throughout the domain). Using this result with system of equations (4.3.9) shows that $\hat{\phi}_2$ satisfies

$$\overline{\nabla}^2\hat{\phi}_2 + \hat{\phi}_2 = -\frac{1}{3}\hat{\phi}_0 - 2\overline{\nabla}\cdot\widehat{\nabla}\hat{\phi}_0 - 2\mathrm{i}\frac{\partial}{\partial T}\hat{\phi}_0 \tag{4.3.11}$$

everywhere.

4.3.1.2 Inner problem

The complete inner region problem is stated as

$$\nabla_{IR}^2\Phi + \frac{\partial^2\Phi}{\partial Z^2} = 0 \quad \text{in the fluid,} \tag{4.3.12a}$$

$$\epsilon^2\frac{\partial^2\Phi}{\partial t'^2} + \frac{\partial\Phi}{\partial Z} = 0 \quad \text{for} \quad Z = 0 \quad \text{and} \quad |r| > a, \tag{4.3.12b}$$

$$\frac{\partial\Phi}{\partial Z} = 0 \quad \text{on} \quad Z = -1, \tag{4.3.12c}$$

$$\frac{\partial\Phi}{\partial N} = 0 \quad \text{on} \quad S_C, \tag{4.3.12d}$$

where ∇^2_{IR} is the horizontal Laplacian in inner region coordinates. For fast wave motion that is time-harmonic we use

$$\Phi = \mathrm{Re}\left[\varphi^S(X,Y,Z;\hat{X},\hat{Y},T)\mathrm{e}^{-\mathrm{i}t'}\right]$$

to obtain a multiple scales problem of

$$\epsilon^2\left(\nabla^2_{IR} + 2\epsilon^2\nabla_{IR}\cdot\widehat{\nabla}\right)\varphi^S + \frac{\partial^2\varphi^S}{\partial Z^2} = 0 \quad \text{in the fluid,} \tag{4.3.13a}$$

$$\epsilon^2\left(-\varphi^S - 2\mathrm{i}\epsilon^2\frac{\partial\varphi^S}{\partial T} + \epsilon^4\frac{\partial^2\varphi^S}{\partial T^2}\right) + \frac{\partial\varphi^S}{\partial Z} = 0 \quad \text{for} \quad Z = 0 \quad \text{and} \quad |r| > a, \tag{4.3.13b}$$

$$\frac{\partial\varphi^S}{\partial Z} = 0 \quad \text{on} \quad Z = -1, \tag{4.3.13c}$$

$$\frac{\partial\varphi^S}{\partial N} = 0 \quad \text{on} \quad S_C. \tag{4.3.13d}$$

For a leading order inner region solution expanded like

$$\varphi^S \simeq \varphi^S_0 + \epsilon\varphi^S_1 + \ldots \tag{4.3.14}$$

(motivated by the form of the envelope equations used to describe the outer region) we note that slow-time does not appear in the inner region governing equations up to (and including) those that are ord(ϵ), and consequently the inner region solutions that we require are the same as those found for the infinite array.

4.3.1.3 Envelope equations

The so-called envelope equations describe the slow scale dynamics as the waves move through the array. To derive them we consider a separable solution

$$\hat{\phi}_0 = \sum_{q=1}^{Q} A_q(\hat{X},\hat{Y},T)\psi_q(x,y,z) \tag{4.3.15}$$

and apply Green's identity in one primary cell, as in [17], where

$$\psi_q(x,y,z) = D(z/h)\mathrm{e}^{\mathrm{i}\boldsymbol{\beta}^T_q\boldsymbol{r}} = D(Z)\mathrm{e}^{\mathrm{i}\boldsymbol{\beta}^T_q\boldsymbol{R}_j}\mathrm{e}^{\mathrm{i}(\boldsymbol{\beta}^T_q/\beta)\boldsymbol{r}'_j} \tag{4.3.16}$$

for

$$D(Z) = -\frac{\mathrm{i}}{2}\cosh\epsilon(Z+1).$$

Although we earlier stated $\hat{\phi}_0$ is independent of depth we note that, whilst the ψ_q introduced here seems to contradict that statement, ψ_q is actually independent of depth to leading order because $D(Z) = 1$ at leading order. The concept of the multiple scales solution that we will develop is that we've chosen the ψ_q's such that they are valid at the point in wave frequency space that we are perturbing from; the A_q's pick up the perturbations from that point in the case where cylinders are present.

We construct a composite function to describe the fluid in the entire primary cell (which includes the inner and outer regions) where the truncation of the expansions of the inner and outer solutions are chosen (we use here the same notation as [34] for describing the matching principle) so that we have enough equations when matching between the two for the unknowns. Such a composite function is taken as (chosen with the benefit of hindsight: it is used now for ease of presentation)

$$\phi^c = \hat{\phi}^{(4)} + \varphi^{(1)} - \varphi^{(1,4)} \tag{4.3.17}$$

where the inner region's outer expansion is subtracted to avoid double counting the intermediate region that is shared between both fields, as was done in [31] (this was not done in [17]). Applying Green's identity to ϕ^c and ψ_q^* over the primary cell (the superscript asterisk denotes the complex conjugate) yields

$$\iiint\limits_V \left\{\phi^c \nabla^2 \psi_q^* - \psi_q^* \nabla^2 \phi^c\right\}\, dv = \iint\limits_{\partial V} \left\{\phi^c \frac{\partial \psi_q^*}{\partial n} - \psi_q^* \frac{\partial \phi^c}{\partial n}\right\}\, ds$$

in dimensional coordinates, where V is the volume of the cell, defined by the boundary surface ∂V; the surface ∂V consists of the free surface S_F, the structures' wetted surface S_C, the vertical surfaces S_V that bound one cell and the bed S_B. By definition we have $\nabla^2 \psi_q^* = 0$, and the surface integrals on S_B and S_V disappear by the bed condition and the Bloch condition respectively. Writing everything in terms of the appropriate coordinates we hence have

$$\begin{aligned} -\iiint\limits_V \left\{\psi_q^* \left(\epsilon^2 \overline{\nabla}^2 + \frac{\partial^2}{\partial Z^2}\right) \phi^c\right\}\, dv' \\ = \iint\limits_{S_F} \left\{\phi^c \frac{\partial \psi_q^*}{\partial Z} - \psi_q^* \frac{\partial \phi^c}{\partial Z}\right\}\, ds' + \epsilon^2 \iint\limits_{S_C} \left\{\varphi^{(1)} \frac{\partial \psi_q^*}{\partial N} - \psi_q^* \frac{\partial \varphi^{(1)}}{\partial N}\right\}\, dS \end{aligned} \tag{4.3.18}$$

where it is noted that $\phi^c = \varphi^{(1)}$ on the structure whilst dv' and dS are used to represent the surface integral in terms of outer and inner coordinates respectively and N is the normal in

inner coordinates. Let us introduce the notation I_V^S, I_F^S, I_a^S and I_b^S to represent the different integrals in equation (4.3.18), so that we have

$$I_V^S = I_F^S + \epsilon^2(I_a^S - I_b^S). \tag{4.3.19}$$

Dealing with the volume integral in eqn (4.4.19) first, and denoting the inner region horizontal Laplacian $\overline{\nabla}_{IR}^2$, we have that

$$\begin{aligned} I_V^S &= -\iiint_V \left\{ \psi_q^* \left(\epsilon^2 \overline{\nabla}^2 + \frac{\partial^2}{\partial Z^2} \right) \hat{\phi}^{(4)} + \psi_q^* \left(\overline{\nabla}_{IR}^2 + \frac{\partial^2}{\partial Z^2} \right) \left(\varphi^{(1)} - \varphi^{(1,4)} \right) \right\} \, dv' \\ &= -\iiint_V \left\{ \psi_q^* \left(\epsilon^2 \overline{\nabla}^2 + \frac{\partial^2}{\partial Z^2} \right) \hat{\phi}^{(4)} \right\} \, dv' \end{aligned} \tag{4.3.20}$$

by the governing field equation in the inner region. Substituting for $\hat{\phi}^{(4)}$, using the governing equations (4.3.10) and (4.3.11) and truncating at leading order yields

$$I_V^S \simeq 2\epsilon^4 \iiint_V \left\{ \psi_q^* \overline{\nabla} \cdot \widehat{\nabla} \hat{\phi}_0 \right\} \, dv'. \tag{4.3.21}$$

Using (4.3.15) with p as the dummy index, noting that $\overline{\nabla}\psi_p = \mathrm{i}(\boldsymbol{\beta}_p^T/\beta)\psi_p$ and $\widehat{\nabla} A_p$ depends on the slow coordinates only, we thus have

$$I_V^S \simeq 2\epsilon^4 \sum_{p=1}^{Q} \mathrm{i} \frac{\boldsymbol{\beta}_p^T}{\beta} \cdot \widehat{\nabla} A_p \iiint_V \psi_q^* \psi_p \, dv'. \tag{4.3.22}$$

Using [17, appendix A] and the definition of the reciprocal lattice vector, the integral over V is

$$\iiint_V \psi_q^* \psi_p \, dv' \simeq \frac{1}{4} \mathrm{e}^{\mathrm{i}(\boldsymbol{\beta}_p^T \boldsymbol{R}_j - \boldsymbol{\beta}_q^T \boldsymbol{R}_j)} \delta_{qp} \beta^2 A^c = \frac{1}{4} \delta_{qp} \beta^2 A^c \tag{4.3.23}$$

where $\beta^2 A^c$ is the non-dimensional area of one lattice cell ($\beta^2 A^c = \beta^2 L^2$ for a square lattice with sides L; note that A^c is equivalent to $\mathcal{A}$ in [17, equation A6]). Thus

$$I_V \simeq \frac{\mathrm{i}}{2} \epsilon^4 \frac{\boldsymbol{\beta}_q^T}{\beta} \beta^2 A^c \cdot \widehat{\nabla} A_q \quad \text{for} \quad q = 1, \ldots, Q. \tag{4.3.24}$$

We now turn our attention to the integral on the free surface. Note that

$$\left. \frac{\partial \psi_q^*}{\partial Z} \right|_{Z=0} = \epsilon^2 \psi_q^* \Big|_{Z=0} \tag{4.3.25}$$

and so we thus have

$$\begin{aligned} I_F = & \iint\limits_{S_F} \left\{ \hat{\phi}^{(4)} \epsilon^2 \psi_q^* \Big|_{Z=0} - \psi_q^* \Big|_{Z=0} \frac{\partial \hat{\phi}^{(4)}}{\partial Z} \right\} \, ds' \\ & + \iint\limits_{S_F} \left\{ \left(\varphi^{(1)} - \varphi^{(1,4)} \right) \epsilon^2 \psi_q^* \Big|_{Z=0} - \psi_q^* \Big|_{Z=0} \frac{\partial}{\partial Z} \left(\varphi^{(1)} - \varphi^{(1,4)} \right) \right\} \, \epsilon^2 dS \end{aligned} \tag{4.3.26}$$

where the second integral has been written in terms of inner region coordinates. The second integral is zero at leading order; for its first component, $\left(\varphi^{(1)} - \varphi^{(1,4)}\right)$ appears at $O(\epsilon^4)$ and so only the leading order is required thus $\left(\varphi^{(1)} - \varphi^{(1,4)}\right) = 0$ and for its second component $\dfrac{\partial}{\partial Z}\left(\varphi^{(1)} - \varphi^{(1,4)}\right) = 0$. By using the free surface conditions acting on $\hat{\phi}_0$, $\hat{\phi}_2$, and $\hat{\phi}_4$ before truncating at leading order we thus have

$$I_F \simeq - \iint\limits_{S_F} \left\{ \psi_q^* \left(2\mathrm{i}\epsilon^4 \frac{\partial \hat{\phi}_0}{\partial T} \right) \right\} \, ds'. \tag{4.3.27}$$

Using (4.3.15) with p as the dummy variable yields

$$I_F \simeq -2\mathrm{i}\epsilon^4 \sum_{p=1}^{Q} \frac{\partial A_p}{\partial T} \iint\limits_{S_F} \psi_q^* \psi_p \, ds' = -\frac{\mathrm{i}}{2} \epsilon^4 \beta^2 A^c \frac{\partial A_q}{\partial T}, \tag{4.3.28}$$

(the integral is similar to that calculated above as part of the volume integral – although ψ_q^* is now being evaluated on $Z = 0$) where we have, again, been forced to take $p = q$.

For the integral across the structure, we note when the structures are held fixed $I_b^S = 0$. To calculate the integral I_a^S we re-apply Green's identity. Substituting the form of $\varphi^{(1)}$ into I_a^S yields

$$\begin{aligned} I_a^S &= \iint\limits_{S_C} \left(C_0^S + \epsilon \varphi_1^S \right) \frac{\partial \psi_q^*}{\partial N} \, dS, \\ &\equiv I_{a1}^S + I_{a2}^S \end{aligned} \tag{4.3.29}$$

where C_0^S and the form of φ^S are known from the patching solutions. Note that we have introduced the notation I_{a1}^S and I_{a2}^S to represent the two parts of the integral I_a^S. We begin by evaluating I_{a1}^S. As a consequence of the divergence theorem we have that the integral of the normal derivative of a function across and into a structure's boundary is zero (provided that

function is harmonic within the region), that is to say that

$$\iint\limits_{S_C} \frac{\partial \psi_q^*}{\partial N}\, dS = -\iint\limits_{S_W} \left.\frac{\partial \psi_q^*}{\partial N}\right|_{Z=0} dS \tag{4.3.30}$$

for the surface that the structure cuts on the free surface S_W. We thus have that

$$\iint\limits_{S_C} \frac{\partial \psi_q^*}{\partial N}\, dS = \iint\limits_{S_W} \left.\frac{\partial \psi_q^*}{\partial Z}\right|_{Z=0} dS \simeq \frac{\mathrm{i}}{2}\mathrm{e}^{\mathrm{i}\boldsymbol{\beta}_q^T \boldsymbol{R}_j}\epsilon^2 W \tag{4.3.31}$$

for the non-dimensional water plane area W so that

$$I_{a1}^S = \frac{\mathrm{i}}{2}\mathrm{e}^{\mathrm{i}\boldsymbol{\beta}_q^T \boldsymbol{R}_j}\epsilon^2 C_0^S W. \tag{4.3.32}$$

To evaluate I_{a2}^S we note that, in inner region coordinates,

$$\begin{aligned}\psi_q^* &= D^*(Z)\mathrm{e}^{-\mathrm{i}\boldsymbol{\beta}_q^T \boldsymbol{R}_j}\mathrm{e}^{-\mathrm{i}\epsilon R\cos(\theta-\tau_q)} \\ &= \frac{\mathrm{i}}{2}\mathrm{e}^{-\mathrm{i}\boldsymbol{\beta}_q^T \boldsymbol{R}_j}\left[1-\mathrm{i}\epsilon R\cos(\theta-\tau_q)\right] + O(\epsilon^2)\end{aligned} \tag{4.3.33}$$

so that

$$\frac{\partial \psi_q^*}{\partial N} = \frac{\epsilon}{2}\mathrm{e}^{-\mathrm{i}\boldsymbol{\beta}_q^T \boldsymbol{R}_j}\frac{\partial \chi}{\partial N} + O(\epsilon^2) \tag{4.3.34}$$

for $\chi = R\cos(\theta-\tau_q)$. From (4.3.29), we thus have

$$I_{a2}^S \simeq \frac{\epsilon^2}{2}\mathrm{e}^{-\mathrm{i}\boldsymbol{\beta}_q^T \boldsymbol{R}_j}\iint\limits_{S_C} \varphi_1^S \frac{\partial \chi}{\partial N}\, dS. \tag{4.3.35}$$

Consider the function $\chi = R\cos(\theta-\tau_q)$ and apply Green's identity in the inner region only to the two functions φ_1^S and χ to give

$$\begin{aligned}&\iiint\limits_V \varphi_1^S\left(\overline{\nabla}_{IR}^2 + \frac{\partial^2}{\partial Z^2}\right)\chi - \chi\left(\overline{\nabla}_{IR}^2 + \frac{\partial^2}{\partial Z^2}\right)\varphi_1^S\, dV^{IR} \\ &\qquad = \iint\limits_{S_C} \varphi_1^S\frac{\partial \chi}{\partial N} - \chi\frac{\partial \varphi_1^S}{\partial N}\, dS + \iint\limits_{S_\infty} \varphi_1^S\frac{\partial \chi}{\partial R} - \chi\frac{\partial \varphi_1^S}{\partial R}\, dS\end{aligned} \tag{4.3.36}$$

where S_∞ defines the cylinder that is the inner region boundary and it is noted that the surface integrals on the free surface and bed each disappear. By definition of χ and the governing fluid equation on φ_1^S the volume integral on the left hand side disappears, and by the body condition in the inner region for φ_1^S the second component of the integral across the body disappears, so

that

$$\iint\limits_{S_C} \varphi_1^S \frac{\partial \chi}{\partial N}\, dS = -\iint\limits_{S_\infty} \varphi_1^S \frac{\partial \chi}{\partial R} - \chi \frac{\partial \varphi_1^S}{\partial R}\, dS \tag{4.3.37}$$

which is equivalent to stating

$$\begin{aligned}\iint\limits_{S_C} \varphi_1^S \frac{\partial \chi}{\partial N}\, dS = &-\lim_{\hat{R}\to\infty} \iint\limits_{S_\infty} C_1^S + \left(\boldsymbol{E}_1^S\right)^T \left(\hat{R} + \frac{\mathfrak{D}_1}{\hat{R}}\right) \begin{pmatrix}\cos\theta \\ \sin\theta\end{pmatrix} \cos(\theta - \tau_q)\, dS \\ &+ \lim_{\hat{R}\to\infty} \iint\limits_{S_\infty} C_1^S + \hat{R}\cos(\theta-\tau_q) \left(\boldsymbol{E}_1^S\right)^T \left(1 - \frac{\mathfrak{D}_1}{\hat{R}^2}\right) \begin{pmatrix}\cos\theta \\ \sin\theta\end{pmatrix}\, dS\end{aligned} \tag{4.3.38}$$

where it is noted that the summations contained within φ_1^S have disappeared as $\hat{R} \to \infty$. Hence we have that

$$I_{a2}^S \simeq -\frac{\epsilon^2}{2} \mathrm{e}^{-\mathrm{i}\boldsymbol{\beta}_q^T \boldsymbol{R}_j} \left\{ 2\pi \mathfrak{D}_1 \left(\boldsymbol{E}_1^S\right)^T \begin{pmatrix}\cos\tau_q \\ \sin\tau_q\end{pmatrix} \right\} \tag{4.3.39}$$

We thus have, finally, from (4.3.29)

$$I_a^S = \frac{\mathrm{i}}{2} \mathrm{e}^{-\mathrm{i}\boldsymbol{\beta}_q^T \boldsymbol{R}_j} \epsilon^2 \left\{ W \frac{\pi a^2}{h^2} + 2\mathrm{i}\pi \mathfrak{D}_1 \left(\boldsymbol{E}_1^S\right)^T \begin{pmatrix}\cos\tau_q \\ \sin\tau_q\end{pmatrix} \right\} \tag{4.3.40}$$

Note that the integral across the structure can be calculated directly (i.e. without reapplying Green's identity) for the case of a truncated cylinder, which has been done as an exercise and is contained within the appendix.

Matching the inner expansion of the outer region solution

$$\begin{aligned}\hat{\phi}^{(0,1)} &= -\frac{\mathrm{i}}{2} \sum_{p=1}^{Q} A_p \mathrm{e}^{\mathrm{i}\boldsymbol{\beta}_p^T \boldsymbol{R}_j} \left[1 + \mathrm{i}\epsilon R \cos(\theta - \tau_p)\right] \\ &= -\frac{\mathrm{i}}{2} \sum_{p=1}^{Q} A_p \mathrm{e}^{\mathrm{i}\boldsymbol{\beta}_p^T \boldsymbol{R}_j} \left[1 + \mathrm{i}\epsilon R (\boldsymbol{e}_{1p})^T \begin{pmatrix}\cos\theta \\ \sin\theta\end{pmatrix}\right]\end{aligned} \tag{4.3.41}$$

with the outer expansion of the inner region solution

$$\varphi^{(1,0)} = C_0^S + \epsilon R \left(\boldsymbol{E}_1^S\right)^T \begin{pmatrix}\cos\theta \\ \sin\theta\end{pmatrix} \tag{4.3.42}$$

gives the values of the constants to be

$$C_0^S = -\frac{\mathrm{i}}{2}\sum_{p=1}^{Q} A_p \mathrm{e}^{\mathrm{i}\boldsymbol{\beta}_p^T \boldsymbol{R}_j} \tag{4.3.43}$$

$$\boldsymbol{E}_1^S = \frac{1}{2}\sum_{p=1}^{Q} A_p \mathrm{e}^{\mathrm{i}\boldsymbol{\beta}_p^T \boldsymbol{R}_j} (\boldsymbol{e}_{1p})^T. \tag{4.3.44}$$

Putting each of our calculations back into Green's identity (4.3.19), and multiplying through by $2/(\mathrm{i}\beta^2 A^c)$, yields

$$\frac{\partial A_q}{\partial T} + \frac{\boldsymbol{\beta}_q^T}{\beta}\cdot\widehat{\nabla} A_q = -\frac{\mathrm{i}}{2\beta^2 A^c}\sum_{p=1}^{Q}\left\{W - 2\pi\mathfrak{D}_1 \boldsymbol{e}_{1p}^T \boldsymbol{e}_{1q}\right\} A_p \quad \text{for} \quad q = 1,\ldots,Q. \tag{4.3.45}$$

where it is noted that by the definition of the reciprocal lattice vector $\mathrm{e}^{-\mathrm{i}\boldsymbol{\beta}_q^T \boldsymbol{R}_j}\mathrm{e}^{\mathrm{i}\boldsymbol{\beta}_p^T \boldsymbol{R}_j} = 1$.

Comparison with Li and Mei [17] Dimensionalising our envelope equations as given in (4.3.45) by transforming our operators for this section as

$$\frac{\partial}{\partial T} \to \frac{1}{\epsilon^2}\frac{1}{\omega}\frac{\partial}{\partial t} \quad \text{and} \quad \widehat{\nabla} \to \frac{1}{\epsilon^2}\frac{1}{\beta}\widehat{\nabla}_{2D}, \tag{4.3.46}$$

where $\widehat{\nabla}_{2D}$ is the Laplacian in two-dimensional space coordinate (in original coordinates) yields

$$\frac{\partial A_q}{\partial t} + \frac{\omega}{\beta}\frac{\boldsymbol{\beta}_q^T}{\beta}\cdot\widehat{\nabla} A_q = -\frac{\mathrm{i}\pi\omega}{2\beta^2 A^c}\epsilon^2\sum_{p=1}^{Q}\left\{\frac{a^2}{h^2} - 2\mathfrak{D}_1 \boldsymbol{e}_{1p}^T \boldsymbol{e}_{1q}\right\} A_p \quad \text{for} \quad q = 1,\ldots,Q. \tag{4.3.47}$$

For cylinders extending throughout the depth we have $\mathfrak{D}_1 = a^2/h^2$, whilst $\omega/\beta \simeq \sqrt{gh}$ is the waves' group velocity in shallow water to leading order. Using these values results in

$$\frac{\partial A_q}{\partial t} + \sqrt{gh}\frac{\boldsymbol{\beta}_q^T}{\beta}\cdot\widehat{\nabla} A_q = -\frac{\mathrm{i}}{2}\beta^2 a^2 \frac{\pi\sqrt{gh}}{\beta A^c}\sum_{p=1}^{Q}\left\{1 - 2\boldsymbol{e}_{1p}^T \boldsymbol{e}_{1q}\right\} A_p \quad \text{for} \quad q = 1,\ldots,Q \tag{4.3.48}$$

which is precisely [17, equation 44] for the group speed in shallow water $\sqrt{gh}$.

Recovery of infinite array solution The infinite array leading order solution is

$$\hat{\phi} = \frac{\pi L^2}{A^c}\sum_{q=1}^{Q} U_q \mathrm{e}^{\mathrm{i}r'\cos(\theta-\tau_q)}, \tag{4.3.49}$$

(Note that in this chapter we use A^c to represent the area of a lattice cell and so we amend the infinite array solutions throughout – i.e. for deep water too – accordingly) whilst the strip array solution has been found using the leading order solution

$$\hat{\phi} = \left(-\frac{\mathrm{i}}{2}\right) \mathrm{e}^{z'} \sum_{q=1}^{Q} A_q \mathrm{e}^{\mathrm{i}\boldsymbol{\beta}_q^T \boldsymbol{r}} = -\frac{\mathrm{i}}{2} \mathrm{e}^{z'} \sum_{q=1}^{Q} A_q \mathrm{e}^{\mathrm{i}\boldsymbol{\beta}_q^T \boldsymbol{r}} \tag{4.3.50}$$

meaning that we need to use $U_q = -(\mathrm{i}/2)A_q$ when comparing the solutions which, whilst making no difference to the recovery of the scattering solution, is accounted for here for completeness. Let us hence consider amplitudes of the form

$$A_p(\hat{X}, \hat{Y}, T) = \frac{2\pi \mathrm{i} L^2}{A^c} U_p^S \mathrm{e}^{-\mathrm{i}\Omega T} \tag{4.3.51}$$

for constants U_p^S. Amplitudes that do not vary with space are equivalent to the waves found in the infinite array problem. Having considered the fast-time dependence in

$$\Phi = \mathrm{Re}\left[\hat{\phi}(x', y', Z; \hat{X}, \hat{Y}, T)\mathrm{e}^{-\mathrm{i}\omega t}\right],$$

we have that the time dependence found in the infinite array solutions is related to the strip array time dependence via $\mathrm{e}^{-\mathrm{i}\omega t} \equiv \mathrm{e}^{-\mathrm{i}\omega t}\mathrm{e}^{-\mathrm{i}\Omega T}$. When used with the applicable dispersion relations, this becomes

$$\mathrm{e}^{-\mathrm{i}k\sqrt{gh}t} \equiv \mathrm{e}^{-\mathrm{i}\beta\sqrt{gh}t}\mathrm{e}^{-\mathrm{i}\Omega T}$$

so that, when everything is put in terms of t', we have non dimensional frequency

$$\frac{k}{\beta} = 1 + \epsilon^2 \Omega \tag{4.3.52}$$

and so

$$\Omega = \frac{(k-\beta)\,(1/\beta)}{(\beta h)^2}. \tag{4.3.53}$$

Using the constant form of A_p, as given in (4.3.51), with this relationship between Ω and k in the envelope equations yields

$$\frac{(k-\beta)\,(1/\beta)}{(\beta h)^2} a_q = \frac{1}{2\beta^2 A^c} \sum_{p=1}^{Q} \left[W - 2\pi \mathfrak{D}_1 \boldsymbol{e}_{1p}^T \boldsymbol{e}_{1q}\right] a_p \quad \text{for} \quad q = 1, \ldots, Q. \tag{4.3.54}$$

The infinite array scattering solution (in shallow water) was found to be

$$\frac{(k^2-\beta_q^2)L^2}{(kh)^2}U_p^S-\frac{L^2}{A^c}\sum_{q=1}^{Q}U_q^S\left[W-2\pi\mathfrak{D}_1\boldsymbol{e}_{1q}^T\boldsymbol{e}_{1p}\right]=0\quad\text{for}\quad p=1,\ldots,Q \tag{4.3.55}$$

Taking $k\to\beta$ so that $\beta=\beta_q$ in this solution (and dividing through by $2\beta^2L^2$) yields

$$\frac{(k-\beta)(1/\beta)}{(\beta h)^2}U_q^S\;=\frac{1}{\beta^2A^c}\sum_{p=1}^{Q}\left[W-2\pi\mathfrak{D}_1\boldsymbol{e}_{1p}^T\boldsymbol{e}_{1q}\right]U_q^S\quad\text{for}\quad q=1,\ldots,Q \tag{4.3.56}$$

giving agreement with the strip array solution when there is no spatial variation.

4.3.1.4 Obtaining system of equations for solving numerically

Consider a strip of truncated circular cylinders occupying $0\le x'\le\beta s$ and $y'=\pm\infty$. Without loss of generality, we define a forward going wave to have a positive x-component with an angle measured relative to the positive x-axis of $0\le\tau_1<\pi/2$, so that any backward propagating waves will have an angle lying between $(\pi/2,\pi]$ with a negative x-component. We require that the width βs of the array be of strict order $1/\epsilon^2$ so that the array is wide enough for resonance to be observed, and hence write that $S=\epsilon^2 s$. Note that inside the array the envelope equations (4.3.45) hold, whilst outside the array they reduce to

$$\frac{\partial A_q}{\partial T}+\frac{\boldsymbol{\beta}_q^T}{\beta}\cdot\widehat{\nabla}A_q=0\quad\text{for}\quad q=1,\ldots,Q. \tag{4.3.57}$$

For the leading order outer solution

$$\hat{\phi}_0=\sum_{q=1}^{Q}A_q(\hat{X},\hat{Y},T)\psi_q(x,y,z) \tag{4.3.58}$$

we denote the constants differently, depending on whether we are inside or outside the strip. Thus

$$A_q=\begin{cases}A_q^- & ;\hat{X}<0\\ A_q & ;0\le\hat{X}\le\beta S,\\ A_q^+ & ;\beta S<\hat{X}\end{cases} \tag{4.3.59}$$

so that the incident wave, with wavenumber $\boldsymbol{\beta}_1$, takes the form

$$A_1^-(\hat{X},\hat{Y},T)=A_0\mathrm{e}^{\mathrm{i}[\mathcal{K}\hat{X}\cos\tau_1+\mathcal{K}\hat{Y}\sin\tau_1-\Omega T]} \tag{4.3.60}$$

for a prescribed amplitude A_0 with detuning wavenumber $\epsilon^2\mathcal{K}$ and detuning frequency $\epsilon^2\Omega$. For our non-dimensional problem, the detuning frequency and wavenumber are equivalent.

The Bloch condition dictates the form that the solutions take in the $\hat{Y}$ direction (the direction of which the array is infinite) and we thus consider solutions of the form

$$\begin{pmatrix} A_q^-(\hat{X},\hat{Y},T) \\ A_q(\hat{X},\hat{Y},T) \\ A_q^+(\hat{X},\hat{Y},T) \end{pmatrix} = A_0 \begin{pmatrix} B_q^-(\hat{X}) \\ B_q(\hat{X}) \\ B_q^+(\hat{X}) \end{pmatrix} \mathrm{e}^{\mathrm{i}[\mathcal{K}\hat{Y}\sin\tau_1 - \Omega T]} \tag{4.3.61}$$

and furthermore (from (4.3.58), use continuity of the velocity potential and the derivative of velocity potential to show that we only) require continuity of the velocity potential (and hence amplitudes) at the boundary points $\hat{X}=0$ and $\hat{X}=\beta S$ so that

$$B_q^-(0) = B_q(0), \tag{4.3.62}$$

$$B_q(\beta S) = B_q^+(\beta S). \tag{4.3.63}$$

Further boundary conditions are obtained by noting that for $\hat{X}<0$ the only forward propagating wave is the incident wave, whilst for $\hat{X}>\beta S$ there are no backward propagating waves. When $\cos\tau_q > 0$ we have a forward propagating wave, whilst when $\cos\tau_q < 0$ we have a backward propagating wave. Thus our boundary conditions are

$$B_q^- = 0 \quad \text{for any } q = 2,\ldots,Q \text{ such that } \cos\tau_q > 0 \tag{4.3.64}$$

$$B_q^+ = 0 \quad \text{for any } q = 1,\ldots,Q \text{ such that } \cos\tau_q < 0. \tag{4.3.65}$$

Outside the strip, we use (4.3.61) with (4.3.57) to give

$$\frac{dB_q^\pm}{d\hat{X}} = \mathrm{i}\mathcal{K}\frac{(1-\sin\tau_1\sin\tau_q)}{\cos\tau_q}B_q^\pm \quad \text{for} \quad q=1,\ldots,Q \tag{4.3.66}$$

which has a general solution of the form

$$B_q^\pm(\hat{X}) = b_q^\pm \mathrm{e}^{\mathrm{i}K_q\hat{X}} \tag{4.3.67}$$

for

$$K_q = \mathcal{K}\frac{(1-\sin\tau_1\sin\tau_q)}{\cos\tau_q}.$$

Inside the strip, we use (4.3.61) with (4.3.45) to give

$$\frac{dB_q}{d\hat{X}} = \frac{\mathrm{i}}{\beta^2 A^c}\frac{1}{\cos\tau_q}\left[\beta^2 A^c \mathcal{K}(1-\sin\tau_1\sin\tau_q)B_q - \frac{1}{2}\sum_{p=1}^{Q}\left[W - 2\pi\mathfrak{D}_1 \boldsymbol{e}_{1p}^T \boldsymbol{e}_{1q}\right]B_p\right] \tag{4.3.68}$$

for $q = 1, \ldots, Q$. In matrix form this is

$$\frac{d}{d\hat{X}}\begin{pmatrix} B_1 \\ \vdots \\ B_Q \end{pmatrix} = \underline{\underline{\mathrm{F}}}^S \begin{pmatrix} B_1 \\ \vdots \\ B_Q \end{pmatrix} \tag{4.3.69}$$

where $\underline{\underline{\mathrm{F}}}^S$ is a $Q \times Q$ matrix with entries

$$F_{ij}^S = \frac{\mathrm{i}}{\beta^2 A^c}\frac{1}{\cos\tau_i}\left[\delta_{ij}\beta^2 A^c \mathcal{K}(1-\sin\tau_1\sin\tau_i) - \frac{1}{2}\left(W + 2\pi\mathfrak{D}_1 \boldsymbol{e}_{1i}^T \boldsymbol{e}_{1j}\right)\right] \tag{4.3.70}$$

for the Kronecker delta function δ_{ij}.

4.3.2 The radiation problem

4.3.2.1 Outer and inner problems

The outer problem is stated as

$$\epsilon^2 \overline{\nabla}^2 \Phi + \frac{\partial^2 \Phi}{\partial Z^2} = 0 \quad \text{in the fluid,} \tag{4.3.71a}$$

$$\epsilon^2 \frac{\partial^2 \Phi}{\partial t'^2} + \frac{\partial \Phi}{\partial Z} = 0 \quad \text{for} \quad Z = 0 \quad \text{and} \quad |r| > a, \tag{4.3.71b}$$

$$\frac{\partial \Phi}{\partial Z} = 0 \quad \text{on} \quad Z = -1. \tag{4.3.71c}$$

and, as with the scattering problem – for fast wave motion that is time-harmonic, that is $\Phi = \mathrm{Re}\left[\varphi^S(X, Y, Z; \hat{X}, \hat{Y}, T)\mathrm{e}^{-\mathrm{i}t'}\right]$ – we consider a separable solution of the form

$$\hat{\phi}_{02}^R = \sum_{q=1}^{Q} A_q(\hat{X}, \hat{Y}, T)\psi_q(x, y, z) \tag{4.3.72}$$

with ψ_q as defined previously. In the outer region, the ansatz

$$\hat{\phi} = \frac{1}{\epsilon^2}\hat{\phi}_{02}^R + \hat{\phi}_0^R + \epsilon^2 \hat{\phi}_2^R$$

is motivated by the infinite array solution. The slow-time equations in the fluid and on the free surface and bed for $\hat{\phi}_{02}^R$, $\hat{\phi}_0^R$ and $\hat{\phi}_2^R$ all correspond respectively with the problems for $\hat{\phi}_0^S$, $\hat{\phi}_2^S$ and

$\hat{\phi}_4^S$ as given in systems (4.3.7)-(4.3.9) (it is the matching with the inner region solution – which depends on the body condition – that distinguishes the outer region between the scattering and radiation problems).

The complete inner region problem is stated as

$$\nabla_{IR}^2\Phi + \frac{\partial^2\Phi}{\partial Z^2} = 0 \quad \text{in the fluid,} \tag{4.3.73a}$$

$$\epsilon^2\frac{\partial^2\Phi}{\partial t'^2} + \frac{\partial\Phi}{\partial Z} = 0 \quad \text{for} \quad Z = 0 \quad \text{and} \quad |r| > a, \tag{4.3.73b}$$

$$\frac{\partial\Phi}{\partial Z} = 0 \quad \text{on} \quad Z = -1, \tag{4.3.73c}$$

as well as a body condition, which in inner region coordinates (derived directly from that given in the problem formulation section) is

$$\frac{\partial\varphi}{\partial Z} = \frac{\omega^2 a}{g}u_3 = \epsilon^2 u_3 \tag{4.3.74}$$

For the radiation problem we force a structure to move with velocity

$$\epsilon^2 u_3 = \gamma(\hat{X},\hat{Y},T)\mathrm{e}^{-\mathrm{i}(\omega/\beta\sqrt{gh})t'}\mathrm{e}^{\mathrm{i}\boldsymbol{\beta}^T\boldsymbol{R}_j}$$

for non-dimensional complex amplitude of the structure's vertical velocity $\gamma(\hat{X},\hat{Y},T)$ which has been forced to evolve on the slow scales as waves move across the strip array. Expanding the complex amplitude of the structure's vertical velocity in powers of ϵ^2, the body condition for the radiation problem hence becomes

$$\frac{\partial\varphi^R}{\partial Z} = \mathrm{e}^{\mathrm{i}\boldsymbol{\beta}^T\boldsymbol{R}_j}\left(\gamma_0(\hat{X},\hat{Y},T) + \epsilon^2\gamma_2(\hat{X},\hat{Y},T) + \dots\right) \quad \text{on} \quad S_{Bj}. \tag{4.3.75}$$

For an inner region ansatz of

$$\varphi_R = \frac{1}{\epsilon^2}\varphi_{02}^R + \frac{1}{\epsilon}\varphi_{01}^R + \log\epsilon\,\varphi_{00}^R + \varphi_0^R + \dots \tag{4.3.76}$$

we thus have a homogeneous body condition for φ_{02}^R, φ_{01}^R and φ_{00}^R and

$$\frac{\partial\varphi_0^R}{\partial Z} = \mathrm{e}^{\mathrm{i}\boldsymbol{\beta}^T\boldsymbol{R}_j}\gamma_0 \tag{4.3.77}$$

after dropping the dependence of the γ's on $(\hat{X},\hat{Y},T)$ for ease of notation. We note that slow-time does not appear in the inner region governing equations up to (and including) those that

are ord(1), and consequently the inner region solutions that we require are the same as those found for the infinite array. Going forward in this section, we will drop the R subscript from the velocity potential.

4.3.2.2 Envelope equations

We apply Green's identity to the composite function (chosen with the benefit of hindsight: it is used now for ease of presentation)

$$\phi^c = \hat{\phi}^{(2)} + \varphi^{(0)} - \varphi^{(0,2)} \tag{4.3.78}$$

(The truncation of the expansions of the inner and outer solutions are chosen so that we have enough equations when matching between the two for the unknowns) and ψ_q^* to obtain

$$I_V^R = I_F^R + \epsilon^2 (I_a^R - I_b^R). \tag{4.3.79}$$

with each integral notation following from the previous section; recall that I_a^R is the contribution from the integral over $\varphi^{(0)}(\partial\psi_q^*/\partial N)$ and I_b^R is the contribution from the integral over $\psi_q^*(\partial\varphi^{(0)}/\partial N)$ (which was equal to zero for the scattering problem). The arguments for evaluating the integrals I_V^R, I_F^R and I_S^R follow straightforwardly from those of the scattering problem, albeit that the terms appear at different orders of ϵ, due to the different ansatz under consideration here. Similarly to the scattering problem, we note that slow-time does not appear in the inner region governing equations up to (and including) those that are strictly of order ϵ^0, and consequently the leading order inner region solutions are the same as those found for the infinite array. We thus have

$$I_V^R \simeq \frac{\mathrm{i}}{2}\epsilon^2 \frac{\boldsymbol{\beta}_q}{\beta}\beta^2 A^c \cdot \widehat{\nabla} A_q \quad \text{for} \quad q = 1, \ldots, Q. \tag{4.3.80}$$

$$I_F^R \simeq -\frac{\mathrm{i}}{2}\epsilon^2 \beta^2 A^c \frac{\partial A_q}{\partial T} \tag{4.3.81}$$

$$I_a^R \simeq \frac{\mathrm{i}}{2}\mathrm{e}^{-\mathrm{i}\boldsymbol{\beta}_q^T \boldsymbol{R}_j} \left\{ W C_{02}^R - 2\mathrm{i}\pi\mathfrak{D}_1 \left(\boldsymbol{E}_1^S\right)^T \begin{pmatrix} \cos\tau_q \\ \sin\tau_q \end{pmatrix} \right\} \tag{4.3.82}$$

Matching the inner expansion of the outer region solution

$$\begin{aligned}\hat{\phi}^{(-2,-1)} &= -\frac{\mathrm{i}}{2}\sum_{p=1}^{Q} A_p \mathrm{e}^{\mathrm{i}\boldsymbol{\beta}_h^T \boldsymbol{R}_j}\left[\frac{1}{\epsilon^2} - \frac{\mathrm{i}}{\epsilon}R\cos(\theta-\tau_p)\right] \\ &= -\frac{\mathrm{i}}{2}\sum_{p=1}^{Q} A_p \mathrm{e}^{\mathrm{i}\boldsymbol{\beta}_h^T \boldsymbol{R}_j}\left[\frac{1}{\epsilon^2} - \frac{\mathrm{i}}{\epsilon}R(\boldsymbol{e}_{1p})^T\begin{pmatrix}\cos\theta\\ \sin\theta\end{pmatrix}\right]\end{aligned} \tag{4.3.83}$$

with the outer expansion of the inner region solution

$$\varphi^{(-1,-2)} = \frac{1}{\epsilon^2}C_{02}^R + \frac{1}{\epsilon}R\left(\boldsymbol{E}_{11}^R\right)^T\begin{pmatrix}\cos\theta\\ \sin\theta\end{pmatrix} \tag{4.3.84}$$

gives the values of the constants to be

$$C_{02}^R = -\frac{\mathrm{i}}{2}\sum_{p=1}^{Q} A_p \mathrm{e}^{\mathrm{i}\boldsymbol{\beta}_p^T \boldsymbol{R}_j} \tag{4.3.85}$$

$$\boldsymbol{E}_{11}^R = -\frac{1}{2}\sum_{p=1}^{Q} A_p \mathrm{e}^{\mathrm{i}\boldsymbol{\beta}_p^T \boldsymbol{R}_j}(\boldsymbol{e}_{1p})^T. \tag{4.3.86}$$

Furthermore, for circular cylinders with base S_1 and sides S_2, we have that

$$\begin{aligned}I_b^R &= \iint_{S_1}\psi_q^*\frac{\partial\varphi^{(0)}}{\partial Z}\,dS + \iint_{S_2}\psi_q^*\frac{\partial\varphi^{(0)}}{\partial R}\,dS \\ &= \frac{\mathrm{i}}{2}\mathrm{e}^{-\mathrm{i}\boldsymbol{\beta}_q^T\boldsymbol{R}_j}\int_0^{a/h}\int_0^{2\pi}\mathrm{e}^{\mathrm{i}\boldsymbol{\beta}^T\boldsymbol{R}_j}\gamma_0\;Rd\theta dR + 0 \\ &= \frac{\mathrm{i}}{2}W\gamma_0.\end{aligned} \tag{4.3.87}$$

Putting each of our calculations back into Green's identity (4.3.79) and multiplying through by $2/(\mathrm{i}\beta^2 A^c)$, yields

$$\frac{\partial A_q}{\partial T} + \frac{\boldsymbol{\beta}_q}{\beta}\cdot\widehat{\nabla}A_q = -\frac{\mathrm{i}}{2\beta^2 A^c}\sum_{p=1}^{Q}\left\{W - 2\pi\mathfrak{D}_1\boldsymbol{e}_{1p}^T\boldsymbol{e}_{1q}\right\}A_p - \frac{W}{\mathrm{i}\beta^2 A^c}\gamma_0 \quad \text{for} \quad q=1,\ldots,Q. \tag{4.3.88}$$

Recovery of infinite array solution Comparing the infinite array leading order solution with the strip array leading order solution, we see that we need to consider amplitudes of the form

$$A_p(\hat{X},\hat{Y},T) = \frac{2\pi\mathrm{i}L^2}{A^c}U_p^R\mathrm{e}^{-\mathrm{i}\Omega T}$$

for constants U_p^R. Using this form of A_p with $\gamma_0 = \mathrm{e}^{-\mathrm{i}\Omega T}$ and equation (4.3.53) inside the envelope equations (4.3.88) yields

$$\frac{(k-\beta)\,(1/\beta)}{(\beta h)^2}U_q^R = \frac{1}{2\beta^2 A^c}\sum_{q=1}^{Q}\left[W - 2\pi\mathfrak{D}_1 \boldsymbol{e}_{1q}^T\boldsymbol{e}_{1p}\right]U_q^R - \frac{W}{2\pi\beta^2 L^2} \quad \text{for} \quad q = 1,\ldots,Q. \tag{4.3.89}$$

The infinite array radiation solution in shallow water was found to be

$$\frac{(k^2-\beta_q^2)L^2}{(kh)^2}U_p^R - \frac{L^2}{A^c}\sum_{q=1}^{Q}\left[W - 2\pi\mathfrak{D}_1 \boldsymbol{e}_{1q}^T\boldsymbol{e}_{1p}\right]U_q^R = -\frac{W}{\pi}, \quad p = 1,\ldots,Q \tag{4.3.90}$$

Taking $k \to \beta$ so that $\beta = \beta_q$ (and dividing through by $2\beta^2 L^2$) in this solution yields

$$\frac{(k-\beta)(1/\beta)}{(\beta h)^2}U_q^R = \frac{1}{2\beta^2 A^c}\sum_{p=1}^{Q}\left[W - 2\pi\mathfrak{D}_1 \boldsymbol{e}_{1p}^T\boldsymbol{e}_{1q}\right]U_p^R - \frac{W}{2\pi\beta^2 L^2}, \quad q = 1,\ldots,Q \tag{4.3.91}$$

giving agreement with the strip array solution when there is no spatial variance.

4.3.3 Freely-floating structures

The non-dimensional freely floating body condition is

$$\frac{\partial\varphi_F}{\partial Z} = \epsilon^2 u_3^j \quad \text{on} \quad S_{Bj}, \tag{4.3.92}$$

where we drop the superscript R for this section. The structures are not being forced to move with a velocity that is slowly evolving across the array, hence there is no slow-time evolution built into the freely floating condition; they are instead moving with a velocity that depends on the slow evolution of the waves themselves and so their (slow scale) movement is picked up from the slow evolution of the waves (i.e. the $A_p\mathrm{e}^{\mathrm{i}\boldsymbol{\beta}_p^T\boldsymbol{R}_j}$'s); for this reason we don't include the phase difference within the body boundary condition.

The equation of motion

$$u_3^j = \frac{C_{02}}{\epsilon^2}\frac{W}{W+\kappa-\mathrm{i}\lambda} = -\frac{1}{\epsilon^2}\frac{W}{W+\kappa-\mathrm{i}\lambda}\frac{\mathrm{i}}{2}\sum_{p=1}^{Q}A_p\mathrm{e}^{\mathrm{i}\boldsymbol{\beta}_p^T\boldsymbol{R}_j} \tag{4.3.93}$$

after matching $\varphi^{(-1,-2)}$ with $\hat{\phi}^{(-2,-1)}$. The application of Green's identity to the composite

function ϕ_c and ψ_q^* in one cell is represented by the expression

$$I_V = I_F + \epsilon^2 \left(I_a - I_b \right), \tag{4.3.94}$$

which is defined in the obvious way, as per the formulation in the radiation solution, where

$$I_b^F = \frac{\mathrm{i}}{2} \mathrm{e}^{-\mathrm{i}\boldsymbol{\beta}_p^T \boldsymbol{R}_j} W \epsilon^2 u_3^j \tag{4.3.95}$$

(note that in the calculation for I_b^R in the radiation problem, the phase factor $\mathrm{e}^{-\mathrm{i}\boldsymbol{\beta}_p^T \boldsymbol{R}_j}$ cancelled with the phase factor $\mathrm{e}^{\mathrm{i}\boldsymbol{\beta}_p^T \boldsymbol{R}_j}$ from the body condition).

Amending (4.3.88) appropriately means that the application of Green's identity in one cell thus yields

$$\frac{\partial A_q}{\partial T} + \frac{\boldsymbol{\beta}_q}{\beta} \cdot \widehat{\nabla} A_q = -\frac{\mathrm{i}}{2\beta^2 A^c} \sum_{p=1}^{Q} \left[\frac{W(\kappa - \mathrm{i}\lambda)}{W + \kappa - \mathrm{i}\lambda} - 2\pi \mathfrak{D}_1 \boldsymbol{e}_{1q}^T \boldsymbol{e}_{1p} \right] A_p \tag{4.3.96}$$

The discussion found in §4.3.1.4 also applies here. Following the same discussion and methods, the differential equation for the shallow water freely-floating problem, in matrix form, is

$$\frac{d}{d\hat{X}} \begin{pmatrix} B_1 \\ \vdots \\ B_Q \end{pmatrix} = \underline{\underline{\mathrm{F}}} \begin{pmatrix} B_1 \\ \vdots \\ B_Q \end{pmatrix} \tag{4.3.97}$$

where $\underline{\underline{\mathrm{F}}}$ is a $Q \times Q$ matrix with entries

$$F_{ij} = \frac{\mathrm{i}}{\beta^2 A^c} \frac{1}{\cos \tau_i} \left[\delta_{ij} \beta^2 A^c \mathcal{K} (1 - \sin \tau_1 \sin \tau_i) - \frac{1}{2} \left(\frac{W(\kappa - \mathrm{i}\lambda)}{W + \kappa - \mathrm{i}\lambda} - 2\pi \mathfrak{D}_1 \boldsymbol{e}_{1q}^T \boldsymbol{e}_{1p} \right) \right] \tag{4.3.98}$$

for the Kronecker delta function δ_{ij}. The boundary conditions, regarding left- and right-going waves applies here also.

Recovery of infinite array solution Considering wave amplitudes of the form

$$A_p(\hat{X}, \hat{Y}, T) = \frac{2\pi \mathrm{i} L^2}{A^c} U_p \mathrm{e}^{-\mathrm{i}\Omega T}$$

for constants U_p for the reasons outlined previously inside the envelope equations (4.3.96) yields

$$\frac{(k - \beta)\,(1/\beta)}{(\beta h)^2} U_q = \frac{1}{\beta^2 A^c} \sum_{p=1}^{Q} \left[\frac{W(\kappa - \mathrm{i}\lambda)}{W + \kappa - \mathrm{i}\lambda} - 2\pi \mathfrak{D}_1 \boldsymbol{e}_{1q}^T \boldsymbol{e}_{1p} \right] U_p, \quad q = 1, \ldots, Q. \tag{4.3.99}$$

The infinite array freely-floating solution was found to be

$$\frac{(k^2-\beta_q^2)L^2}{(kh)^2}U_p = \frac{L^2}{A^c}\sum_{q=1}^{Q}\left[\frac{W(\kappa-\mathrm{i}\lambda)}{W+\kappa-\mathrm{i}\lambda} - 2\pi\mathfrak{D}_1\boldsymbol{e}_{1q}^T\boldsymbol{e}_{1p}\right]U_q, \quad p=1,2,\ldots Q. \tag{4.3.100}$$

Taking $k\to\beta$ so that $\beta=\beta_q$ (and dividing through by β^2L^2) in this solution yields

$$\frac{(k-\beta)(1/\beta)}{(\beta h)^2}U_q = \frac{1}{\beta^2A^c}\sum_{p=1}^{Q}\left[\frac{W(\kappa-\mathrm{i}\lambda)}{W+\kappa-\mathrm{i}\lambda} - 2\pi\mathfrak{D}_1\boldsymbol{e}_{1p}^T\boldsymbol{e}_{1q}\right]U_p, \quad p=1,2,\ldots Q. \tag{4.3.101}$$

giving agreement with the strip array solution when there is no spatial variation.

4.4 Finite depth and the deep water limit

The work in this section is effectively an account of the solution given in [18], where it is assumed that the size of the structures present are very small when compared with the depth of the water. We also wish to consider small structures relative to the depth, but we on the other hand wish to consider structures in deep water, that is in the limit as the water's depth grows infinitely large. Therefore the work in this section is presented up to the point of obtaining the envelope equations (for both the scattering and radiation problems) in terms of the wave frequency ω (i.e. without using the dispersion relation). Only once these have been obtained do we use the finite depth dispersion relation in order to recover the solutions found in [18] before continuing on our way with using the deep water dispersion relation in order that we may find solutions that are comparable to our infinite array work. We only consider the deep water case for the freely-floating solution.

We look for solutions as $k\to\beta$ and the length scale b introduced in § 4.2 is chosen to be $b=a$ and, for deep water, the unperturbed wavenumber is $\beta=\omega^2/g$. We assume that the size of each structure is characterised by a length a that is much smaller than the wavelength $2\pi/\beta$, that is $\epsilon=\beta a\ll 1$, and that a/h and βL are ord(1) so that $a/L\ll 1$. In the inner region the motion takes place on the length scale a, but in the outer region the motion takes place on the length scale β^{-1}. Hence suitable inner coordinates are

$$X=x/a,\ Y=z/a,\ Z=z/a,\ R=r_j/a, \tag{4.4.1}$$

and the inner region potential is $\varphi(X, Y, Z, \epsilon) \equiv \phi(x, y, z)$, while suitable outer coordinates are

$$x' = \beta x, \quad y' = \beta y, \quad z' = \beta z, \quad r'_j = \beta r_j,$$

and the potential is $\hat{\phi}(x', y', z', \epsilon) \equiv \phi(x, y, z)$. Spherical coordinates centred on the origin O are also used; these are denoted by $(\tilde{R}, \psi, \theta) = (\tilde{R}, \cos^{-1}(Z/\tilde{R}), \theta)$ for the inner region, and $(\tilde{r}, \psi, \theta) = (\tilde{r}, \cos^{-1}(z/\tilde{r}), \theta)$ for the outer region. For $\beta a \ll 1$, we expect our solutions to satisfy the dispersion relation $\omega^2 = g\beta \tanh \beta h$ and so it is convenient to introduce a non-dimensional fast-time quantity

$$t' = \sqrt{\beta g}\, t.$$

We also need to define slow scale coordinates

$$\hat{X} = \epsilon^2 x', \quad \hat{Y} = \epsilon^2 y', \quad T = \epsilon^2 t',$$

to describe the evolution of waves as they propagate through the array. We assume that the fast motion of the waves is time harmonic by writing

$$\Phi = \mathrm{Re}\left[\hat{\phi}(x', y', Z; \hat{X}, \hat{Y}, T)\mathrm{e}^{-\mathrm{i}(\omega/\sqrt{\beta g})t'}\right] \tag{4.4.2}$$

so that fast-time is separated out of the problem. Hence, we note that our differential operators become

$$\frac{\partial}{\partial x'} \to \frac{\partial}{\partial x'} + \epsilon^2 \frac{\partial}{\partial \hat{X}} \quad ; \quad \frac{\partial^2}{\partial x'^{\,2}} \to \frac{\partial^2}{\partial x'^{\,2}} + 2\epsilon^2 \frac{\partial}{\partial x'}\frac{\partial}{\partial \hat{X}} + \mathrm{O}(\epsilon^4), \tag{4.4.3}$$

where the relationship between y' and $\hat{Y}$ follows similarly so that we also have

$$\overline{\nabla}^2 \to \overline{\nabla}^2 + 2\epsilon^2 \overline{\nabla} \cdot \widehat{\nabla} + \epsilon^4 \widehat{\nabla}^2 \tag{4.4.4}$$

where $\widehat{\nabla}$ is the horizontal Laplacian in slow coordinates and $\overline{\nabla}$ is the horizontal Laplacian in outer region coordinates. Furthermore we have

$$\frac{\partial}{\partial t'} \to \epsilon^2 \frac{\partial}{\partial T} \quad \text{so that} \quad \frac{\partial^2}{\partial t'^{\,2}} \to \epsilon^4 \frac{\partial^2}{\partial T^2}. \tag{4.4.5}$$

4.4.1 The scattering problem

4.4.1.1 Outer problem

The outer region problem is stated as

$$\overline{\nabla}^2\Phi + \frac{\partial^2\Phi}{\partial z'^2} = 0 \quad \text{in the fluid,} \tag{4.4.6a}$$

$$\frac{\partial^2\Phi}{\partial t'^2} + \frac{\partial\Phi}{\partial z'} = 0 \quad \text{for} \quad z' = 0 \quad \text{and} \quad |r| > a, \tag{4.4.6b}$$

as well as, for water of finite depth a bed condition

$$\frac{\partial\Phi}{\partial z'} = 0 \quad \text{on} \quad z' = -1, \tag{4.4.7}$$

while for deep water we require

$$|\nabla\Phi| \to 0 \quad \text{as} \quad z' \to -\infty. \tag{4.4.8}$$

(We note now that when we come to applying Green's identity in a single cell, the surface integral across the bottom of the cell – whether we are considering finite depth or deep water – is zero. For this reason, and to avoid repetition, from this point onwards we omit stating the finite depth bed and deep water condition each time we state an outer problem).

Using the form of Φ given in (4.4.2) generates the multiple scales problem of

$$\left(\overline{\nabla}^2 + 2\epsilon^2\overline{\nabla}\cdot\widehat{\nabla} + \epsilon^4\widehat{\nabla}^2\right)\hat{\phi}^S + \frac{\partial^2\hat{\phi}^S}{\partial z'^2} = 0 \quad \text{in the fluid,} \tag{4.4.9a}$$

$$\left(-\frac{\omega^2}{\beta g}\hat{\phi}^S - 2\mathrm{i}\epsilon^2\frac{\omega}{\sqrt{\beta g}}\frac{\partial\hat{\phi}^S}{\partial T} + \epsilon^4\frac{\partial^2\hat{\phi}^S}{\partial T^2}\right) + \frac{\partial\hat{\phi}^S}{\partial z'} = 0 \quad \text{for} \quad Z = 0 \quad \text{and} \quad |r| > a, \tag{4.4.9b}$$

Motivated by the infinite array solution, where our outer solutions were constructed from fundamental solutions of the form $g_{mn} = g^{(1)}_{mn} + \epsilon^2 g^{(2)}_{mn}$, consider the ansatz

$$\hat{\phi}^S = \hat{\phi}^S_0 + \epsilon^2\hat{\phi}^S_2 + \dots$$

Going forward, we drop the superscript S from our outer velocity potentials. Substituting this

into the system (4.4.9) yields

$$\overline{\nabla}^2\hat{\phi}_0 + \frac{\partial^2\hat{\phi}_0}{\partial z'^2} = 0 \quad \text{in the fluid,} \tag{4.4.10a}$$

$$\frac{\partial}{\partial z'}\hat{\phi}_0 - \frac{\omega^2}{g\beta}\hat{\phi}_0 = 0 \quad \text{for} \quad z' = 0 \quad \text{and} \quad |r| > a, \tag{4.4.10b}$$

$$\frac{\partial^2\hat{\phi}_2}{\partial z'^2} = -\overline{\nabla}^2\hat{\phi}_2 - 2\epsilon^2\overline{\nabla}\cdot\widehat{\nabla}\hat{\phi}_0 \quad \text{in the fluid,} \tag{4.4.11a}$$

$$-\frac{\omega^2}{\beta g}\hat{\phi}_2 - 2\mathrm{i}\frac{\omega}{\sqrt{\beta g}}\frac{\partial\hat{\phi}_0}{\partial T} + \frac{g\beta}{\beta g}\frac{\partial\hat{\phi}_2}{\partial z'} = 0 \quad \text{for} \quad z' = 0 \quad \text{and} \quad |r| > a. \tag{4.4.11b}$$

4.4.1.2 Inner problem

The complete inner region problem is stated as

$$\nabla_{IR}^2\Phi + \frac{1}{\epsilon^2}\frac{\partial^2\Phi}{\partial Z^2} = 0 \quad \text{in the fluid,} \tag{4.4.12a}$$

$$\epsilon\frac{\partial^2\Phi}{\partial t'^2} + \frac{\partial\Phi}{\partial Z} = 0 \quad \text{for} \quad Z = 0 \quad \text{and} \quad |r| > a, \tag{4.4.12b}$$

$$\frac{\partial\Phi}{\partial N} = 0 \quad \text{on} \quad S_C. \tag{4.4.12c}$$

For fast wave motion that is time-harmonic we use

$$\Phi = \mathrm{Re}\left[\varphi^S(X, Y, Z; \hat{X}, \hat{Y}, T)\mathrm{e}^{-\mathrm{i}(\omega/\sqrt{\beta g})t'}\right]$$

to obtain a multiple scales problem of

$$\epsilon^2\left(\nabla_{IR}^2 + 2\epsilon^2\nabla_{IR}\cdot\widehat{\nabla}\right)\varphi + \frac{\partial^2\varphi}{\partial Z^2} = 0 \quad \text{in the fluid,} \tag{4.4.13a}$$

$$\epsilon\left(-\varphi - 2\mathrm{i}\epsilon^2\frac{\partial\varphi}{\partial T} + \epsilon^4\frac{\partial^2\varphi}{\partial T^2}\right) + \frac{\partial\varphi}{\partial Z} = 0 \quad \text{for} \quad Z = 0 \quad \text{and} \quad |r| > a, \tag{4.4.13b}$$

$$\frac{\partial\varphi}{\partial N} = 0 \quad \text{on} \quad S_C. \tag{4.4.13c}$$

For a leading order inner region solution expanded like

$$\varphi^S \simeq \varphi_0^S + \epsilon\varphi_1^S + \ldots \tag{4.4.14}$$

(motivated by the form of the envelope equations used to describe the outer region) we note that slow-time does not appear in the inner region governing equations up to (and including) those that are ord(ϵ), and consequently the inner region solutions that we require are the same as those found for the infinite array.

4.4.1.3 Envelope equations

The so called envelope equations describe the slow scale dynamics as the waves move through the array. To derive them we consider a separable solution

$$\hat{\phi}_0 = \sum_{q=1}^{Q} A_q(\hat{X}, \hat{Y}, T)\psi_q(x', y', z'), \tag{4.4.15}$$

for

$$\psi_q(x', y', z') = -\frac{\mathrm{i}\sqrt{\beta g}}{\omega} D(z')\mathrm{e}^{\mathrm{i}\boldsymbol{\beta}_q^T \boldsymbol{R}_j}\mathrm{e}^{\mathrm{i}(\boldsymbol{\beta}_q^T/\beta)\boldsymbol{r}'_j} \tag{4.4.16}$$

where

$$D(z') = \frac{\cosh(z' + \beta h)}{\cosh \beta h}$$

Note that we've chosen the ψ_q's such that they are valid at the point in wavenumber space we are perturbing from; the A_q's pick up the perturbations from that point in the case where cylinders are present.

We formalise the solution given in [18] by constructing a composite function to describe the fluid in the entire primary cell (which includes the inner and outer region) where the truncation of the expansions of the inner and outer solutions are chosen so that we have the correct order of equations when applying Green's identity. Such a composite function is taken as (chosen with the benefit of hindsight: it is used now for ease of presentation)

$$\phi^c = \hat{\phi}^{(2)} + \varphi^{(0)} - \varphi^{(0,2)} \tag{4.4.17}$$

where the inner region's outer expansion is included to avoid double counting the intermediate region that is shared between both fields. Applying Green's identity to ϕ^c and ψ_q^* over the primary cell (the superscript asterisk denotes that the complex conjugate has been taken) yields

$$\iiint_V \left\{\phi^c \nabla^2 \psi_q^* - \psi_q^* \nabla^2 \phi^c\right\}\, dv = \iint_{\partial V} \left\{\phi^c \frac{\partial \psi_q^*}{\partial n} - \psi_q^* \frac{\partial \phi^c}{\partial n}\right\}\, ds$$

in dimensional coordinates, where V is the volume of the cell, defined by the boundary surface ∂V; the surface ∂V consists of the free surface S_F, the cylinders wetted surface S_C, the vertical surfaces S_V that describe one cell and the bed S_B. By definition we have $\nabla^2\psi_q^* = 0$, and the surface integrals on S_B and S_V disappear by the deep water condition and the Bloch condition respectively. Writing everything in terms of the appropriate coordinates, and using the scattering boundary condition on the inner region solution we hence have

$$\begin{aligned} -\iiint_V \left\{\psi_q^*\left(\overline{\nabla}^2 + \frac{\partial^2}{\partial z'^2}\right)\phi^c\right\}\, dv' \\ = \iint_{S_F}\left\{\phi^c\frac{\partial\psi_q^*}{\partial z'} - \psi_q^*\frac{\partial\phi^c}{\partial z'}\right\}\, ds' + \epsilon\iint_{S_C}\left\{\varphi^{(1)}\frac{\partial\psi_q^*}{\partial N} - \psi_q^*\frac{\partial\varphi^{(1)}}{\partial N}\right\}\, dS \end{aligned} \tag{4.4.18}$$

where it is noted that $\phi^c = \varphi^{(1)}$ on the structure and dS is used to represent the surface integral in terms of inner region coordinates and N is the normal in inner region coordinates. Let us introduce the notation I_V^S, I_F^S, I_a^S and I_b^S to represent the different integrals in (4.4.18) so that we have

$$I_V^S = I_F^S + \epsilon(I_a^S + I_b^S) \tag{4.4.19}$$

to represent the application of Green's identity in one cell.

Dealing with the volume integral in eqn (4.4.19) first, and denoting the inner region horizontal Laplacian $\overline{\nabla}_{IR}^2$, we have that

$$\begin{aligned} I_V^S &= -\iiint_V \left\{\psi_q^*\left(\overline{\nabla}^2 + \frac{\partial^2}{\partial z'^2}\right)\hat{\phi}^{(2)} + \psi_q^*\frac{1}{\epsilon^2}\left(\overline{\nabla}_{IR}^2 + \frac{\partial^2}{\partial Z^2}\right)\left(\varphi^{(1)} - \varphi^{(1,2)}\right)\right\}\, dv' \\ &= -\iiint_V \left\{\psi_q^*\left(\overline{\nabla}^2 + \frac{\partial^2}{\partial z'^2}\right)\hat{\phi}^{(2)}\right\}\, dv' \end{aligned} \tag{4.4.20}$$

by the governing field equation in the inner region. Substituting for $\hat{\phi}^{(2)}$, using the governing field equations and then truncating at leading order yields

$$I_V^S \simeq 2\epsilon^2\iiint_V \left(\psi_q^*\overline{\nabla}\cdot\widehat{\nabla}\hat{\phi}_0\right)\, dv' = 2\epsilon^2\iiint_V \left\{\psi_q^*\overline{\nabla}\cdot\widehat{\nabla}\left(\sum_{q=1}^{Q} A_q\psi_q\right)\right\} dv', \quad q = 1,\ldots,Q. \tag{4.4.21}$$

Using (4.4.15) with p as the dummy index, noting that $\overline{\nabla}\psi_p = \mathrm{i}(\boldsymbol{\beta}_p/\beta)\psi_p$ and $\widehat{\nabla}A_p$ depends on

the slow coordinates only, we thus have

$$I_V^S \simeq 2\mathrm{i}\epsilon^2 \frac{\beta g}{\omega^2}\beta^2 A^c \left[\int_{-\beta h}^{0} D^2(z')\ dz'\right] \frac{\boldsymbol{\beta}_p^T}{\beta} \cdot \sum_{q=1}^{Q} \widehat{\nabla} A_q, \quad q = 1, \ldots, Q \tag{4.4.22}$$

where $\beta^2 A^c$ is the non-dimensional area of one lattice cell ($\beta^2 A^c = \beta^2 L^2$ for a square lattice); it comes from the horizontal component of the volume integral as demonstrated in [17]; the Kronecker delta function that appears in said calculation forces $p = q$. The integral through the depth is calculated as

$$\int_{-\beta h}^{0} D^2(z')\ dz' = \frac{1}{2}\tanh\beta h \left[1 + \frac{\beta h}{\sinh(\beta h)\cosh(\beta h)}\right] \tag{4.4.23}$$

We now turn our attention to the integral on the free surface. Note that

$$\left.\frac{\partial \psi_q^*}{\partial z'}\right|_{z'=0} = D'(z')\ \psi_q^*\Big|_{z'=0} \tag{4.4.24}$$

where

$$D'(z')\Big|_{z'=0} = \left.\frac{\sinh(z'+\beta h)}{\cosh\beta h}\right|_{z'=0} = \tanh\beta h \tag{4.4.25}$$

in the outer region but (for calculating I_a^S later) note that

$$D'(\epsilon Z)\Big|_{Z=0} = \epsilon \left.\frac{\sinh(\epsilon Z+\beta h)}{\cosh\beta h}\right|_{Z=0} = \epsilon\tanh\beta h \tag{4.4.26}$$

in the inner region. By definition, we have

$$\begin{aligned} I_F^S = &\iint_{S_F} \left\{ \hat{\phi}^{(2)} D'(z')\psi_q^*\Big|_{z'=0} - \psi_q^*\Big|_{z'=0} \frac{\partial \hat{\phi}^{(2)}}{\partial z'} \right\}\ ds' \\ &+ \iint_{S_F} \left\{ \left(\varphi^{(0)} - \varphi^{(0,2)}\right) D'(\epsilon Z)\psi_q^*\Big|_{Z=0} - \psi_q^*\Big|_{z'=0} \frac{1}{\epsilon}\frac{\partial}{\partial Z}\left(\varphi^{(0)} - \varphi^{(0,2)}\right) \right\}\ \epsilon^2 dS \\ &\qquad\qquad\qquad\qquad\qquad\qquad\qquad\qquad\qquad\qquad\qquad\qquad q = 1, \ldots, Q, \end{aligned} \tag{4.4.27}$$

where the second integral has been written in terms of inner region coordinates. The second integral is zero, because $\varphi^{(0)} - \varphi^{(0,2)} = 0$. By using the free surface conditions acting on $\hat{\phi}_0$ and

$\hat{\phi}_2$ we obtain

$$I_F^S \simeq -\iint_{S_F} \left\{ \psi_q^* \Big|_{z'=0} \left(2\mathrm{i}\epsilon^2 \frac{\omega\sqrt{\beta g}}{g\beta} \frac{\partial \hat{\phi}_0}{\partial T} \right) \right\} \, ds', \quad q = 1, \ldots, Q. \tag{4.4.28}$$

Using (4.4.15) with p as the dummy variable yields

$$I_F \simeq -2\mathrm{i}\epsilon^2 \frac{\sqrt{\beta g}}{\omega} \beta^2 A^c \frac{\partial A_q}{\partial T}, \quad q = 1, \ldots, Q \tag{4.4.29}$$

(the integral is similar to that calculated above as part of the volume integral – although ψ_q is now being evaluated on $z' = 0$) where we have, again, been forced to take $p = q$.

For the integral across the structure, we note that for the scattering problem $I_b^S = 0$. By definition we have that

$$I_a^S = \iint_{S_C} C_0^S \frac{\partial \psi_q^*}{\partial N} \, dS \quad \text{for} \quad q = 1, \ldots, Q, \tag{4.4.30}$$

where $\varphi^{(0)} = C_0^S$ to leading order. As a consequence of the divergence theorem we know that the integral of the normal derivative of a function across and into a structure's boundary is zero, that is to say that

$$\begin{aligned} \iint_{S_C} \frac{\partial \psi_q^*}{\partial N} \, dS &= -\iint_{S_W} \frac{\partial \psi_q^*}{\partial N} \Big|_{Z=0} \, dS \\ &= \iint_{S_W} \frac{\partial \psi_q^*}{\partial Z} \Big|_{Z=0} \, dS \\ &\simeq \frac{\mathrm{i}\sqrt{\beta g}}{\omega} D'(\epsilon Z) \Big|_{Z=0} \, \mathrm{e}^{-\mathrm{i}\boldsymbol{\beta}_q^T \boldsymbol{R}_j} W \end{aligned} \tag{4.4.31}$$

for $q = 1, \ldots, Q$, where S_W is the surface that the structure cuts on the free surface and W is the (non-dimensional) water plane area. For a circular cylinder with a radius non-dimensionalised by a we have $W = \pi$ giving

$$I_a^S \simeq \frac{\mathrm{i}\sqrt{\beta g}}{\omega} \epsilon \tanh \beta h \, \mathrm{e}^{-\mathrm{i}\boldsymbol{\beta}_q^T \boldsymbol{R}_j} \pi C_0^S, \quad q = 1, \ldots, Q. \tag{4.4.32}$$

Matching the outer region solution's inner expansion $\hat{\phi}^{(0,0)}$, written in terms of dummy

variable p, with the inner region solution's outer expansion $\varphi^{(0,0)}$ yields

$$C_0^S = -\frac{\mathrm{i}\sqrt{\beta g}}{\omega}\sum_{p=1}^{Q} A_p \mathrm{e}^{\mathrm{i}\boldsymbol{\beta}_p^T \boldsymbol{R}_j} \tag{4.4.33}$$

so that

$$I_a^S \simeq \epsilon\pi \sum_{p=1}^{Q} A_p \tag{4.4.34}$$

where it is noted that by the definition of the reciprocal lattice vector $\mathrm{e}^{-\mathrm{i}\boldsymbol{\beta}_q^T \boldsymbol{R}_j}\mathrm{e}^{\mathrm{i}\boldsymbol{\beta}_p^T \boldsymbol{R}_j} = 1$. Putting each of our calculations back into Green's identity (4.4.19), and multiplying through by $\omega/(2\mathrm{i}\beta A^c)$ yields

$$\sqrt{\beta g}\frac{\partial A_q}{\partial T} + \frac{\omega}{2}\left(1 + \frac{\beta h}{\sinh(\beta h)\cosh(\beta h)}\right)\frac{\boldsymbol{\beta}_q^T}{\beta}\cdot\widehat{\nabla} A_q = -\frac{\mathrm{i}\pi\omega}{2\beta^2 A^c}\sum_{p=1}^{Q} A_p, \quad q = 1,\ldots,Q. \tag{4.4.35}$$

Comparison with Garnaud and Mei [18] Putting our envelope equations as given in (4.4.35) back into dimensional form by transforming our operators

$$\frac{\partial}{\partial T} \to \frac{1}{\epsilon^2}\frac{1}{\sqrt{\beta g}}\frac{\partial}{\partial t} \quad \text{and} \quad \widehat{\nabla} \to \frac{1}{\epsilon^2}\frac{1}{\beta}\widehat{\nabla}_{2D}, \tag{4.4.36}$$

where $\widehat{\nabla}_{2D}$ is the Laplacian in two-dimensional space coordinate in original coordinates, we obtain

$$\frac{\partial A_q}{\partial t} + C_g\frac{\boldsymbol{\beta}_q^T}{\beta}\cdot\widehat{\nabla}_{2D} A_q = -\frac{\mathrm{i}\pi\omega}{2}\frac{a^2}{A^c}\sum_{p=1}^{Q} A_p, \quad q = 1,\ldots,Q. \tag{4.4.37}$$

This is analogous to [18, equation (4.17)] for their group speed [18, equation (3.8)]

$$C_g = \frac{\omega}{2\beta}\left(1 + \frac{2\beta h}{\sinh(2\beta h)}\right).$$

Deep water envelope equations for the scattering problem We continue going forward with this scattering solution under the deep water assumption, that is that $\beta h \to \infty$, so that $\omega^2 = g\beta$ so that from (4.4.35)

$$\frac{\partial A_q}{\partial T} + \frac{1}{2}\frac{\boldsymbol{\beta}_q^T}{\beta}\cdot\widehat{\nabla} A_q = -\frac{\mathrm{i}\pi}{2\beta^2 A^c}\sum_{p=1}^{Q} A_p \quad \text{for} \quad q = 1,\ldots,Q. \tag{4.4.38}$$

The discussion found in §4.3.1.4 also applies here. Following the same discussion and methods, the differential equation for the deep water scattering problem, in matrix form, is

$$\frac{d}{d\hat{X}}\begin{pmatrix} B_1 \\ \vdots \\ B_Q \end{pmatrix} = \underline{\underline{\mathrm{F}}}^S \begin{pmatrix} B_1 \\ \vdots \\ B_Q \end{pmatrix} \tag{4.4.39}$$

where $\underline{\underline{\mathrm{F}}}^S$ is a $Q \times Q$ matrix with entries

$$F^S_{ij} = \frac{\mathrm{i}}{\beta^2 A^c}\frac{1}{\cos\tau_i}\left[\delta_{ij}\beta^2 A^c \mathcal{K}(2 - \sin\tau_1 \sin\tau_i) - \pi\right] \tag{4.4.40}$$

for the Kronecker delta function δ_{ij}. The boundary conditions, regarding left- and right-going waves applies here also.

Recovery of infinite array solution The infinite array leading order solution is

$$\hat{\phi} = \sum_{q=1}^{Q} U_q \mathrm{e}^{\mathrm{i}r' \cos(\theta - \tau_q)}, \tag{4.4.41}$$

whilst the strip array solution has been found using the leading order solution

$$\hat{\phi} = \left(-\frac{\sqrt{\beta g}\mathrm{i}}{\omega}\right)\mathrm{e}^{z'}\sum_{q=1}^{Q} A_q \mathrm{e}^{\mathrm{i}\boldsymbol{\beta}_q^T \boldsymbol{r}} = -\mathrm{i}\mathrm{e}^{z'}\sum_{q=1}^{Q} A_q \mathrm{e}^{\mathrm{i}\boldsymbol{\beta}_q^T \boldsymbol{r}} \tag{4.4.42}$$

meaning that we need to use $U_q = -\mathrm{i}A_q$ when comparing the solutions which, whilst making no difference to the recovery of the scattering solution, is accounted for here for completeness.

Let us hence consider amplitudes of the form

$$A_p(\hat{X}, \hat{Y}, T) = \mathrm{i}U_p^S \mathrm{e}^{-\mathrm{i}\Omega T} \tag{4.4.43}$$

for constants U_p^S (i.e. amplitudes that do not vary over space). Having considered the fast-time dependence in $\Phi = \mathrm{Re}\left[\hat{\phi}(x', y', Z; \hat{X}, \hat{Y}, T)\mathrm{e}^{-\mathrm{i}\omega t}\right]$, we have that the time dependence found in the infinite array solutions is related to the strip array time dependence via $\mathrm{e}^{-\mathrm{i}\omega t} \equiv \mathrm{e}^{-\mathrm{i}\omega t}\mathrm{e}^{-\mathrm{i}\Omega T}$. When used with the applicable dispersion relations, this becomes

$$\mathrm{e}^{-\mathrm{i}\sqrt{kg}t} \equiv \mathrm{e}^{-\mathrm{i}\sqrt{\beta g}t}\mathrm{e}^{-\mathrm{i}\Omega T}$$

so that, when everything is put in terms of t', we have non dimensional frequency

$$\sqrt{\frac{k}{\beta}} = 1 + \epsilon^2\Omega \tag{4.4.44}$$

so that $k/\beta = 1 + 2\epsilon^2\Omega + \epsilon^4\Omega^2$ and so

$$\Omega \simeq \frac{(k-\beta)\,(1/2\beta)}{(\beta a)^2}. \tag{4.4.45}$$

Using the form of A_p, as given in (4.4.43), with this relationship between Ω and k in the envelope equations (4.4.38) yields

$$\frac{(k-\beta)\,(1/\beta)}{(\beta a)^2}U_q^S - \frac{\pi}{\beta^2 A^c}\sum_{p=1}^{Q} U_q^S = 0, \quad q = 1, \ldots, Q. \tag{4.4.46}$$

The infinite array scattering solution in deep water was found to be

$$\frac{(k^2-\beta_q^2)L^2}{(ka)^2}U_p^S - \frac{\pi L^2}{A^c}\sum_{q=1}^{Q} 2U_q^S = 0, \quad p = 1, \ldots, Q \tag{4.4.47}$$

Taking $k \to \beta$ so that $\beta = \beta_q$ in the infinite array solution (and dividing through by $\beta^2 L^2$) yields

$$\frac{(k-\beta)(1/\beta)}{(\beta a)^2}U_q^S - \frac{\pi}{\beta^2 A^c}\sum_{p=1}^{Q} U_p^S = 0, \quad q = 1, \ldots, Q \tag{4.4.48}$$

giving agreement with the strip array solution when there is no spatial variation.

4.4.2 The radiation problem

4.4.2.1 Inner and outer problems

The outer region problem is stated as

$$\overline{\nabla}^2\Phi + \frac{\partial^2\Phi}{\partial z'^2} = 0 \quad \text{in the fluid,} \tag{4.4.49a}$$

$$\frac{\partial^2\Phi}{\partial t'^2} + \frac{\partial\Phi}{\partial z'} = 0 \quad \text{for} \quad z' = 0 \quad \text{and} \quad |r| > a, \tag{4.4.49b}$$

as well as, for water of finite depth a bed condition

$$\frac{\partial\Phi}{\partial z'} = 0 \quad \text{on } S_B \tag{4.4.50}$$

while for deep water we require

$$|\nabla\Phi| \to 0 \quad \text{as} \quad z' \to -\infty. \tag{4.4.51}$$

As with the scattering problem – for fast wave motion that is time-harmonic, that is $\Phi = \mathrm{Re}\left[\varphi^S(X,Y,Z;\hat{X},\hat{Y},T)\mathrm{e}^{-\mathrm{i}(\omega/\sqrt{\beta g})t'}\right]$ – we consider a separable solution of the form

$$\hat{\phi}^R_{01} = \sum_{q=1}^{Q} A_q(\hat{X},\hat{Y},T)\psi_q(x,y,z) \tag{4.4.52}$$

with ψ_q as defined previously. In the outer region, the ansatz

$$\hat{\phi} = \frac{1}{\epsilon}\hat{\phi}^R_{01} + \epsilon\hat{\phi}^R_1 + \epsilon^3\hat{\phi}^R_3 + \ldots$$

is motivated by the infinite array solution. The slow-time equations in the fluid and on the free surface (as well as either the bed or deep water condition) for $\hat{\phi}^R_{01}$ and $\hat{\phi}^R_1$ correspond respectively with the problems for $\hat{\phi}^S_0$ and $\hat{\phi}^S_2$ as given in the systems of equations (4.4.10) and (4.4.11); As with the shallow water problem, it is the matching with the inner region solution – which depends on the body condition – that distinguishes the outer region between the scattering and radiation problems.

The complete inner region problem is

$$\nabla^2_{IR}\Phi + \frac{1}{\epsilon^2}\frac{\partial^2\Phi}{\partial Z^2} = 0 \quad \text{in the fluid,} \tag{4.4.53a}$$

$$\epsilon\frac{\partial^2\Phi}{\partial t'^2} + \frac{\partial\Phi}{\partial Z} = 0 \quad \text{for} \quad Z = 0 \quad \text{and} \quad |r| > a, \tag{4.4.53b}$$

as well as a body condition, which in inner region coordinates (derived directly from that given in the problem formulation section) is

$$\frac{\partial\varphi}{\partial Z} = \frac{\omega^2 a}{g}u_3 = \epsilon u_3 \tanh\beta h \tag{4.4.54}$$

For the radiation problem we force a structure to move with velocity

$$\epsilon\tanh\beta h u_3 = \gamma(\hat{X},\hat{Y},T)\mathrm{e}^{-\mathrm{i}(\omega/\sqrt{\beta g})t'}\mathrm{e}^{\mathrm{i}\boldsymbol{\beta}^T\boldsymbol{R}_j}$$

for non-dimensional complex amplitude of the structure's vertical velocity $\gamma(\hat{X},\hat{Y},T)$ which will evolve on the slow scales as waves move across the strip array. Expanding the complex amplitude

of the structure's vertical velocity in powers of ϵ^2, the body condition for the radiation problem hence becomes

$$\frac{\partial \varphi^R}{\partial Z} = \mathrm{e}^{\mathrm{i}\boldsymbol{\beta}^T \boldsymbol{R}_j} \left(\gamma_0(\hat{X}, \hat{Y}, T) + \epsilon^2 \gamma_2(\hat{X}, \hat{Y}, T) + \dots \right) \quad \text{on} \quad S_{Bj}, \tag{4.4.55}$$

for both the arbitrary depth and deep water case. For an inner region ansatz of

$$\varphi^R = \frac{1}{\epsilon} \varphi^R_{01} + \varphi^R_0 \tag{4.4.56}$$

the body condition for the radiation problem becomes

$$\frac{\partial \varphi_{01}}{\partial Z} = 0 \tag{4.4.57a}$$

$$\frac{\partial \varphi_0}{\partial Z} = \mathrm{e}^{\mathrm{i}\boldsymbol{\beta}^T \boldsymbol{R}_j} \gamma_0 \tag{4.4.57b}$$

after dropping the dependence of the γ's on $(\hat{X}, \hat{Y}, T)$ for ease of notation. We note that slow-time does not appear in the inner region governing equations up to (and including) those that are ord(1), and consequently the inner region solutions that we require are the same as those found for the infinite array. Going forward in this section, we will drop the R subscript from the velocity potential.

4.4.2.2 Envelope equations

We apply Green's identity to the composite function (chosen with the benefit of hindsight: it is used now for ease of presentation)

$$\phi^c = \hat{\phi}^{(1)} + \varphi^{(0)} - \varphi^{(0,1)} \tag{4.4.58}$$

(The truncation of the expansions of the inner and outer solutions are chosen so that on applying Green's identity, we have all of the required leading order terms of the solutions for each of the integrals) and ψ^*_q to obtain

$$I^R_V = I^R_F + \epsilon(I^R_a - I^R_b). \tag{4.4.59}$$

where the notation is used to represent the same components of the integrals we are required to calculate. The arguments for evaluating the integrals I^R_V, I^R_F and I^R_S follow straight forwardly from those of the scattering problem, albeit that the terms appear at different orders of ϵ, due

to the different ansatz under consideration here. Similarly to the scattering problem, we note that slow-time does not appear in the inner region governing equations up to (and including) those that are ord(1), and consequently the leading order inner region solutions are the same as those found for the deep water infinite array. We thus have

$$I_V^R \simeq \mathrm{i}\epsilon\beta^2 A^c \left(1 + \frac{\beta h}{\sinh(\beta h)\cosh(\beta h)}\right) \frac{\boldsymbol{\beta}_p^T}{\beta} \cdot \sum_{q=1}^{Q} \widehat{\nabla} A_q \tag{4.4.60}$$

$$I_F^R \simeq -2\mathrm{i}\epsilon \frac{\sqrt{\beta g}}{\omega} \beta^2 A^c \frac{\partial A_q}{\partial T} \tag{4.4.61}$$

$$I_a^R \simeq \frac{\mathrm{i}\sqrt{\beta g}}{\omega} \epsilon \tanh \beta h \ \mathrm{e}^{-\mathrm{i}\boldsymbol{\beta}_q^T \boldsymbol{R}_j} \pi \frac{C_{01}^R}{\epsilon} \tag{4.4.62}$$

with each being defined for $q = 1, \ldots, Q$.

Matching the outer region solution's inner expansion $\hat{\phi}_R^{(-1,-1)}$, written in terms of dummy variable p, with the inner region solution's outer expansion $\varphi_R^{(-1,-1)}$ yields

$$C_{01}^R = -\frac{\mathrm{i}\sqrt{\beta g}}{\omega} \sum_{p=1}^{Q} A_p \mathrm{e}^{\mathrm{i}\boldsymbol{\beta}_p^T \boldsymbol{R}_j} \tag{4.4.63}$$

so that

$$I_a^R \simeq \pi \sum_{p=1}^{Q} A_p \tag{4.4.64}$$

where it is noted that by the definition of the reciprocal lattice vector $\mathrm{e}^{-\mathrm{i}\boldsymbol{\beta}_q^T \boldsymbol{R}_j} \mathrm{e}^{\mathrm{i}\boldsymbol{\beta}_p^T \boldsymbol{R}_j} = 1$. Furthermore, for circular cylinders with bases S_1 (note that $\partial\varphi^{(0)}/\partial N = 0$ on the cylinders' sides) that have been scaled by their radii a, we have that

$$\begin{aligned} I_b^R &= \iint_{S_1} \psi_q^* \frac{\partial \varphi^{(0)}}{\partial Z} \, dS \\ &\simeq \frac{\mathrm{i}\sqrt{\beta g}}{\omega} \mathrm{e}^{-\mathrm{i}\boldsymbol{\beta}_q^T \boldsymbol{R}_j} \int_0^{a/a} \int_0^{2\pi} \mathrm{e}^{\mathrm{i}\boldsymbol{\beta}^T \boldsymbol{R}_j} \gamma_0 \, R d\theta dR \\ &= \frac{\mathrm{i}\sqrt{\beta g}}{\omega} \pi \gamma_0. \end{aligned} \tag{4.4.65}$$

Putting each of our calculations back into Green's identity (4.4.59), and multiplying through by

$\omega/(2\mathrm{i}\beta A^c)$ yields

$$\sqrt{\beta g}\frac{\partial A_q}{\partial T}+\frac{\omega}{2}\left(1+\frac{\beta h}{\sinh(\beta h)\cosh(\beta h)}\right)\frac{\boldsymbol{\beta}_q^T}{\beta}\cdot\widehat{\nabla}A_q=-\frac{\mathrm{i}\pi\omega}{2\beta^2A^c}\left(\sum_{p=1}^{Q}A_p-\frac{\mathrm{i}\sqrt{\beta g}}{\omega}\gamma_0\right),\quad q=1,\ldots,Q. \tag{4.4.66}$$

Comparison with Garnaud and Mei [18] Putting our envelope equations as given in (4.4.66) back into dimensional form by transforming our operators as done in the recovery of the Garnaud and Mei scattering solution, we obtain

$$\frac{\partial A_q}{\partial t}+C_g\frac{\boldsymbol{\beta}_q^T}{\beta}\cdot\widehat{\nabla}_{2D}A_q=-\frac{\mathrm{i}\pi\omega}{2}\frac{a^2}{A^c}\left(\sum_{p=1}^{Q}A_p-\frac{\mathrm{i}\sqrt{\beta g}}{\omega}\gamma_0\right),\quad q=1,\ldots,Q. \tag{4.4.67}$$

On comparing our body condition (4.4.55) with [18, equation (5.4c)] we see that the amplitude of our velocity γ_0 is related to their amplitude of displacement ζ_0 through $\gamma_0\equiv-\mathrm{i}(\omega/\sqrt{\beta g})\zeta_0$ and hence these envelope equations are analogous to [18, equation (4.17)] for their group speed C_g given in [18, equation (3.8)].

Deep water envelope equations for the radiation problem We continue going forward with this solution for the radiation problem under the deep water assumption, that is that $\beta h\to\infty$, so that $\omega^2=g\beta$ so that from (4.4.66)

$$\frac{\partial A_q}{\partial T}+\frac{1}{2}\frac{\boldsymbol{\beta}_q^T}{\beta}\cdot\widehat{\nabla}A_q=-\frac{\mathrm{i}\pi}{2\beta^2A^c}\left(\sum_{p=1}^{Q}A_p-\mathrm{i}\gamma_0\right),\qquad q=1,\ldots,Q. \tag{4.4.68}$$

Recovery of infinite array solution Comparing the infinite array leading order solution with the strip array leading order solution, we see that we need to consider amplitudes of the form

$$A_p(\hat{X},\hat{Y},T)=\mathrm{i}U_p^R\mathrm{e}^{-\mathrm{i}\Omega T}$$

for constants U_p^R. Using this form of A_p with $\gamma_0=\mathrm{e}^{-\mathrm{i}\Omega T}$ and equation (4.4.45) inside the envelope equations (4.4.68) yields

$$\frac{(k-\beta)\,(1/\beta)}{(\beta a)^2}U_q^R-\frac{\pi}{\beta^2A^c}\sum_{p=1}^{Q}U_p^R=-\frac{\pi}{\beta^2A^c},\quad q=1,\ldots,Q. \tag{4.4.69}$$

The infinite array solution to the radiation problem (in deep water) was found to be

$$\frac{(k^2-\beta_q^2)L^2}{(ka)^2}U_p^R - \frac{\pi}{A^c}\sum_{q=1}^{Q} 2U_q^R = -\frac{2\pi}{A^c}, \quad p=1,\ldots,Q \tag{4.4.70}$$

Taking $k \to \beta$ so that $\beta = \beta_q$ in the infinite array solution (and dividing through by $\beta^2 L^2$) yields

$$\frac{(k-\beta)(1/\beta)}{(\beta a)^2}U_q^R - \frac{\pi}{\beta^2 A^c}\sum_{p=1}^{Q} U_p^R = -\frac{\pi}{\beta A^c}, \quad q=1,\ldots,Q \tag{4.4.71}$$

giving agreement with the strip array solution when there is no spatial variation.

4.4.3 Freely-floating structures

We consider only the case of deep water in this section and hence $\beta h \to \infty$ means that $\omega^2 = \beta g$. The non-dimensional freely floating body condition is

$$\frac{\partial \varphi}{\partial Z} = \epsilon u_3^j \quad \text{on} \quad S_{Bj}. \tag{4.4.72}$$

where for this problem we again drop the subscript R. The equation of motion

$$u_3^j = \frac{C_{01}}{\epsilon}\frac{W}{W+\kappa-\mathrm{i}\lambda} = -\frac{\mathrm{i}}{\epsilon}\frac{W}{W+\kappa-\mathrm{i}\lambda}\sum_{p=1}^{Q} A_p \mathrm{e}^{\mathrm{i}\boldsymbol{\beta}_p^T \boldsymbol{R}_j} \tag{4.4.73}$$

after matching $\varphi^{(-1,-1)}$ with $\hat{\phi}^{(-1,-1)}$. The application of Green's identity to the composite function ϕ_c and ψ_q^* in one cell is represented by the expression

$$I_V = I_F + \epsilon^2 \left(I_a - I_b\right), \tag{4.4.74}$$

which is defined in the obvious way, as per the formulation in the radiation solution, where

$$I_b = \mathrm{i}\pi\epsilon u_3^j \mathrm{e}^{-\mathrm{i}\boldsymbol{\beta}_p^T \boldsymbol{R}_j} \tag{4.4.75}$$

(note that in the calculation for I_b^R in the radiation problem, the phase factor $\mathrm{e}^{-\mathrm{i}\boldsymbol{\beta}_p^T \boldsymbol{R}_j}$ cancelled with the phase factor $\mathrm{e}^{\mathrm{i}\boldsymbol{\beta}_p^T \boldsymbol{R}_j}$ from the body condition).

Amending (4.4.66) appropriately means that the application of Green's identity in one cell

thus yields

$$\frac{\partial A_q}{\partial T} + \frac{1}{2}\frac{\boldsymbol{\beta}_q^T}{\beta} \cdot \widehat{\nabla} A_q = -\frac{\mathrm{i}\pi}{2\beta^2 A^c}\frac{\kappa - \mathrm{i}\lambda}{W + \kappa - \mathrm{i}\lambda}\sum_{p=1}^{Q} A_p, \quad q = 1, \ldots, Q. \tag{4.4.76}$$

The discussion found in §4.3.1.4 also applies here. Following the same discussion and methods, the differential equation for the shallow water freely-floating problem, in matrix form, is

$$\frac{d}{d\hat{X}}\begin{pmatrix} B_1 \\ \vdots \\ B_Q \end{pmatrix} = \underline{\underline{\mathrm{F}}}\begin{pmatrix} B_1 \\ \vdots \\ B_Q \end{pmatrix} \tag{4.4.77}$$

where $\underline{\underline{\mathrm{F}}}$ is a $Q \times Q$ matrix with entries

$$F_{ij} = \frac{\mathrm{i}}{\beta^2 A^c}\frac{1}{\cos\tau_i}\left[\delta_{ij}\beta^2 A^c \mathcal{K}(1 - \sin\tau_1 \sin\tau_i) - \frac{(\kappa - \mathrm{i}\lambda)\pi}{W + \kappa - \mathrm{i}\lambda}\right] \tag{4.4.78}$$

for the Kronecker delta function δ_{ij}. The boundary conditions, regarding left- and right-going waves applies here also.

Recovery of infinite array solution Considering wave amplitudes of the form

$$A_p(\hat{X}, \hat{Y}, T) = \mathrm{i}U_p \mathrm{e}^{-\mathrm{i}\Omega T}$$

for constants U_p for the reasons outlined previously inside the envelope equations (4.4.76) yields

$$\frac{(k - \beta)\,(1/\beta)}{(\beta a)^2}U_q = \frac{\pi}{\beta^2 A^c}\frac{\kappa - \mathrm{i}\lambda}{W + \kappa - \mathrm{i}\lambda}\sum_{p=1}^{Q} U_p, \quad q = 1, \ldots, Q. \tag{4.4.79}$$

The infinite array freely-floating solution (in deep water) was found to be

$$\frac{(k^2 - \beta_q^2)L^2}{(ka)^2}U_p = \frac{2\pi L^2}{\beta^2 A^c}\sum_{q=1}^{Q}\frac{\kappa - \mathrm{i}\lambda}{\pi + \kappa - \mathrm{i}\lambda}U_q, \quad p = 1, 2, \ldots Q. \tag{4.4.80}$$

Taking $k \to \beta$ so that $\beta = \beta_q$ and dividing through by $\beta^2 L^2$ in this solution yields

$$\frac{(k - \beta)(1/\beta)}{(\beta a)^2}U_q = \frac{\pi}{\beta^2 A^c}\frac{\kappa - \mathrm{i}\lambda}{\pi + \kappa - \mathrm{i}\lambda}\sum_{p=1}^{Q} U_p, \quad q = 1, 2, \ldots Q. \tag{4.4.81}$$

giving agreement with the strip array solution when there is no spatial variation.

4.5 Results and discussion

The approach we take is to choose an area of the unperturbed dispersion diagram (i.e. the relationship between k^2 and β^2 when no cylinders are present) to perturb from (by introducing cylinders). We present the strip array solutions for the same phase vector βL (and other physical parameters) that were used in the infinite array solutions. Comparing the strip array solutions with the infinite array solutions by using the relationship

$$\frac{k}{\beta} = 1 + \epsilon^2 \Omega \tag{4.5.1}$$

for shallow water and

$$\sqrt{\frac{k}{\beta}} = 1 + \epsilon^2 \Omega \tag{4.5.2}$$

for deep water allows for a deeper understanding. The unperturbed dispersion relations for our region of interest is shown in figure 4.2. Having presented diagrams for two plane waves to correspond with the results in chapter 2 for shallow water and deep water, we then consider briefly results for three plane waves alongside the corresponding infinite array results, allowing us to illustrate the relationship between infinite arrays and strip arrays for more than two plane waves.

Ultimately, for each set of results, we are interested in the wave intensities at the entry point (reflected waves) and the exit point (transmitted waves) of the strip array for an incident wave of prescribed amplitude. We wish to see how the radii of the cylinders, the width of the array and the depth of submergence of the cylinders effects the wave intensities for the scattering and freely floating problems. The number of waves present in a solution - including the incident wave - is determined by our location in figure 4.2 ; our results are organised into the number of waves present, and then the nature of these waves.

4.5.1 Two plane waves

At the point $(kL, q_1 L, q_2 L) = (\pi, \pi, 0)$, we have

$$\boldsymbol{\beta}_1 L = (\pi, 0) \quad \text{and} \quad \boldsymbol{\beta}_2 L = (-\pi, 0)$$

which are chosen to represent an incident and backward scattered wave respectively.

We expect the band gaps calculated in Chapter 2 to define the frequencies for which the

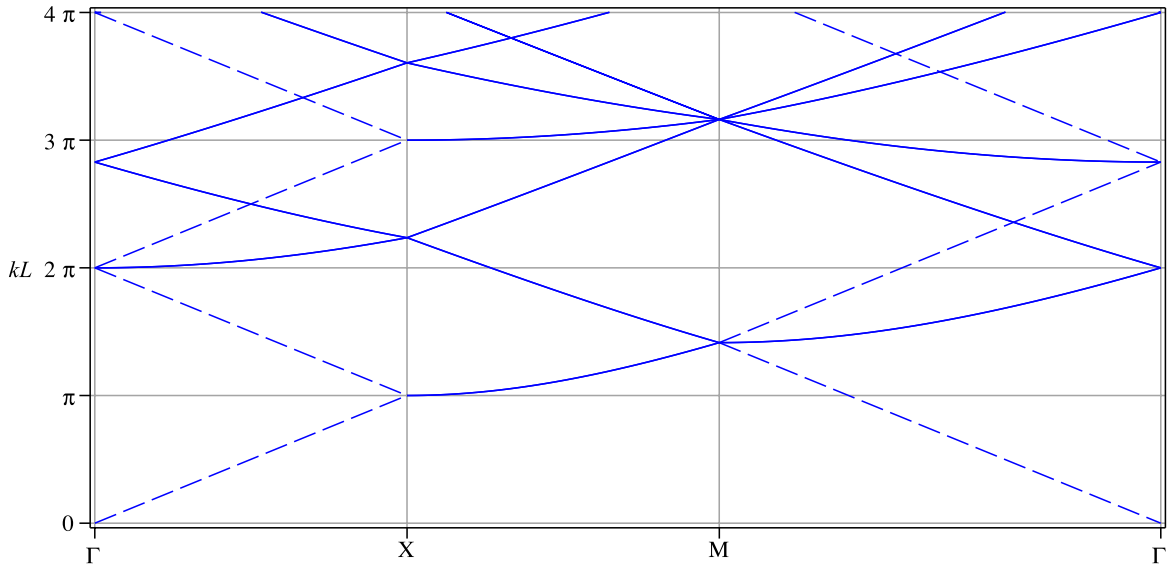

Figure 4.2 Position of poles in wavenumber (or, equivalently, frequency) space for a square lattice with cell side L for $Q = 1$ (– – –) and $Q = 2$ (———): the abscissae is the modulus of $\boldsymbol{\beta} = (q_1, q_2)$ along the edges of the first irreducible Brillouin zone so that ΓX corresponds to $q_1 L \in [0, \pi]$ and $q_2 L = 0$, XM corresponds to $q_2 L \in [0, \pi]$ and $q_1 L = 0$, and $M\Gamma$ corresponds to $q_1 L = q_2 L \in [0, \pi]$.

incident wave cannot propagate through the strip array giving total (or near total) reflection and hence no transmitted waves. We begin this subsection by giving a detailed analysis of the first set of results. Figures 4.3a and 4.3c shows the transmitted and reflected wave intensities on the edge of a strip array (of width $\beta S = 15$, corresponding to approximately 50 cylinders) for various radii a/h in the case of fixed truncated cylinders. It is apparent that the infinite array solutions demonstrated in figure 2.4a served as a very good indication as to what to expect for the strip array; inside the band gaps the wave intensity of the incident wave, evaluated at the exit point of the array, $|B_1(S)|$ is zero whilst the wave intensity of the backward scattered wave $|B_2(0)|$ is increased for the same frequencies. This indeed confirms that there are frequency parameters kL for which the incident wave cannot propagate through the array and hence is totally reflected.

We have complete qualitative agreement with the infinite array results for each set of results here. In the case of surface-piercing fixed truncated cylinders in shallow water, we have shown in figure 4.3 that the band gap widens as the radii a/h is increased but only one side of the band gap's boundary (namely that associated with $kL < \pi$) is affected by changing the depth of submergence d/h of the cylinders. Figure 4.4 confirms that only the lower edge of the band gap is affected by changing the radii or the depth of submergence when the cylinders are made to be bottom mounted. For freely floating cylinders in shallow water (see figure 4.5), we see that

only the upper edge of the band gap is affected by the radii of the cylinders. In the case of deep water, figure 4.6 also agrees with the infinite array solutions: only the upper edge of the band gap is affected as the water-plane radius increases from zero, and by allowing the structure to move.

4.5.2 Three plane waves

In order that we can analyse three plane waves, we need to find points of three solutions in figure 4.2; such points are found at noticeably higher values of kL and consequently it must be noted that at such points we are possibly violating the assumption that βh is small (e.g. at the three-mode point found at $\beta L = 5\pi/2$ when $h/L = 0.05$ we have $\beta h = 0.39$). We hence proceed on the understanding that the results described here are illustrative. At $(kL, q_1 L, q_2 L) = (5\pi/2, \pi/2, 0)$ we have the phase vectors

$$\boldsymbol{\beta}_1 L = (3\pi, 0) \quad ; \quad \boldsymbol{\beta}_2 L = (-\pi, 2\pi) \quad ; \quad \boldsymbol{\beta}_3 L = (-\pi, -2\pi)$$

which are chosen to represent an incident wave that propagates forwards, and two scattered waves both propagating backwards. Figure 4.7a shows the direction of the three phase vectors at this point, whilst figure 4.7b is the infinite array solution for cylinders of various radii a/h that are fixed to the ocean bed.

Strengths of three wave intensities on the edge of the array for various slow frequencies Ω are shown in figures 4.8 and 4.9; we look at the effect of increasing the radii a/h in figure 4.8 for a fixed array width, and then look at varying the width of the array βS for a fixed radii a/h in figure 4.9. Again, there is clear evidence that there are wave-numbers (e.g. approximately $2.47\pi \geq kL \leq 2.53\pi$ for $a/h = 1$, $\beta S = 240$ – corresponding to approximately 50 cylinders) for which the incident wave cannot get through the array; i.e. nothing is transmitted and we have total reflection that is that the wave intensities of the backward propagating waves $B_2(0)$ and $B_3(0)$ are at their maximum value, whilst for values of kL outside this range more of the incident wave is transmitted at the exit point of the array but less is reflected at the entry point. We observe that for larger radii, akin to the infinite array band results, the range of kL for which the incident wave cannot propagate is narrowed.

Figure 4.9 indicates that for larger array widths βS the band gap becomes better defined. This is what one might suspect, because a wider array is becoming more like the infinite array that we considered in Chapter 2.

The infinite array solution for these phase vectors, demonstrated graphically in 4.7b, did not

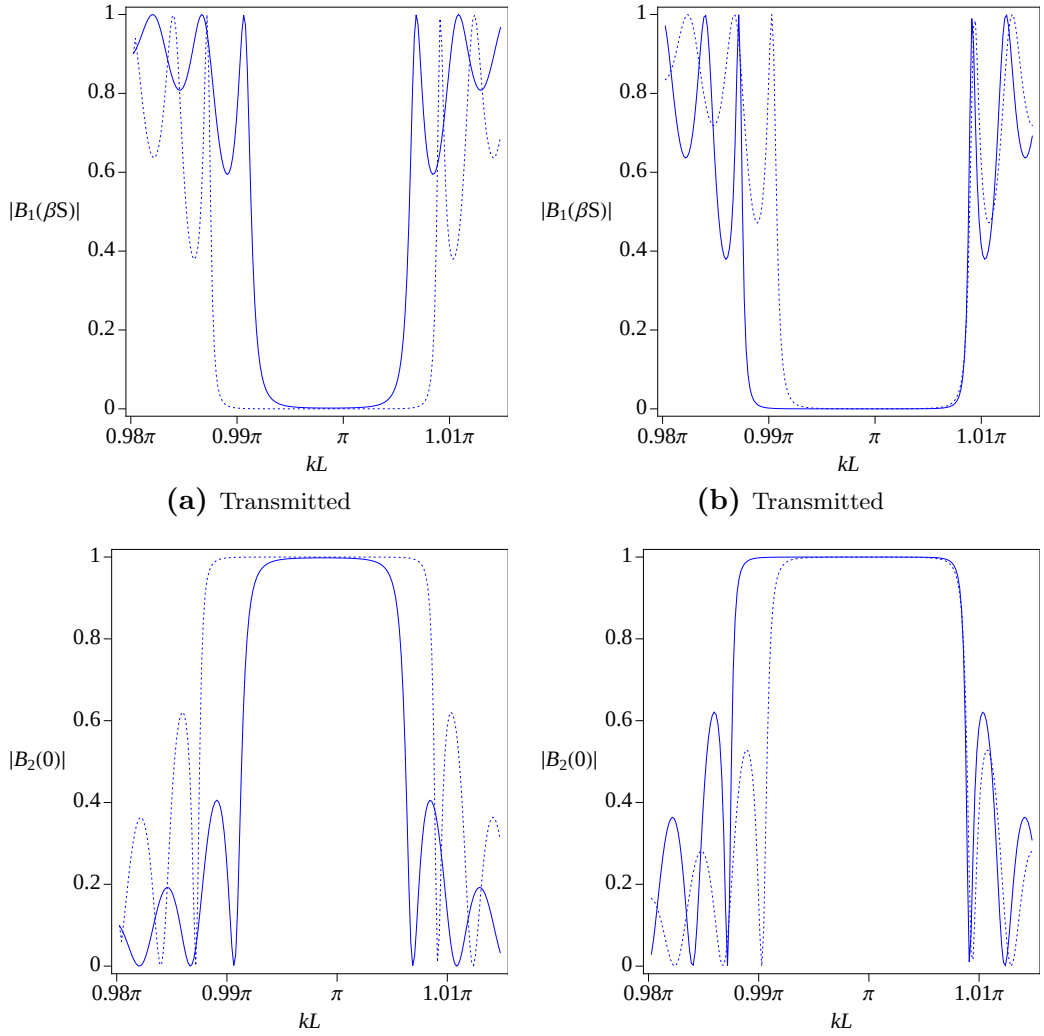

Figure 4.3 Perturbation of two plane waves for fixed surface-piercing cylinders in shallow water (array width is approx. 50 cylinders) for $L/h = 20$: (a)&(c) kL *vs.* $q_1 L$ for $d/h = 0.8$ with $a/h = 0.8$ (——) , $a/h = 1$ (· · · · · ·) for comparison with figure 2.4a; (b)&(d) kL *vs.* $q_1 L$ for $a/h = 1$ with $d/h = 0.8$ (——), $d/h = 0.6$ (· · · · · ·) for comparison with figure 2.4b.

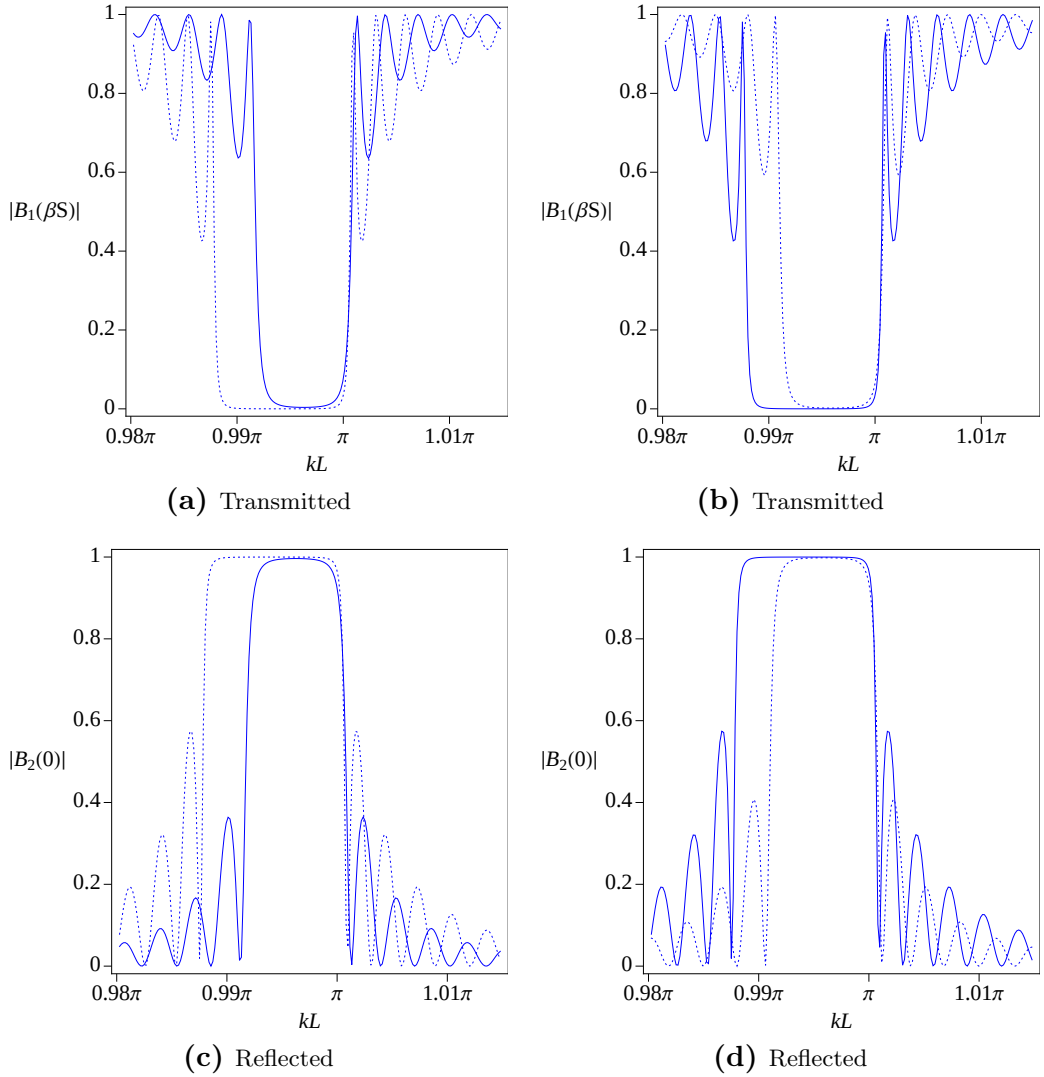

(a) Transmitted **(b)** Transmitted

(c) Reflected **(d)** Reflected

Figure 4.4 Perturbation of two plane waves for fixed bottom-mounted cylinders in shallow water (array width is approx. 75 cylinders) for $L/h = 20$: (a)&(c) kL *vs.* q_1L for $d/h = 0.8$ with $a/h = 0.8$ (——) , $a/h = 1$ (· · · · ·) for comparison with figure 2.5a; (b)&(d) kL *vs.* q_1L for $a/h = 1$ with $d/h = 0.8$ (——), $d/h = 0.6$ (· · · · ·) for comparison with figure 2.5b.

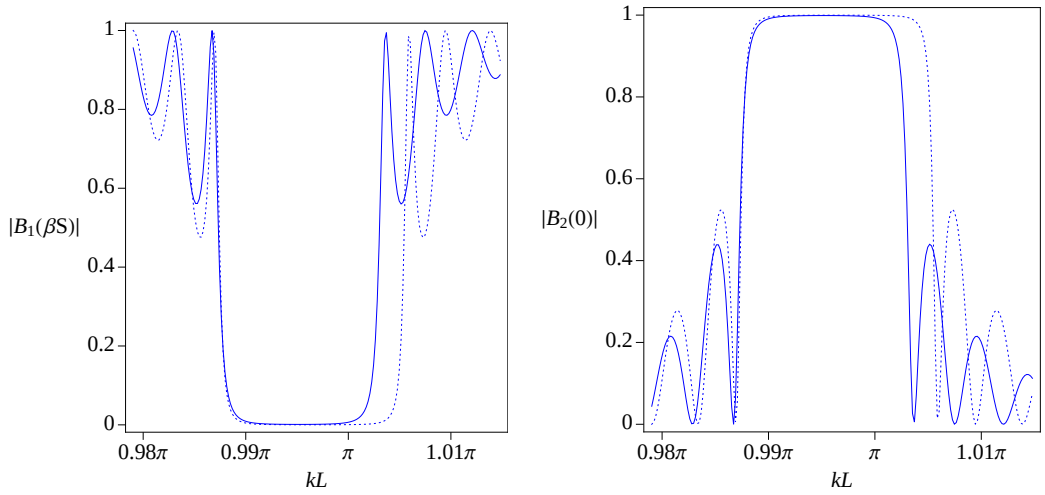

(a) Transmitted **(b)** Reflected

Figure 4.5 Perturbation of two plane waves for freely-floating surface-piercing cylinders in shallow water (array width is approx. 50 cylinders) for $L/h = 20$, $d/h = 0.8$ and $a/h = 1$: kL *vs.* $q_1 L$ for $\kappa = 1$ (——), $\kappa = 4$ (· · · · · ·) for comparison with figure 2.6.

suggest that there are localised bandgaps in the neighbourhood of $(kL, q_1 L, q_2 L) = (5\pi/2, \pi/2, 0)$. However the infinite array solution did tell us that only backward propagating waves may exist in the approximate wave-number range of $2.47\pi \leq kL \leq 2.53\pi$ (the group speed, given by the negative gradient $\partial\omega/\partial t$, implies that the direction of energy propagation is in the negative x direction), which is exactly what we have observed here.

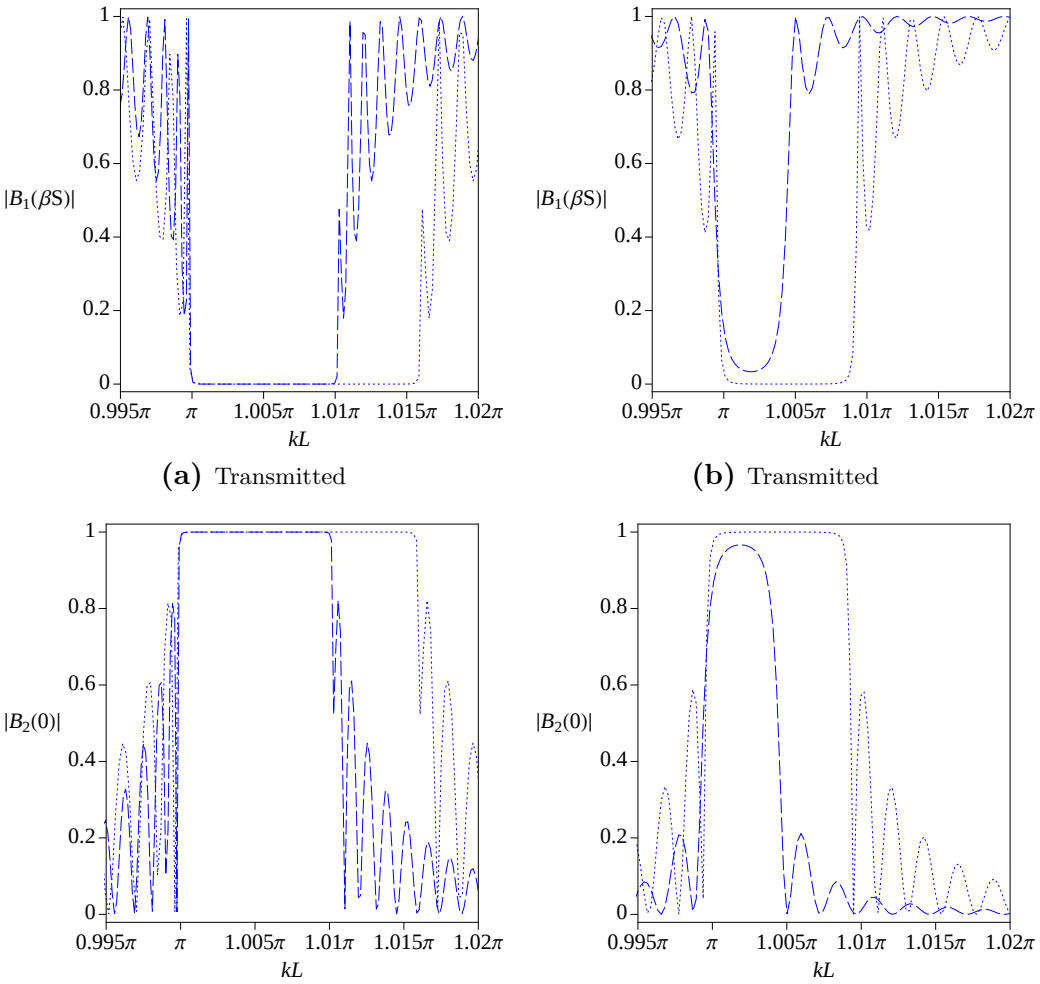

(a) Transmitted **(b)** Transmitted

(c) Reflected **(d)** Reflected

Figure 4.6 Perturbation of two plane waves for surface-piercing structures in deep water (array width is approx. 100 cylinders): kL *vs.* $q_1 L$ for (a)&(c) a fixed structure of radius $a/L = 0.04$ (——) , $a/L = 0.05$ (· · · · · ·) for comparison with figure 2.7a; (b)&(d) freely-floating structures for $a/L = 0.05$ with $\kappa = 1$ (——), $\kappa = 4$ (· · · · · ·) for comparison with figure 2.7b.

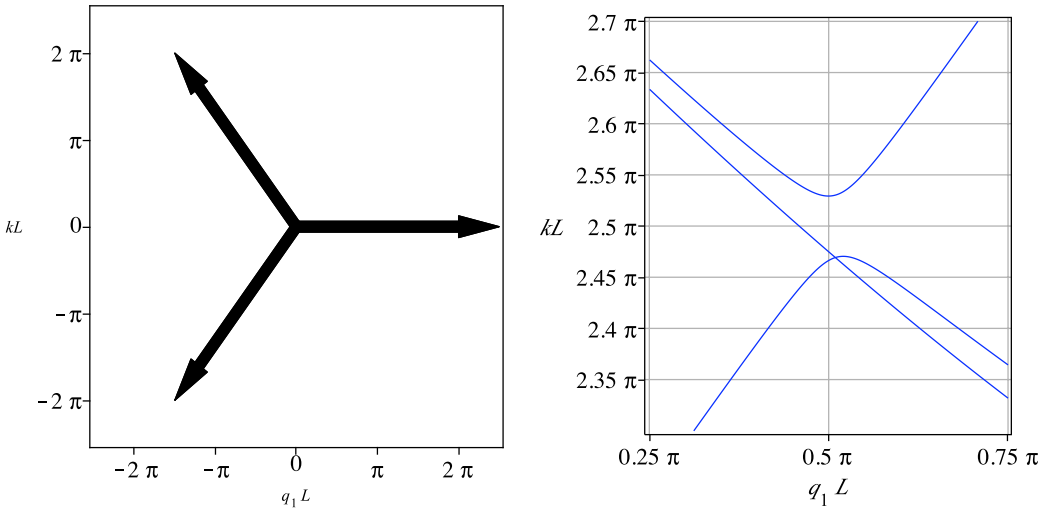

Figure 4.7 At $(kL, q_1L, q_2L) = (5\pi/2, \pi/2, 0)$ we have (a) an incident wave and two backward propagating waves; (b) the solution for an infinite array for cylinders fixed to the ocean bed for $a/h = 1$.

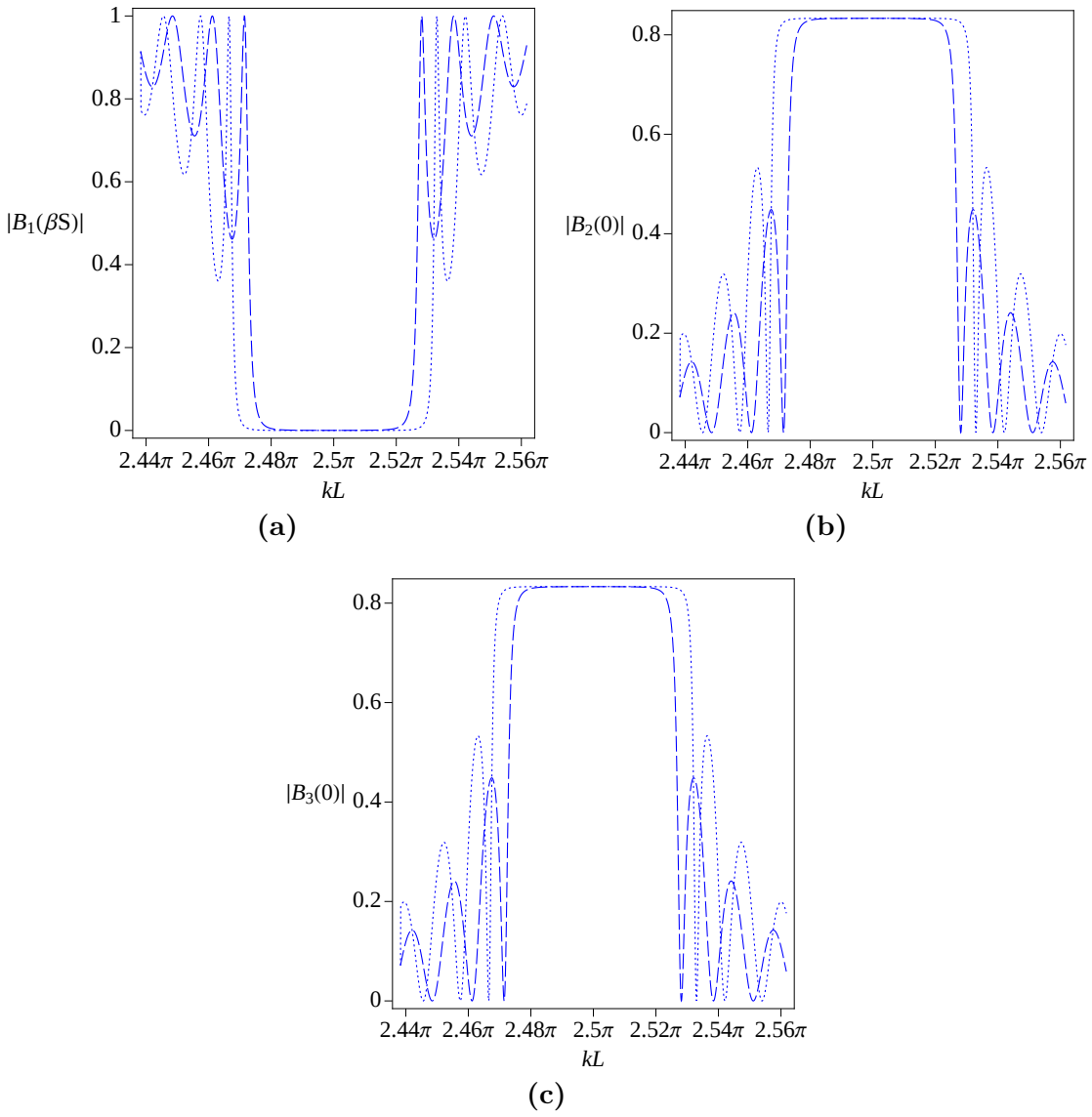

Figure 4.8 Backward, backward propagation for cylinders fixed to the bed in shallow water for $a/h = 0.9$ (– – –), $a/h = 1$ (· · · · · ·) with $\beta S = 240$, corresponding to approximately 50 cylinders: (a) Transmission coefficient $|B_1(S)|$; (b) Reflection coefficient $|B_2(0)|$; (c) Reflection coefficient $|B_3(0)|$

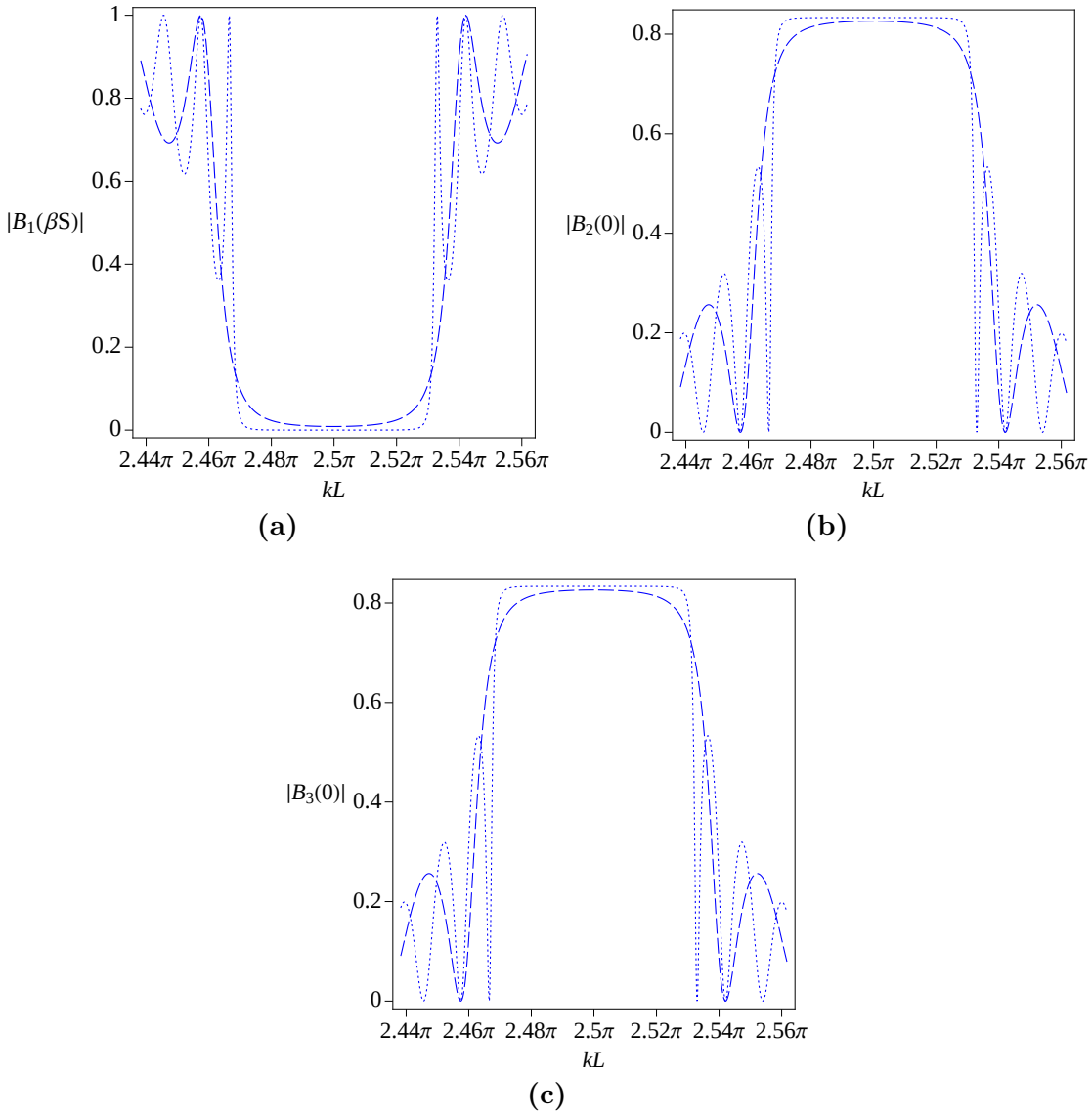

Figure 4.9 Backward, backward propagation for cylinders fixed to the bed in shallow water for $\beta S = 120$ (– – –) and $\beta S = 240$ (· · · · · ·), corresponding to approximately 25 and 50 cylinders respectively, with $a/h = 1$: (a) Transmission coefficient $|B_1(S)|$; (b) Reflection coefficient $|B_2(0)|$; (c) Reflection coefficient $|B_3(0)|$

4.5.3 Structure of the solutions

The link that we have established between the infinite array perturbations and the strip array perturbations from the solutions that exist in the case of no cylinders can be made more definite when we consider the structure of the solutions. Let us recall that the strip array solution is

$$\begin{aligned}\hat{\phi}_0 &= \sum_{q=1}^{Q} A_q(\hat{X},\hat{Y},T)\psi_q(x,y,z) \\ &= \sum_{q=1}^{Q}\left[A_0\sum_{p=1}^{Q} c_{pq}\boldsymbol{v}_p \mathrm{e}^{\lambda_p \hat{X}}\right]\psi_q(x,y,z),\end{aligned} \tag{4.5.3}$$

where $\boldsymbol{v}_p$ are the eigenvectors with associated eigenvalues λ_p for the matrix $\underline{\underline{\mathrm{F}}}^S$; this matrix $\underline{\underline{\mathrm{F}}}^S$ describes the perturbations from the unperturbed point in the case of no cylinders (i.e. where the ψ_q's are valid), and thus we can deduce the relationship between this $\underline{\underline{\mathrm{F}}}^S$ and the infinite array solutions which describe a perturbation from the same point. At the three mode point previously under investigation, i.e. at $(kL, q_1L, q_2L) = (5\pi/2, \pi/2, 0)$, let us consider what happens as kL is increased from $kL = 5\pi/2$. As kL is increased we obtain two values of q_1L less that $\pi/2$ and one greater than $\pi/2$; this corresponds to $\underline{\underline{\mathrm{F}}}^S$ having two negative imaginary eigenvalues and one positive imaginary eigenvalue. For a sufficient decrease in kL, this situation is reversed.

Chapter 5

Conclusion

Approximate methods have been used to show how the frequency, and hence the speed, of a wave of given length and direction is changed by the presence of a periodic lattice of structures that may be fixed, or allowed to float freely. Different water depths have been considered.

We began by considering the case of an array that was infinite in two horizontal directions, and solved the water-wave problem using the method of matched asymptotic expansions. Two particular approximations have been studied. One approximation is valid for shallow water and the other for deep water, but in both cases the structure is assumed to be small relative to the wavelength, and the wavelength is taken to be of a similar magnitude to the array periodicity. For a given wave vector, wave propagation is possible only at discrete frequencies which may be isolated ($Q = 1$), or close to one or more other frequencies that arise from the splitting of degeneracies ($Q > 1$). For $Q = 1$, the shallow-water theory for fixed, surface-piercing circular cylinders shows that the primary effect is to reduce the frequency, relative to that in the absence of structures, when the cylinder is longer than a certain length, but to increase the frequency when it is shorter than that length. However, for a submerged structure the frequency is always decreased. In deep water, the presence of a fixed compact, surface-piercing structure always leads to an increase in frequency. In both deep and shallow water, allowing the structure to float freely with a positive mooring stiffness decreases the frequency of wave propagation compared to that when the structure is fixed. For $Q > 1$ the theory allows, in particular, explicit formulae to be obtained for the width of local band gaps. One feature of these solutions is that one edge of the band gap can be unaffected by changes in the geometrical and mooring parameters.

The Rayleigh-Ritz method was used to solve the same infinite array problem for fixed cylinders, but of course the problem could be solved without having to make assumptions on the length scales involved. Furthermore the method afforded us the ability to compute complete

band diagrams which we have been able to use to aid an investigation into negative refraction which, in turn, motivated a search for complete band gaps. We have been able to reproduce the localised band gap diagrams which were found using the asymptotic methods, where good agreement was observed between the two different approaches of solutions. In the case of deep water, the best agreement was observed when the length of the cylinders was reduced to zero (representing a disc on the free surface).

Finally, we looked at the water-wave problem for a strip array (that is, where the array stretches to infinity in only one horizontal direction), which was solved using a combination of the method of multiple scales and the method of matched asymptotic expansions. Considering a strip array allowed us to consider the properties of the transmitted and reflected waves for a given incident wave, and in particular how the transmitted and reflected waves were affected for different physical parameters. A correspondence was made between the band gaps found for the infinite array problem and the complete reflection (and hence zero transmission) for the strip array problem.

An obvious extension is to consider other modes of motion. The general theory laid out in the first chapter allows for six degrees of freedom, but we have only considered heave throughout. Whilst it may be that the algebra becomes cumbersome, multiple interacting modes could be looked at. A further possible extension of this work, motivated by the real life application of Very Large Floating Structures, is to introduce a platform between the floating structures, that is to link the structures together so that complete modules of structures may be considered. Some progress has been made in [47], where structures are linked together in clusters.

Appendix A

Infinite array

A.1 Convergence of a lattice sum

We consider here the convergence of certain lattice sums. For simplicity in the presentation, we consider only a rectangular lattice and that part Λ^+ of the lattice that lies in the first quadrant (similar arguments apply to the other three quadrants). For a rectangular lattice, each lattice point is readily identified with a pair $(p,q) \in \mathbb{Z} \times \mathbb{Z}$ so that, for some $F(r_j) \equiv f(p,q)$, a lattice sum

$$\sum_{\boldsymbol{R}_j \in \Lambda^+}{}' F(r_j) = \sum_{p,q}{}' f(p,q), \tag{A.1.1}$$

where the last summmation is over all non-negative integer pairs excluding $p = q = 0$. If for all (x,y) in the first quadrant R, $f(x,y) > 0$ and $f(x,y) \geq f(\xi,\eta)$ whenever $\xi \geq x$ and $\eta \geq y$ then, by the integral test for double series [48, § 32],

$$\sum_{p,q}{}' f(p,q) \text{ converges } \iff \iint_R f(x,y)\,\mathrm{d}x\,\mathrm{d}y \text{ converges.} \tag{A.1.2}$$

We now consider the convergence of the specific lattice sum

$$S_{mn} = \sum_{\boldsymbol{R}_j \in \Lambda^+}{}' \mathrm{e}^{\mathrm{i}\boldsymbol{\beta}^T \boldsymbol{R}_j} \left[I^c_{mn}(r_j, z; k) + I^s_{mn}(r_j, z; k) \right] \mathrm{e}^{\mathrm{i}\theta_j}, \quad m \geq n \geq 0, \tag{A.1.3}$$

where

$$I^c_{mn}(r, z; k) = \int_0^\infty \frac{\nu^{m+2} \cos \nu z}{\nu^2 + k^2} K_n(\nu r)\,\mathrm{d}\nu \tag{A.1.4}$$

and

$$I^s_{mn}(r,z;k) = k\int_0^\infty \frac{\nu^{m+1}\sin\nu z}{\nu^2+k^2}K_n(\nu r)\,\mathrm{d}\nu. \tag{A.1.5}$$

When extended to the complete lattice Λ, the sum S_{mn} is proportional to the lattice sum appearing in equation (2.4.7), with the latter written in dimensional coordinates so as to display explicitly the dependence on k. The series S_{mn} is absolutely convergent provided

$$S^c_{mn} = {\sum_{\boldsymbol{R}_j\in\Lambda^+}}' |I^c_{mn}(r_j,z;k)| \quad \text{and} \quad S^s_{mn} = {\sum_{\boldsymbol{R}_j\in\Lambda^+}}' |I^s_{mn}(r_j,z;k)| \tag{A.1.6}$$

both converge. Choose a $k_0>0$, then for $k\geq k_0$

$$|I^c_{mn}(r,z;k)| \leq \int_0^\infty \frac{\nu^{m+2}K_n(\nu r)}{\nu^2+k_0^2}\,\mathrm{d}\nu \equiv \widehat{I}_{mn}(r), \tag{A.1.7}$$

say, which exists provided $m+3>n$. From the properties of the modified Bessel function K_n, $\widehat{I}_{mn}(r)$ is a monotonically decreasing function of r and from [49, equation 5.2.28]

$$\widehat{I}_{mn}(r) \sim \frac{D_{mn}}{r^{m+3}} \quad \text{as} \quad r\to\infty \tag{A.1.8}$$

for some constant D_{mn}. Thus, for the required range $m\geq n\geq 0$, the conditions of the integral test for double series are satisfied and S^c_{mn} converges for all $k\geq k_0>0$ (and hence S^c_{mn} has no singularities as a function of k except possibly at $k=0$). A similar argument applies to S^s_{mn} because

$$|I^s_{mn}(r,z;k)| \leq k|z|\int_0^\infty \frac{\nu^{m+2}K_n(\nu r)}{\nu^2+k_0^2}\,\mathrm{d}\nu = k|z|\widehat{I}_{mn}(r). \tag{A.1.9}$$

A.2 Calculation of shallow water inner region dipole coefficient

A *patching* method is used here to determine the dipole coefficient $\mathfrak{D}_1$ needed in the shallow-water solution for a truncated circular cylinder of non-dimensional radius a/h and height d/h. (By *patching* we mean equating solutions at a shared boundary – this is in contrast to *matching*, where we mean equating solutions within a shared region.) The method follows that used in [50] for the problem of wave radiation by a truncated circular cylinder. Here we treat the case of a surface-piercing cylinder, the dipole coefficient takes the same value for a bottom-mounted cylinder of the same height.

The aim is to determine the asymptotic form as $R \to \infty$ of the inner region eigenfunction F_1 defined in equation (2.3.16). The solution is effected by further dividing the inner region into two smaller regions: an exterior region in $R > a/h$, and an interior region in $R < a/h$ that lies beneath the cylinder when the cylinder is surface piercing. The interior problem is

$$\nabla^2 \varphi_1^{S(i)} = 0 \qquad \text{in the fluid,} \tag{A.2.1}$$

$$\frac{\partial}{\partial Z}\varphi_1^{S(i)} = 0 \qquad \text{on } Z = -1, \tag{A.2.2}$$

$$\frac{\partial}{\partial Z}\varphi_1^{S(i)} = 0 \qquad \text{on } Z = -d/h \tag{A.2.3}$$

and the appropriate form for the desired eigenfunction is

$$\varphi_1^{S(i)} = (\boldsymbol{E}_1^S)^T \sum_{n=0}^{\infty} \epsilon_n \mathfrak{C}_n^S \frac{I_1(\alpha_n R)}{I_1(\alpha_n a/h)} \cos[\alpha_n(Z+1)] \begin{pmatrix} \cos\theta \\ \sin\theta \end{pmatrix} \tag{A.2.4}$$

where the $\mathfrak{C}_n^S$'s are to be found, $\alpha_n = n\pi h/l$, and ϵ_n is the Neumann symbol defined by $\epsilon_0 = 1$ and $\epsilon_n = 2$ for $n \geq 1$. The exterior problem is

$$\nabla^2 \varphi_1^{S(e)} = 0 \quad \text{in the fluid,} \tag{A.2.5}$$

$$\frac{\partial}{\partial Z}\varphi_1^{S(e)} = 0 \quad \text{on } Z = 0, \tag{A.2.6}$$

$$\frac{\partial}{\partial Z}\varphi_1^{S(e)} = 0 \quad \text{on } Z = -1, \tag{A.2.7}$$

$$\frac{\partial}{\partial R}\varphi_1^{S(e)} = 0 \quad \text{on } R = a/h \text{ and } Z \in (-d/h, 0) \tag{A.2.8}$$

for which the appropriate general solution is

$$\varphi_1^{S(e)} = (\boldsymbol{E}_1^S)^T \left[(R + \mathfrak{D}_1 R^{-1}) + \sum_{n=1}^{\infty} \mathfrak{D}_n^S \frac{K_1(n\pi R)}{K_1(n\pi a/h)} \cos[n\pi(Z+1)] \right] \begin{pmatrix} \cos\theta \\ \sin\theta \end{pmatrix}, \tag{A.2.9}$$

where $\boldsymbol{E}_1^S$ and the $\mathfrak{D}_n^S$'s are the constants to be found.

Continuity of φ_1^S across $R = a/h$ for $-1 < Z < -d/h$ gives

$$\frac{a}{h} + \mathfrak{D}_1 \frac{h}{a} + \sum_{n=1}^{\infty} \mathfrak{D}_n^S \cos[n\pi(Z+1)] = \sum_{n=0}^{\infty} \epsilon_n \mathfrak{C}_n^S \cos[\alpha_n(Z+1)], \tag{A.2.10}$$

and then multiplication by $\cos[\alpha_m(Z+1)]$ and integration over $Z \in (-1, -d/h)$ yields

$$\delta_{m0} \frac{l}{h} \left[\frac{a}{h} + \mathfrak{D}_1 \frac{h}{a} \right] + \sum_{n=1}^{\infty} \mathfrak{D}_n^S c_{mn} = \mathfrak{C}_m^S \frac{l}{h}, \quad m = 0, 1, 2, ..., \tag{A.2.11}$$

where

$$c_{mn} = \int_{-1}^{-d/h} \cos\alpha_m(Z+1)\cos n\pi(Z+1)\,\mathrm{d}Z = \begin{cases} l/h, & m = n = 0; \\ l/2h, & m/n = l/h; \\ \dfrac{(-1)^m n\pi \sin(n\pi l/h)}{(n^2\pi^2 - \alpha_m^2)}, & \text{otherwise.} \end{cases} \tag{A.2.12}$$

Continuity of $\partial\varphi_1^S/\partial R$ across $R = a/h$ for $-1 < Z < -d/h$ and the body boundary condition on $R = a/h$ for $-d/h < Z < 0$ give

$$1 - \mathfrak{D}_1\frac{h^2}{a^2} + \sum_{n=1}^{\infty}\mathfrak{D}_n^S q_n^1\cos[n\pi(Z+1)] = \begin{cases} \displaystyle\sum_{n=0}^{\infty}\epsilon_n\mathfrak{C}_n^S p_n^1\cos[\alpha_n(Z+1)], & Z \in (-1,-d/h); \\ 0, & Z \in (-d/h, 0), \end{cases} \tag{A.2.13}$$

where

$$p_n^1 = \alpha_n\frac{I_1'(\alpha_n a/h)}{I_1(\alpha_n a/h)} \quad \text{and} \quad q_n^1 = n\pi\frac{K_1'(n\pi a/h)}{K_1(n\pi a/h)}, \quad n \geq 1, \tag{A.2.14}$$

are introduced for convenience of notation (note that $p_0^1 = h/a$ whilst q_0^1 isn't defined). Multiplication by $\cos[m\pi(Z+1)]$ and integration over $Z \in (-1, 0)$ yields

$$1 - \frac{h^2}{a^2}\mathfrak{D}_1 = \mathfrak{C}_0^S\frac{l}{a}, \quad m = 0, \tag{A.2.15}$$

$$\frac{1}{2}\mathfrak{D}_m^S q_m^1 = \sum_{n=0}^{\infty}\epsilon_n\mathfrak{C}_n^S p_n^1 c_{nm}, \quad m = 1, 2, 3, \ldots. \tag{A.2.16}$$

Solution of (A.2.16) for $\mathfrak{D}_n^S$ and substitution of the result, along with (A.2.15), into (A.2.11) yields

$$\sum_{n=0}^{\infty}\left[\delta_{mn} - 2\epsilon_n\frac{h}{l}p_n^1 f_{mn}^1\right]\mathfrak{C}_n^S = \delta_{m0}\left(\frac{a}{h} + \mathfrak{D}_1\frac{h}{a}\right) \quad \text{for } m = 0, 1, 2, \ldots, \tag{A.2.17}$$

where

$$f_{mn}^1 = \sum_{s=1}^{\infty}\frac{c_{ms}c_{ns}}{q_s^1}, \tag{A.2.18}$$

which may be solved by truncation.

A.3 Alternative deep water solution (changing the ansatz)

The zero eigenvalue obtained in § 2.6.2.2 is potentially problematic as, when adopting the ansatz in equation (2.4.8), we make the assumption that each $\Delta_q = \mathrm{ord}(1)$ as $\epsilon \to 0$. Let us modify the ansatz to

$$(k^2 - \beta_q^2)L^2 = \epsilon^3 \Delta_q \tag{A.3.1}$$

with $\Delta_q = \mathrm{ord}(1)$ as $\epsilon \to 0$. What follows is only a slight and straightforward adaption of the work that is contained within § 2.4.1. With the aid of equation (A.3.1), we may write

$$\begin{aligned} G_{mn}(r',\theta,z') = \hat{\phi}_{m|n|}(r',z')\mathrm{e}^{\mathrm{i}n\theta} + {\sum_{\boldsymbol{R}_j \in \Lambda}}' \mathrm{e}^{\mathrm{i}\boldsymbol{\beta}^T \boldsymbol{R}_j} K_{m|n|}(r_j', z')\mathrm{e}^{\mathrm{i}n\theta_j} \\ + \frac{(-1)^m}{(m-|n|)!}\pi \mathrm{i}\, \mathrm{e}^{z'} \xi_n \sum_p (-1)^{n-p} \left[\sum_{q=1}^{Q} \frac{\sigma_{n-p,q}^{(1)}}{\epsilon^3 \Delta_q} + \sigma_{n-p}^{(2)} \right] J_p(r')\mathrm{e}^{\mathrm{i}p\theta}, \end{aligned} \tag{A.3.2}$$

and it is again convenient to define

$$g_{mn}(r',\theta,z') = \epsilon^3 G_{mn}(r',\theta,z') = g_{mn}^{(1)}(r',\theta,z') + \epsilon^3 g_{mn}^{(2)}(r',\theta,z'), \tag{A.3.3}$$

where $g_{mn}^{(1)}$ contains the terms in $\sigma_{n,q}^{(1)}$, and $g_{mn}^{(2)}$ all other terms. We recall that

$$g_{mn}^{(1)}(r',\theta,z') = \frac{(-1)^m}{(m-|n|)!}\pi \mathrm{i}\, \mathrm{e}^{z'} \xi_n (-1)^n \sum_{q=1}^{Q} \frac{\sigma_{n,q}^{(1)}}{\Delta_q} \mathrm{e}^{\mathrm{i}r' \cos(\theta - \tau_q)}, \tag{A.3.4}$$

which is a combination of deep-water plane waves. The outer region solution is written as

$$\hat{\phi}_S^{(3)} = \sum_{m,n} \mathfrak{a}_{mn}^S \left[g_{mn}^{(1)}(r',\theta,z') + \epsilon^3 g_{mn}^{(2)}(r',\theta,z') \right] + \sum_{m,n} \left\{ \epsilon \mathfrak{b}_{mn}^S + \epsilon^2 \mathfrak{c}_{mn}^S + \epsilon^3 \mathfrak{d}_{mn}^S \right\} g_{mn}^{(1)}(r',\theta,z'). \tag{A.3.5}$$

The form of the inner solution was given in § 2.4.1 as

$$\varphi_S^{(1)} = \varphi_0^S + \epsilon \varphi_1^S \tag{A.3.6}$$

(where possible intermediate terms are omitted to simplify the presentation). A zero eigenvalue

found when using the original ansatz corresponds to $C_0^S = 0$, so that the inner solutions for the new ansatz become

$$\varphi_0^S = C_0^S = 0 \tag{A.3.7}$$

and

$$\varphi_1^S = C_1^S + C_0^S(Z + \chi_0) + (\boldsymbol{E}_1^S)^T \left[\tilde{R}\sin\psi \begin{pmatrix}\cos\theta\\ \sin\theta\end{pmatrix} + \boldsymbol{\chi}_1\right], \tag{A.3.8}$$

where we recall that as $\tilde{R} \to \infty$

$$\chi_0 \sim \frac{B_0^S}{\tilde{R}} \quad \text{and} \quad \boldsymbol{\chi}_1 \sim \underline{\underline{\mathrm{M}}}\frac{\sin\psi}{\tilde{R}^2}\begin{pmatrix}\cos\theta\\ \sin\theta\end{pmatrix}, \tag{A.3.9}$$

for a constant B_0 and a matrix $\underline{\underline{\mathrm{M}}}$ that is determined by the shape of the structures. The outer expansion of the inner solution is given as

$$\varphi_S^{(1,3)} = C_0^S + \epsilon\left\{C_1^S + C_0^S\left((Z + \frac{B_0^S}{\tilde{R}}\right) + (\boldsymbol{E}_1^S)^T\left[\tilde{R}\sin\psi\begin{pmatrix}\cos\theta\\ \sin\theta\end{pmatrix} + \underline{\underline{\mathrm{M}}}\frac{\sin\psi}{\tilde{R}^2}\begin{pmatrix}\cos\theta\\ \sin\theta\end{pmatrix}\right]\right\}. \tag{A.3.10}$$

When expressed in terms of the outer coordinates, the most singular term at $\mathrm{ord}(\epsilon^3)$ in the outer expansion of $\varphi_S^{(1)}$ is in $1/\tilde{r}^2$. Thus, there can be no terms more singular than this at $\mathrm{ord}(\epsilon^3)$ in the outer solution and, taking into account the singular terms in $\hat{\phi}_{mn}$ as shown in equation (2.4.1), this gives

$$\mathfrak{a}_{mn}^S = 0 \quad \text{for} \quad m \geq 1 \tag{A.3.11}$$

meaning that the inner expansion of the outer solution is

$$\begin{aligned}\hat{\phi}_S^{(3,1)} =& \pi\mathrm{i}\sum_{q=1}^{Q}\frac{1}{\Delta_q}\left[\sigma_{0,q}^{(1)}\mathfrak{a}_{00}^S - \sigma_{0,q}^{(1)}\mathfrak{a}_{10}^S + \sigma_{1,q}^{(1)}\mathfrak{a}_{11}^S - \sigma_{-1,q}^{(1)}\mathfrak{a}_{1,-1}^S\right]\\ &\cdot\left[1 + \epsilon\tilde{R}\cos\psi + \mathrm{i}\epsilon\tilde{R}\sin\psi\,\boldsymbol{e}_{1q}^T\begin{pmatrix}\cos\theta\\ \sin\theta\end{pmatrix}\right]\\ &+ \epsilon^3\left[\frac{\mathfrak{a}_{00}^S}{\epsilon\tilde{R}} + \mathfrak{a}_{10}^S\overline{\phi}_{10} - \mathfrak{a}_{11}^S\frac{\sin\psi}{\epsilon^2\tilde{R}^2}\mathrm{e}^{\mathrm{i}\theta} - \mathfrak{a}_{1,-1}^S\frac{\sin\psi}{\epsilon^2\psi^2}\mathrm{e}^{-\mathrm{i}\theta}\right] + \epsilon\sum_{m,n}\mathfrak{b}_{mn}^S\end{aligned} \tag{A.3.12}$$

where $\overline{\phi}_{10}$ is the outer expansion of $\hat{\phi}_{01}$ that is not actually needed as it has nothing to match within the inner region (we expect $\epsilon^3\overline{\phi}_{10}$ to take the form $\epsilon^3 P_1^0(\cos\psi)/\tilde{r}^2 \equiv \epsilon\cos\psi/\tilde{R}^2$ for which

there is nothing for it to match with in the inner region).

An application of the matching principle $\varphi_S^{(1,3)} \equiv \hat{\phi}_S^{(3,1)}$ gives, among other relationships (including that C_0^S, $\mathfrak{a}_{00}^S$, and $\mathfrak{a}_{10}^S$ all equal zero)

$$-\pi \sum_{q=1}^{Q} \frac{1}{\Delta_q} \left[\sigma_{1,q}^{(1)} \mathfrak{a}_{11}^S - \sigma_{-1,q}^{(1)} \mathfrak{a}_{1,-1}^S \right] \boldsymbol{e}_{1q}^T = (\boldsymbol{E}_1^S)^T, \tag{A.3.13a}$$

$$-\mathfrak{a}_{11}^S (1, \mathrm{i})^T - \mathfrak{a}_{1,-1}^S (1, -\mathrm{i})^T = (\boldsymbol{E}_1^S)^T \underline{\underline{\mathrm{M}}} \tag{A.3.13b}$$

and, to unify the deep- and shallow- water cases we define

$$U_q^S = \frac{\mathrm{i}}{\Delta_q} \left[-4\mathrm{e}^{\mathrm{i}\tau_q} \mathfrak{a}_{11}^S - 4\mathrm{e}^{-\mathrm{i}\tau_q} \mathfrak{a}_{1,-1}^S \right] \tag{A.3.14}$$

to obtain

$$\sum_{q=1}^{Q} \left[\delta_{pq} \Delta_p + \frac{4\pi L^2}{A} \boldsymbol{e}_{1q}^T \underline{\underline{\mathrm{M}}} \boldsymbol{e}_{1p} \right] U_q^S = 0, \quad p = 1, 2, \ldots Q. \tag{A.3.15}$$

as the eigenvalue relation to determine the allowable values of k.

Appendix B

Strip array

B.1 Shallow water scattering problem: direct calculation of body integral

Here we calculate directly the integral across the structure for the shallow water scattering problem for use in applying Green's identity in one lattice cell. (In the main body of text, this integral was found by reapplying Green's identity in the near field; this direct calculation is included for verification of the method used in the main body of text).

Denoting the base of the cylinder as S_1 and the sides S_2 we have

$$I_S = \iint_{S_1} \varphi^{(1)(i)} \frac{\partial \psi_q^*}{\partial Z} \, dS^{NF} + \iint_{S_2} \varphi^{(1)(e)} \frac{\partial \psi_q^*}{\partial R} \, dS^{NF} \tag{B.1.1}$$

where the superscript (i) and (e) denote the near field interior and exterior solutions respectively. We note that, in near field coordinates,

$$\begin{aligned} \psi_q^* &= D(Z) \mathrm{e}^{\mathrm{i}\boldsymbol{\beta}_q^T \boldsymbol{R}_j} \mathrm{e}^{-\mathrm{i}\epsilon R\cos(\theta-\tau_q)} \\ &\simeq -\frac{\mathrm{i}}{2} \mathrm{e}^{\mathrm{i}\boldsymbol{\beta}_q^T \boldsymbol{R}_j} \left[1 + \frac{\epsilon^2 (Z+1)^2}{2}\right] \left[1 - \mathrm{i}\epsilon R\cos(\theta-\tau_q) + \frac{1}{2}\epsilon^2 R^2 \cos^2(\theta-\tau_q)\right] \end{aligned} \tag{B.1.2}$$

so that

$$\frac{\partial \psi_q^*}{\partial R} = -\frac{\mathrm{i}}{2} \mathrm{e}^{\mathrm{i}\boldsymbol{\beta}_q^T \boldsymbol{R}_j} \left[-\mathrm{i}\epsilon\cos(\theta-\tau_q) + \epsilon^2 R\cos^2(\theta-\tau_q)\right] + O(\epsilon^3) \tag{B.1.3}$$

Since $\dfrac{\partial \psi_q^*}{\partial Z}$ is strictly of order ϵ^2, we only require the leading order constant of $\varphi^{(1)(i)}$ to calculate

the integral over S_1

$$\begin{aligned} I_S = & \iint\limits_{S_1} C_0^S \frac{\partial \psi_q^*}{\partial Z}\, dS^{NF} + \iint\limits_{S_2} \varphi^{(1)(e)} \frac{\partial \psi_q^*}{\partial R}\, dS^{NF} \\ \simeq & -\frac{\mathrm{i}}{2} \mathrm{e}^{\mathrm{i}\boldsymbol{\beta}_q^T \boldsymbol{R}_j} \left\{ \iint\limits_{S_1} C_0^S \epsilon^2 (Z+1)\, dS^{NF} \right. \\ & \left. + \iint\limits_{S_2} \varphi^{(1)(e)} \left[-\mathrm{i}\epsilon \cos(\theta - \tau_q) + \epsilon^2 R \cos^2(\theta - \tau_q) \right]\, dS^{NF} \right\} \\ = & -\frac{\mathrm{i}}{2} \mathrm{e}^{\mathrm{i}\boldsymbol{\beta}_q^T \boldsymbol{R}_j} \left\{ -\mathrm{i}\epsilon \iint\limits_{S_2} \varphi^{(1)(e)} \cos(\theta - \tau_q)\, dS^{NF} \right. \\ & \left. + \epsilon^2 \left[\iint\limits_{S_2} C_0^S R \cos^2(\theta - \tau_q)\, dS^{NF} + \iint\limits_{S_1} C_0^S (Z+1)\, dS^{NF} \right] \right\} \end{aligned} \tag{B.1.4}$$

where only the constant C_0^S is needed from $\varphi^{(1)(e)}$ in the second integral. Denoting each of the three surface integrals I_a, I_b and I_c respectively, let us first calculate I_a. To do so, let us consider the function $\chi = R\cos(\theta - \tau_q)$ and apply Green's identity in the near field only to the two functions $\varphi^{(1)(e)}$ and χ to give

$$\begin{aligned} & \iiint\limits_V \varphi^{(1)(e)} \left(\overline{\nabla}_{NF}^2 + \frac{\partial^2}{\partial Z^2} \right) \chi - \chi \left(\overline{\nabla}_{NF}^2 + \frac{\partial^2}{\partial Z^2} \right) \varphi^{(1)(e)} \\ & \qquad = \iint\limits_{S_B} \varphi^{(1)(e)} \frac{\partial \chi}{\partial N} - \chi \frac{\partial \varphi}{\partial N}^{(1)(e)}\, dS^{NF} + (-1) \iint\limits_{S_\infty} \varphi^{(1)(e)} \frac{\partial \chi}{\partial R} - \chi \frac{\partial \varphi}{\partial R}^{(1)(e)}\, dS^{NF} \end{aligned} \tag{B.1.5}$$

where it is noted that the surface integrals on the free surface and bed each disappear, S_∞ defines the cylinder that is the near field boundary and the factor of (-1) is included to account for the fact that Green's identity has the normal pointing into the region. (Our normal is defined to be pointing out of the fluid, i.e. in the opposite direction). By definition of χ and the governing fluid equation on $\varphi^{(1)(e)}$ the volume integral on the left hand side disappears, and by the body condition on $\varphi^{(1)(e)}$ the second component of the integral on the body disappears leaving us with

$$0 = \iint\limits_{S_1} \varphi^{(1)(e)} \frac{\partial \chi}{\partial Z}\, dS^{NF} + \underbrace{\iint\limits_{S_2} \varphi^{(1)(e)} \frac{\partial \chi}{\partial R}\, dS^{NF}}_{= I_a} - \iint\limits_{S_\infty} \varphi^{(1)(e)} \frac{\partial \chi}{\partial R} - \chi \frac{\partial \varphi}{\partial R}^{(1)(e)}\, dS^{NF} \tag{B.1.6}$$

By definition of χ the integral over S_1 disappears so that we have

$$\begin{aligned} I_a &= \iint_{S_\infty} \varphi^{(1)(e)} \frac{\partial \chi}{\partial R} - \chi \frac{\partial \varphi}{\partial R}^{(1)(e)} \, dS^{NF} \\ &= \lim_{\hat{R}\to\infty} \iint_{S_\infty} \left\{ C_0^S + \epsilon \left(\boldsymbol{E}_1^S\right)^T \left(\hat{R} + \frac{\mathfrak{D}_0^S}{\hat{R}} \right) \begin{pmatrix} \cos\theta \\ \sin\theta \end{pmatrix} \right\} \cos(\theta - \tau_q) \, dS^{NF} \\ &\quad - \lim_{\hat{R}\to\infty} \iint_{S_\infty} \cos(\theta - \tau_q) \hat{R} \epsilon \left(\boldsymbol{E}_1^S\right)^T \left(1 - \frac{\mathfrak{D}_0^S}{\hat{R}^2} \right) \begin{pmatrix} \cos\theta \\ \sin\theta \end{pmatrix} \, dS^{NF} \end{aligned} \tag{B.1.7}$$

where it is noted that the summations contained within $\varphi^{(1)(e)}$ disappear as $\hat{R} \to \infty$. We thus have

$$\begin{aligned} I_a &= \lim_{\hat{R}\to\infty} \int_{-1}^{0} \int_{0}^{2\pi} \left\{ C_0^S + 2\epsilon \frac{\mathfrak{D}_0^S}{\hat{R}} \left(\boldsymbol{E}_1^S\right)^T \begin{pmatrix} \cos\theta \\ \sin\theta \end{pmatrix} \right\} \cos(\theta - \tau_q) \, \hat{R} d\theta dZ \\ &= 2\pi\epsilon \mathfrak{D}_0^S \left(\boldsymbol{E}_1^S\right)^T \begin{pmatrix} \cos\tau_q \\ \sin\tau_q \end{pmatrix} \end{aligned} \tag{B.1.8}$$

The surface integrals I_b and I_c are easily computed as

$$\begin{aligned} I_b &= \int_{-d/h}^{0} \int_{0}^{2\pi} C_0^S \frac{a}{h} \cos^2(\theta - \tau_q) \, \frac{a}{h} d\theta dZ = \frac{d}{h} \frac{a^2}{h^2} \pi C_0^S; \\ I_c &= \int_{0}^{a/h} \int_{0}^{2\pi} C_0^S \frac{l}{h} \, R d\theta dR = \frac{l}{h} \frac{a^2}{h^2} \pi C_0^S \end{aligned} \tag{B.1.9}$$

Hence, from (B.1.4) we have

$$I_S \simeq -\frac{\mathrm{i}}{2} \mathrm{e}^{\mathrm{i}\boldsymbol{\beta}_q^T \boldsymbol{R}_j} \epsilon^2 \pi \left\{ -2\mathrm{i}\mathfrak{D}_0^S \left(\boldsymbol{E}_1^S\right)^T \begin{pmatrix} \cos\tau_q \\ \sin\tau_q \end{pmatrix} + \frac{a^2}{h^2} C_0^S \right\} \tag{B.1.10}$$

Putting each of our calculations back into Green's identity yields

$$-\frac{\mathrm{i}}{2} \frac{\boldsymbol{\beta}_q}{\beta} \beta^2 A^c \cdot \widehat{\nabla} A_q = \frac{\mathrm{i}}{2} \beta^2 A^c \frac{\partial A_q}{\partial T} - \frac{\mathrm{i}}{2} \mathrm{e}^{\mathrm{i}\boldsymbol{\beta}_q^T \boldsymbol{R}_j} \pi \left\{ \frac{a^2}{h^2} C_0^S - 2\mathrm{i}\mathfrak{D}_0^S \left(\boldsymbol{E}_1^S\right)^T \boldsymbol{e}_{1q} \right\} \quad \text{for} \quad q = 1, \ldots, Q. \tag{B.1.11}$$

Bibliography

[1] Xtreme! Engineering. Riding the wave of the future. `http://www.xtreme.hawaii.edu/research-projects/vlfs/`, 2002.

[2] BBC News website. Floating wind turbine launched. `http://news.bbc.co.uk/1/hi/business/8085551.stm`, 2009.

[3] C. M. Linton and P. McIver. *Handbook of Mathematical Techniques for Wave/Structure Interactions*. Chapman and Hall/CRC, Boca Raton, 2001.

[4] C. C. Mei, M. Stiassnie, and D. P. Yue. *Theory and Applications of Ocean Surface Waves, Part 1: Linear Aspects*. World Scientific, Singapore, 2005.

[5] P. McIver. Wave interaction with arrays of structures. *Applied Ocean Research*, 24:121–126, 2002.

[6] C. M. Linton and D. V. Evans. The interaction of waves with arrays of vertical circular cylinders. *Journal of Fluid Mechanics*, 215:549–569, 1990.

[7] Hiroshi Kagemoto and Dick K. P. Yue. Interactions among multiple three-dimensional bodies in water waves: an exact algebraic method. *Journal of Fluid Mechanics*, 166:189–209, 1986.

[8] M. Kashiwagi. Hydrodynamic interactions among a great number of columns supporting a very large flexible structure. *Journal of Fluids and Structures*, pages 1013–34, 2000.

[9] M. A. Peter, M. H. Meylan, and C. M. Linton. Water-wave scattering by a periodic array of arbitrary bodies. *Journal of Fluid Mechanics*, 548:237–256, 2006.

[10] M. A. Peter and M. H. Meylan. Water-wave scattering by a semi-infinite periodic array of arbitrary bodies. *Journal of Fluid Mechanics*, 575:473–494, 2007.

[11] C. M. Linton, R. Porter, and I. Thompson. Scattering by a semi-infinite periodic array and the excitation of surface waves. *SIAM Journal on Applied Mathematics*, 67:1233–1258, 2007.

[12] I. Thompson, C. M. Linton, and R. Porter. A new approximation method for scattering by long finite arrays. *Quarterly Journal of Mechanics and Applied Mathematics*, 61:333–352, 2008.

[13] C. M. Linton. Water waves over arrays of horizontal cylinders: band gaps and bragg resonance. *Journal of Fluid Mechanics*, 670:504–526, 2011.

[14] C. M. Linton and D. V. Evans. The interaction of waves with a row of circular cylinders. *Journal of Fluid Mechanics*, 251:687–708, 1993.

[15] M. A. Peter and M. H. Meylan. Water-wave scattering by vast fields of bodies. *SIAM Journal on Applied Mathematics*, 70(5):1567–1586, 2009.

[16] L. G. Bennetts. Wave attenuation through multiple rows of scatterers with differing periodicities. *SIAM Journal on Applied Mathematics*, 71:540–558, 2011.

[17] Y. Li and C. C. Mei. Multiple resonant scattering of water waves by a two-dimensional array of vertical cylinders: Linear aspects. *Physical Review E*, 76:016302–1–23, 2007.

[18] X. Garnaud and C. C. Mei. Bragg scattering and wave-power extraction by an array of small buoys. *Proceedings of the Royal Society A*, 466:79–106, 2010.

[19] P. McIver. Approximations to wave propagation through doubly-periodic arrays of scatterers. *Waves in Random and Complex Media*, 17(4):439–453, 2007.

[20] P. McIver. Water-wave propagation through an infinite array of cylindrical structures. *Journal of Fluid Mechanics*, 424:101–125, 2000.

[21] X. Hu, Y. Shen, X. Liu, R. Fu, J. Zi, X. Jiang, and S. Feng. Band structures and band gaps of liquid surface waves propagating through an infinite array of cylinders. *Physical Review E*, 68:037301–1–4, 2003.

[22] J. P. Dowling. Photonic & sonic band-gap and metamaterial bibliography. `http://phys.lsu.edu/~jdowling/pbgbib.html`, 2008.

[23] X. Hu, Y. Shen, X. Liu, R. Fu, and J. Zi. Superlensing effect in liquid surface waves. *Physical Review E*, pages 030201–1–4, 2004.

[24] L. Feng, X-P Liu, Y-B Chen, Z-P Huang, Y-W Mao, Y-F Chen, J Zi, and Y-Y Zhu. Negative refraction of acoustic waves in two-dimensional sonic crystals. *Physical Review B*, 72(033108), 2005.

[25] J. Dong, X. Hu, and H. Wang. Existing conditions of full bandgaps and absolute negative refraction in metallic-dielectric photonic crystal. *Chinese Physics*, 16(4):1057–61, 2007.

[26] G. D. Crapper. *Introduction to Water Waves*. Ellis Horwood Limited, England, 1984.

[27] X. Garnaud and C. C. Mei. Wave-power extraction by a compact array of buoys. *Journal of Fluid Mechanics*, 635:389–413, 2009.

[28] A. Krynkin and P. McIver. Approximations to wave propagation through a lattice of Dirichlet scatterers. *Waves in Random and Complex Media*, 19(2):347–365, 2009.

[29] S. Guo and P. McIver. Propagation of elastic waves through a lattice of cylindrical cavities. *Proceedings of the Royal Society of London*, 467:2962–2982, 2011.

[30] J. D. Joannopoulos, S. G. Johnson, J. N. Winn, and R. D. Meade. *Photonic Crystals: Molding the Flow of Light*. Princeton University Press, Princeton, 2008.

[31] S. Guo. *PhD thesis "Asymptotic Analysis of Wave Propagation through Periodic Arrays and Layers"*. Loughborough University, 2011.

[32] B. G. Carter and P. McIver. Water-wave propagation through an infinite array of floating structures. *Journal of Engineering Mathematics*, doi: 10.1007/s10665-012-9569-6, 2012.

[33] E. J. Hinch. *Perturbation Methods*. Cambridge University Press, Cambridge, 1991.

[34] D. G. Crighton and F. G. Leppington. Singular perturbation methods in acoustics: diffraction by a plate of finite thickness. *Proceedings of the Royal Society of London*, 335:313–339, 1973.

[35] M. Abramowitz and I. A. Stegun. *Handbook of Mathematical Functions*. Dover Publications, New York, 1965.

[36] C. M. Linton. Lattice sums for the Helmholtz equation. *SIAM Review*, 52:630–674, 2010.

[37] G. K. Batchelor. *An Introduction to Fluid Dynamics*. Cambridge University Press, Cambridge, 1967.

[38] P. McIver. Low frequency asymptotics of hydrodynamic forces on fixed and floating structures. In M. Rahman, editor, *Ocean Waves Engineering*, pages 1–49. Computational Mechanics Publications, Southampton, 1994.

[39] I. Stakgold. *Green's functions and boundary value problems*. Wiley-Interscience, New York, 1998.

[40] C. J. Fitzgerald and P. McIver. Passive trapped modes in the water-wave problem for a floating structure. *Journal of Fluid Mechanics*, 657:456–477, 2010.

[41] G. F. C. Duff and D. Naylor. *Differential Equations of Applied Mathematics*. John Wiley and Sons, 1966.

[42] H.J.P Morand and R. Ohayon. *Fluid Structure Interaction*. Wiley-Blackwell, 1995.

[43] R.V. Craster, J. Kaplunov, E. Nolde, and S. Guenneau. Bloch dispersion and high frequency homogenization for separable doubly-periodic structures. *Wave Motion*, 49(2):333 – 346, 2012.

[44] X. Zhang and Z. Liu. Negative refraction of acoustic waves in two-dimensional phononic crystals. *Applied Physics Letters*, 85(2):341–343, 2004.

[45] A. Sukhovich, l. Jing, and J.H. Page. Negative refraction and focusing of ultrasound in two-dimensional phononic crystals. *Physical Review B*, 77:014301–1–9, 2008.

[46] M. Ke, Z. Liu, C. Qui, W. Wang, J. Shi, W. Wen, and P. Sheng. Negative-refraction imaging with two-dimensional phononic crystals. *Physical Review B*, 72:064306–1–5, 2005.

[47] A. Krynkin and P. McIver. Wave propagation through a doubly-periodic array of clusters. *Unpublished manuscript*.

[48] T. J. I'A Bromwich. *An Introduction to the Theory of Infinite Series*. Merchant Books, 2008.

[49] N. Bleistein and R. A. Handelsman. *Asymptotic Expansions of Integrals*. Dover, New York, 1986.

[50] R. W. Yeung. Added mass and damping of a vertical cylinder in finite-depth waters. *Applied Ocean Research*, 3(3):119–33, 1981.